

The Eurasia Proceedings of Science, Technology, Engineering & Mathematics

EPSTEM

VOLUME 30 ICBAST CONFERENCE

ISSN: 2602-3199

ISBN: 978-625-6959-57-6

ICBAST 2024: 4th International Conference on Basic Sciences and Technology

November 14-17, 2024 Antalya, Turkey

Edited by: Prof.Dr. Mehmet Ozaslan - Gaziantep University, Turkey

ICBAST 2024

4th International Conference on Basic Sciences and Technology (ICBAST)

Proceedings Book

Editor

Mehmet Ozaslan
Gaziantep University, Turkey

ISBN: 978-625-6959-57-6

Copyright 2024

Published by the ISRES Publishing

Address: Askan Mah. Akinbey Sok. No: 5-A/Konya/Turkey

Web: www.isres.org

Contact: isrespublishing@gmail.com

<https://www.2024.icbast.net>

Dates: November 14-17, 2024

Location: Antalya, Turkey



This work is licensed under a [Creative Commons Attribution-NonCommercial-ShareAlike 4.0 International License](https://creativecommons.org/licenses/by-nc-sa/4.0/).

About Editor

Prof Dr. Mehmet Ozaslan

Department of Biology, Gaziantep University, Turkey

Website: mehmetozaslan.com

E-mail: ozaslanmd@gantep.edu.tr

Language Editor

Lecturer Ceren Dogan

School of Foreign Languages, Necmettin Erbakan University, Turkey

Email: cerendogan@erbakan.edu.tr

CONFERENCE PRESIDENTS

Dr. Mehmet Ozaslan - Gaziantep University, Turkey

SCIENTIFIC BOARD

Bahar Tercan - Institute for Systems Biology, USA
Besnik Hajdari - University "isa Boletini" Mitrovica, Kosovo
Bogdan Patrut - Alexandru Ioan Cuza Ţiiversitesi , Romania
Chalavadi Sulochana - Gulbarga University, India
Dariusz Jacek Jakóbczak - Technical University of Koszalin, Poland
Dehini Rachid -University of Bechar, Algeria
Ebba Ossiannilsson - Swedish Association for Distance Education, Swedish
Eleonora Guseinoviene - Klaipeda University, Lithuania
Elena Krelja Kurelovic - Polytechnic of Rijeka, Croatia
Eva Trnova - Masaryk University, Czech Republic
Farhad Balash - Kharazmi University, Iran
Gabriel Delgado-Toral - Universidad Nacional Autónoma de México, Mexico
Gordana Savic - University of Belgrade, Serbia
Isti Hidayah - Semarang State University, Indonesia
Jose Manuel Lopez Guede - University of Basque Country, Spain
Marija Stanić - University of Kragujevac, Serbia
Mehmet Ozaslan - Gaziantep University, Turkey
M. Hanefi Calp - Karadeniz Technical University, Turkey
Mohamed Ahmed - Mansoura University, Egypt
Nicu Bizon - Pitesti University, Romania
Pandian Vasant - Teknology Petronas University, Romania
Rajnalkar Laxman - Gulbarga University, India
Sanaa Al-Delaimy - Mosul University, Iraq
Servet Yatin - Quincy College, United States
Shynar Baimaganbetova - Nazarbayev University, Kazakhstan
Yiyang Chen - Soochow University (CN), China
Zairi Ismael Rizman - MARA University of Technology, Malaysia
Zipporah Pewat Duguryil - Federal College of Education, Nigeria

ORGANIZING COMMITTEE

Besnik Hajdari - University "isa Boletini" Mitrovica, Kosovo
Cemil Aydogdu - Hacettepe University
Danielle Gonçalves de Oliveira Prado-Federal Technological University of Paraná, Brazil
Dariusz Jacek Jakóbczak - Technical University of Koszalin, Poland
Halil Snopce - South East European University, Macedonia
Jaya Bishnu Pradhan-Tribhuvan University, Mahendra Ratna Campus, Nepal
Mehmet Ozaslan - Gaziantep University, Turkey
Mohammad Sarwar - Scialert, Dubai, United Arab Emirates
Murat Beytur - Kafkas University
M. Hanefi Calp - Karadeniz Technical University, Turkey
Shaymaa Fadhel Abbas Albaayit - Baghdad University, Iraq
Zairi Ismael Rizman - MARA University of Technology, Malaysia

Editorial Policies

ISRES Publishing follows the steps below in the proceedings book publishing process.

In the first stage, the papers sent to the conferences organized by ISRES are subject to editorial oversight. In the second stage, the papers that pass the first step are reviewed by at least two international field experts in the conference committee in terms of suitability for the content and subject area. In the third stage, it is reviewed by at least one member of the organizing committee for the suitability of references. In the fourth step, the language editor reviews the language for clarity.

Review Process

Abstracts and full-text reports uploaded to the conference system undergo a review procedure. Abstracts will be evaluated on the basis of abstracts/proposals. The conference system allows the full text to be sent if the abstract is accepted. Participants must wait for the evaluation results after uploading their article abstracts to the conference system. If their abstracts are accepted, they can upload their full texts to the conference system. The full texts are then sent to at least two reviewers for review. The conference has a double-blind peer-review process. Any paper submitted for the conference is reviewed by at least two international reviewers with expertise in the relevant subject area. Based on the reviewers' comments, papers are accepted, rejected or accepted with revision. If the comments are not addressed well in the improved paper, then the paper is sent back to the authors to make further revisions. The accepted papers are formatted by the conference for publication in the proceedings.

Aims & Scope

Technology and basic sciences are closely related fields. Developments and innovations in one of them affect the other. Therefore, the focus of the conference is on studies related to these two fields. Studies in the fields of technology and basic sciences are accepted to the conference even if they are not associated with other field. The conference committee thinks that a study in only one field (for example, mathematics, physics, etc.) will contribute to other field (such as technology) in future studies, even if it is not associated with the presentation at the conference. In line with this perspective, studies in the following fields are accepted to the conference: Biology, Chemistry, Physics, Mathematics and Technology.

The aim of the conference is to bring together researchers and administrators from different countries, and to discuss theoretical and practical issues in all fields of technology and basic science

Articles: 1- 16

CONTENTS

On the Finite Element Modeling of Metal/Ceramic Functionally Graded Beams Subjected to Non-Uniform Static Bending Process / Pages: 1-8

Abdelmadjid Si - Salem, Baya Allala, Souad Ait - Taleb, Fatma Kheloui - Taouche, Soraya Ferhat

Construction of an Integral Distribution Function of Random Variables Determining the Impact of Wind Power Plant on Birds in accordance with the Predictive Analysis by Experts Process / Pages: 9-16

Vladimir Yeremeev, Andrey Naidysh, Oksana Stokan

Application of Magnetic Biochar@Alginate Composite as Adsorbent for Effective Removal of Methylene Blue from Aqueous Media Process / Pages: 17-27

Serife Parlayici, Erol Pehlivan

Lignin Extraction and Characterization from Lavender Waste Process / Pages: 28-38

Halil Sen, Hale Secilmis, Asem Assani, Canan Sen

Comparative Soil-Plant Relationship of Pyrus L. Species under in Situ and Ex Situ Conditions Process / Pages: 39-46

Elman Osman Isgender, Panah Muradov, Sabina Jafarzadeh

Synthesis and Study of the Complex Compound of Isonicotinamide with Zinc Nitrate Process / Pages: 47-55

Lobar Sharipova, Mavluda Ibragimova, Oybek Khudoyberganov, Farhod Khallokov, Khayrulla Bobakulov, Zubayda Abdullaeva

Evaluation of Antioxidant and Anti-Inflammatory Activities of Aqueous Extract of Malva Sylvestris Leaves in Association with Serum Albumin Process / Pages: 56-63

Idir Moualek, Karima Benarab, Karim Houali

Phenological and Morphological Characters Analysis of Vicia Narbonensis L. and Vicia Sativa L. in a Semi-Arid Context Process / Pages: 64-71

Farid Djellal, Selma Mahmah, Azeddine Mouhous, Si Ammar Kadi, Amar Mebarkia

Chemical Properties of Agricultural Soils after Applications of Municipal Sewage Sludge Process / Pages: 72-77

Rabia Cherfouh, Khaled Ouali, Si Ammar Kadi, Azeddine Mouhous, Ali Bouzouren, Zahia Dorbane, Nacima Zimbri - Zirmi, Houci Guermah, Farid Djellal, Idir Moualek, Dahia Saidj

Energy Audit of an Enterprise from Machine Industry Process / Pages: 78-84

Slav Valchev, Ana Semerdzhieva, Stanislava Tasheva

Early Predictors of Cognitive Decline and Stroke Process / Pages: 85-89

Galya Atanasova

Basic Principles of Infection Control and Implementation Strategies Process / Pages: 90-96

Mehmet Erdem, Makhzuna Khamdamova, Mehmet Ozaslan

The Properties of Waste Cooking Oil Soap with Avocado Waste Extract as Filler Process / Pages: 97-106

Nisrina Zahira Putri Irawan, Heli Siti Halimatul Munawaroh, Sjaeful Anwar

Cluster Analysis of Sleep Health and Lifestyle Data Using Ward Algorithm and Euclidean Distance Process / Pages: 107-113

Mawar Idah Shonia, Noorma Yulia Megawati, Gunardi Gunardi, Asrul Khasanah

The Impact of Climate Change on the Morphology of Marine Topography Using GNSS Process / Pages: 114-120

Sotiris Lycourghiotis, Elizabeth Paraskevi Crawford

Research into Alternative Resources to Improve Animal Feed: The Case of Azolla Process / Pages: 121-128

Mouhous Azedine, Amina Ait - Allaoua, Lisa Chettouh, Nadir Semsoum, Nassima Zirmi - Zembri, Zahia Dorbane, Dyhia Saidj, Hocine Guermah, Farid Djellal, Rabia Cherfouh, Ali Bouzourene, Si Ammar Kadi

The Eurasia Proceedings of Science, Technology, Engineering & Mathematics (EPSTEM), 2024

Volume 30, Pages 1-8

ICBAST 2024: International Conference on Basic Sciences and Technology

On the Finite Element Modeling of Metal/Ceramic Functionally Graded Beams Subjected to Non-Uniform Static Bending

Abdelmadjid Si-Salem

Mouloud Mammeri University of Tizi Ouzou

Baya Allala

Mouloud Mammeri University of Tizi Ouzou

Souad Ait-Taleb

Mouloud Mammeri University of Tizi Ouzou

Fatma Kheloui-Taouche

Mouloud Mammeri University of Tizi Ouzou

Soraya Ferhat

Mouloud Mammeri University of Tizi Ouzou

Abstract: Currently, several approaches focused on the optimization of materials design and solutions to respond to the ecological and economic concerns through the development of novel materials and structures. In this connection, functionally graded materials (FGM) known as a new generation of composites with optimized mechanical properties which vary according to a continuous function-law to avoid interfacial debonding and stresses concentration were largely investigated. Accordingly, the main purpose of this work is to advocate a new way to simulate the mechanical behavior of simply supported FGM beams submitted to non-uniform static bending through a finite element modeling (FEM). The power-law function which governs the stiffness distribution of the used metal and ceramic materials are explicitly presented. In addition, a mesh sensitivity was established to assess the optimal mesh size of the modeled FGM based-beams. The simulation outcomes presented in the form stress and strain cartographies were correlated with a good agreement to the analytical results from the literature in term of qualitative and quantitative validations.

Keywords: Composite based-beams, FGM, Non-uniform bending, FEM simulations, Elastic behavior.

Introduction

Specific applications and environmental conditions lead manufacturers to choose a new material that guarantees economy, performance and extended service life (Bouzeboudja & Salem, 2023; Si Salem et al., 2022). Researchers are mostly applied to optimize solutions of already existing materials (Ait Taleb et al., 2022; Ali Ahmed et al., 2022). However, in some cases scientific were leaded to develop and design completely new materials (Bagheri et al., 2023; Medjmadj et al., 2022). Consequently, functional gradient materials (FGMs) were appeared as a novel generation of composite materials with optimized mechanical and physical properties which transit according to a gradually continuous function law through the material thickness (Medjmadj et al., 2023; Shinde & Sayyad, 2022).

Regarding the experimental and manufacturing difficulties, FGMs based-structures have been deeply investigated in the literature using analytical formulation (Do & Lee, 2018; Garg et al., 2021; Katili & Katili, 2020). Accordingly, Medjmadj et al. (2023) introduced a theoretical approach to predict the flexural response of functionally graded beams validated using microscopic images and experimental observations. In addition,

- This is an Open Access article distributed under the terms of the Creative Commons Attribution-Noncommercial 4.0 Unported License, permitting all non-commercial use, distribution, and reproduction in any medium, provided the original work is properly cited.

- Selection and peer-review under responsibility of the Organizing Committee of the Conference

© 2024 Published by ISRES Publishing: www.isres.org

Katili & Katili (2020) proposed a novel beam element based on two-node approach by using the first-order deformation model applied on FGM based-beams. By using analytical and numerical methods, Vo et al. (2014) focused the post-elastic behavior of a fully composited beam with metal facesheets under tangential loading. Based on the discrete shear projection approach Katili et al. (2023) studied the buckling of functionally graded material multilayer structures by means of quadrilateral elements.

However, these analytical resolution methods lead to an underestimation of the exact response of such structures under loading. To overcome these convergence problems, simulation procedures using finite elements approaches were investigated in the literature (Do & Lee, 2018; Jongpradist et al., 2024; Sharma and Singh 2021). In this regards, Sharma & Singh (2021) used the explicit differential quadrature technique to simulate the features functionally graded beams with various boundary conditions. The authors outcomes were validated on the basis of several mathematical approaches issued form the open literature. In addition, Sadowski et al. (2015) presented several numerical models of FGM structural parts using finite element analysis and the mechanical response were confronted with previously advocated simplified analytical model. Chaker et al. (2021) established a numerical model able to solve the convergence problems due to the finite elements meshes of solid and shell members.

According to the above literature review, the numerical investigations on the flexural behavior of FGM based-beam using 3D simulations were few. In this connection, the aim of this work is to highlight the mechanical behavior of simply supported FGM based-beams loaded under uniform and no uniform bending, using fully 3D simulations on the basis on finite elements analysis. The originality of this work is to propose a numerical approach to resolve the differential equation governing the bending response of FGM beams, while considering the impacts of shear and buckling. Consequently, 3D modeling based on the finite element method is carried out on ABAQUS and validated by using previously published theoretical and numerical works. In order to demonstrate the effectiveness of the model in terms of strength and deformability prediction, results in terms of deflections, strains and normal/shear stress are highlighted and deeply discussed.

Problem Formulation

In order to develop a reliable numerical procedure, the analytically studied and designed functionally graded materials based-beam by (Katili & Katili, 2020) was simulated in the present investigation. The beam was made of a metal phase in the flexural zone with is functionally graded to reach a ceramic phase in the beam's top compressive zone, as shown in Figure. 1. Rectangular Timoshenko beam with L length was modeled, with a beam non-dimensional width $b = 1$ and $L/h=16$ ratio to represent performance in thin problems. It is important to notice that the two materials phases are entirely continuous without any bonding interface and slip behavior.

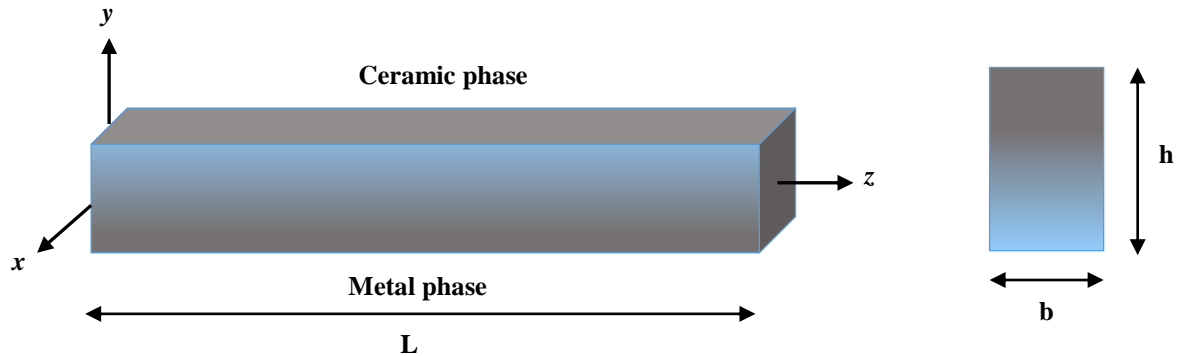


Figure 1. Geometric features of the simulated and modeled FGM based-beam.

The stiffens $E(y)$ and density $d(y)$ variation through the beam thickness was largely modeled in the literature using the power law functions in Equation. 1 and 2 respectively. Nevertheless, the Poisson's ratio is considered not varying according to the FGM beam height.

$$E(y) = E_c + \left(\frac{y}{h} + \frac{1}{2}\right)^p (E_m - E_c) \quad (1)$$

$$d(y) = d_c + \left(\frac{y}{h} + \frac{1}{2}\right)^p (d_m - d_c) \quad (2)$$

In which E_m and d_m are correspondingly the Elastic modulus and the relative-density of the metal phase. While E_c and d_c are separately the Elastic modulus and the density of the ceramic phase, the p -parameter governs the functionally transition from the metal to the ceramic phases. When p - tends to null value, the beam is full metal rich-composition. The full ceramic rich-composition was reached when high p -values were considered. The elastic behavior of the such FGM based-beams was generally evaluated using analytical approaches, such as high-order beam theories, which is based on many assumptions (Ait Taleb et al., 2017; Ait Taleb et al., 2020; Taleb et al., 2015). In this respect, a new three-dimensional numerical-way to model the power law function of the Equation 1 and 2 using finite element simulations in the below sections.

Simulation Procedure

Full 3D simulations and modeling were conducted on simply supported FGM based-beams using ABAQUS as used by Djenad et al (2022); Djenad et al. (2023); Salem et al.(2015); Taleb et al.(2015). The different steps followed in the modeling, starting from the geometric conditions creation to the results extraction are listed in the below section:

Geometry, Boundaries and Materials

The geometric model and the adoption of finite element models for the mesh are generated in three-dimensional (3D) space, while taking into account the actual behavior of the constituent material. Rectangular Timoshenko beam with non-dimensional span and unit width was simulated. While, $L/h=16$ was considered to represent performance in thin problems as studied by Katili & Katili (2020); Nguyen et al. (2013) and validated by Katili et al. (2020); Vo et al. (2014). It is significant to clarify that the two materials phases are modeled to be continuous without any bonding interface and tangential behavior during the transition.

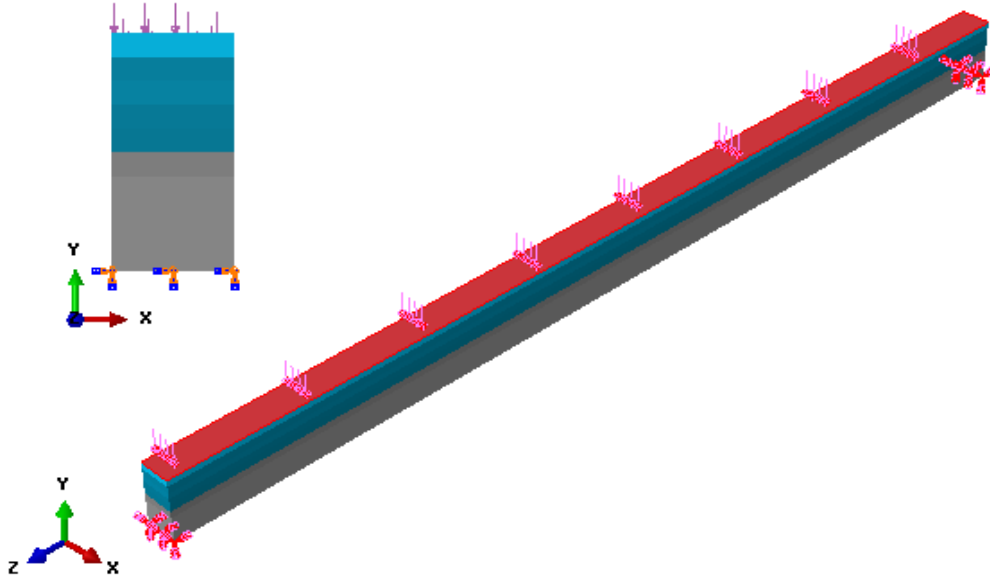


Figure 2. Geometric and boundaries conditions of the modeled FGM based-beam

The frontiers conditions and the loading configuration in the present simulations were correspondingly to the theoretical models of (Katili & Katili, 2020). In order to ensure the boundary conditions and the non-uniform bending load, reference points were assigned to analytical-rigid shells located on the at the position $z = 0$ and $z = L$. The interface among the reference points and the beam was ensured by the rigid body constraint of (ABAQUS, 2014) which may allocate regularly the support to all nodes of the modeled FGM based-beam depicted in Figure. 2. The rotations and axial displacement of the right reference point were allowed, while, the vertical translations in the direction of the Y axis was restrained. The general static step was assumed to prevent to convergence problems. The fully-static analysis method was implemented with tiny loading increments with a smooth-step way. The loading was applied on the ceramic phase surface as illustrated in Figure. 2

The numerical analysis is carried out on a ceramic-metal phases constituting a graded beam submitted to a non-uniformly scattered bending load. Considered materials are metal at the bottom surface of the beam with Young

modulus $E_m = 70$ GPa, density $\rho_m = 2702$ kg/cm³ and poisson's ratio $\nu_m = 0.3$. The ceramic phase of the top beam surface was modeled with: Young modulus $E_c = 200$ GPa, density $\rho_c = 3960$ kg/cm³ and poisson's ratio $\nu_c = 0.3$. Several configuration of the functional degradation were considered according to the p-parameter values, as depicted in Figure 3, which illustrates the variation of the bema stiffness through the thickness. In addition, full rich ceramic and metal beam were also modeled.

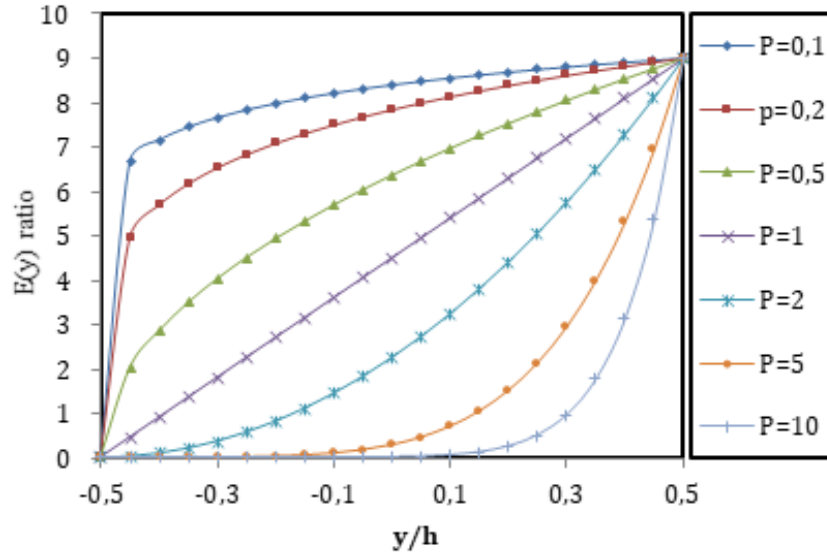


Figure 3. Evolution of the stiffness according to the FGM based-beam thickness.

Finite Elements and Stability

Hexahedral elements with first-order linear shape functions and 8 nodes were used to mesh the beam. These 3D HEX8, ABAQUS elements C3D8 are very efficient for linear geometry and offer the possibility of reduced integration (Djenad, et al., 2023; Si Salem et al., 2017). It gives also the ability to mesh the same part differently to highlight the most deformable surfaces. A mesh sensitivity study has been carried out for the beam, in order to define the optimum size of finite elements to best converge towards the exact solution. To this end, a comparative study was carried out with various dimensions, namely: 20 mm, 15 mm, 10 mm, 8 mm, 6 mm, 4mm, 2mm, 1mm and 0.5mm. Observation shows that the curves of the Figure 4 stabilized with a quasi-constant displacement at an approximately 10 mm value. As a result, the beam is meshed with 5mm finite elements in all three spatial directions, providing a highly refined mesh.

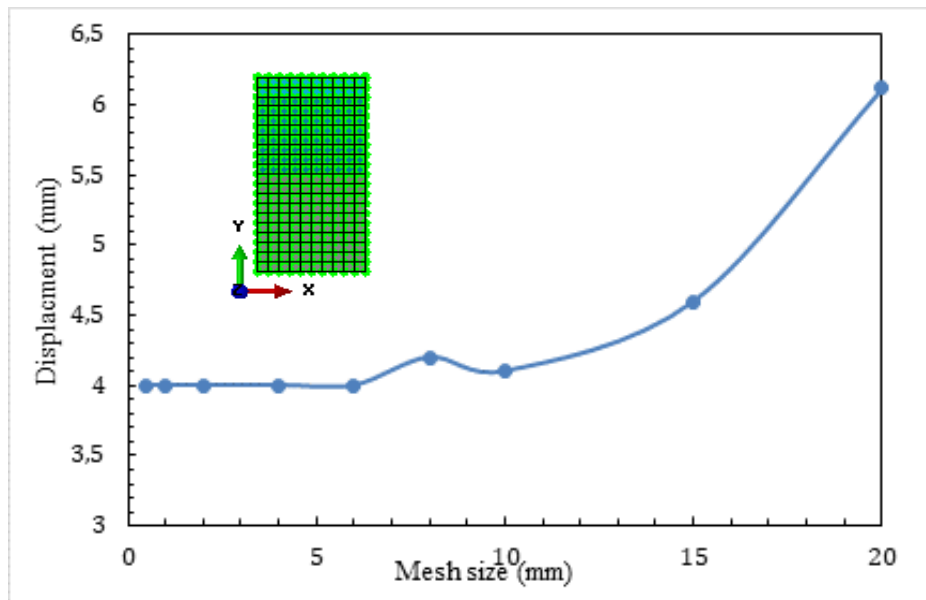


Figure 4. Mesh stability curve of the used C3D8 FE elements.

Numerical Outcomes

In this section, the obtained results from the numerical simulations carried out on the mechanical behavior of the FGM based-beams under bending were presented and interpreted. In this respect, all the findings and results in terms of displacements and stresses under mechanical loading are quantitatively and qualitatively discussed.

FEM Validation

The numerical procedure and the proposed finite element model are validated using analytical results issued from the literature review is carried out. Accordingly, a comparison between the present study results and the theoretical model is done in Figure 5.

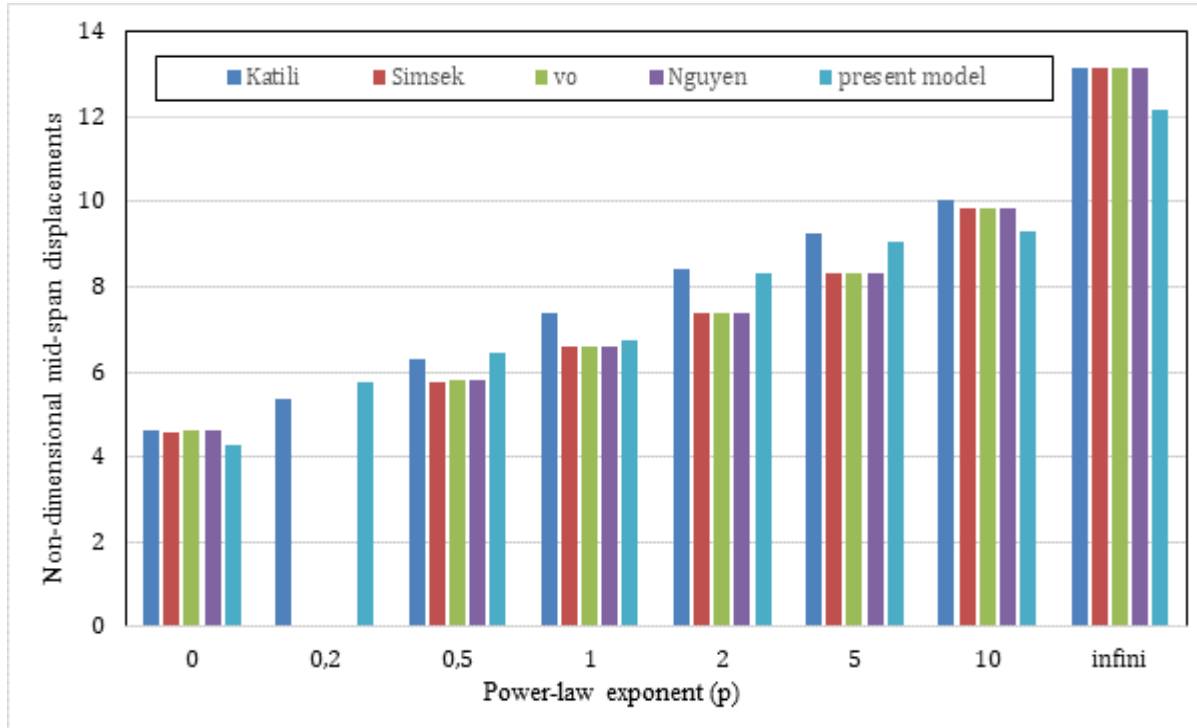


Figure 5. Histogram of non-dimensional mid span deflections comparison.

The obtained results in Table 1 and Figure 5 reveal a good agreement between the present numerical approach and analytical ones in terms of the general behavior of the FGM beams below flexural loading. Analysis of these results shows that displacement increases proportionally with the material p-parameter. The maximum error of the proposed model is less than 1% in all cases, validating the numerical models developed to predict the response of FGM beams under static bending. Physically this error is due to the perfect conditions of the analytical formulation in terms of geometric and loading values.

Mid-Span Deflections Evolution

The FGM beam non-dimensional displacements under mechanical loading for various p-parameters according to the z/L ratio are shown in Figure 6. From these curves, one can conclude that the displacement increases with the material p-parameter, and the ultimate value was reached at the beam mid-span. As the p-value increases, the transition from the ceramic to the metallic phase becomes higher, giving the FGM beam low stiffness which leads to high displacement values. In terms of qualitative observation, the cartographies of displacement evolution through the functionally graded material based-beam are shown in Figure 7.

From the mappings, it is observed that the maximum displacement for all cases of p-parameters appears at the beam mid-span, then propagates respectively towards the simply-supports, the displacement value was null at the supports. The displacement is greater for full-ceramic beams corresponding to $p = \text{infinite}$ with 12.216 mm, compared to one of the full-metal beams ($p=0$) with 4.257 mm. This is due to the influence of the Young's

modulus, which is higher for the ceramic phase than for the metal one. Based on the obtained outcomes in terms of displacement, it can be concluded that the suggested model is capable to predict the response of FGM beams.

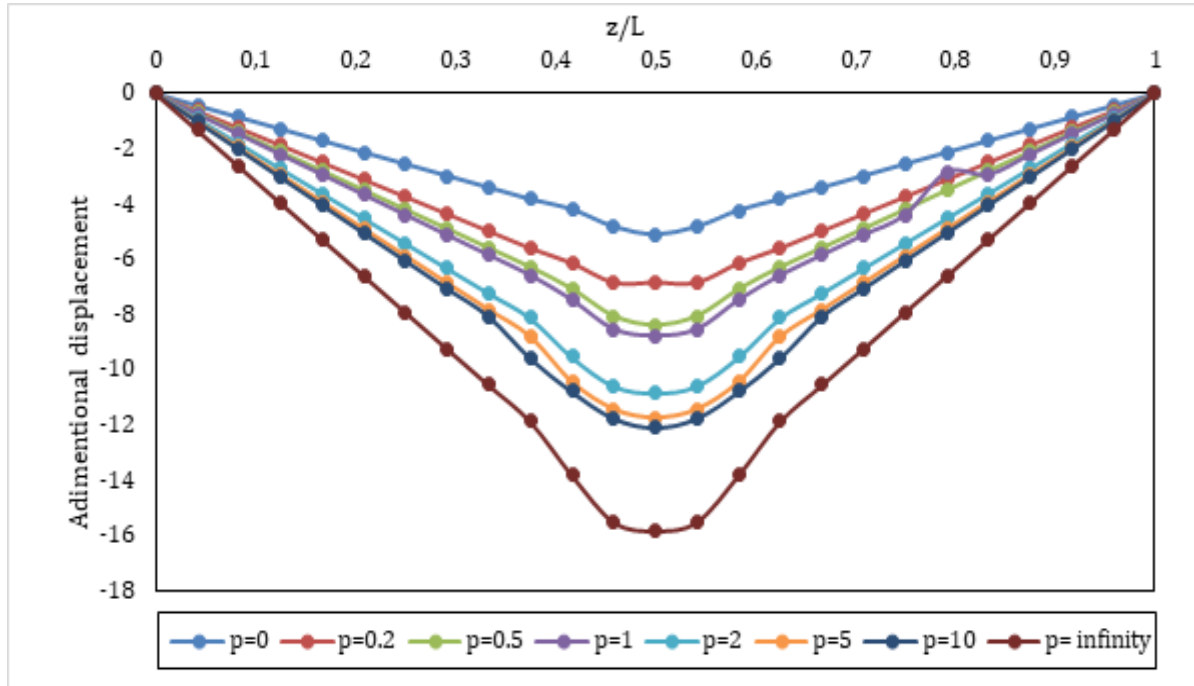


Figure 6. Non-dimensional deflections according to the beam span.

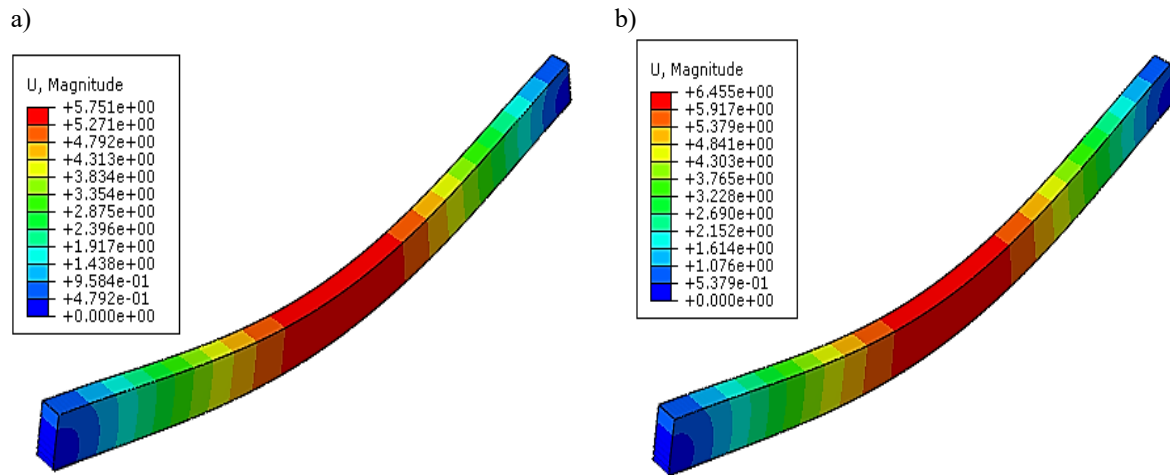


Figure 7. Cartography maps of non-dimensional deflections according to the beam span: a) $p = 0.2$; b) $p = 0.5$

Conclusion

In this work, a numerical approach is developed under FEM ABAQUS code to propose and validate a model susceptible to resolve the behavior governed by the power law function of FGM based-beams under non-uniform bending. Consequently, the various achieved outcomes enabled us to list the below conclusions:

- The established numerical model predicts with a satisfactory agreement the mid-span displacements of the FGM based-beam, through confrontation with analytical models available in the scientific literature;
- By increasing the p -parameter value of the power law function, great degradation from the ceramic matrix to the metal core is observed., which confers to the FGM beam low stiffness and accordingly large displacements;
- As the power-law exponent p -value decreases, the functionally degradation tends to a smooth transition from the ceramic phase to the metal matrix, conferring to the FGM beam low strengths and stresses;

Recommendations

The critical analysis of the obtained outcomes allowed us to identify future aspects for improving and overcoming the limitations of the present work. Indeed, the further perspectives should be formulated to take into account the effect of material porosity when evaluating the stiffness of the FGM based-beam.

Scientific Ethics Declaration

The authors declare that the scientific ethical and legal responsibility of this article published in EPSTEM Journal belongs to the authors.

Acknowledgements or Notes

* This article was presented as a poster presentation at the International Conference on Basic Sciences and Technology (www.icbast.net) held in Antalya/Turkey on November 14-17, 2024.

References

- Ait Taleb, S., Si Salem, A., & Ait tahar, K. (2017). Behaviour of a new graded beam reinforced with externally bonded composite sheets: theoretical and experimental studies. *European Journal of Environmental and Civil Engineering*, 21(9), 1171-1185.
- Ait Taleb, S., Si Salem, A., & Ait Tahar, K. (2020). Experimental and theoretical modeling coupled to a reliability approach for flexural failure prediction in hybrid composite beams. *Asian Journal of Civil Engineering*, 21(3), 495-504.
- Ali Ahmed, C., Si Salem, A., Ait Taleb, S., & Ait Tahar, K. (2024). Experimental behavior and reliability of predamaged concrete columns externally repaired with FRP spiral strips under axial compression. *World Journal of Engineering*, 21(1), 115-126.
- Bagheri, H., Kiani, Y., & Eslami, M. R. (2023). Geometrically nonlinear response of FGM beams on elastic foundation subjected to thermal shock. *Iranian Journal of Science and Technology, Transactions of Mechanical Engineering*, 47(1), 187-201.
- Bouzeboudja, F., & Si Salem, A. (2023). Experimental investigation on flexural behavior of textile-reinforced concrete: effect of reinforcement type and dune sand addition. *World Journal of Engineering*, 1-16
- Chaker, A., Koubaa, S., Mars, J., Vivet, A., & Dammak, F. (2021). An efficient ABAQUS solid shell element implementation for low velocity impact analysis of FGM plates. *Engineering with Computers*, 37, 2145-2157.
- Djenad, S., Taleb, S. A., Salem, A. S., & Bouzidi, M. A. (2022). NLFEA based design optimization of GFRP strips in partially confined concrete. *Procedia Structural Integrity*, 37, 321-329.
- Djenad, S., Ait Taleb, S., & Si Salem, A. (2023). Finite element modeling of partially-confined concrete and RC columns with embedded hexagonal-FRP strips under axial and horizontal loading. *Structures* 54: 369–85.
- Garg, A., Belarbi, M. O., Chalak, H. D., & Chakrabarti, A. (2021). A review of the analysis of sandwich FGM structures. *Composite Structures*, 258, 113427.
- Jongpradist, P., Tongthong, S., Kongwat, S., Ruangjirakit, K., Thongchom, C., & Hasegawa, H. (2024, January). Optimizing functionally graded hexagonal crash boxes with honeycomb filler for enhanced crashworthiness. *Structures*, 59, 105775.
- Katili, A. M., & Katili, I. (2020). A simplified UI element using third-order Hermitian displacement field for static and free vibration analysis of FGM beam. *Composite Structures*, 250, 112565.
- Katili, I., Batoz, J. L., Bouabdallah, S., Maknun, I. J., & Katili, A. M. (2023). Discrete shear projection method for mechanical buckling analysis of FGM sandwich plates. *Composite Structures*, 312, 116825.
- Katili, I., Syahril, T., & Katili, A. M. (2020). Static and free vibration analysis of FGM beam based on unified and integrated of Timoshenko's theory. *Composite Structures*, 242, 112130.
- Li, L., Nie, L., & Ren, Y. (2024). Low-velocity impact response of the post-buckled FG-MEE plate resting on visco-Pasternak foundation: Magneto-electro-mechanical effects-based interaction analysis. *Composite Structures*, 331, 117869.
- Liang, Y., Zheng, S., Wang, H., & Chen, D. (2024). Nonlinear isogeometric analysis of axially functionally graded graphene platelet-reinforced composite curved beams. *Composite Structures*, 330, 117871.

- Medjmadj, S., Ait Taleb, S., & Si Salem, A. (2024). Analytical modeling of the bending behavior of plaster/cork functionally graded core sandwich beams: analysis and experimental validation. *Iranian Journal of Science and Technology, Transactions of Mechanical Engineering*, 48(3), 1489-1507.
- Nguyen, T. K., Vo, T. P., & Thai, H. T. (2013). Static and free vibration of axially loaded functionally graded beams based on the first-order shear deformation theory. *Composites Part B: Engineering*, 55, 147-157.
- Sadowski, T., Birsan, M., & Pietras, D. (2015). Multilayered and FGM structural elements under mechanical and thermal loads. Part I: Comparison of finite elements and analytical models. *Archives of Civil and Mechanical Engineering*, 15(4), 1180-1192.
- Salem, A. S., & Taleb, S. A. (2015). Static and dynamic behavior of composite concrete-based beams with embedded Polymer/FRP Components. *Procedia Engineering*, 114, 173-180.
- Sharma, P., & Singh, R. (2021). A numerical study on free vibration analysis of axial FGM beam. *Materials Today: Proceedings*, 44, 1664-1668.
- Shinde, B. M., & Sayyad, A. S. (2022). A new higher order shear and normal deformation theory for FGM sandwich shells. *Composite Structures*, 280, 114865.
- Si Salem, A., Ait Taleb, S., & Ait Tahar, K. (2017). A finite element approach for predicting the flexural response of light weight FRP-concrete beams under cyclic loading. In *Applied Mechanics, Behavior of Materials, and Engineering Systems: Selected contributions to the 5th Algerian Congress of Mechanics, CAM2015, El-Oued, Algeria, October 25–29* (pp. 355-363). Springer International Publishing.
- Salem, A. S., Djenad, S., & Taleb, S. A. (2022). Experimental Axial Compressive Behavior of Partially Confined Concrete Columns with Combined External and Internal FRP Strips. *The Eurasia Proceedings of Science Technology Engineering and Mathematics*, 21, 356-362.
- Şimşek, M. (2009). Static analysis of a functionally graded beam under a uniformly distributed load by Ritz method. *International Journal of Engineering and Applied Sciences*, 1(3), 1-11.
- Taleb, S. A., & Salem, A. S. (2015). Bending and shear behavior of a composite beam strengthened and double-confined with FRP-jacket. *Procedia Engineering*, 114, 165-172.
- Taleb, S. A., Medjmadj, S., & Salem, A. S. (2022). Modeling the nonlinear behavior of predamaged reinforced concrete beams retrofitted with bonded and jacketed frp sheets. *The Eurasia Proceedings of Science Technology Engineering and Mathematics*, 21, 288-294.
- Van Do, V. N., & Lee, C. H. (2018). Numerical investigation on post-buckling behavior of FGM sandwich plates subjected to in-plane mechanical compression. *Ocean Engineering*, 170, 20-42.
- Vo, T. P., Thai, H. T., Nguyen, T. K., & Inam, F. (2014). Static and vibration analysis of functionally graded beams using refined shear deformation theory. *Meccanica*, 49, 155-168.

Author Information

Abdelmadjid Si Salem

University Mouloud Mammeri of Tizi Ouzou
Tizi Ouzou, 15000, Algeria
Contact e-mail: abdelmadjid.sisalem@ummto.dz

Baya Allala

University Mouloud Mammeri of Tizi Ouzou
Tizi Ouzou, 15000, Algeria

Souad Ait-Taleb

University Mouloud Mammeri of Tizi Ouzou
Tizi Ouzou, 15000, Algeria

Fatma Kheloui-Taouche

University Mouloud Mammeri of Tizi Ouzou
Tizi Ouzou, 15000, Algeria

Soraya Ferhat

University Mouloud Mammeri of Tizi Ouzou
Tizi Ouzou, 15000, Algeria

To cite this article:

Si-Salem, A., Allala, B., Ait-Taleb, S., Kheloui-Taouche, F., & Ferhat, S. (2024). On the finite element modeling of metal/ceramic functionally graded beams subjected to non-uniform static bending. *The Eurasia Proceedings of Science, Technology, Engineering & Mathematics (EPSTEM)*, 30, 1-8.

The Eurasia Proceedings of Science, Technology, Engineering & Mathematics (EPSTEM), 2024

Volume 30, Pages 9-16

ICBAST 2024: International Conference on Basic Sciences and Technology

Construction of an Integral Distribution Function of Random Variables Determining the Impact of Wind Power Plant on Birds in accordance with the Predictive Analysis by Experts

Vladimir Yeremeev
Melitopol State University

Andrey Naidysh
Melitopol State University

Oksana Stokan
Melitopol State University

Abstract: The team of scientists led by ornithologist V. D. Siokhin proposed a method for predicting the impact of planned wind power plants (WPP) on avifauna using expert assessment. The method for modeling the differential $p(x)$ and integral $F(x)$ distribution functions of the sum of several random variables with distribution densities $p_1(x_1), p_2(x_2), p_3(x_3), \dots$, determining the probability of bird interaction on the territory of a wind farm and adjacent buffer zones is developed in this article. The function $p(x)$, which is a convolution of $p_1(x_1), p_2(x_2), p_3(x_3), \dots$, is represented as an improper integral with infinite limits. An algorithm for calculating $p(x)$ and $F(x)$ is proposed by replacing an improper integral with an integral having finite limits and subsequent numerical integration taking into account the specified accuracy. Testing of the method for calculating the functions $p(x)$ and $F(x)$ was carried out on two examples with known solutions. One of the tests was carried out on two differential functions of distribution subjecting the normal law with mathematical expectations a_1 and a_2 , and variances σ_1^2 and σ_2^2 . It is known that the distribution of such a sum obeys the normal law with mathematical expectation a equal to the sum of a_1 and a_2 , and variance σ^2 equal to the sum of σ_1^2 and σ_2^2 . The results of calculations of the functions $p(x)$ and $F(x)$ using numerical methods for the number of nodes of 100 and more coincide with known solutions with an error of 10^{-15} , which indicates the high accuracy of the proposed method. The found integral distribution function allows us to determine the probability characteristics of the impact of wind farms on birds.

Keywords: Integration, Mathematical statistics, Numerical method, Random variable distribution function.

Introduction

The team of scientists led by ornithologist V.D. Siokhin proposed a method for predicting the impact of planned wind power plants (WPP) on avifauna using expert assessment. The theory of distribution of a system of random variables given by a vector $(\alpha_1, \alpha_2, \dots, \alpha_n)$ on Borel sets B_1, B_2, \dots, B_n from $B(-\infty, +\infty)$ is described in many monographs and textbooks (Gnedenko & Kolmogorov, 1949; Kremer, 2004; Gmurman, 1999; Samarova, n.d.). A system of random variables defining a random vector $(\alpha_1, \alpha_2, \dots, \alpha_n)$ when the condition is met

$$P(\alpha_1 \in B_1, \alpha_2 \in B_2, \dots, \alpha_n \in B_n) = P(\alpha_1 \in B_1) \cdot P(\alpha_2 \in B_2) \cdot \dots \cdot P(\alpha_n \in B_n), \quad (1)$$

it is called independent in aggregate.

The distribution function of a random vector $(\alpha_1, \alpha_2, \dots, \alpha_n)$ in the space of n variables $(x_1, x_2, \dots, x_n) \in R^n$ is determined by equality

$$F_{\alpha_1, \alpha_2, \dots, \alpha_n}(x_1, x_2, \dots, x_n) = P(\alpha_1 \leq x_1, \alpha_2 \leq x_2, \dots, \alpha_n \leq x_n) \quad (2)$$

For a continuous random vector, there is a non-negative function $p_{\alpha_1, \alpha_2, \dots, \alpha_n}(x_1, x_2, \dots, x_n)$, which is called the distribution density, that for any Borel set $B \in (R^n)$ ensures the following equality

$$P\{(\alpha_1, \alpha_2, \dots, \alpha_n) \in B\} = \int_B p_{\alpha_1, \alpha_2, \dots, \alpha_n}(x_1, x_2, \dots, x_n) dx_1 dx_2, \dots, dx_n. \quad (3)$$

The distribution function for any random vector is determined by multidimensional integrals

$$F_{\alpha_1, \alpha_2, \dots, \alpha_n}(x_1, x_2, \dots, x_n) = \int_{-\infty}^{x_1} \dots \int_{-\infty}^{x_n} p_{\alpha_1, \alpha_2, \dots, \alpha_n}(x_1, x_2, \dots, x_n) dx_1 dx_2, \dots, dx_n. \quad (4)$$

The multidimensional integral of the distribution density over the entire area of its definition is equal to one:

$$\int_{-\infty}^{\infty} \dots \int_{-\infty}^{\infty} p_{\alpha_1, \alpha_2, \dots, \alpha_n}(x_1, x_2, \dots, x_n) dx_1 dx_2, \dots, dx_n = 1. \quad (5)$$

Formulas (3)-(5) can be used to find the distribution function of the sum of random variables. In most cases, taking integrals in an analytical form is not possible and finding the vector (2) is reduced to numerical modeling of the true distribution law. Therefore, the analysis of calculation methods is an urgent task.

Method

Analysis of Recent Research and Publications

The integral $F_{ak}(x)$ and differential $p_{ak}(x)$ functions for the one-dimensional distribution of random variables, which are a special case of the multidimensional distribution (4), have the form

$$F_{\alpha_k}(x) = \int_{-\infty}^x p_{\alpha_k}(x) dx_k. \quad (6)$$

$$p_{\alpha_k}(x) = \int_{-\infty}^x \left(\int_{-\infty}^{+\infty} \dots \int_{-\infty}^{+\infty} p_{\alpha_1, \alpha_2, \dots, \alpha_n}(x_1, x_2, \dots, x_n) dx_1 \dots dx_{k-1} dx_{k+1} \dots dx_n \right) dx_k. \quad (7)$$

A large number of publications (Tregubova & Hartov, 2022; Rozovsky, 2022; Ganin & Polenin, 2015) have been devoted to the distribution of the sum of continuous random variables. It can be obtained from formulas (6), (7). Let us consider two independent random variables α_1, α_2 with distribution densities $p_{a1}(x_1), p_{a2}(x_2)$. The differential distribution function of the sum $\alpha = \alpha_1 + \alpha_2$ according to (7) is determined by the formula (Samarova, n.d)

$$p_{\alpha}(x) = \int_{-\infty}^{+\infty} p_{\alpha_1}(x_1) p_{\alpha_2}(x - x_1) dx_1, \quad (8)$$

which is actually a convolution of two functions $p_{a1}(x_1), p_{a2}(x_2)$.

According to definition (6), the integral distribution function for the sum of two random variables α_1 and α_2 has the form

$$F_{\alpha}(x) = P(\alpha = \alpha_1 + \alpha_2 \leq x) = \int_{-\infty}^x p_{\alpha}(x) dx. \quad (9)$$

The differential distribution function (8) can be easily generalized to the case of the sum of three or more random variables.

Example. Let the random variable U be equal to the sum of three independent random variables $U = \alpha_1 + \alpha_2 + \alpha_3$ with known distribution densities $p_{\alpha 1}(x_1)$, $p_{\alpha 2}(x_2)$, $p_{\alpha 3}(x_3)$. Since the differential distribution function of the sum of two random variables $\alpha_1 + \alpha_2$ is determined by formula (9), then the integral

$$p_{\alpha}(u) = \int_{-\infty}^{+\infty} \left(\int_{-\infty}^{+\infty} p_{\alpha_1}(x_1) p_{\alpha_2}(t - x_1) dx_1 \right) p_{\alpha_3}(u - t) dt; u, t, x_1 \in [-\infty, +\infty]. \quad (10)$$

determines the distribution density of the sum of three random variables $\alpha_1 + \alpha_2 + \alpha_3$.

Formulas (6)-(10) allow us to construct a numerical model for the integral and differential distribution functions of the sum of random variables in the space of n variables $(x_1, x_2, \dots, x_n) \in R^n$.

The Purpose of the Work and the Task Statement

The purpose of the research is to develop an algorithm for numerical modeling of distribution functions of the sum of random variables. To achieve the goal, it is necessary to solve the following tasks: to analyze numerical methods for calculating improper integrals; to select an algorithm for calculating integrals of type (8)-(10) and estimate its error in calculating the integral and differential distribution functions of the sum of random variables.

Results and Discussion

Let's consider an algorithm for calculating improper integrals of type (8)-(10) by numerical method. The first step involves converting them into certain integrals with a given accuracy.

As an example, we replace the integral (9) with its approximate value $\int_a^x p_{\alpha}(x) dx$, $x \in [a, b]$ ensuring an error of no more than α for all x on the segment $[a, b]$:

$$\left| \int_a^x p_{\alpha}(x) dx - \int_{-\infty}^x p_{\alpha}(x) dx \right| < \alpha; x \in [a, b]. \quad (11)$$

The exact value of the first definite integral in condition (11) can be represented as an integral sum [10]:

$$\int_a^x p_{\alpha}(x) dx = S = \sum_{i=1}^n p_{\alpha}(x_i^*) h_i, x \in [a, b], \quad (12)$$

where $p_{\alpha}(x_i^*)$ is the value of the integrand function at the point x_i^* belonging to the i interval h_i , $\sum h_i = b - a$.

Since the value of $F(x)$ belongs to the segment $[0, 1]$, the value of the integral sum at $x = b$ must correspond the condition:

$$|1 - S| < \alpha. \quad (13)$$

The definition of an improper integral (12) is reduced to the calculation of the integral sum S . The accuracy of the calculation results depends on the correctness of replacing the infinite limits with finite values and the error

in calculating the integral sum. One of the most common ways to calculate a certain integral is based on the use of Newton–Cotes quadrature formulas («Methods of numerical integration», n.d.).

The simplest quadrature formulas are implemented in the methods of trapezoids («Numerical methods of calculating the definite integral», n.d.), left, right and middle rectangles («Method of rectangles», n.d.) and parabolas («Numerical methods of calculating the definite integral», n.d.). These methods are widely used in the educational process and in solving many applied problems. In case of the method of average rectangles with a constant step $h_i=h$ the integral sum S in formula (12) is represented as

$$S \approx S^* = h \sum_{i=1}^{i=n} p(x_i + h/2). \quad (14)$$

The use of formula (14) provides an error of no more than (Fikhtenholtz, 1969):

$$\varepsilon = n | p''(x^*) | h^3 / 24 \quad (15)$$

where n – is the number of intervals, $nh=b-a$, $\varepsilon=p''(x^*)$ - is the maximum value of the second derivative function at the point $x^* \in [a, b]$.

The actual error turns out to be less than the value determined by the integral sum (15). It was shown in (Yeremeev, 2023) that its value, found for functions in the case of an absolute value of the second derivative of the order of one with the number of intervals $n=1000$, is about 10^{-8} , which is quite acceptable for numerical modeling of distribution functions of random variables. For large values of the second derivative, as well as when finding the distribution of the sum of several random variables, more accurate methods may be required, for example, Simpson or Gauss methods. Using a variable interval value can also significantly improve the accuracy. One of the simple ways to determine the h_{i+1} interval relates its length to the length of the previous h_i interval using the formula:

$$h_{i+1} = h_i | p'(t_i) / p'(t_{i+1}) | \quad (16)$$

where $p'(t_i)$ and $p'(t_{i+1})$ are the first derivatives at the nodes t_i and t_{i+1} .

The algorithm for numerical modeling of distribution functions of the sum of random variables is presented in the form of the following steps:

- replacement of an improper integral with a definite integral with finite integration limits to ensure a given accuracy,
- choice of a numerical integration method,
- testing a numerical model using well-known accurate methods for calculating distribution functions.

The testing was performed using two examples. Let two random variables α_1, α_2 with distribution densities be given

$$p_1(x) = \begin{cases} 0, & x < 0 \\ 0 \leq x \leq 1, \\ 0, & x > 1 \end{cases} \quad (17)$$

$$p_2(x) = \begin{cases} 0, & x < 0 \\ e^{-x}, & 0 \leq x < \infty. \end{cases} \quad (18)$$

Differential and integral distribution functions of the sum of two random variables defined by formulas (17), (18), (8), (9), have the form of:

$$p(x) = \begin{cases} 0, x < 0, \\ 1 - e^{-x}, x \in [0, 1], \\ e^{-x}(e - 1), x > 1. \end{cases} \quad (19)$$

$$F(x) = \begin{cases} 0, x < 0 \\ \int_0^x (1 - e^{-x}) dx = x + e^{-x} - 1, 0 \leq x \leq 1 \\ e^{-1} + \int_1^x e^{-x}(e - 1) dx = e^{-1} + (e - 1)(e^{-1} - e^{-x}), 1 \leq x < \infty. \end{cases} \quad (20)$$

The distribution function of the sum of two random variables (8), (9) was calculated in two ways: by the method of average rectangles, formula (14); using analytical formulas (19), (20).

The accuracy of presenting the results in the form of a numerical model for the distribution of the sum of random variables depends on the choice of the limits of integration of a certain integral $[a, b]$ and the method of calculating the integral sum. The largest error in calculating the function $p(x)$ is expected at $x=b$. The value of the distribution density $p(x)$ depending on b for $a=0$ and the number of intervals n from 10 to 104 is given in Table 1.

Table 1. The results of calculations

b	$b=5$	$b=10$	$b=15$	$b=20$
$n=10^2$	0,0115776	0,0000780	0,0000005	$<10^{-15}$
$n=10^3$	0,0115776	0,0000780	0,0000005	$<10^{-15}$
$n=10^4$	0,0115777	0,0000780	0,0000005	$<10^{-15}$

According to Table 1, fairly good results are achieved at $b \geq 5$ and the number of partitions $n \geq 10^2$, where the error is provided at the level of $5 \cdot 10^{-8}$ or less. Close accuracy is obtained when calculating the integral function. The second test was carried out using the example of the distribution of the sum of two random variables with a normal distribution. Let there be two normal distributions with mathematical expectations $a_1=0$, $a_2=3$ and standard deviations $\sigma_1=1$ and $\sigma_2=2$:

$$p_1(x_1) = \frac{1}{\sqrt{2\pi}} e^{-\frac{x_1^2}{2}}, p_2(x_2) = \frac{1}{2\sqrt{2\pi}} e^{-\frac{(x_2-3)^2}{8}}. \quad (21)$$

Figure 1 shows graphs of the distribution density for two functions $p_1(x_1)$, $p_2(x_2)$, corresponding to the normal law (21), and the distribution density $p(x)$ for the sum $x=x_1+x_2$, calculated using convolution (8) by the method of rectangles.

It is known (Lemons, 2003; «Sum of normally distributed random variables», n.d.) that the mathematical expectation a and the variance σ_2 of the sum of two random variables obeying the normal law are equal, respectively, to the sum of mathematical expectations and variances of its terms, i.e.: $a=a_1+a_2$, $\sigma_2=\sigma_{21}+\sigma_{22}$. Therefore, the distribution density of the sum of two random variables determined by formulas (21) has the form:

$$p(x) = \frac{1}{\sqrt{10\pi}} e^{-\frac{(x-3)^2}{10}}. \quad (22)$$

Calculations of the distribution density of the sum of two random variables $x=x_1+x_2$ in accordance with formula (22), and the same sum calculated using convolution (8) by the numerical method for the number of intervals $n=10$ differ only in the second significant digit. Increasing the number of intervals to $n=30$ ensures an accuracy of at least 10^{-10} (Table 2).

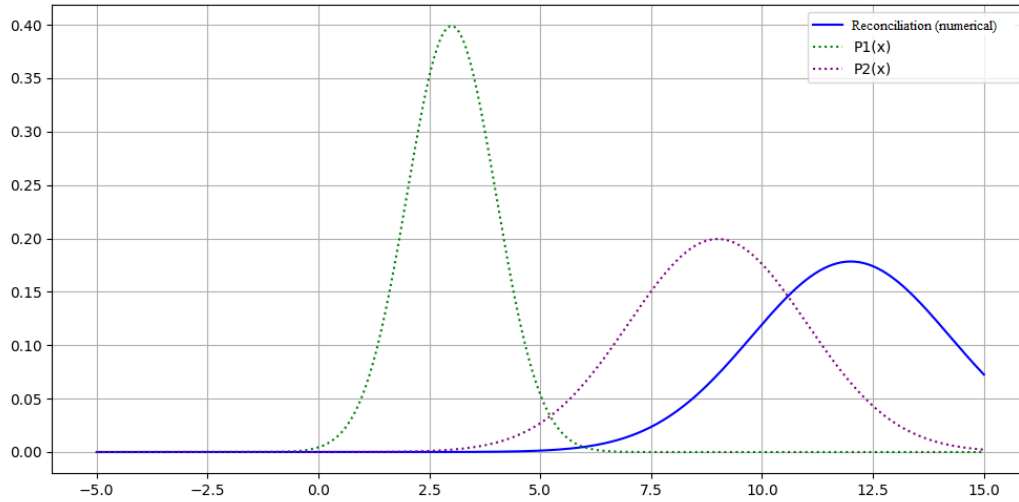


Figure 1. Distribution densities of the random numbers

Table 2. The results of calculating

x	3	6	9	12
$p(x)$, formula (8)	0.0000541551	0.0048748912	0.072537074	0.17841241
$p(x)$, $n=30$, convolution	0.0000541551	0.0048748912	0.072537074	0.17841241

With an increase in the number of intervals to 100, 1000, 10000, the accuracy of calculations increases to 10^{-15} - 10^{-19} . The integral distribution function of the random variable X for the normal law (22) is determined by the formula:

$$F(x) = \frac{1}{2}(1 + \Phi(t)), \quad (23)$$

where $t=(x-3)/\sqrt{5}$, $\Phi(t)$ - is the Laplace integral:

$$\Phi(t) = \frac{2}{\sqrt{2\pi}} \int_0^t e^{-\frac{t^2}{2}} dt.$$

Test calculations of the integral function for different values of n are given in Table 3.

Table 3. The results of calculating

x	3	6	9	12
Formula (23)	0,5000	0,9101	0,9963	1,0000
Formula (6), $n=30$	0,5053	0,9109	0,9965	0,9998
Formula (6), $n=100$	0,5016	0,9104	0,9964	0,9998
Formula (6), $n=300$	0,5005	0,9102	0,9964	0,9998
Formula (6), $n=1000$	0,5002	0,9102	0,9963	0,9998

According to the calculation results presented in Table 3, the error of the numerical method for determining the integral distribution function for the sum of two normally distributed random variables at $n = 30$ is about 10^{-3} . Increasing the number of intervals to $n = 1000$ reduces the error by an order to $2 \cdot 10^{-4}$. Based on the verification carried out (Tables 1-3, Figure 1), it can be argued that numerical modeling of the distribution function for the sum of several random variables provides a sufficiently high accuracy.

Conclusion

There it has been developed the method for determining the distribution functions of the sum of random variables by replacing an improper integral with an integral with finite integration limits and then choosing a

numerical integration method. The method was tested using the examples with two distribution densities $p_{a1}(x_1)$, $p_{a2}(x_2)$, for which the law of distribution of the sum of random variables $\alpha_1 + \alpha_2$ is known. In the first test, the distribution density $p_{a1}(x_1)$ corresponded to a uniform distribution on the interval $[0, 1]$, and $p_{a2}(x_2)$ to an exponential distribution on the half-interval $[0, +\infty)$. In the second test, we analyzed the sum of two differential distribution functions obeying the normal law. The accuracy of calculations of the distribution density of the sum of two random variables turned out to be about 10^{-15} . The accuracy of calculating the integral function was lower: in the first case, it was no worse than 10^{-7} , and in the second - about 10^{-4} . If necessary, the accuracy of calculations can be improved by optimizing the numerical algorithm, namely:

- the implementation of a more accurate method for calculating the integral sum,
- the use of a variable step, determined, for example, by the formula (16).

The found integral distribution function allows determining probabilistic characteristics of the impact of wind farms on birds that fly through them or adjacent buffer zones.

Recommendations

The obtained data can be used in applied mathematical statistics in the study of measurement error, the results of which depend on the action of several factors.

Scientific Ethics Declaration

The authors declare that the scientific ethical and legal responsibility of this article published in EPSTEM journal belongs to the authors.

Acknowledgements or Notes

* This article was presented as an oral presentation at the International Conference on Basic Sciences and Technology (www.icbast.net) held in Antalya/Turkey on November 14-17, 2024.

* The work was carried out under the state order FRRS-2023-0035 «Assessment of the state of seasonal ornithological complexes and transcontinental migrations at monitoring sites of the Azov-Black Sea region and Sivash, development of software for modeling and managing natural complexes».

References

- Fikhtengol'ts, G. M. (1969). Course of differential and integral calculus. *M.: Science*, 2, 153.
- Ganin, M.P., & Polenin, V.I. (2015). Distributions of sums of a random number of continuous random variables. *Scientific periodical, Ceteris Paribus. Phys.-Mat. Sciences*, 3.
- Gmurman, V.E. (199). *Probability theory*. Moscow: Higher School.
- Gnedenko, B.V., & Kolmogorov, A.N. (1949). *Limit distributions for sums of independent random variables*. Moscow: Fizmatgiz.
- ITMO University. (n.d). *Methods of numerical integration*. Retrieved from http://aco.ifmo.ru/el_books/numerical_methods/lectures/glava2.html.
- Kremer, N.S. (2004). *Probability theory and mathematical statistics*. Moscow: Izd. UNITI-Dana.
- Lemons, D. S., & Langevin, P. (2002). *An introduction to stochastic processes in physics*. JHU Press.
- Mathprofi. (n.d.). *Method of rectangles*. Retrieved from http://mathprofi.ru/metod_prjamougolnikov.html.
- Rozovsky, L.V. (2022). Large evasions of the sum of independent random variables whose distributions have rapidly decreasing tails. *Probability Theory and Its Applications*, 67(3), 456-470.
- Samarova, S.S. (n.d). *Joint distribution of random variables*. Retrieved from [https://old.mipt.ru/education/chair/mathematics/study/methods/%D0%A1%D0%A0%D0%A1%D0%92_%D0%A1%D0%B0%D0%BC%D0%BE%D1%80%D0%BE%D0%B2%D0%B0\(2\).pdf](https://old.mipt.ru/education/chair/mathematics/study/methods/%D0%A1%D0%A0%D0%A1%D0%92_%D0%A1%D0%B0%D0%BC%D0%BE%D1%80%D0%BE%D0%B2%D0%B0(2).pdf)
- Tomsk Polytechnic University. (n.d). *Numerical methods of calculating the definite integral*. Retrieved from https://portal.tpu.ru/SHARED/k/KRAYNOV/Study/Tab1/Tab2nd_task.pdf.

- Tregubova, K. A., & Khartov, A. A. (2022). Sums of independent random variables and the generalized Dickman laws. *Zapiski Nauchnykh Seminarov POMI*, 515, 199-213.
- Wikipedia. (n.d). *Sum of normally distributed random variables*. Retrieved from https://en.wikipedia.org/wiki/Sum_of_normally_distributed_random_variables.
- Yeremeev, V.S., Goncharov, A.Yu., & Nikulin. M.A. (2023, May 23). Comparative analysis of accuracy of calculation of definite integrals by different methods. *Modern problems of geometrical modeling and information technologies*. Melitopol: MSU. 7-19.

Author Information

Vladimir Yeremeev

Federal State Budgetary Educational Institution of Higher Education «Melitopol State University»
Melitopol, Russia

Andrey Naidysh

Federal State Budgetary Educational Institution of Higher Education «Melitopol State University»
Melitopol, Russia

Oksana Stokan

Federal State Budgetary Educational Institution of Higher Education «Melitopol State University»
Melitopol, Russia
Contact e-mail: oksana.stokan0@mail.ru

To cite this article:

Yeremeev, V., Naidysh, A., & Stokan, O. (2024). Construction of an integral distribution function of random variables determining the impact of wind power plant on birds in accordance with the predictive analysis by experts. *The Eurasia Proceedings of Science, Technology, Engineering & Mathematics (EPSTEM)*, 30, 9-16.

The Eurasia Proceedings of Science, Technology, Engineering & Mathematics (EPSTEM), 2024

Volume 30, Pages 17-27

ICBAST 2024: International Conference on Basic Sciences and Technology

Application of Magnetic Biochar@Alginate Composite as Adsorbent for Effective Removal of Methylene Blue from Aqueous Media

Serife Parlayıcı

Konya Technical University

Erol Pehlivan

Konya Technical University

Abstract: In recent years, magnetic biochar has been widely used for the removal of dyes in polluted water due to its magnetic separation abilities and has been used as composite adsorbents by incorporating different biomasses into its structure for the removal of such pollutants. In this study, a new composite magnetic biochar@alginate composite (mBC@Alg) was synthesized as an alternative adsorbent for the removal of methylene blue (MB) from aqueous solutions. The primary focus of this intensive preparation procedure is on the synthesis, characterization, and optimization of the mBC@Alg for enhanced MB adsorption capacity. The composite material was characterized using FT-IR analysis and scanning electron microscopy (SEM). Batch adsorption studies experiments were performed to determine the removal efficiencies, pH, adsorbent dose, contact time and initial concentration of MB molecules. Various adsorption isotherms such as Freundlich, Langmuir, Scatchard and Dubinin-Radushkevich were used to describe the adsorption behavior at equilibrium. The Langmuir adsorption isotherm was identified as the most appropriate model to explain the observed adsorption phenomena, and the adsorption capacity of mBC@Alg for MB was determined to be 416.67 mg/g using this isotherm. Kinetic studies were carried out using pseudo-first-order and pseudo-second-order kinetic models and it was concluded that the experimental data fit well with the second-order kinetic model. The adsorbent properties of the mBC@Alg composite are particularly effective in removing MB molecules from aqueous solutions.

Keywords: Biochar, Alginate, Nano-Fe₃O₄, Methylene blue, Kinetics

Introduction

Dyes, and pigments from various human activities pose significant environmental risks, especially when discharged into aqueous medium. Due to their resistance to natural degradation, these substances threaten both human health and environmental safety. They can lead to adverse effects, including genetic mutations, allergic reactions, and cancer. Additionally, these contaminants harm aquatic ecosystems by lowering dissolved oxygen levels, reducing light penetration, and inhibiting photosynthesis.

The pollution of water bodies by organic dyes has become a pressing environmental concern, largely driven by industrial activities like textile dyeing, printing, and leather processing (Parlayıcı & Pehlivan, 2021). Among these dyes, methylene blue (MB) is widely utilized across multiple industries; however, its release into water systems poses serious health and ecological risks due to its toxicity, persistence, and potential for bioaccumulation. Consequently, developing efficient and sustainable methods for removing MB from aqueous environments is crucial to safeguard both environmental quality and public health (Jiang et al., 2018; Kasbaji et al., 2023). Adsorption has emerged as one of the most effective techniques for dye removal, given its simplicity, low energy requirements, and high efficiency. Recently, biochar (BC) — a carbon-rich adsorbent derived from biomass — has garnered attention as an eco-friendly adsorbent due to its porous structure, large surface area,

- This is an Open Access article distributed under the terms of the Creative Commons Attribution-Noncommercial 4.0 Unported License, permitting all non-commercial use, distribution, and reproduction in any medium, provided the original work is properly cited.

- Selection and peer-review under responsibility of the Organizing Committee of the Conference

© 2024 Published by ISRES Publishing: www.isres.org

and modifiable functional groups (Srivatsav et al., 2020; Vafakish et al., 2024; Parlayıcı et al., 2024; Suratman et al., 2024). However, conventional BC often lacks the magnetic properties needed for easy separation from treated water, which can complicate its practical application. To address this limitation, researchers have focused on enhancing biochar with magnetic nanoparticles, creating magnetic BC that can be easily separated via external magnetic fields (Feng et al., 2021; Yi et al., 2020).

Natural biopolymers (chitosan, cellulose, lignin, and alginate) demonstrated excellent affinity toward heavy metals and dyes through different mechanisms including, electrostatic attraction, complexation, chelation, and ion exchange (Doyo et al., 2023; Fouda-Mbanga et al., 2021; Kasbaji et al., 2024). In addition to magnetic modification, incorporating BC into a composite with biocompatible materials such as alginate can further enhance its adsorption capacity and structural integrity (Salem et al., 2023). Alginate, a natural polysaccharide derived from brown algae, is commonly used due to its non-toxicity, biodegradability, and gelling properties (Liu et al., 2023; Bahsaine et al., 2024; Aichour et al., 2024; Parlayıcı & Pehlivan, 2023). The combination of magnetic BC and alginate creates a robust, multifunctional composite that can effectively capture and remove pollutants like MB from water.

This study examines the use of a mBC@Alg composite as an adsorbent for removing MB from aqueous solutions. The research includes the synthesis, characterization, and evaluation of the mBC@Alg composite's adsorption performance, focusing on its adsorption capacity, kinetics, and the influence of factors such as pH, contact time, and initial dye concentration. The results provide insights that support the development of efficient, reusable, and eco-friendly adsorbents for water purification, presenting a promising approach to mitigating water pollution.

Method

Materials

All analytical-grade chemicals were used as received, without any further purification. MB was obtained from Acros Organics (New Jersey, USA). Sigma-Aldrich was the supplier of both the sodium alginate powder and the iron oxide (Fe_3O_4) nanopowder. Hydrochloric acid (HCl) and sodium hydroxide (NaOH) were purchased from Merck.

Preparation of Adsorbent

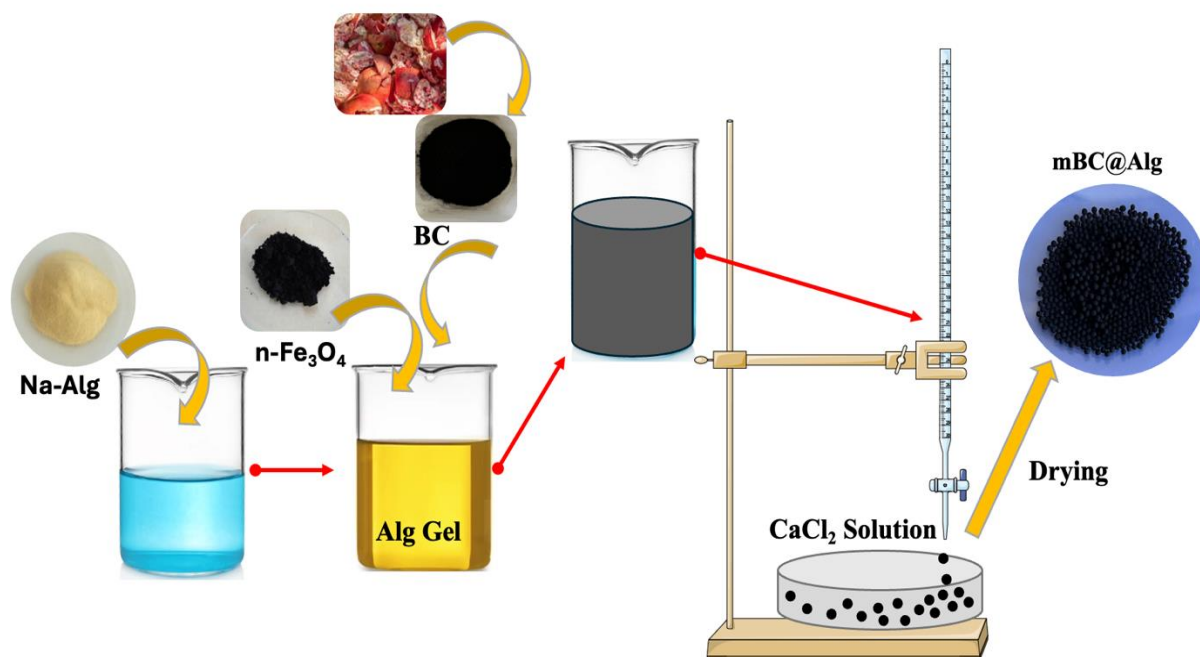


Figure 1. Synthesis scheme of mBC@Alg composite.

The pomegranate was obtained from a local market in Turkey. The peel and fruit parts were separated. The peels were washed with pure water and dried in an oven for 24 hours. The dried seeds were heated at 600 °C in a Magma THERM MT1210/B2 muffle furnace for 3 hours and converted to BC in the presence of low oxygen (Amalina et al., 2022). The BC, cooled in a desiccator, was ground into a powder. Particles of 125 µm in size, obtained by sieving, were used in the preparation of the composite.

For the preparation of mBC@Alg, sodium alginate was first dissolved in 100 ml (5% w/v) distilled water. It was mixed on a magnetic stirrer for about 4 hours to obtain a homogeneous gel. Meanwhile, a suspension of 2.5 g of nano-Fe₃O₄ in 20 ml of distilled water and a suspension of 2.5 g of BC in 20 ml of distilled water were prepared. These suspensions were mixed individually at 300 rpm for 2 hours. The prepared suspensions were then added to the prepared alginate gel and mixed on a magnetic stirrer for 6 hours until a homogeneous solution was formed. Spheres were created by adding the mixture dropwise into a 0.5 M CaCl₂ solution using an injector, and the spheres formed were mixed on a magnetic stirrer at 100 rpm for about 3 hours. The beads were left in this solution overnight, then collected by filtration and thoroughly washed with water until a neutral pH was achieved. Finally, the beads were filtered out and dried at 60 °C for 24 hours (Figure 1).

Characterization

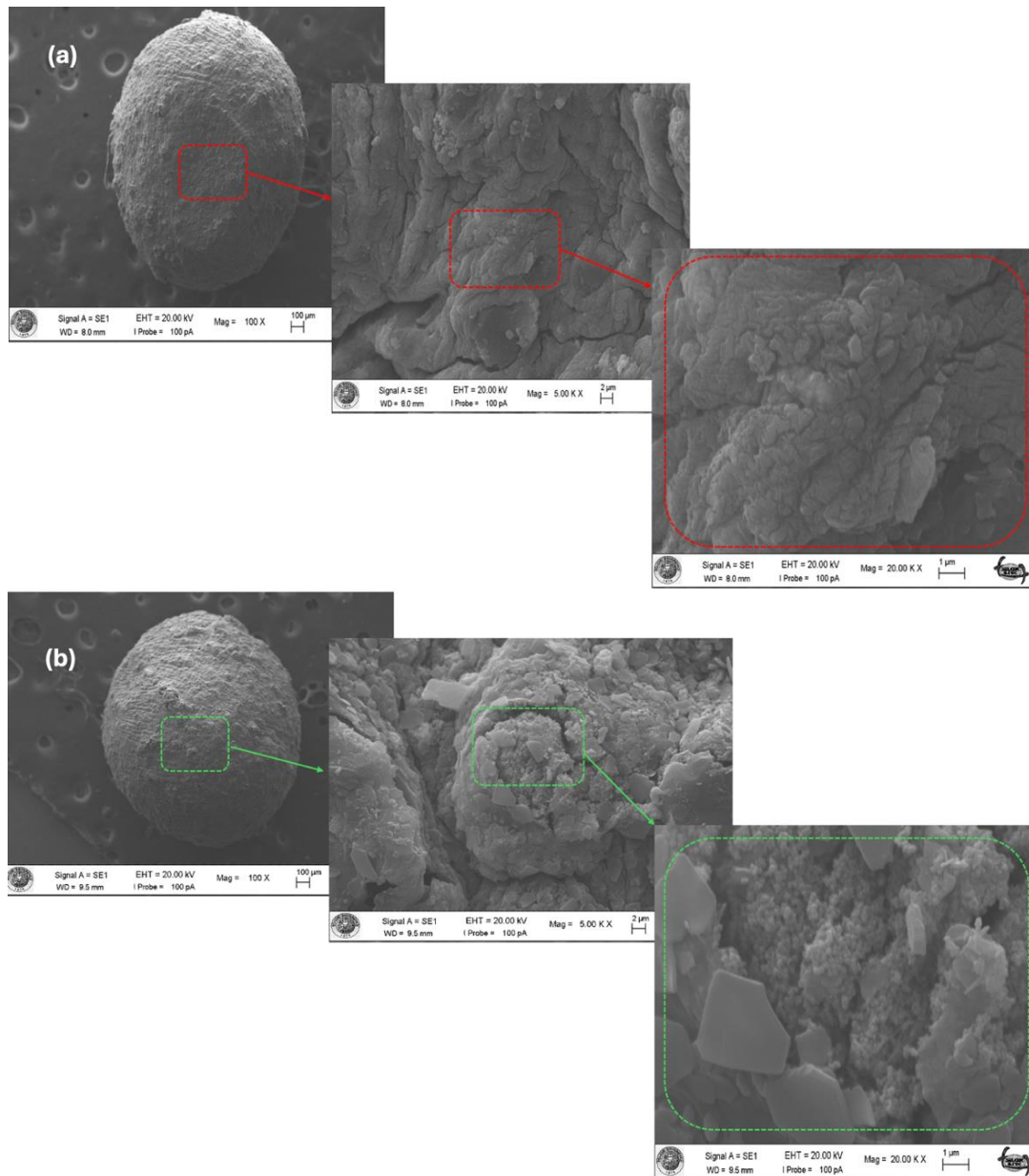


Figure 2. SEM image mBC@Alg composite (a) and after MB adsorption (b).

The morphology of mBC@Alg before and after the adsorption of MB ions was examined using SEM imaging. A thorough understanding of the structure and morphology of the mBC@Alg is necessary to evaluate its efficacy and potential interactions with MB. The adsorption efficiency of the composite is directly impacted by the surface properties, particle size, porosity, and overall structural integrity that may be shown by scanning electron microscopy (SEM). According to SEM pictures, the mBC@Alg has a porous surface structure with different levels of homogeneity and roughness, which is crucial for increasing adsorption sites and surface area. It appears that the magnetic characteristics were successfully incorporated into the composite because the magnetic particles contained in the BC matrix are clearly distributed. When Figure 2a. is examined, the roughness of the surface draws attention. As can be seen from Figure 2b., MB ions were coated on the pores and accumulations were seen on the surface. This showed that MB ions were adsorbed to the mBC@Alg surface.

Important information about the chemical structure and functional groups of the mBC@Alg composite can be obtained from its Fourier Transform Infrared (FT-IR) spectrum. Characteristic peaks in the FT-IR analysis show the presence of functional groups in the matrix of the alginate and biochar components (Thakur et al., 2016, Kusuktham et al., 2014). These peaks are frequently observed in areas that correlate to C=O stretching, O–H stretching, and C–O–C vibrations. Iron oxide (FeO₄) nanoparticles, which may exhibit unique peaks associated with Fe–O stretching, are commonly used to add magnetic characteristics. According to the FT-IR spectrum of mBC@Alg, it was observed that the stretching vibration peak of O–H is represented in the range of 3270 cm⁻¹. The peak at 1590 cm⁻¹ is caused by carboxyl –C=O stretching vibrations. The vibration peak at 1420 cm⁻¹ is aromatic C=C stretching vibrations. The stretching at 1016 cm⁻¹ corresponds to the ether –C–O and alcohol –C–O stretching. The characteristic absorption bands associated with Fe₃O₄ nanoparticles are observed at 535 cm⁻¹, which is related to the stretching modes of the Fe–O bond.

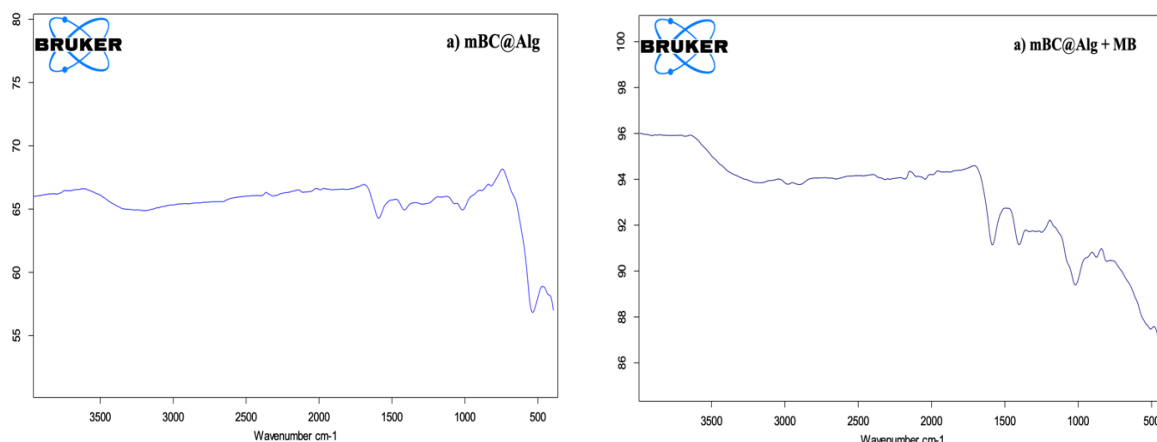


Figure 3. FT-IR spectra of MB before adsorption by mBC@Alg (a) and after adsorption by mBC@Alg (b).

Results and Discussion

Effect of pH on MB adsorption

One important aspect affecting the effectiveness of dye removal from wastewater is the impact of pH on the adsorption of MB by a composite adsorbent (Liu et al., 2022). The ionization state of the adsorbent and the adsorbate are both significantly influenced by the pH of the solution. The attraction between positively charged MB molecules and negatively charged sites on the composite can be strengthened in acidic environments by protonating functional groups on the surface of the BC (Xu et al. 2024). The deprotonation of these groups, on the other hand, may decrease the adsorption capability in alkaline circumstances because of increased electrostatic repulsion. Therefore, maximizing the effectiveness of the mBC@Alg composite in wastewater treatment applications requires an understanding of the ideal pH range for MB adsorption.

The remaining MB concentrations measured at pH levels 2, 3, 4, 5, 6, 7, and 8 after the 60-minute equilibrium period were analyzed to determine how pH affected the adsorption of MB ions by mBC@Alg composite. The adsorption process is further affected by the interaction between pH and the structural characteristics of the mBC@Alg composite. Variations in pH can influence the surface charge, porosity, and availability of active sites on the composite material. Research indicates that hydrophobic interactions between MB and the BC

matrix might be enhanced at certain pH levels, resulting in improved adsorption efficiency. Thus, it is crucial to thoroughly investigate how pH impacts adsorption kinetics and equilibrium to develop effective treatment strategies. The optimal pH range for enhancing the removal efficiency of MB is between pH 6 and pH 8 (Figure 4.).

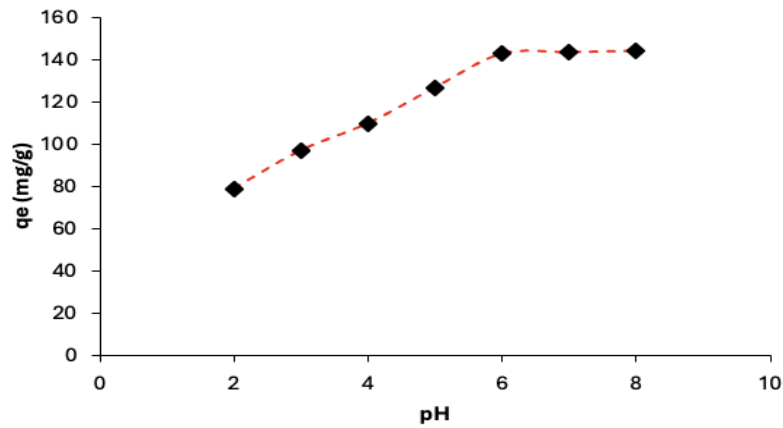


Figure 4. Effect of pH on MB adsorption.

Effect of Contact Time on MB Ions Adsorption

The effect of contact time on MB adsorption was studied at various intervals (5, 15, 30, 60, 120, 180, and 240 minutes) with an adsorbent dosage of 2 g/L, at pH 6, and a temperature of 25 °C. An optimal contact time of 60 minutes was selected for further experiments. A key factor influencing the effectiveness of pollutant removal from aqueous solutions is the role of contact time in the adsorption of MB onto a mBC@Alg composite. Typically, the adsorption capacity increases with longer contact times due to enhanced interactions between the MB and the surface functional groups of the composite material. Initially, adsorption occurs rapidly as accessible sites on the mBC@Alg composite surface are filled. However, as these sites become occupied, the adsorption rate diminishes, leading to a state of equilibrium (Figure 5). An optimal contact time of 60 minutes was selected for further experiments. Understanding this relationship is essential for optimizing the design of mBC@Alg composite in wastewater treatment, as it helps determine the optimal contact time required to achieve maximum removal efficiency of MB.

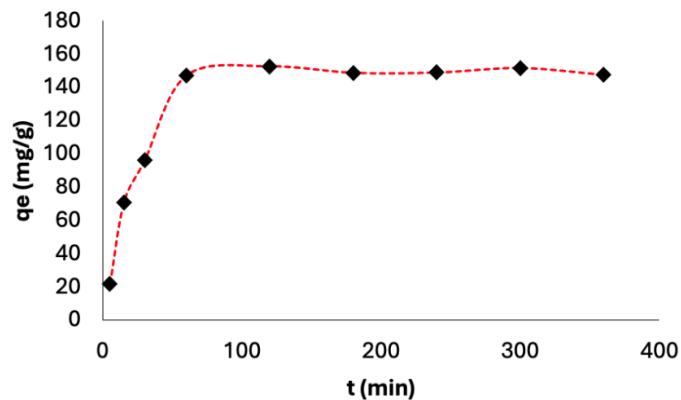


Figure 5. Effect of contact time on MB adsorption.

Adsorbent Dose Effect

The effect of adsorbent dosage (Figure 6.) on the removal of MB ions was investigated through adsorption experiments at various doses (0.25, 0.50, 1.0, 1.25, 1.50, and 2.0 g/L). The optimal adsorbent dosage was determined to be 1.25 g/L.

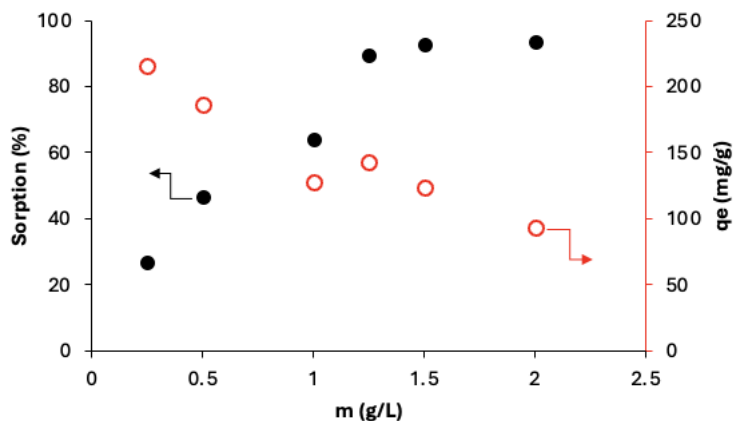


Figure 6. Effect of adsorbent dosage on MB adsorption.

Effect of Initial Concentration on MB Adsorption

The starting concentration of MB in a solution significantly influences the adsorption capacity of mBC@Alg composite. As the initial concentration rises, the force driving mass transfer between the liquid phase and the solid adsorbent intensifies, leading to increased adsorption rates. When concentrations are low, the available sites on the mBC@Alg composite are not fully engaged, resulting in lower removal efficiencies. However, as the concentration increases, more MB ions interact with the surface functional groups of the composite, thereby enhancing the overall adsorption capacity. This relationship underscores the importance of initial concentration in assessing the effectiveness of the adsorbent material. The adsorption capacity was evaluated by varying the initial MB concentration (25, 50, 100, 150, 200, 250, 300, 400, and 500 ppm).

Although higher initial concentrations generally improve adsorption, this trend has its limits as shown in Figure 7. At elevated concentrations, the mBC@Alg composite may reach a saturation point where most adsorption sites are filled. Beyond this saturation level, the adsorption rate may decline, leading to diminishing returns in MB removal efficiency. Additionally, factors such as competition among MB ions for available sites and possible aggregation of the composite can hinder effective uptake at very high concentrations.

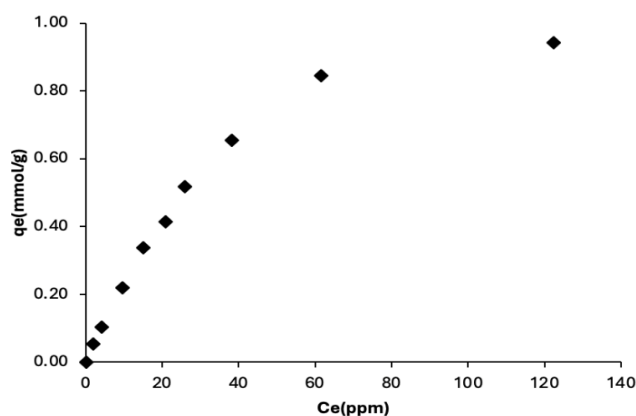


Figure 7. Effect of initial concentration on MB adsorption.

Adsorption Isotherms

Understanding the effectiveness of mBC@Alg composite as adsorbent for MB treatment requires an understanding of adsorption isotherms. These isotherms provide insights into how pollutants interact with the composite material at various concentrations, enabling researchers to analyze and predict the adsorption behavior of contaminants, including organic dyes. Key factors like maximal adsorption capacity and surface heterogeneity can be found by analyzing the data using different models, such as Freundlich, Langmuir, Scatchard and D-R isotherms (Langmuir, 1917, Freundlich, 1906, Scatchard, 1949, Dubinin and Radushkevich,

1947) (Figure 8.). These parameters are crucial for improving the design and use of these composites in practical situations (Parlayici & Pehlivan, 2024).

The appropriateness of the Langmuir isotherm model in characterizing the adsorption behavior of contaminants on mBC@Alg composite suggests a monolayer adsorption mechanism, in which each adsorption site accommodates only one molecule of the adsorbate (Huangfu et al., 2023). This model is based on the premise of uniform adsorption sites and a limited number of available locations, which corresponds well to the properties of these composites, especially when their surface functionalization is tailored for specific contaminants (Qi, et al., 2018). The maximum adsorption capacity, denoted as q_e , is a vital parameter derived from the Langmuir isotherm, indicating how effectively the composite can bind pollutants. q_e was calculated as 416.7 mg/g. A higher value q_e reflects an increased ability of the adsorbent to capture contaminants, underscoring its potential for effective use in wastewater treatment. Therefore, the Langmuir model not only facilitates predictions of adsorption performance but also serves as a guide for optimizing the design of mBC@Alg composite to maximize MB removal efficiency.

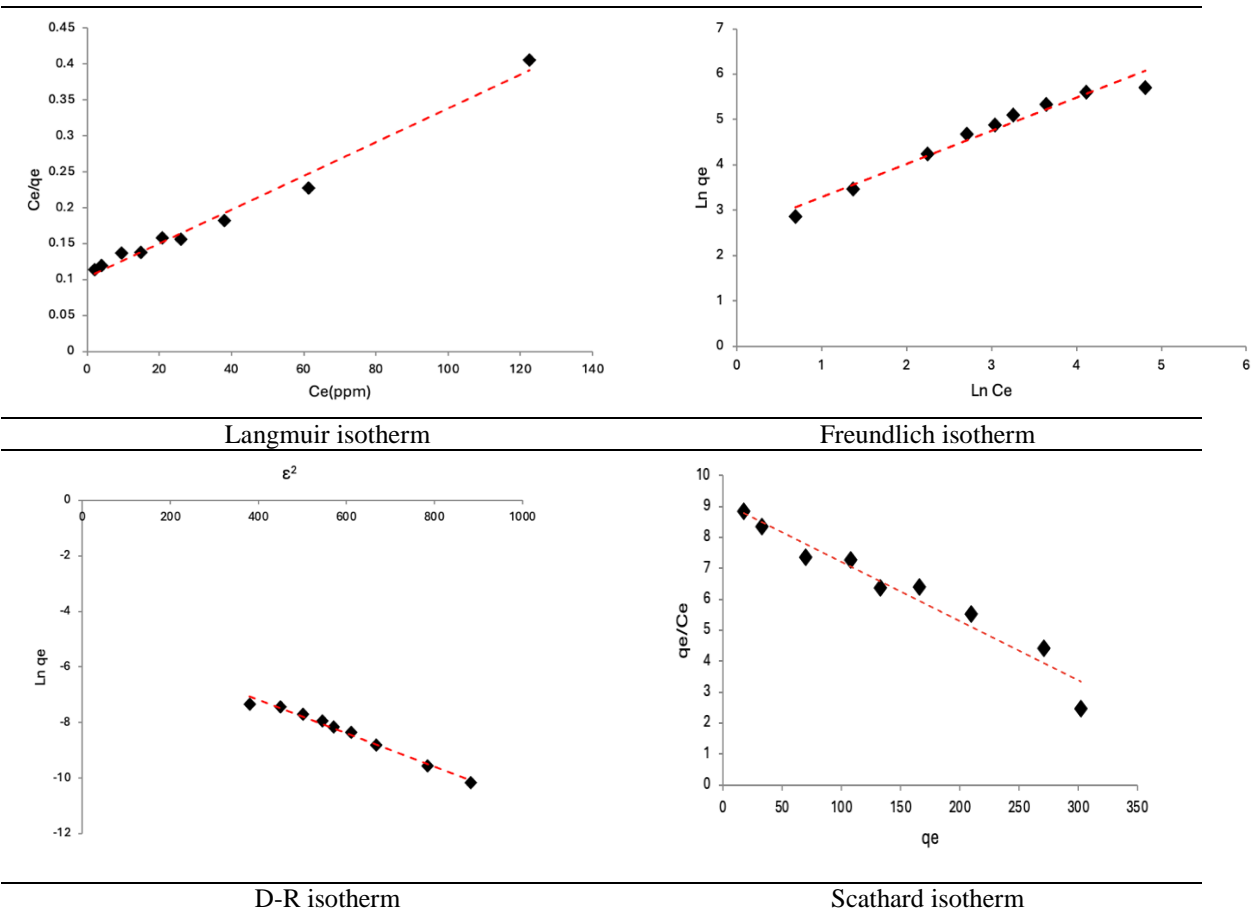


Figure 8. Langmuir, Freundlich, Scatchard and D-R isotherm graphs for mBC@Alg composite.

Table 1. Adsorption isotherm parameters for removal of MB.

Model	Equation	Parameters for dye			
Langmuir	$\frac{C_e}{q_e} = \frac{C_e}{A_s} + \frac{1}{K_b A_s}$	q_e 416.7	K_b 0.0232	R^2 0.984	R_L 0.177
Freundlich	$\ln q_e = \ln K_f + \frac{1}{n} \ln C_e$	K_f 12.96	n 1.37	R^2 0.965	
D-R	$\ln q_e = \ln q_m - \beta \epsilon^2$	X_m 0.008	K 0.006	E 9.13	R^2 0.984
Scatchard	$q_e/C_e = Q_s K_s - q_e K_s$	Q_s 475.22	K_s 0.019	R^2 0.947	

Adsorption Kinetic Modeling

Understanding the rate and mechanism of contaminant uptake in dye treatment applications involves kinetic modeling of MB adsorption onto mBC@Alg composite. Kinetic models such as pseudo-first-order and pseudo-second-order provide information on the factors that influence the rate at which MB molecules adsorb onto the composite surface. The pseudo-first-order model typically captures the initial rapid adsorption phase in which many adsorption sites are rapidly filled. In contrast, the so-called second-order model usually provides a better fit over longer time periods, suggesting that the adsorption process may be chemically controlled rather than entirely governed by diffusion.

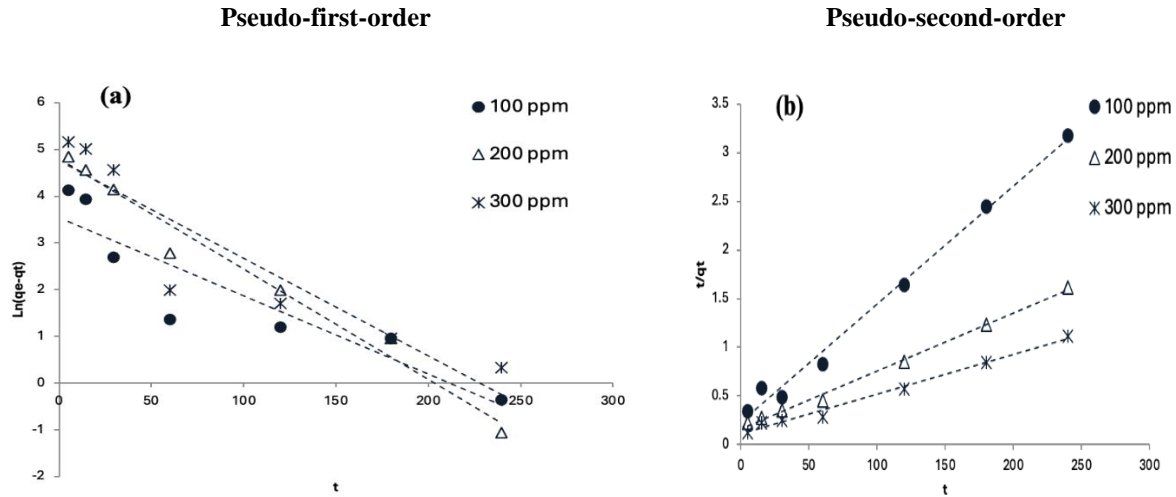


Figure 9. Graphs of pseudo-first-order and pseudo-second kinetic models for MB adsorption.

Table 2. Comparison of the pseudo-first-order, pseudo-second-order adsorption rate constants and calculated and experimental q_e values obtained at different initial MB concentrations.

$C_o(\text{ppm})$	$q_{e \text{ exp}}$	Pseudo First-order			Pseudo Second- order		
		k_1	q_e	R^2	k_2	q_e	R^2
100	76.30	0.0167	34.50	0.836	0.0006	82.64	0.992
200	149.01	0.0236	120.71	0.978	0.0002	169.49	0.996
300	217.04	0.0209	116.56	0.853	0.0002	243.90	0.989

By analyzing the kinetic parameters derived from these models, including rate constants and equilibrium times, they can optimize operational conditions to achieve maximum MB removal efficiency. The applicability of the pseudo-second-order rate mechanism for MB adsorption kinetic modeling on mBC@Alg composite highlights the complexity and efficiency of the adsorption process. This model is particularly relevant as it indicates that the rate of MB adsorption is primarily influenced by chemical interactions between the pollutant and the active sites on the composite surface, rather than merely by physical diffusion. The pseudo-second-order model provided a better fit for experimental data over extended time periods, suggesting that adsorption sites become increasingly occupied as equilibrium is approached (Figure 9). This behavior is crucial for practical applications, as it implies that the adsorbent can effectively bind higher concentrations of MB, making it a promising solution for dye treatment.

Thermodynamic Parameters

The thermodynamic parameters associated with MB adsorption on mBC@Alg composite provide critical insights into the nature of the adsorption process and its feasibility under varying temperature conditions. The effect of temperature on MB adsorption was investigated over a temperature range of 25 °C, 35 °C, and 45 °C (Figure 10.) and thermodynamic parameters were calculated. These parameters such as the change in Gibbs free energy (ΔG°), enthalpy (ΔH°), and entropy (ΔS°) can be derived from equilibrium data given in the Table 3., offering a comprehensive understanding of the energetic and disorder aspects of the adsorption process. A negative ΔG° value indicates that the adsorption is spontaneous, while positive ΔH° values suggest an endothermic process, implying that higher temperatures favor the adsorption of MB. Conversely, a positive ΔS°

value reflects an increase in randomness at the solid-liquid interface during the adsorption, which is indicative of favorable interactions between the composite material and the dye molecules. The value of ΔG° (Gibbs free energy change) becomes more negative as the temperature rises (Table 3), indicating that the process becomes more thermodynamically favorable at higher temperatures. This suggests that the uptake efficiency is greater at higher temperatures, where the more negative ΔG° values signify a stronger tendency for the process to occur spontaneously (Bahrami et al., 2024).

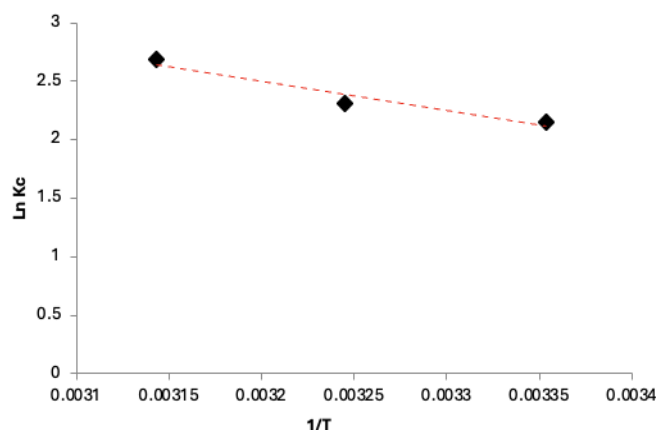


Figure 10. $\ln K_c - 1/T$ plot

Table 3. Thermodynamic parameters for MB adsorption

ΔS°	ΔH°	ΔG° (J mol ⁻¹)			R^2
J K ⁻¹ mol ⁻¹	J mol ⁻¹	T=298.15K	T=308.15K	T=318.15K	
87.85	20934.24	-5254.98	-6133.37	-7011.76	0.934

Conclusion

The study demonstrated that mBC@Alg composite is an effective and environmentally friendly adsorbent for removing MB from aqueous media. By integrating BC with alginate and magnetic particles, the composite combines high adsorption efficiency, easy recovery, and reusability, providing a sustainable approach to wastewater treatment. The experiments demonstrated that optimal conditions for effective MB removal included an equilibrium time of 60 minutes, an initial pH of 6, an initial dye concentration of 200 ppm, and a composite dosage of 2 g/L. The adsorption process was shown to follow Langmuir isotherm and pseudo-second-order kinetic models, indicating a monolayer adsorption mechanism with strong interaction between MB and the mBC@Alg composite. The pseudo-second-order kinetics model was selected for time-dependent studies to accurately describe the adsorption process and predict the rate of MB removal over time. Furthermore, the magnetic properties of the composite allowed facile separation from the solution, making it practical for real-world applications. The reusability studies revealed that mBC@Alg composite could maintain substantial adsorption capacity over multiple cycles, reinforcing its economic and environmental viability. In conclusion, mBC@Alg composite is a promising adsorbent for the removal of MB from water systems, highlighting its potential application in industrial wastewater management and environmental remediation efforts. Future research could explore its application for various other pollutants and optimization in industrial-scale setups to fully realize its potential in diverse environmental applications.

Scientific Ethics Declaration

The authors declare that the scientific ethical and legal responsibility of this article published in EPSTEM Journal belongs to the authors.

Acknowledgements or Notes

* This article was presented as an oral presentation at the International Conference on Basic Sciences and Technology (www.icbast.net) held in Antalya/Turkey on November 14-17, 2024.

References

- Aichour, A., Djafer Khodja, H., Zaghouane-Boudiaf, H., Iborra, C. V., & Polo, M. S. (2024). Kinetic adsorption studies of methylene blue and crystal violet dyes removal in single and competitive systems using lemon peels/activated carbon/alginate composite. *Reaction Kinetics, Mechanisms and Catalysis*, 1-20.
- Bahrami, M., Amiri, M. J., Rajabi, S., & Mahmoudi, M. (2024). The removal of methylene blue from aqueous solutions by polyethylene microplastics: Modeling batch adsorption using random forest regression. *Alexandria Engineering Journal*, 95, 101-113.
- Bahsaine, K., Benzeid, H., Zari, N., & Bouhfid, R. (2024). Biochar-alginate beads derived from argan nutshells for effective methylene blue removal: A sustainable approach to wastewater treatment. *International Journal of Biological Macromolecules*, 136853.
- Doyo, A. N., Kumar, R., & Barakat, M. A. (2023). Recent advances in cellulose, chitosan, and alginate based biopolymeric composites for adsorption of heavy metals from wastewater. *Journal of the Taiwan Institute of Chemical Engineers*, 151, 105095.
- Dubinin, M.M., Radushkevich, L.V., (1947).. Equation of the characteristic curve of activated charcoal. *Proc. Acad. Sci. USSR Phys. Chem. Sect.* 55, 331-333.
- Feng, Z., Yuan, R., Wang, F., Chen, Z., Zhou, B., & Chen, H. (2021). Preparation of magnetic biochar and its application in catalytic degradation of organic pollutants: A review. *Science of the Total Environment*, 765, 142673.
- Fouda-Mbanga, B. G., Prabakaran, E., & Pillay, K. (2021). Carbohydrate biopolymers, lignin based adsorbents for removal of heavy metals (Cd²⁺, Pb²⁺, Zn²⁺) from wastewater, regeneration and reuse for spent adsorbents including latent fingerprint detection: A review. *Biotechnology Reports*, 30, e00609.
- Freundlich, H. (1907). Über die adsorption in lösungen. *Zeitschrift für physikalische Chemie*, 57(1), 385-470.
- Huangfu, C., Yu, S., Tong, B., Yang, A., Lyu, J., & Guo, X. (2023). Efficient lithium extraction from aqueous solutions by MIL-100 (Fe): A study on adsorption kinetics, thermodynamics and mechanism. *Separation and Purification Technology*, 322, 124365.
- Jiang, N., Shang, R., Heijman, S. G., & Rietveld, L. C. (2018). High-silica zeolites for adsorption of organic micro-pollutants in water treatment: A review. *Water research*, 144, 145-161.
- Kasbaji, M., Mennani, M., Boussetta, A., Grimi, N., Barba, F. J., Mbarki, M., & Moubarik, A. (2023). Bio-adsorption performances of methylene blue (MB) dye on terrestrial and marine natural fibers: Effect of physicochemical properties, kinetic models and thermodynamic parameters. *Separation Science and Technology*, 58(2), 221-240.
- Kasbaji, M., Mennani, M., Barhoumi, S., Esshouba, Y., Oubenali, M., Ablouh, E. H., Kassab, Z & El Achaby, M. (2024). Synergy of magnetic nanoparticles and sodium alginate-coated lignin for effective pollutant remediation, simple recovery, and cost-effective regeneration. *Langmuir*, 40, 20657-20678.
- Langmuir, I. (1917). The constitution and fundamental properties of solids and liquids. II. Liquids. *Journal of the American Chemical Society*, 39(9), 1848-1906.
- Liu, X. J., Li, M. F., Ma, J. F., Bian, J., & Peng, F. (2022). Chitosan crosslinked composite based on corncob lignin biochar to adsorb methylene blue: Kinetics, isotherm, and thermodynamics. *Colloids and Surfaces A: Physicochemical and Engineering Aspects*, 642, 128621.
- Liu, H., Zhu, J., Li, Q., Li, L., Huang, Y., Wang, Y., Fan, G. & Zhang, L. (2023). Adsorption performance of methylene blue by KOH/FeCl₃ modified biochar/alginate composite beads derived from agricultural waste. *Molecules*, 28(6), 2507.
- Qi, X., Wei, W., Su, T., Zhang, J., & Dong, W. (2018). Fabrication of a new polysaccharide-based adsorbent for water purification. *Carbohydrate Polymers*, 195, 368-377.
- Parlayıcı, Ş., & Pehlivan, E. (2023). An ecologically sustainable specific method using new magnetic alginate-biochar from acorn cups (*Quercus coccifera* L.) for decolorization of dyes. *Polymer Bulletin*, 80(10), 11167-11191.
- Parlayıcı, Ş., Bahadır, M., & Pehlivan, E. (2024). Nanoporous carbonaceous materials (biochar and activated carbon): recent progress and potential applications for arsenic removal. *Journal of Dispersion Science and Technology*, 1-22.
- Parlayıcı, Ş., & Pehlivan, E. (2024). Methylene blue removal using nano-TiO₂/MWCNT/Chitosan hydrogel composite beads in aqueous medium. *Chemosphere*, 365, 143244.
- Pehlivan, E., & Parlayıcı, Ş. (2021). Fabrication of a novel biopolymer-based nanocomposite (nanoTiO₂-chitosan-plum kernel shell) and adsorption of cationic dyes. *Journal of Chemical Technology & Biotechnology*, 96(12), 3378-3387.

- Salem, D. B., Ouakouak, A., Touahra, F., Hamdi, N., Eltaweil, A. S., Syed, A., Boopathy, R. & Tran, H. N. (2023). Easy separable, floatable, and recyclable magnetic-biochar/alginate bead as super-adsorbent for adsorbing copper ions in water media. *Bioresource Technology*, 383, 129225.
- Scatchard, G. (1949). The attractions of proteins for small molecules and ions. *Annals of the New York Academy of Sciences*, 51(4), 660-672.
- Srivatsav, P., Bhargav, B. S., Shanmugasundaram, V., Arun, J., Gopinath, K. P., & Bhatnagar, A. (2020). Biochar as an eco-friendly and economical adsorbent for the removal of colorants (dyes) from aqueous environment: A review. *Water*, 12(12), 3561
- Suratman, A., Astuti, D. N., Kusumastuti, P. P., & Sudiono, S. (2024). Okara biochar immobilized calcium-alginate beads as eosin yellow dye adsorbent. *Results in Chemistry*, 7, 101268.
- Thakur, S., Pandey, S., & Arotiba, O. A. (2016). Development of a sodium alginate-based organic/inorganic superabsorbent composite hydrogel for adsorption of methylene blue. *Carbohydrate Polymers*, 153, 34-46.
- Vafakish, B., Babaei-Ghazvini, A., & Acharya, B. (2024). Unraveling the mechanisms of methylene blue adsorption onto biochar: a robust and sustainable approach for water remediation. *International Journal of Environmental Science and Technology*, 1-12.
- Xu, R., Wei, J., Cheng, D., Wang, W., Hong, L., Chen, Y., & Guo, Y. (2024). Abundant porous biochar derived from luffa vine for removal of methylene blue: Selective adsorption and mechanistic studies. *Industrial Crops and Products*, 219, 119114.
- Yi, Y., Huang, Z., Lu, B., Xian, J., Tsang, E. P., Cheng, W., Fang, J., & Fang, Z. (2020). Magnetic biochar for environmental remediation: A review. *Bioresource Technology*, 298, 122468.

Author Information

Şerife Parlayıcı

Department of Chemical Engineering,
Konya Technical University, Campus,
42250 Selçuklu-Konya,Türkiye

Erol Pehlivan

Department of Chemical Engineering,
Konya Technical University, Campus,
42250 Selçuklu-Konya,Türkiye
Contact e-mail: erolpehlivan@gmail.com.tr

To cite this article:

Parlayıcı, S.. & Pehlivan, E. (2024). Application of magnetic biochar@alginate composite as adsorbent for effective removal of methylene blue from aqueous media. *The Eurasia Proceedings of Science, Technology, Engineering & Mathematics (EPSTEM)*, 30, 17-27.

The Eurasia Proceedings of Science, Technology, Engineering & Mathematics (EPSTEM), 2024

Volume 30, Pages 28-38

ICBAST 2024: International Conference on Basic Sciences and Technology

Lignin Extraction and Characterization from Lavender Waste

Halil Sen

Burdur Mehmet Akif Ersoy University

Hale Secilmis

Burdur Mehmet Akif Ersoy University

Asem Assani

Burdur Mehmet Akif Ersoy University

Canan Sen

Burdur Mehmet Akif Ersoy University

Abstract: Today, the vast majority of plastic products are produced from petroleum-based chemicals. This has led to a great dependence on non-renewable energy sources in the production of many commonly used products. As the world population increases, the demand for such products and therefore oil also increases. However, fossil fuel resources are limited and will inevitably be depleted over time. Lignocellulosic biomasses, which are the most abundant natural carbon sources on earth, are the best alternative to fossil fuel sources. Lignocellulosic biomass is important for reducing and utilizing agroforestry residues for potential use in the production of biochemicals, biofuels, biomaterials, and other value-added products. "Green" biomass fractionation methodologies are being developed to reduce environmental impact. In our study, NaOH-water and KOH-water mixtures of 0.5%, 1%, 2%, 4%, 6%, 8%, 10% and 15% were used to extract lignin from waste lavender fibers. Characterization analyses of the isolated lignin were performed using thermal and spectroscopic techniques. T_{dehyde} , T_g and T_m values were measured from the DSC curves of the extracts. Decomposition temperature values of 5%, 10% and 25% of the TGA curves were calculated. The presence of functional groups in lignin was emphasized from the FTIR spectra. Absorbance values were also measured by UV-VIS spectroscopy. Lignin obtained from lavender waste is a sustainable and environmentally friendly alternative.

Keywords: Lignin, Extraction, Characterization, Biomass, Lavender

Introduction

Today, the vast majority of plastic products are produced from petroleum-based chemicals. As the world population increases, the demand for such products and therefore for petroleum is increasing. However, fossil fuel resources are limited and will inevitably be depleted over time. Lignocellulosic biomasses, which are the most abundant natural carbon sources on earth, are the best alternative to fossil fuel sources. Lignocellulosic biomasses consist of three main polymers: cellulose, hemicellulose and lignin (Eraslan, 2020). Since 1838, when Anselme Payen first discovered the material that forms a shell between cellulose and hemicellulose, later called "lignin", numerous studies have been conducted to investigate the structure and properties of lignin. Lignin ranks second in quantity in terrestrial regions of the Earth's surface and plays an important role in ensuring water conduction for plants and protecting them from pathogen attacks. In terms of chemical structure, lignin is a potential source of valuable phenolic compounds when degraded. Compared to other sustainable carbon-based sources, these large resources constitute a potential advantage for lignin utilization. Lignin is one of the main components of the cell walls of vascular plants and constitutes 18-25% of the biomass. In softwood

- This is an Open Access article distributed under the terms of the Creative Commons Attribution-Noncommercial 4.0 Unported License, permitting all non-commercial use, distribution, and reproduction in any medium, provided the original work is properly cited.

- Selection and peer-review under responsibility of the Organizing Committee of the Conference

© 2024 Published by ISRES Publishing: www.isres.org

species, it constitutes 25-35%. Lignin, which contains 30% of the world's organic carbon, is the most abundant natural polymer after cellulose (Alonso et al., 2006; Kapluhan, 2014; Méchin et al., 2007). Chemically, lignins are considered complex polyphenols. Despite many studies, their chemistry, biosynthesis and molecular biology have not been fully understood so far (Boerjan et al., 2003).

Lignin is effective and economical. It has been developed via phenol and aldehyde or by lignin modification. It can be used as a rubber thickener, polyol, rubber packing. It has many areas of use, from composite materials to unsaturated polyesters.

- Kraft lignin products are often used in high-end applications such as foam fire extinguishers.
- It has been used to stabilize foam and in printing inks for high-speed rotary presses, as an extender/modifier, and as a reinforcing pigment in rubber (Cerro et al., 2020).
- It is used as a binder in glass wool building insulation.
- Lignin improves the performance of energy storage devices.
- Lignosulfonate acts as a dust suppressant/inhibitor due to its tendency to bind with other polar and non-polar compounds.
- It is also used for dust control in ceramics.
- Adding alkaline lignins as fiber to human foods or as roughage to pet foods are potential uses of lignin. Extensive research in this area has shown that high dietary intake is associated with lower colon incidence (Meister, 2002).
- Lignin can be used in the production of biodegradable polymers. Studies are being conducted on the use of lignin, especially in the search for biodegradable alternatives to plastics and packaging materials.
- Lignin can also be used as an additive to strengthen polymer composite materials. Such composite materials can be used in many areas such as building materials, automotive parts and packaging materials by increasing their durability and mechanical properties.
- Lignin can be used as a first-class raw material in the production of chemical products. Phenolic compounds obtained from lignin can be used in the production of various industrial chemicals such as phenols, vanillin and other biologically active compounds.
- Lignin is one of the main components of biomass and can be used as fuel for energy production. Gasification or pyrolysis of biomass obtained from lignin is a potential method for bioenergy production.
- Lignin can be used as a soil amendment in agricultural applications. Especially in organic farming, lignin-based fertilizers and soil conditioners can increase soil fertility and support plant health.

There are studies in the literature that address different aspects of the extraction, characterization and structural transformation of lignin from different biomass sources. (Quesada-Medina et al. (2010), focused on the organosolv extraction of lignin from the hydrolyzed form of almond hulls and used the delta-value theory to optimize and understand the extraction process. The study highlighted the role of solvent properties in improving lignin recovery. Wen et al. (2013), investigated the structural and physical properties of bamboo lignin, revealing its unique properties and potential applications. Wen et al. (2014), investigated the chemical transformations of lignin during ionic liquid pretreatment and presented information on how these liquids alter the structure of lignin. Wu et al. (2017), described the isolation of lignin from Masson's pine by liquid-liquid extraction using aqueous NaOH solution. Rashid et al. (2018), investigated the kinetics and optimization of lignin extraction from different oil palm biomass types, focusing on process efficiency and conditions. Achinivu (2018), investigated the use of protic ionic liquids for lignin extraction, highlighting the unique properties this method imparts to lignin and lignin characterization. These studies represent important advances in lignin extraction methods and their potential applications, particularly in the context of bio-based materials and green chemistry.

Method

DSC Analysis

For the characterization of the isolated lignin in the study, PERKIN ELMER brand 400 model DSC system was used. The temperature was started at -25°C and 400°C was reached with 10°C increases per minute. Approximately 10 mg of isolated lignin was studied and the analyses were carried out in nitrogen atmosphere (Watkins et al., 2015).

TGA Analysis

In the experimental phase, SEIKO SII brand TG/DTA 7200 model device was used. In the study, starting from room temperature (25-30°C), it was increased to 1000°C with 10°C increments per minute. Approximately 10 mg of isolated lignin was used. Endothermic and exothermic data were evaluated from the thermograms obtained from this temperature program. The studies were carried out in nitrogen atmosphere (Watkins et al., 2015).

FTIR Analysis

In the study, SHIMADZU brand model device was used. In the study, measurements were made between 4000-400 cm⁻¹. Pellets were prepared with KBr and measurements were made (Watkins et al., 2015).

Spectroscopic Analyses

In the study, in the comparison phase of extraction efficiency, Lambda 25 brand PERKIN ELMER model spectrophotometer system was used.

Sample Preparation

2 g of dried lavender fibers were taken and kept in 20 mL %0,5, %1,0, %2, %4, %6, %8, %10, ve %15 sodium hydroxide solution for 30 min at ambient temperature. In order to increase the yield, extractions were carried out in an ultrasonic water bath. The fibers were washed with plenty of water to remove alkali residues on the fiber surface. The processed fibers were then dried in an oven at 80°C for 48 h (Teli & Jadhav, 2017).

2 g of dried lavender fibers were taken and kept in 20 mL of 0.5%, 1.0%, 2%, 4%, 6%, 8%, 10%, and 15% potassium hydroxide solution for 30 min at ambient temperature. Extractions were carried out in an ultrasonic water bath to increase the yield. The fibers were washed with plenty of water to remove alkali residues on the fiber surface. The processed fibers were then dried in an oven at 80 ° C for 48 h (Tang et al., 2020).

Results and Discussion

DSC Results

DSC, one of the most preferred thermal analysis systems, is one of the most widely used techniques to study the physico-chemical properties of polymers and to monitor the structural dependence on thermal degradation of natural lignocellulosic fibers. With DSC, two important temperature values are considered in the process of understanding and interpreting the structure of the polymers obtained. The first one is the Glass Transition Temperature (T_g) and the other one is the Crystal Melting Point (T_m). In our study, firstly, the curves obtained from DSC studies of lignin were analyzed and T_g and T_m values were calculated using the thermograms obtained. The T_g value of lignin is primarily influenced by molecular weight, but also by factors such as thermal history, the presence of low molecular weight contaminants (including water and solvents) and crosslinking (Hodge, 1994; Rials & Glasser, 1990).

In conventional DSC studies, the glass transition temperature (T_g) of a polymer is obtained from the second heating scan, while the first scan (above its T_g) is usually used to remove the thermal history stored in the glassy state of the polymer. T_g is an important thermal property of lignin. However, it is not easy to obtain an accurate value due to the inhomogeneous chemical structure, composition and water content of the lignin obtained after extraction (Aminzadeh et al., 2017). This difficulty can be attributed to the heterogeneity of lignin chemistry as well as the wide molecular weight distributions caused by isolation procedures.

In general, T_g depends on the molecular weight of the polymer and has been found at temperatures between 90 and 180°C for non-derivatized lignins (Cachet et al., 2014; Crestini et al., 2011; Sevastyanova et al., 2014). Furthermore, the glass transition temperature of lignins is influenced by the content of both phenolic hydroxyl and methoxyl groups (syringyl content) as well as the degree of condensation (number of C-C linkages) (Cachet et al., 2014; Cazacu et al., 2013; Doherty et al., 2011).

In the DSC degradation curves of lignin obtained using NaOH-water mixture in Figure 1, the peak with a maximum in the range of 39-56°C in a broad endothermic region corresponds to the dehydration temperature (T_{dehyd}) of lignin. In addition, the glass transition temperature (T_g) of lignin was measured in the range of 100-150°C. In their study, Ház et al. (2019) measured the T_{dehyd} value between 76,7°C; Tejado et al. (2007), measured the T_g value between 100-138°C. Gordobil et al. (2014), measured the T_g value between 88-154°C in lignin species isolated from spruce and eucalyptus. Sameni et al. (2014), gave the T_g value of lignin obtained from wood and eucalyptus waste between 130-190°C.

The large/different molecular weight of lignin has been attributed to its chemically heterogeneous properties and also to isolation procedures. In general, T_g depends on the molecular weight of the polymer and was found at temperatures between 90 and 180°C for non-derivatized lignins .(Cachet et al., 2014; Crestini et al., 2011; Sevastyanova et al., 2014) Furthermore, the T_g values of lignins depend on the content of both phenolic hydroxyl and methoxyl groups (syringyl content), as well as on various molecular factors such as the number of C-to-C bonds, interchain hydrogen bonding, crosslinking density, rigid phenyl groups and molecular mass (Cachet et al., 2014; Cazacu et al., 2013; Doherty et al., 2011; Heitner et al., 2016).

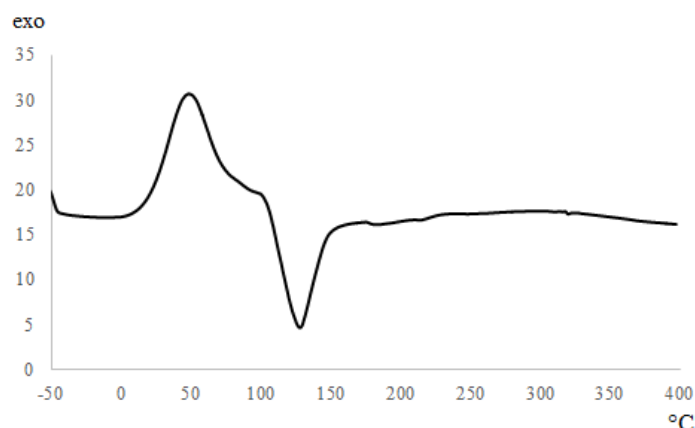


Figure 1. DSC thermogram of lignin extracts obtained using NaOH-water mixture

Table 1. DSC data of lignin extracts obtained using NaOH-water mixture

Ratio, %	T_{dehyd}	T_g	T_m
0.5	46	100	300
1	39	126	301
2	56	120	330
4	40	150	324
6	39	136	322
8	43	125	314
10	43	124	311
15	43	123	309

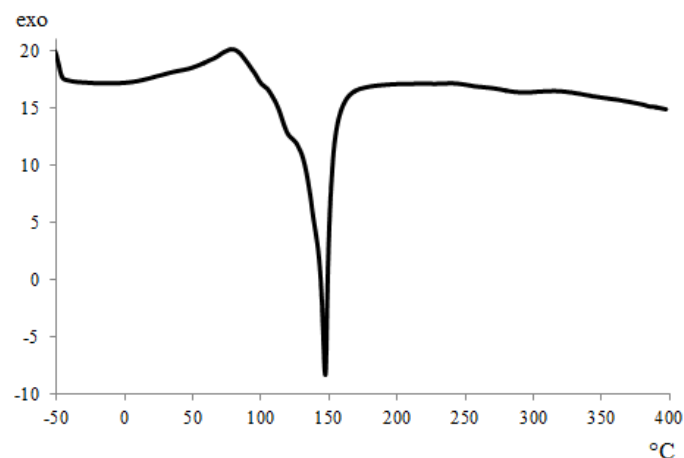


Figure 2. DSC thermogram of lignin extracts obtained using KOH-water mixture

Table 2. DSC data of lignin extracts obtained using KOH-water mixture

Ratio, %	T _{dehyd}	T _g	T _m
0.5	36	131	299
1	38	147	300
2	42	111	306
4	47	150	320
6	63	146	327
8	55	151	306
10	50	157	318
15	55	146	311

Lignin with various oxygen-containing functional groups belonging to lignin thermally decomposes over a wide temperature range and their degradation occurs at different temperatures. The cleavage of functional groups results in the formation of low molecular weight products, while at higher temperatures the complete rearrangement of the lignin backbone leads to 30-50% carbonization and the release of volatile products. The breakage of aryl-ether bonds leads to the formation of highly reactive and unstable free radicals that can further react through rearrangement, electron abstraction or radical-radical interactions to form highly stable products (Afifi et al., 1989). The presence of water facilitates oxygen-assisted decomposition of lignin (Butt & Kalsi, 2006).

Lignin obtained when the predominant Aryl-ether bonds form more than half of the inter-unit bonds has lower thermal stability. Therefore, they can be degraded at low temperatures, even below 310°C. β -ether bonds have different pyrolytic cleavage mechanisms depending on the side chain structure of the lignin. Methyl-, dimethyl-, ethyl- and vinylphenols are formed from the corresponding guaiacol intermediates by cleavage of O-C (alkyl) and O-C (aryl) bonds and show increased yields at high temperatures. Demethylation of dimethoxy groups leads to the conversion of phenols to pyrocatecho at 350-450°C, when pyrolysis is almost complete (Murwanashyaka et al., 2001).

Cleavage of the aromatic C-O bond in lignin leads to the formation of one-oxygen atom products, while cleavage of the methyl C-O bond forms two-oxygen atom products. Cleavage of the side chain C-C bond occurs between the aromatic ring and the α -C atom. Low heating rates favor the formation of oxygen-containing compounds, while rapid heating rates lead to the formation of more hydrocarbons and alkyl-phenol derivatives (Demirbas et al., 2004)

TGA Results

Thermal degradation in polymers is another important parameter to be known in order to establish thermal processing and lifetime conditions. The lignin molecule has great potential for use as a biomaterial. It can be used as a macromonomer or as a filler in other natural and synthetic polymers. The thermal properties of lignin are therefore important when considering the effect of adding lignin to the polymeric system. In general, high molecular weight, high purity and high thermal stability are important properties for polymers.

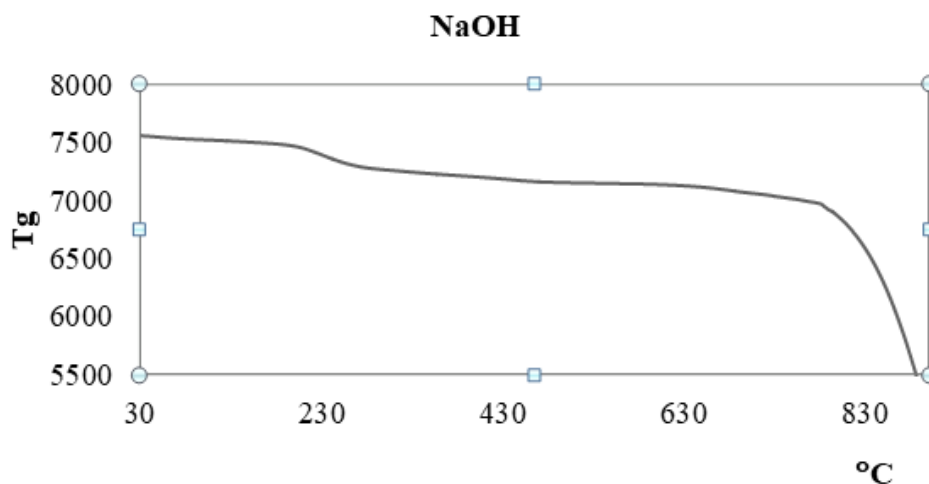


Figure 3. TGA thermogram of lignin extracts obtained using NaOH-water mixture

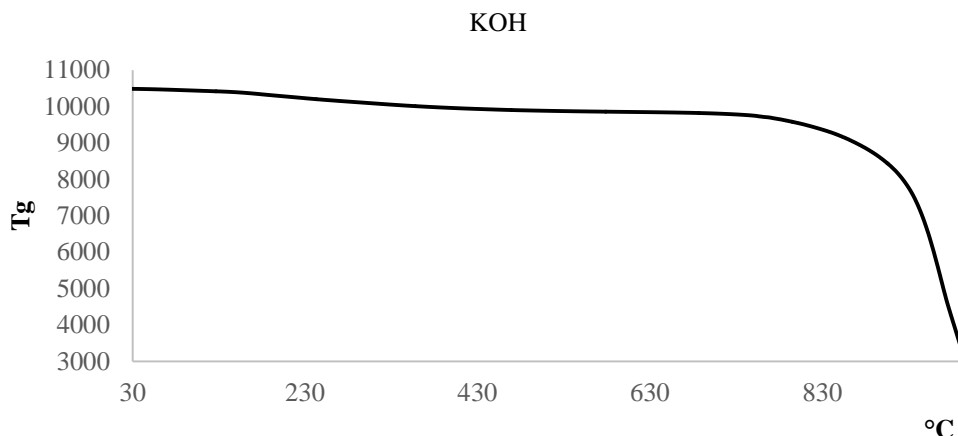


Figure 4. TGA thermogram of lignin extracts obtained using KOH-water mixture

Thermogravimetric (TG) and first derivative (DTG) curves obtained for lignins extracted under nitrogen atmosphere are presented. All lignin samples exhibited several distinct weight loss stages.

Table 3. TGA results of lignin extracts obtained using NaOH-water mixture

Ratio, %	%5	%10	%25	Residue amount at 900°C, %
0.5	300.04	401.13	402.52	38.22
1	345.62	392.63	401.11	88.91
2	430.68	807.95	879.43	29.67
4	783.60	842.41	888.13	28.21
6	91.83	128.73	890.11	25.33
8	93.12	250.33	879.36	35.13
10	96.43	381.52	855.13	36.23
15	97.50	228.11	833.21	40.13

Lignin degradation isolated with NaOH occurs over a wide temperature range. At 0.5% NaOH, 5% mass loss is approximately 300.04°C, while at 15% KOH this temperature is 97.50°C. As the NaOH content increases, 5% mass losses decrease to 100°C and below. The first stage (30-184°C) is a mass loss due to the evaporation of physically adsorbed moisture. The measured values for 0.5%, 1%, 2%, 4%, 6%, 8%, 10%, 15% are 99°C, 93°C, 184°C, 113°C, 69°C, 71°C, 55°C and 59°C, respectively. The second stage degradation curve (114-265°C) is mainly attributed to the dehydration of chemically bound water and hydroxyl groups in lignin (Zhao and Liu, 2010). The measured values for 0.5%, 1%, 2%, 4%, 6%, 8%, 10%, 15% are 184°C, 132°C, 265°C, 211°C, 122°C, 129°C, 114°C and 131°C, respectively.

The third stage corresponds to the partial decomposition of carboxylic and anhydride groups and hemicellulose remaining in the kraft lignin (Bal et al., 2004). The measured values for 0.5%, 1%, 2%, 4%, 6%, 8%, 10%, 15% are 760°C, 758°C, 770°C, 743°C, 688°C, 675°C, 641°C and 635°C, respectively. Lignin is the most difficult to decompose compared to cellulose and hemicellulose. Its decomposition occurs slowly over the entire temperature range from ambient to 900°C, but at a very low mass loss rate (Yang et al., 2007). Its degradation increased to 770°C up to 2% and then decreased again.

Table 4. TGA results of lignin extracts obtained using KOH-water mixture

Ratio, %	%5	%10	%25	Residue amount at 900°C, %
0.5	396.36	819.33	927.48	72.26
1	742.47	812.51	870.59	35.54
2	543.66	804.83	868.78	35.70
4	371.13	788.48	859.10	39.71
6	50.11	773.55	849.12	45.76
8	90.34	242.99	600.00	34.23
10	97.41	375.52	848.35	38.14
15	96.71	111.49	859.67	41.45

Lignin degradation isolated with KOH also occurs over the same wide temperature range as NaOH. At 0.5% KOH, the 5% mass loss was approximately 396.36°C, while at 15% KOH this temperature was calculated as 96.71°C. As the KOH content increased, the 5% mass losses decreased to 100°C and below.

The first stage (30-145°C) is a mass loss due to the evaporation of physically adsorbed moisture. The measured values for 0.5%, 1%, 2%, 4%, 6%, 8%, 10%, 15% are 118°C, 133°C, 120°C, 145°C, 141°C, 72°C, 52°C and 55°C, respectively. The second stage degradation curve (102-359°C) is mainly attributed to the dehydration of chemically bound water and hydroxyl groups in lignin (Zhao and Liu, 2010). The measured values for 0.5%, 1%, 2%, 4%, 6%, 8%, 10%, 15% are 258°C, 224°C, 260°C, 359°C, 204°C, 138°C, 102°C and 116°C, respectively. The third stage corresponds to the partial decomposition of carboxylic and anhydride groups and hemicellulose remaining in the kraft lignin (Bal et al., 2004). This stage is very sharp in the thermograms. The measured values for 0.5%, 1%, 2%, 4%, 6%, 8%, 10%, 15% are 730°C, 740°C, 758°C, 740°C, 738°C, 688°C, 612°C and 630°C, respectively.

Lignin is the most difficult to decompose compared to cellulose and hemicellulose. Its decomposition occurs slowly over the entire temperature range from ambient to 900°C, but at a very low mass loss rate (Yang et al., 2007). Its degradation increased to 758°C up to 2% and then decreased again.

FTIR Results

Lignin is one of the most complex biopolymers as it contains a variety of bonds and functional groups. Its complex nature results in overlapping infrared spectra, making it difficult to read the peaks accurately

Table 5. FTIR bands of lignin

Wavelength (cm ⁻¹)	IR Band description
3427-3442	O-H stretching in aliphatic and phenolic OH structures
2924-2938	C-H stretching in methyl groups
2842-2854	C-H stretching in methylene groups
1711-1730	C=O stretching in unconjugated ketones and carboxyl groups; saturated esters
1611	Stretching of C=O conjugated to aromatic rings (conjugated carbonyl)
1590-1598	Aromatic skeleton ring vibration (S > G) + C=O stretching
1560-1514	Aromatic skeleton ring vibrations (G > S)
1452-1466	C-H asymmetric deformations in methyl and methylene groups
1419-1427	Aromatic skeleton ring vibrations
136-1378	Aliphatic C-H symmetric deformation in methyl (not methoxyl) + O-H deformation in phenols
1328-1330	S ring vibration + G ring substitution in position 5
1264-1269	Ring respiratory vibration and C-O stretching
1217-1235	C-O stretching in phenols and ethers
1222-1149	C-H stretching in G ring and Aromatic C-H bonds in plane deformation (S)
1082	C-O stretching of secondary alcohols and aliphatic ethers
1034	Aromatic C-H in-plane deformations in G units + C-O deformations in primary alcohols.
835/855	Aromatic C-H out-of-plane deformation (only in GS and H lignin types)

In lignin, the band around 3427 cm⁻¹ corresponds to the frequency of O-H stretching in aliphatic or phenolic hydroxyl groups. The bands at 2924 cm⁻¹ to 2938 cm⁻¹ and 2842 cm⁻¹ to 2854 cm⁻¹ indicate C-H stretching in methyl and methylene groups, respectively. In kraft lignin, the broad band around 1661 cm⁻¹ corresponds to an aromatic conjugated carboxylate structure; the band around 3427 cm⁻¹ corresponds to the frequency of O-H stretching in aliphatic or phenolic hydroxyl groups. FT-IR spectra of all lignin samples show bands at about 1600, 1515 and 1425 cm⁻¹ corresponding to aromatic ring vibrations of the phenyl propane skeleton. In kraft lignin, the common weak bands around 1367 cm⁻¹ to 1378 cm⁻¹ are due to aliphatic C-H symmetric deformation in methyl groups and O-H deformation in phenolic groups. The bands around 1264 cm⁻¹ to 1269 cm⁻¹ indicate the vibration of the guaiacyl ring.

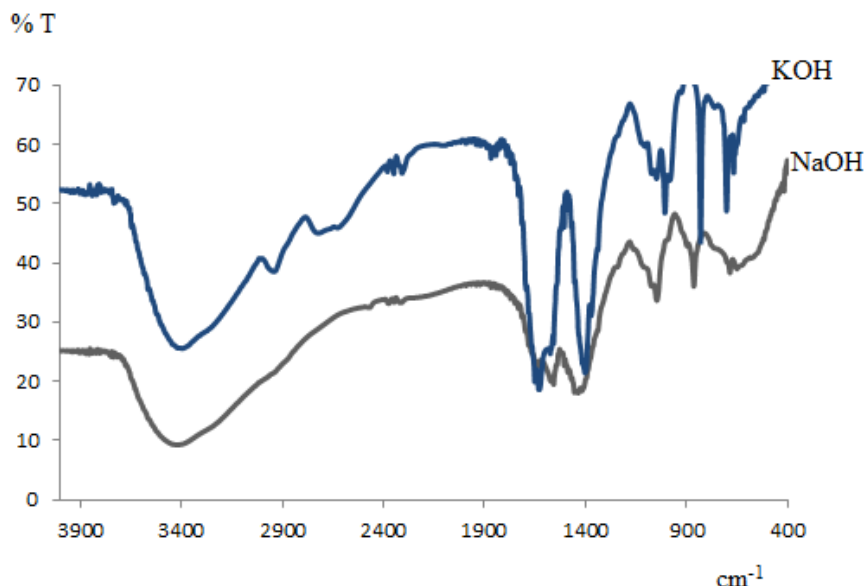


Figure 5. FTIR spectra of NaOH and KOH extracts

UV Results

Given the presence of lignins in the spectroscopic analysis, total phenolic analysis was performed from the initial residue for lignin determination.

Table 6. Total phenolic results of lignin extracts obtained using NaOH-water mixture

Ratio, %	A
0.5	0.1740
1	0.2359
2	0.1614
4	0.2749
6	0.3272
8	0.3793
10	0.3412
15	0.3512

Table 7. Total phenolic results of lignin extracts obtained using KOH-water mixture

Ratio, %	A
0.5	0.1487
1	0.2563
2	0.1526
4	0.2409
6	0.2811
8	0.3090
10	0.3735
15	0.4511

The total phenolic absorbance value of both NaOH and KOH 2% mixture is lower than the other values. The main components of lignin are phenolics. The decrease in the amount of phenolics indicates that lignin is isolated from lavender. The highest lignin yield was obtained at 2% of both bases. These results are similar to the third stage temperature values obtained from TGA. The same amount of starting material was used in both studies. When the absorbance values obtained were compared, higher lignin isolation was realized with 2% 2% KOH. Lignins contain many functional chemical groups such as hydroxyl (phenolic or alcoholic), methoxyl, carbonyl and carboxyl in various amounts depending on the source and isolation process applied (Gosselink et al., 2004; Sun et al., 2000)

Conclusion

In this study, it was observed that analytical techniques such as DSC, TGA, FTI) and UV play an important role in lignin characterization and applications. These techniques were used to determine the thermal properties, chemical composition and structural properties of lignin.

The combination of these analytical techniques provides a comprehensive approach to lignin characterization. DSC, TGA, FTIR and UV are used as powerful tools to evaluate the thermal properties, thermal stability, chemical composition and structural properties of lignin-based materials.

As a result, analytical techniques such as DSC, TGA, FTIR and UV provide valuable scientific information in lignin research and applications. The use of these techniques is an important step in the development of lignin-based products, the establishment of waste management strategies and the development of sustainable industries. In future studies, it is expected that lignin applications will be further expanded and diversified with further improvement and optimization of these analytical techniques.

Scientific Ethics Declaration

The authors declare that the scientific ethical and legal responsibility of this article published in EPSTEM Journal belongs to the authors.

Acknowledgements or Notes

* This article was presented as an oral presentation at the International Conference on Basic Sciences and Technology (www.icbast.net) held in Antalya/Turkey on November 14-17, 2024.

* This work was supported by Burdur Mehmet Akif Ersoy University Scientific Research Projects (BAP) Coordinator under the Project number of [0796-YL-21].

References

- Achinivu, E. C. (2018). Protic ionic liquids for lignin extraction—A lignin characterization study. *International Journal of Molecular Sciences*, 19(2).
- Afifi, A. I., Hindermann, J. P., Chornet, E., & Overend, R. P. (1989). The cleavage of the arylOCH₃ bond using anisole as a model compound. *Fuel*, 68(4), 498–504.
- Alonso, D., Etienne, R. S., & Mckane, A. J. (2006). The merits of neutral theory. *Trends in Ecology & Evolution*, 21(8), 451–457.
- Aminzadeh, S., Zhang, L., & Henriksson, G. (2017). A possible explanation for the structural inhomogeneity of lignin in LCC networks. *Wood Science and Technology*, 51(6), 1365–1376.
- Boerjan, W., Pilate, G., Morreel, K., Messens, E., Baucher, M., Van Doorselaere, J., Chen, C., Meyermans, H., Pollet, B., Lapierre, C., Jouanin, L., Leplé, J.-C., Ralph, J., Marita, J., Guiney, E., Schuch, W., Petit-Conil, M., & Halpin, C. (2003). Genetic engineering of lignin biosynthesis in poplar and effects on Kraft pulping. *Polyphenols 2002: Recent Advances in Polyphenols Research*, 34–49. <http://hdl.handle.net/1854/LU-216843>
- Butt, A. M., & Kalsi, A. (2006). Inwardly rectifying potassium channels (Kir) in central nervous system glia: A special role for Kir4.1 in glial functions. *Journal of Cellular and Molecular Medicine*, 10(1), 33–44.
- Cachet, N., Camy, S., Benjelloun-Mlayah, B., Condoret, J. S., & Delmas, M. (2014). Esterification of organosolv lignin under supercritical conditions. *Industrial Crops and Products*, 58, 287–297.
- Cazacu, G., Capraru, M., & Popa, V. I. (2013). Advances concerning lignin utilization in new materials. *Advanced Structured Materials*, 18, 255–312.
- Cerro, D., Bustos, G., Villegas, C., Buendia, N., Truffa, G., Godoy, M. P., Rodríguez, F., Rojas, A., Galotto, M. J., Constandil, L., Yáñez-S, M., Romero, J., & Torres, A. (2020). Effect of supercritical incorporation of cinnamaldehyde on physical-chemical properties, disintegration and toxicity studies of PLA/lignin nanocomposites. *International Journal of Biological Macromolecules*, 167, 255–266.
- Crestini, C., Melone, F., Sette, M., & Saladino, R. (2011). Milled wood lignin: A linear oligomer. *Biomacromolecules*, 12(11), 3928–3935.

- Demirbas, N., Karaoglu, S. A., Demirbas, A., & Sancak, K. (2004). Synthesis and antimicrobial activities of some new 1-(5-phenylamino-[1,3,4]thiadiazol-2-yl)methyl-5-oxo-[1,2,4]triazole and 1-(4-phenyl-5-thioxo-[1,2,4]triazol-3-yl)methyl-5-oxo-[1,2,4]triazole derivatives. *European Journal of Medicinal Chemistry*, 39(9), 793–804.
- Doherty, W. O. S., Mousavioun, P., & Fellows, C. M. (2011). Value-adding to cellulosic ethanol: Lignin polymers. *Industrial Crops and Products*, 33(2), 259–276.
- Eraslan, T. (2020). *Daphne oleoides*'den sentezlenen gümüş nanopartiküllerin antioksidan aktivitesinin değerlendirilmesi. <https://acikerisim.erbakan.edu.tr/xmlui/handle/20.500.12452/7149>
- Gordobil, O., Egüés, I., Llano-Ponte, R., & Labidi, J. (2014). Physicochemical properties of PLA lignin blends. *Polymer Degradation and Stability, Complete* (108), 330–338.
- Gosselink, R. J. A., Abächerli, A., Semke, H., Malherbe, R., Käuper, P., Nadif, A., & Van Dam, J. E. G. (2004). Analytical protocols for characterisation of sulphur-free lignin. *Industrial Crops and Products*, 19(3), 271–281.
- Heitner, C., Dimmel, D., & Schmidt, J. (2016). Lignin and lignans: Advances in chemistry. *Lignin and Lignans: Advances in Chemistry*, 1–669.
- Hodge, I. M. (1994). Enthalpy relaxation and recovery in amorphous materials. *Journal of Non-Crystalline Solids*, 169(3), 211–266.
- Kapluhan, E. (2014). Enerji coğrafyası açısından bir inceleme: biyokütle enerjisinin dünya'daki ve türkiye'deki kullanım durumu. *Marmara Coğrafya Dergisi*, 30, 97–125. <https://dergipark.org.tr/tr/pub/iucogرافya/issue/25074/264647>
- Méchin, V., Baumberger, S., Pollet, B., & Lapierre, C. (2007). Peroxidase activity can dictate the in vitro lignin dehydrogenative polymer structure. *Phytochemistry*, 68(4), 571–579.
- Meister, J. J. (2002). Modification of lignin. *Journal of Macromolecular Science - Polymer Reviews*, 42(2), 235–289.
- Murwanashyaka, J. N., Pakdel, H., & Roy, C. (2001). Step-wise and one-step vacuum pyrolysis of birch-derived biomass to monitor the evolution of phenols. *Journal of Analytical and Applied Pyrolysis*, 60(2), 219–231.
- Quesada-Medina, J., López-Cremades, F. J., & Olivares-Carrillo, P. (2010). Organosolv extraction of lignin from hydrolyzed almond shells and application of the delta-value theory. *Bioresource Technology*, 101(21), 8252–8260. <https://doi.org/10.1016/J.BIORTECH.2010.06.011>
- Rashid, T., Gnanasundaram, N., Appusamy, A., Kait, C. F., & Thanabalan, M. (2018). Enhanced lignin extraction from different species of oil palm biomass: Kinetics and optimization of extraction conditions. *Industrial Crops and Products*, 116, 122–136.
- Rials, T. G., & Glasser, W. G. (1990). Multiphase materials with lignin: 5. Effect of lignin structure on hydroxypropyl cellulose blend morphology. *Polymer*, 31(7), 1333–1338.
- Sameni, J., Krigstin, S., Dos, D., Rosa, S., Leao, A., & Sain, M. (2014). Thermal characteristics of lignin residue from industrial processes. *BioResources*, 9(1), 725–737. https://jstatm.textiles.ncsu.edu/index.php/BioRes/article/view/BioRes_09_1_725_Sameni_Thermal_Characteristics_Lignin_Residue
- Sevastyanova, O., Helander, M., Chowdhury, S., Lange, H., Wedin, H., Zhang, L., Ek, M., Kadla, J. F., Crestini, C., & Lindström, M. E. (2014). Tailoring the molecular and thermo-mechanical properties of Kraft lignin by ultrafiltration. *Journal of Applied Polymer Science*, 131(18), 9505–9515.
- Sun, R., Tomkinson, J., Mao, F. C., & Sun, X. F. (2000). *Physicochemical characterization of lignins from rice straw by hydrogen peroxide treatment*. <https://www.semanticscholar.org/paper/physicochemical-characterization-of-lignins-from-by-sun-tomkinson/28fdda7ffeda7ec8b5d3c1d76baf484e2d6da739>
- Tang, P. L., Hassan, O., Yue, C. S., & Abdul, P. M. (2020). Lignin extraction from oil palm empty fruit bunch fiber (OPEFBF) via different alkaline treatments. *Biomass Conversion and Biorefinery*, 10(1), 125–138.
- Tejado, A., Peña, C., Labidi, J., Echeverria, J. M., & Mondragon, I. (2007). Physico-chemical characterization of lignins from different sources for use in phenol–formaldehyde resin synthesis. *Bioresource Technology*, 98(8), 1655–1663.
- Teli, M., & Jadhav, A. (2017). Effect of mercerization on the properties of pandanus odorifer lignocellulosic fibre. *IOSR Journal of Polymer and Textile Engineering*, 04(01), 07–15.
- Watkins, D., Nuruddin, M., Hosur, M., Tcherbi-Narteh, A., & Jeelani, S. (2015). Extraction and characterization of lignin from different biomass resources. *Journal of Materials Research and Technology*, 4(1), 26–32.
- Wen, J. L., Xue, B. L., Xu, F., Sun, R. C., & Pinkert, A. (2013). Unmasking the structural features and property of lignin from bamboo. *Industrial Crops and Products*, 42(1), 332–343.
- Wen, J. L., Yuan, T. Q., Sun, S. L., Xu, F., & Sun, R. C. (2014). Understanding the chemical transformations of lignin during ionic liquid pretreatment. *Green Chemistry*, 16(1), 181–190.
- Wu, W., Jiang, B., Yang, L., & Jin, Y. (2017). Isolation of lignin from masson pine by liquid-liquid extraction based on complete dissolution in NaOH aqueous solution. *Bioresources*, 13(1), 231–240.

Yang, H., Yan, R., Chen, H., Lee, D. H., & Zheng, C. (2007). Characteristics of hemicellulose, cellulose and lignin pyrolysis. *Fuel*, 86(12–13), 1781–1788.

Author Information

Halil Sen

Burdur Mehmet Akif Ersoy University,
Industrial Engineering Department,
İstiklal Kampus,15030, Burdur-Türkiye
Contact e-mail: halilsen@mehmetakif.edu.tr

Hale Secilmis

Burdur Mehmet Akif Ersoy University,
Department of Chemistry,
İstiklal Kampus,15030, Burdur-Türkiye

Asem Assani

Burdur Mehmet Akif Ersoy University,
Burdur-Türkiye

Canan Sen

Burdur Mehmet Akif Ersoy University,
Burdur - Türkiye

To cite this article:

Sen, H., Secilmis, C., Assani, A. & Sen, C. (2024). Lignin extraction and characterization from lavender waste. *The Eurasia Proceedings of Science, Technology, Engineering & Mathematics (EPSTEM)*, 30, 28-38.

The Eurasia Proceedings of Science, Technology, Engineering & Mathematics (EPSTEM), 2024

Volume 30, Pages 39-46

ICBAST 2024: International Conference on Basic Sciences and Technology

Comparative Soil-Plant Relationship of *Pyrus* L. Species under *in Situ* and *Ex Situ* Conditions

Elman Iskender

Ministry of Science and Education of Azerbaijan Republic

Panah Muradov

Ministry of Science and Education of Azerbaijan Republic

Sabina Jafarzadeh

Ministry of Science and Education of Azerbaijan Republic

Abstract. This study conducts a comparative analysis of the soil-plant relationship for *Pyrus* L. species under both *in situ* and *ex situ* conservation environments. It highlights the significance of these conservation strategies, especially given the distinct botanical features of *Pyrus* L. species. The research involved selecting different species within the *Pyrus* genus and systematically gathering sample data. Various methodologies were used to assess both the chemical and physical properties of the soil, employing techniques such as soil texture analysis and nutrient profiling. The findings indicate clear differences in soil-plant interactions across these conservation methods, showcasing how *Pyrus* L. species adapt to their environments and the effectiveness of different protective measures. In particular, the results illustrate the impact of soil composition on plant health and growth in various conservation scenarios. The study concludes by discussing the implications of these findings and suggesting future actions to improve *in situ* and *ex situ* conservation practices. These statements aim to enhance our understanding of *Pyrus* L. species and refine conservation strategies, ultimately supporting the sustainability of these crucial plants.

Keywords: *Pyrus* L. , *In situ*, *Ex situ*, Soil, GIS.

Introduction

The interaction between soil and plants is essential for understanding ecosystem dynamics, particularly for fruit-bearing species like *Pyrus* L. (pear). This genus comprises various species that demonstrate distinct growth behaviors and adaptability to different soil conditions. Studying the comparative soil-plant relationship under *in situ* (natural) and *ex situ* (cultivated) environments provides crucial insights into the ecological needs and agricultural viability of *Pyrus* species. *In situ* settings enable plants to flourish in their native habitats, where optimal soil characteristics and beneficial microbial interactions are present. The author explored how various abiotic factors influence the cultivated dendroflora in Azerbaijan's northeastern region. The research examined the interactions between environmental conditions—such as soil quality, temperature, and moisture—and the growth and health of different tree species (Iskender et al., 2022). These interactions are vital for nutrient cycling and overall plant vitality. In contrast, *ex situ* environments, such as orchards or controlled settings, can significantly modify these relationships, potentially leading to varying growth results. Soil characteristics, such as texture, pH, and organic matter content, influence water retention and nutrient availability. Understanding how these factors affect *Pyrus* species can inform conservation and agricultural practices. The ability of *Pyrus* species to adapt to diverse soil types may reflect their evolutionary background and ecological roles.

Plant growth-promoting bacteria (PGPB) and other beneficial organisms are helping to tackle the challenges of modern agriculture. Recent scientific advancements have created new opportunities for both research and

commercial applications. In our current study, we compiled recent findings and expert insights on this topic. The overall conclusion is that PGPB are becoming increasingly important in agriculture globally, fostering more sustainable and eco-friendly farming practices while decreasing dependence on artificial fertilizers and chemicals (Kisvarga et al., 2023). The relationship between soil and the microbiome is a crucial and emerging area of scientific research today. The extensive use of Plant Growth-Promoting Bacteria (PGPB) could offer a solution to boost and sustain agricultural production while minimizing environmental harm. Recent advancements in genetic technology are also enhancing the capabilities of microorganisms, potentially accelerating their application in the phytoremediation of metal-contaminated soils (Szilvia, et al ,2023).

The phytoremediation process that relies solely on plants can be slow and may limit metal uptake, particularly in soils with high levels of pollutants. (Hansda et al, 2022). Soil health significantly influences the effectiveness of phytoremediation, as it affects both plant growth and the microbial community. Plant–microbe interactions in the soil are crucial for helping plants adapt to metal-contaminated environments and for enhancing their growth. By exploring these interactions, we can improve microbial-assisted phytoremediation and effectively remediate polluted soils (Ma , 2019).

In this study, the authors conducted an inventory of tree and shrub species found on the Huzurlu High Plateau in Gaziantep, Turkey. The research aimed to document the biodiversity of the region and to analyze the ecological characteristics of the identified species. The findings contribute to a better understanding of the local flora and provide valuable information for conservation efforts and sustainable land management practices in the area (Iskender et al., 2005).

The research findings suggest that the fungal biota affecting fruits and berries in Azerbaijan is not at a critical level, with fungal diseases not exceeding a prevalence of 16.1%. This situation is influenced by soil factors, as soil health plays a crucial role in supporting plant immunity and influencing the prevalence of fungal pathogens. However, given the reality of global issues, this statistic should still be viewed as concerning. Therefore, prioritizing the improvement of soil conditions and implementing preventive measures against these threats is essential for safeguarding crop health (Bakshaliyeva et al., 2020).

Numerous multifunctional and agriculturally significant microbes reside within plant internal tissues (Gupta et.al, 2021). These endophytic bacteria can help alleviate stress in plants, but their effectiveness depends on certain conditions, including the presence and concentration of volatile and bioactive compounds such as ethylene, auxins, phenols, polysaccharides, siderophores, and organic acids (Kahtani et al., 2020).

The study focused on the ecological conditions of Absheron and how they could support the growth and survival of these species. The findings underscore the importance of conservation efforts and provide a framework for future introductions, aiming to enhance biodiversity and restore native ecosystems in the region (Iskenderov, 1993)

In this research work soil quality, encompassing factors like nutrient availability, pH, and organic matter content, can significantly influence pollen viability and fertility. *In situ* conditions usually offer a more complex soil ecosystem that enhances nutrient cycling and microbial interactions, resulting in healthier plants with more viable pollen. In contrast, *ex situ* conditions often consist of cultivated soils with reduced biological diversity, which may not provide optimal growth conditions and could lead to diminished pollen quality and fertility (Jafarzadeh & Iskender, 2024).

Significance of *in Situ* and *Ex Situ* Conservation

There are various species of wild fruit plants that are distributed in the forests of Azerbaijan, including the areas in the northeastern part of the Greater Caucasus. These plant species are a source of raw materials for use in various fields of food and industry. Among these plants, pear species that grow naturally in the study area are of special importance in providing the population of the Republic with healthy ecological food products and in terms of other uses. One of the important aspects of the researched plants is that, in addition to being one of the main components of the forest type in the vegetation, research materials have special roles in the formation of associations or formations.

Wildlife and natural resource conservation involve safeguarding, preserving, managing, and restoring ecosystems, including forests and bodies of water. By prioritizing biodiversity conservation, we can secure the

survival of numerous species and habitats facing threats from human activities. There is an urgent need, not only to manage and conserve the biotic wealth, but also restore the degraded ecosystems (Mc Gowen et al., 2016).

In situ conservation involves preserving genetic resources directly within their natural habitats, whether it's safeguarding the genetic diversity of plant species within their native forests or protecting the genetic makeup of animal populations within their natural habitats. It is the process of protecting an endangered plant or animal species in its natural habitat, either by protecting or cleaning up the habitat itself, or by defending the species from predators. It is applied to conservation of agricultural biodiversity in agro forestry by farmers, especially those using unconventional farming practices. *In situ* conservation is being done by declaring area as protected area (Qinglin et al., 2022)

Method

In the 21st century, soil monitoring has gained paramount importance due to climate change, water scarcity issues, and the vulnerability of ecosystems. The necessity to monitor soil environments has become imperative in order to safeguard and preserve them. The soil resource must be recognized as a dynamic living system that emerges through a unique balance and interaction of its biological, chemical, and physical components (Karlen et al., 1997).

Monitoring soil serves not only to manage soil moisture and ensure plant health but also plays a crucial role in understanding various natural processes and water resources, both at the local and regional levels. While many soil sampling methods necessitate composite soil samples obtained by physically mixing soil cores, environmental soil monitoring employs a diverse range of techniques to ensure comprehensive assessment. Utilizing remote sensing for monitoring soil salinity is crucial. Imbalances in soil salinity can adversely affect water quality, crop yields, and infrastructure, underscoring the importance of timely detection and management. Measuring the pH: As many factors such as pollution, climate, and the environment can affect the pH in soil, also helps us understand soil environments.

GIS Applications: *Ex situ* researches were conducted in the Central Botanical Garden of ANAS in 2016. Highly cultivated (N4021'18.1", E4948'51.0"), cultivated (N4021'18.0", E4948'42.0") and poorly cultivated (N4121'26.38", E4848'53.92") 3 soil profile were placed under the soil. Based on the monograph "Modern soil cover of the Greater Caucasus" prepared by the team of the Institute of Soil Science and Agrochemistry of ANAS (M.P. Babayev, Ch.M. Jafarova, A.M. Jafarov, X.M. Gasimov and others) and the 1:100000 scale soil, we determined that *Pyrus* L. species are distributed in situ on northeastern slope of the Greater Caucasus mainly on carbonate mountain-brown, grayish mountain-brown, mountain brown-meadow and mountain gray-brown soils. We placed 4 cuts in Khizi (Altiaghach vil. N40°33'10.60", E48°37'47.04", June 2017) and Guba (Second Nugadi vil. N41°18'47.01", E48°35'47.97" 2017, July) mountain-brown grass, in Siyazan (Dağ Gushchu vil. N40°59'46.09", E48°57'38.20", 2017, July) and in Shabran (Pirabadil vil. N41°12'5.65", E48°48'2.54", 2017, August) under mountain-gray-brown soils.

Granulometric calculation of soil from soil taken from the study area. – N.A. Kachinsky (Kachinsky, 1958), humus – I.V. Tyurin (Mineeva, 1989), total nitrogen Kyeldal (Mineeva, 1989), total phosphorus - Lawrence; total potassium – Smith's method; environmental response - with pH meter, dry residue by Ivanov's method (according to specific gravity); absorbed bases (Ca+Mg) – D.V. Ivanov method, CO₂-Scheibler method; (Mineeva, 1989), carbonation was determined according to CO₂ (Arinushkina, 1970).

The method of using a hydrometer was chosen to determine the soil texture, while the pH of the soil was analyzed in a soil-water suspension with a ratio of 1:2.5. The method of using a hydrometer was chosen to determine the soil texture, while the pH of the soil was analyzed in a soil-water suspension with a ratio of 1:2.5. Cation exchange capacity (CEC) was determined by saturating the samples with sodium acetate; exchangeable cations (Na, K, Ca and Mg) with ammonium acetate; electrical conductivity (EC) in 1.0:2.5 soil-water saturation and organic matter using Walkley-Black method (Arinushkina, 1970; Durak, Saltali, Oghuz & Kilich, 2007).

Soil is a dynamic natural body developed as a result of pedogenic processes through weathering of rocks, consisting of mineral and organic constituents, possessing definite chemical, physical, mineralogical and biological properties, having a variable depth over the surface of the earth, and providing a medium for plant growth. Soil supports terrestrial life through five processes: (1) biomass productivity, (2) restoration and resilience of ecosystems, (3) purification of water, (4) detoxification of pollutants, and (5) cycling of C, N, P, S,

and H₂O (Karlen et al., 1997).

Results and Discussion

The soil-forming rocks of the Central Botanical Garden are composed of sea and lake sediments, fish-ear limestones, gypsum-saline and sandy Absheron clays and their weathering products. M.P. Babayev and etc. based on their research, it was determined that raw and irrigated cultivated types of gray-brown soils are distributed in the area. As we mentioned, based on the laboratory analysis, it was determined that the amount of humus in irrigated gray-brown soils is higher than in raw soils, so the amount of humus in the planting layer (AUa 25-45 cm) of highly cultivated soils is 1.48-2.67%, cultivated gray-brown it varies between 1.38-1.85% in soils, and between 0.44-0.75% in the poorly cultured version. Regarding the amount of total N, nitrogen in the soil of the Central Botanical Garden ranges from 0.07-0.20%, and the ratio of C:N varies between 5.6-7.2. In the irrigated gray-brown soils of the area, the amount of carbonates is high in the upper layer (16-18%), and decreases along the profile (9-14%) (Table 1.).

Table 1. Fertility indicators of central botanical garden soils

Soil profile number	Depth of genetic layers (cm)	Humus, %	Total nitrogen %	Total P ₂ O ₅ %	Total K ₂ O, %	pH (water)	Absorbed sum of bases, mq/ekv	Dry residue,%	Granulometric composition		CO ₂ , %	CaCO ₃ , %
									<0,01 mm	<0,001 mm		
Highly cultivated irrigated gray-brown soil												
1	AU'a 0-25	2,67	0,20	0,18	1,9	7,8	23,0	0,139	32,0	9,0	2,2	18,2
	AU'a 25-45	1,48	0,12	0,16	1,6	7,9	22,0	0,200	29,9	10,1	2,3	15,9
	Bca 45-82	0,52	0,05	0,12	1,4	8,1	19,8	0,122	33,6	13,8	2,4	17,3
	Cl 82-120	0,20	-	0,09	1,0	8,2	17,7	0,130	22,0	8,5	2,1	11,0
	CII 120-153	0,18	-	-	-	8,4	18,4	0,141	29,8	5,7	2,1	-
Cultivated irrigated gray-brown soil												
2	AU'a 0-24	1,85	0,15	0,15	1,7	7,9	23,2	0,082	44,0	19,9	2,0	19,8
	AU'a 24-56	1,38	0,12	0,12	1,3	7,8	18,7	0,112	48,9	15,2	1,9	20,7
	Bca 56-82	0,66	0,05	0,12	1,2	8,0	17,6	0,110	42,3	18,0	2,1	19,0
	Cs 82-113	0,45	-	0,11	0,8	8,1	16,5	0,114	38,0	14,2	2,2	14,7
	Cs 113-150	0,19	-	-	-	8,2	17,1	-	49,3	18,8	-	10,2
Poorly cultivated gray-brown soil												
3	Ala 0-18	0,75	0,07	0,12	1,3	8,0	15,0	0,090	13,8	5,7	2,1	16,0
	B/C 18-34	0,44	0,06	0,11	1,2	8,1	15,7	0,071	15,9	6,9	2,2	15,7
	Cl 34-85	0,38	0,03	0,10	1,0	8,3	15,8	0,078	18,0	5,0	2,3	19,0
	CII 85-120	0,23	-	0,09	0,5	8,4	14,0	0,093	21,4	6,4	2,2	21,9
	Cs 120-165	0,18	-	-	-	8,5	13,2	0,082	30,5	6,2	2,0	22,3

According to the degree of provision of absorbed bases, the highly and medium cultivated gray-brown soils of the Central Botanical Garden are moderately (23.1-23.2 mg-eq), and the poorly cultivated variant is provided to a low extent (15.0-15.7 mg-eq). The amount of Ca²⁺ cation is 46-62% of the total absorbed bases, and the amount of Mg²⁺ is high, 17-39%. The fact that the amount of Na⁺ cation in the profile of these soils is 6.5-8.0% indicates that the soils are acidic. Based on the monograph "Modern soil cover of the Greater Caucasus" prepared by the team of the Institute of Soil Science and Agrochemistry of ANAS (M.P. Babayev, Ch.M. Jafarova, A.M. Jafarov, Kh.M. Gasimov and others), we determined that *Pyrus* L. species are distributed in situ on the northeastern slope of the Great Caucasus mainly on carbonate mountain-brown, grayish mountain-brown, mountain brown-meadow is (6.7-8.3) and mountain gray-brown soils (Babayev et al., 2017).



Altaghach, Khizi district

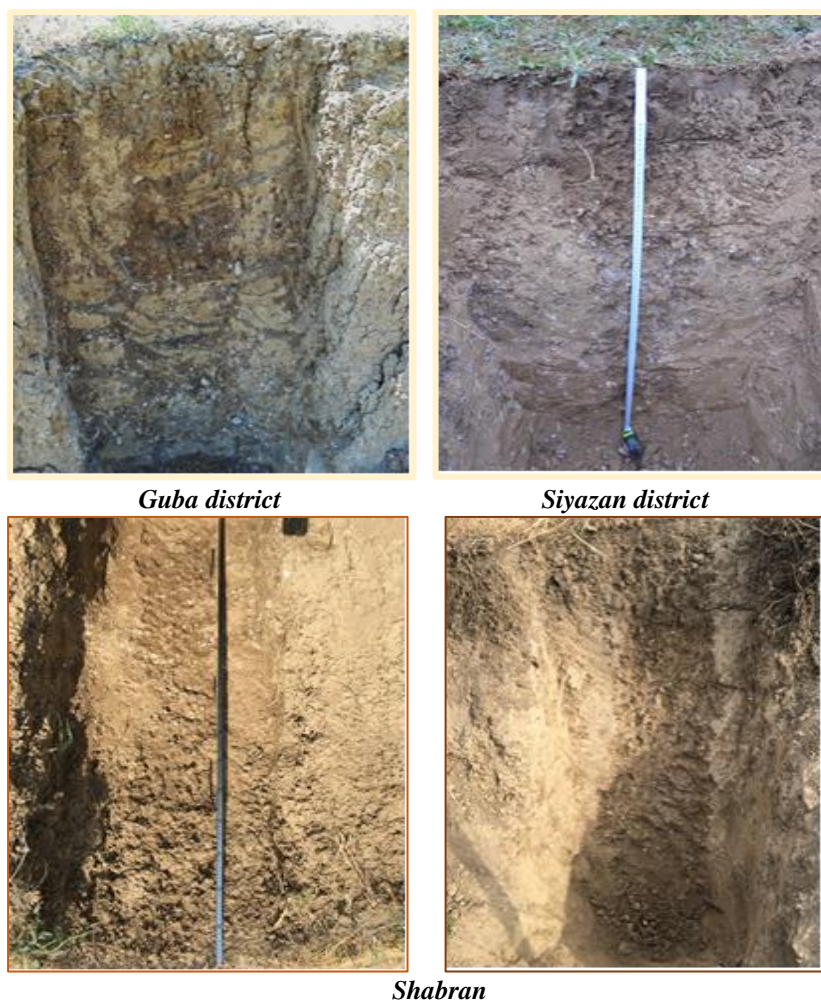


Figure 1. Soil cross section under species of the genus *Pyrus* L. in the northeastern part of the Greater Caucasus.

Figure 1. that illustrates a soil cross-section beneath plants belonging to the genus *Pyrus* L. The setting is specified as the northeastern region of the Greater Caucasus. Mountain brown-meadow soils are spread in the foothills of the Greater Caucasus, in the Guba-Khachmaz sloping plain, and are similar to brown soils in many of their characteristics. However, unlike brown soils, these soils do not obey the zonal law and do not form any belt (Babayev et al., 2017). These soils were mainly formed in hydromorphic conditions, as groundwater is distributed in areas closer to the surface. In the profile of these soils, there is a turf layer in the upper layer, it has a heavier mechanical composition, the carbonate illuvial layer is thinner, and the amount of carbonates is low. Since the forests were cut down in the areas where mountain brown-meadow soils spread for a long time, grass and shrub plants developed in those places. Depending on the amount of precipitation falling on the northeastern slope of the Great Caucasus and the lithological composition of the rocks, the level of groundwater also varies (Babayev et al., 2017). The soil-forming rocks of the areas where mountain brown-meadow soils are spread are composed of ancient alluvial sediments of clayey, gravelly and carbonate origin.

In mountain brown-meadow soils, the amount of humus is 2.3-3.2% in the upper layer, and a sharp decrease is observed towards the depth - 0.6%. The amount of total N is 0.16-0.21% in the upper layer and decreases to 0.10% towards the lower layers (Table 2.). The amount of carbonates in these soils is the same throughout the profile, only in the deep layers there is an increase - 7.0-22.4%.

The absorption capacity of mountain brown-meadow soils varies between 18-24 mg-eg on average, and a decrease is observed along the profile. Although Ca cation dominates in the upper layer of the profile of these soils, it is observed that the amount of Mg^{2+} increases in the lower layers - 7.5-10.47 mg-eg, which, in turn, indicates that Mg^{2+} is spreading in these soils (Babayev et al., 2017). In mountain brown-meadow soils, the reaction of the environment is pH 7.9-8.2 in the upper layers, increasing alkalinity towards the lower layers (Table 2.). According to the mechanical composition of these soils, the clay content increases with depth.

Table 2. Fertility indicators of the soils of the northeastern slope of the greater caucasus

Soil profile number	Depth of genetic layer	Hum us, %	Total nitroge n, %	Total P ₂ O ₅ , %	Total K ₂ O, %	Carbonate, %		pH (water)	Absorb ed sum of bases, mq/ekv	Granulometric composition, %	
						CO ₂	CaCO ₃			<0,01	<0,00 1
Mountain brown-meadow soils											
Altiaghach 4	0-25	2,2	0,16	0,17	2,0	4,2	10.2	7,9	18,00	46,75	17,88
	25-35	2,1	0,12	0,15	2,1	5,0	11.4	8,0	17,30	66,17	19,75
	35-55	1,6	0,11	0,13	1,9	5,2	13.7	8,1	16,42	58,46	26,42
	55-87	1,2	0,10	0,08	2,2	7,8	17.2	8,2	15,36	55,00	20,56
	87-120	0,6	-	0,06	2,3	6,3	22.4	8,3	13,48	37,52	17,76
Guba 5	0-10	3,2	0,21	0,16	2,4	3,3	7.0	8,2	24,30	48,32	18,45
	10-25	2,3	0,17	0,14	2,3	2,4	5.3	8,3	19,12	65,12	26,76
	25-60	2,1	0,14	0,12	2,2	2,8	5.6	8,1	19,35	60,72	12,24
	60-95	1,5	-		2,0	3,3	8.0	8,1	18,16	28,30	10,20
	95-145	1,0	-	0,06	-	4,4	9.9	8,3	17,52	25,45	9,24
Mountain gray-brown soils											
Siyazan 6	0-20	2,2	0,17	0,18	2,3	6,0	13.5	7,5	23,45	70,18	31,70
	20-45	1,6	0,15	0,16	2,2	7,1	14.8	7,7	19,72	69,20	25,00
	45-67	1,3	0,13	0,13	2,1	5,9	14.6	8,1	15,36	66,35	41,36
	67-90	1,0	0,09	0,10	2,0	4,3	10.5	8,3	14,73	69,42	34,82
	90-115	0,5	0,04	0,09	2,0	8,9	22.7	8,2	12,76	60,32	24,70
	115-150	0,2	-	0,08	1,9	8,3	19.3	8,3	11,46	70,26	21,60
Shabran 7	0-7	3,1	0,20	0,09	2,3	5,0	11.6	8,3	17,10	55,32	26,58
	7-25	1,2	0,12	0,07	2,2	5,5	12.4	8,4	15,46	48,00	23,35
	25-60	0,7	0,08	0,05	2,0	6,9	15.2	8,3	18,30	32,35	19,46
	60-100	0,5	0,07	0,01	1,8	9,2	23.8	8,2	17,21	28,52	15,00

On the northeastern slope of the Greater Caucasus, mountain gray-brown soils are spread in the middle of the Gusar foothill plain in the form of a thin strip. Although the amount of humus is 2.2-3.1% in the upper layer, a strong decrease is observed below 30 cm - 1.2% (Table 2). The amount of total nitrogen in the top layer is 0.17-0.20%. It is noteworthy that these soils are highly carbonated and the illuvial-carbonate layer is located in the deep layers of the soil profile: 13.5-22.7%. On the steep slopes in the surrounding areas of Shabran and Siyazan, primitive mountain gray-brown soils are spread, the humus layer is thin in these soils, and skeletal structure is observed below 50-70 cm.

Due to the amount of readily soluble salts, the mountain gray-brown soils are weakly saline - 0.15-0.22%. The mechanical composition of mountain gray-brown soils is clayey and heavy loamy. The amount of silt particles is 26-31%, the amount of particles <0.01 mm in size is 55-70% in the upper layer of the profile, it decreases towards the lower layers and is 28-60% (Table 2).

Conclusion

In summary, the comparative analysis of soil-plant relationships in *Pyrus* L. species under *in situ* and *ex situ* conditions offers valuable insights into their ecological and agricultural relevance. Our results indicate that soil characteristics play a crucial role in influencing the growth, health, and productivity of *Pyrus* species. Typically, *in situ* conditions provide a more integrated environment that fosters natural microbial interactions, leading to better nutrient absorption and disease resistance. While *ex situ* environments can facilitate controlled cultivation, they may introduce factors that affect plant performance differently than in natural settings. Recognizing these differences enables us to optimize agricultural practices to more closely resemble natural conditions, thus promoting healthier plants and higher yields. The ability of *Pyrus* species to adapt to various soil types highlights their potential for cultivation across diverse agricultural landscapes. This research underscores the significance of adopting suitable soil management practices that cater to the specific needs of *Pyrus* species. Employing sustainable soil practices can yield long-term advantages for both agricultural productivity and ecosystem health. By focusing on soil quality and health, we can enhance the resilience of *Pyrus* species against environmental challenges, such as climate change and soil deterioration. In essence, the complex relationship between *Pyrus* species and their soil environments is crucial for both ecological stability and agricultural sustainability. Future research should continue to delve into these relationships, exploring the effects of various

soil amendments and management strategies. Such investigations will be essential for enhancing our comprehension of plant-soil interactions and improving ecosystem health. Ultimately, cultivating a deeper understanding of these relationships can lead to more responsible and effective agricultural and conservation practices. As we advance, it is vital to integrate scientific insights into practical applications that serve both human interests and the environment. Examining the physiological responses of *Pyrus* species to different soil environments can provide insights into their resilience against environmental stressors, such as drought and salinity. This is especially relevant in the context of climate change, which presents significant challenges to both agriculture and natural ecosystems.

In conclusion, examining the comparative soil-plant relationship of *Pyrus* species in both *in situ* and *ex situ* conditions is a vital area of study. It not only deepens our understanding of plant ecology but also offers practical insights for agricultural practices and conservation efforts. Through this investigation, we aim to contribute to the broader field of plant-soil interactions, highlighting the importance of maintaining healthy ecosystems for future generations.

Recommendations

1. Habitat Conservation: Prioritizing the protection of natural habitats where *Pyrus* species flourish to maintain their genetic diversity and ecological functions.
2. Controlled Experiments: Conducting *ex situ* experiments that closely mimic natural conditions to gather data on how *Pyrus* species respond to various soil types and management practices.
3. Nutrient Management Plans: Creation tailored nutrient management plans for *Pyrus* species, focusing on balanced fertilization to minimize reliance on synthetic fertilizers.
4. Environmental Monitoring: Establishment programs to monitor environmental stressors like drought, salinity, and pests, aiding in the development of strategies to mitigate their effects on *Pyrus* species.

Scientific Ethics Declaration

As researchers engaged in the study of *Pyrus* L. species and their interactions with soil environments, we commit to upholding the highest standards of scientific integrity and ethical conduct throughout my work.

Acknowledgements

* This article was presented as a poster presentation at the International Conference on Basic Sciences and Technology (www.icbast.net) held in Antalya/Turkey on November 14-17, 2024.

* We would like to express our gratitude to all those who contributed to the success of this research on *Pyrus* L. species and their soil-plant interactions. We are also grateful to my colleagues and fellow researchers at Institute Soil and Agrochemistry of MSERA, (Ecology of Soil Lab) and Central Botanical Garden whose collaboration and shared knowledge have enriched this work.

References

- ALKahtani, M. D., Fouda, A., Attia, K. A., Al-Otaibi, F., Eid, A. M., Ewais, E. E. D., ... & Abdelaal, K. A. (2020). Isolation and characterization of plant growth promoting endophytic bacteria from desert plants and their application as bioinoculants for sustainable agriculture. *Agronomy*, 10(9), 1325.
- Arinushkina, E. V. (1970). Guide for chemical analysis of soils. *M.: Publishing House of Moscow University*.
- Bakshaliyeva, K.F., Arabova, G.G., Iskandar, E.O., & Muradov, P.Z. (2024) General characteristics of some fruit plants included in the flora of Azerbaijan and their mycobiota. *Advanced Studies in Biology*, 16(1), 35–43.
- Durak, A., Buyukguner, E., & Dogan, H. M. (2010). Determination of physical and chemical properties of the soils under different land managements. *Asian Journal of Chemistry*, 22(8), 6375-6386.
- Gupta, R., Anand, G., Gaur, R., & Yadav, D.(2021) Plant–microbiome interactions for sustainable agriculture: A review. *Physiologia Plantarum*, 27, 165–179.

- Hansda, A., Kisku, P. C., & Kumar, V. (2022). Plant-microbe association to improve phytoremediation of heavy metal. In *Advances in Microbe-Assisted Phytoremediation of Polluted Sites* (pp. 113-146). Elsevier.
- Iskender, E., Aliyeva, A., & Baghirova, S. (2022) Analysis of the relationship of the cultivated dendroflora of the northeastern part of the Greater Caucasus (Azerbaijan) to some abiotic factors. *Acta Botanica Caucasica*, 1(2), 57-67.
- Iskenderov, E.O. (1993) Evaluation of the prospects for the introduction of rare and endangered tree species of the Caucasus in the conditions of Absheron. *Bulletin of the State Scientific Society*, Moscow, issue 168, pp. 8-11.
- İskender, E., Zeynalov, Y., Özaslan, M., Çakır, B. M., Yayla, F., & İncik, F. N. (2005). Tree and shrub species of the Huzurlu High Plateau (Gaziantep, Turkey). *Phytologia Balcanica*, 11(2), 149-156.
- Jafarzadeh, S.A., & Elman Iskandar, E.O. (2024) Comparative study of pollen morphology and fertility in *Pyrus L.* species under *in situ* and *ex situ* conditions in Greater Caucasus, Azerbaijan. *International Scientific Forum "Modern Trends in Sustainable Development of Biological Sciences BIO Web of Conferences* 100, 03006, pp. 1-5.
- Kachinsky, N. A. (1958). Mechanical and microaggregate composition of the soil, methods of its study. *Academy of Science USSR, Moscow. 193p.[in Russian]*.
- Karlen, D. L., Mausbach, M. J., Doran, J. W., Cline, R. G., Harris, R. F., & Schuman, G. E. (1997). Soil quality: a concept, definition, and framework for evaluation (a guest editorial). *Soil Science Society of America Journal*, 61(1), 4-10.
- Ma, Y. (2019). Biotechnological potential of plant-microbe interactions in environmental decontamination. *Frontiers in Plant Science*, 10, 1519.
- McGowan, P. J., Traylor-Holzer, K., & Leus, K. (2017). IUCN guidelines for determining when and how *ex situ* management should be used in species conservation. *Conservation Letters*, 10(3), 361-366.
- Mineeva, V.G (1989). *Practicum on agrochemistry*. p. 340. Moscow: Moscow State University Publishing House.
- Qinglin, S., Liming, L., Jihua, Z., Sangui, Y., Xin, L., Jiaojiao, G., & Yuanrun, Z. (2022) Differences in ecological traits between plants grown *in situ* and *ex situ* and implications for conservation. *Sustainability*, 14(9), 5199.
- Szilvia, K., Dóra, H.-F., Máté, Ö., Katalin, H., András, N., Dezső, K., & László, O. (2023) The role of the plant–soil relationship in agricultural production—with particular regard to PGPB application and phytoremediation. *Microorganisms*, 11(6), 1616.

Author Information

Elman Iskender

Ministry of Science and Education of Azerbaijan Republic,
Institute of Microbiology,
AZ 1004, Baku c., Sebail dist, Str. A. Abbaszade, 115
Contact e-mail: acae55@hotmail.com

Panah Muradov

Ministry of Science and Education of Azerbaijan
Republic, Institute of Microbiology,
AZ 1004, Baku c., Sebail dist, Str. A. Abbaszade, 115

Sabina Jafarzadeh

Ministry of Science and Education of Azerbaijan Republic,
Institute of Microbiology,
AZ 1004, Baku c., Sebail dist, Str. A. Abbaszade, 115

To cite this article:

Iskender, E., Muradov, P., & Jafarzadeh, S. (2024). Comparative soil-plant relationship of *Pyrus L.* species under *in situ* and *ex situ* conditions. *The Eurasia Proceedings of Science, Technology, Engineering & Mathematics (EPSTEM)*, 30, 39-46.

The Eurasia Proceedings of Science, Technology, Engineering & Mathematics (EPSTEM), 2024

Volume 30, Pages 47-55

ICBAST 2024: International Conference on Basic Sciences and Technology

Synthesis and Study of the Complex Compound of Isonicotinamide with Zinc Nitrate

Lobar Sharipova

Branch of Kazan Federal University in the city of Jizzakh

Mavluda Ibragimova

Institute of General and Inorganic Chemistry

Oybek Khudoyberganov

Khorezm Mamun branch of Uzbekistan Academy of Sciences

Farhod Khallokov

Bukhara State Medical Institute named after Abu Ali Ibn Sino

Khayrulla Bobakulov

Institute of the Chemistry of Plant Substances

Zubayda Abdullaeva

Khorezm Mamun branch of Uzbekistan Academy of Sciences

Abstract. A complex compound of zinc nitrate with isonicotinamide was synthesized. The advantages of the mechanochemical (solid-phase) method, the optimal conditions of synthesis are presented IR- and ^1H NMR-spectroscopic analysis provide information about ligands and the complex compound formed on their basis, the nature of the bond, central atom surrounding, polyhedra, valence and deformation vibrations, shifts in proton signals. Crystallographic data of the complex compound were obtained using a Malvern Panalytical Empyrean diffractometer. Analysis of the obtained results was carried out using FULLPROF and VESTA programs. When the lengths and angles of the valence bonds were analyzed using the MOGUL program adapted to the MERCURY complex, it was found that there were no bonds and angles with non-standard values between them. The state of the central atomic spatial structure, hybridization, binding of the isonicotinamide molecule and the nitric acid residue to the zinc atom were studied. Based on the data obtained, it was concluded.

Key words: Complex compound, Infrared and ^1H NMR spectroscopy, Mechanochemical method, Zinc nitrate, Physicochemical methods of analysis.

Introduction

Huge amounts of mixed-ligand complex compounds of transition metals are synthesized in the world. In order to accelerate and increase the yield of the main crops, much attention is paid to stimulants, in particular to groups of metal complexes (Boldyrev, 2006). Metal complexes containing various N,O-donor centers in the ligand environment occupy a special place in modern coordination chemistry (Lomovsky, 2001). Due to the specific effect of their environment on the stereochemistry of polyhedra, they are good models for studying the problem of competitive coordination in the chemistry of complex compounds (Sharipova, 2022). In this regard, it seems important and relevant to search for ways of directed synthesis of polydentate ligands and, based on

- This is an Open Access article distributed under the terms of the Creative Commons Attribution-Noncommercial 4.0 Unported License, permitting all non-commercial use, distribution, and reproduction in any medium, provided the original work is properly cited.

- Selection and peer-review under responsibility of the Organizing Committee of the Conference

© 2024 Published by ISRES Publishing: www.isres.org

them, metal complexes of a certain composition and structure in order to solve theoretical and practical problems of creating new generation materials with predetermined properties (Sharipova et al., 2019). At the same time, the synthesis of effective, new types of complex compounds to increase productivity and their widespread use in agriculture remains an urgent problem (Ibragimova et al., 2016).

The author established the structure of new coordination compounds $[M(HCO_2)_2(NC_5H_4CONH_2)_2(H_2O)_2]$, ($M=Co, Ni$) using X-ray diffraction analysis and the results were entered into the Cambridge Crystallographic Database, (deposits were entered into the Cambridge Crystallographic Database, (deposits №. 2081143 and №. 2092828) (Jumaniyozova, 2021)

The compounds are isostructural and consist of neutral complexes ($CN = 6$), in which the metal atom is bonded to two nicotinamide molecules through nitrogen heteroatoms, two water molecules, and two monodentate formate ions. The coordination polyhedron is a distorted octahedron with the trans arrangement of the nitrogen heteroatoms of the nicotinamide molecules. Between nicotinamide molecules and formate ions, as well as between nicotinamide molecules and water molecules, intracomplex hydrogen bonds are realized in the complex (Jumaniyozova et al, 2021).

The structure of the coordination compound $[Ca(H_2O)_2(C_5H_4NC(O)NH_2)_2(NO_3)_2]$ was established by X-ray diffraction analysis. It was determined that water and nicotinamide molecules are coordinated monodentately through water oxygen atoms and oxygen atoms of the carbonyl group of nicotinamide, nitrate - anions are coordinated bidentately through oxygen atoms. This structure was entered into the Cambridge Crystallographic Database, deposit № 1850646 (Jumanazarova, 2018).

Method

All reagents were readily available from commercial sources and were used as received without further purification. The amount of metal in the synthesized complex was determined on the Novaa 300 apparatus of Analytic Jena (Germany) (Charlot, 2007). Analysis of C H and N were performed on an EuroVector EA3000 Series of CHNS-O Elemental Analysers (Bazhenova, 2008).

Synthesis and Crystallization

Synthesis of the coordination compounds of zinc nitrate with isonicotinamide was carried out by mechanochemical method (solid phase) (Sharipova, 2022). To determine the optimal conditions for the reaction, the mechanochemical reaction was carried out in a ball mill for 0.5 hours using blanks (working part) 1 and 2 (a ball with a diameter of 20 mm). The mass of the working part is 67 grams. The rotation number is 150 rpm. the duration of one is 30 seconds. Three such mixings constitute one cycle, the time between mixing cycles is 2-3 seconds (Sharipova, 2023). Zinc nitrate and isonicotinamide molecules were mixed in an equimolar ratio of 1:2 ($Zn(NO_3)_2 \cdot 6H_2O : 2NC_5H_4CONH_2$). Yield of the complex is 68%. $[ZnC_{12}H_{14}O_9N_6]$ white crystalline substance, $T_m=111$. Elemental analysis for complex $ZnC_{12}H_{14}O_9N_6$ (451,68): calcd. C 31.93; H 3,10; N 18,63%; found: C 32,08; H 3,13; N 18,59% (Sharipova, 2018).

Methods and Refinement

The determination of the structure of the compounds was carried out using a Malvern Panalytical Empyrean diffractometer. XRD data were recorded using $CuK\alpha$ radiation ($\lambda = 1.54 \text{ \AA}$). In this experiment, the accelerating voltage of the radiation generator was set to 45 kV, and the current emission was set to 40 mA. X-ray diffraction radiographs were recorded at $2\theta = 200\text{--}1200$ in a Bregga–Brentano beam geometry with a continuous scanning speed of 0.33 degrees/min (Yakimov & Dubinin 2008). Analysis of the obtained results was carried out using FULLPROF and VESTA programs (Khudoyberganov et al., 2022). When the lengths and angles of the valence bonds were analyzed using the MOGUL program adapted to the MERCURY complex, it was found that there were no bonds and angles with non-standard values between them (Khasanov et al., 2023).

The absorption regions of the IR spectra were recorded on an IR Tracer-100 spectrometer ($500\text{--}4000 \text{ cm}^{-1}$) from SHIMADZU (Nakamoto, 1991). The NMR method is very important in modern chemistry. This is due to the fact that the resonant frequencies of the nuclei depend on the interaction of the magnetic field (Ibragimov et al., 2022) and the distribution of electron densities in the molecule (Sharipova et al., 2023).

The ^1H NMR spectra of the complex compound were recorded on a JNM-ECZ400R spectrometer (Jeol, Japan) at an operating frequency of 400 MHz in methanol deuterium (CD_3OD) solution. Tetramethyl silane ($\text{TMS} - \text{Si}(\text{CH}_3)_4$) (ppm) was used as an internal standard to obtain ^1H NMR spectra (Volovenko et al., 2011). Chemical shifts of protons occupy a limit close to δ 10 ppm and their uncertainty found in experiment equal to $\pm 0,001$ ppm.

Results and Discussion

Description of IR-Analysis

In the IR spectrum of the uncoordinated isonicotinamide molecule, the ring frequency is observed at 1585 cm^{-1} , the frequency of this field increased to 1593 cm^{-1} in the complex state. The ring vibration frequency of isonicotinamide is in the region of $\nu_{\text{CN}}=1019\text{ cm}^{-1}$ and $\delta_{\text{CCN}}=733\text{ cm}^{-1}$, and the vibration frequencies are shifted to the region of 1026 cm^{-1} and 743 cm^{-1} . The valence frequency of ν_{CO} bond of isonicotinamide remained unchanged, i.e. 1681 cm^{-1} . This indicates coordination of the isonicotinamide pyridine ring through a nitrogen heteroatom. In the complex compound, the nitrate anion was represented by $\nu_s(\text{NO}_3)$, a low intensity band at 1027 cm^{-1} , $\nu_{\text{as}}(\text{NO}_3)$ at 1303 cm^{-1} , and $\delta(\text{NO}_3)$ at 815 cm^{-1} .

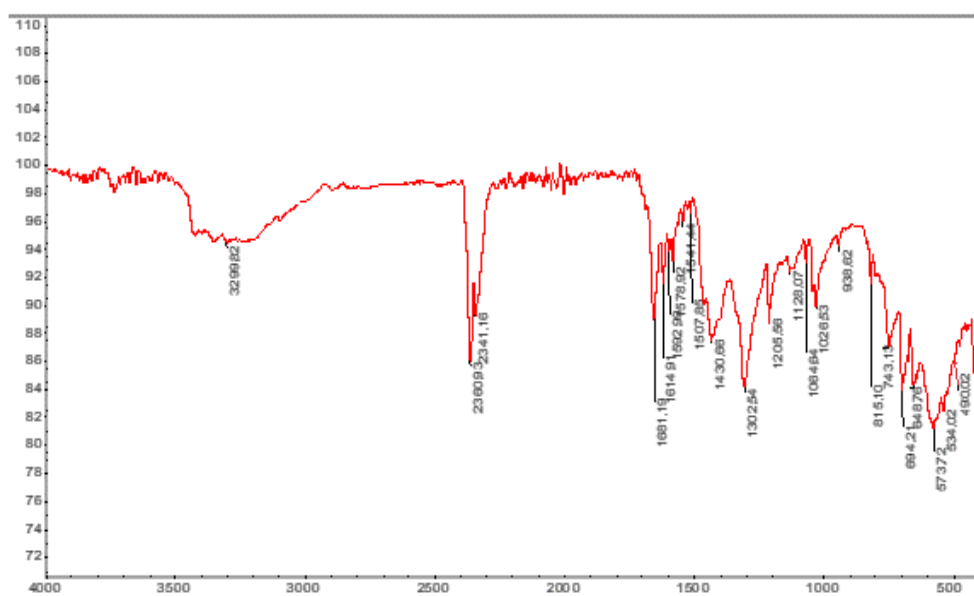


Figure 1. IR-spectrum of the complex compound

Description of NMR Analysis

In the ^1H NMR spectrum of isonicotinic acid amide, the signal of four hydrogen protons in the pyridine ring $\delta=9.028$ ppm at ($\text{H}\alpha$) and multiplet signals ($\text{H}\alpha'$) $\delta=8.686$ ppm., ($\text{H}\gamma$) $\delta=8.282$ ppm., ($\text{H}\beta$) $\delta=8.547, 7.545$ ppm. observed in weak areas (Fig. 3.10). The following chemical shift is observed in the ^1H NMR spectrum of $[\text{Zn}(\text{NO}_3)_2 \cdot 2\text{NC}_5\text{H}_4\text{CONH}_2] \cdot \text{H}_2\text{O}$ complex compound: $\delta=9.040, 9.035$ ppm. at ($\text{H}\alpha$) and multiplet signals ($\text{H}\alpha'$) $\delta=8.698$ ppm, ($\text{H}\gamma$) $\delta=8.348, 8.328$ ppm., ($\text{H}\beta$) $\delta=7.596, 7.594$ ppm.

Comparing the chemical shift values of the protons in the free and coordinated pyridine ring shows that the signals are shifted towards the weak field. This shift indicates that the process of complex generation has gone. The strong shielding of the hydrogen located in the b state in the ligand pyridine ring and the strong descreening when isonicotinamide goes to the complex state are related to the metaorientation property of the nitrogen in the pyridine ring. Descreening in the pyridine ring is caused by the interaction of the unshared electron pair on the nitrogen atom with the 4s and 4p₃ orbitals of zinc. As a result of this interaction, a molecular orbital is formed in which the electron density is transferred to the metal ion. This process causes descreening of hydrogen protons in the pyridine ring. Therefore, based on the data of 1N NMR spectroscopy, it can be concluded that isonicotinamide is coordinated through the nitrogen atom in the pyridine ring.

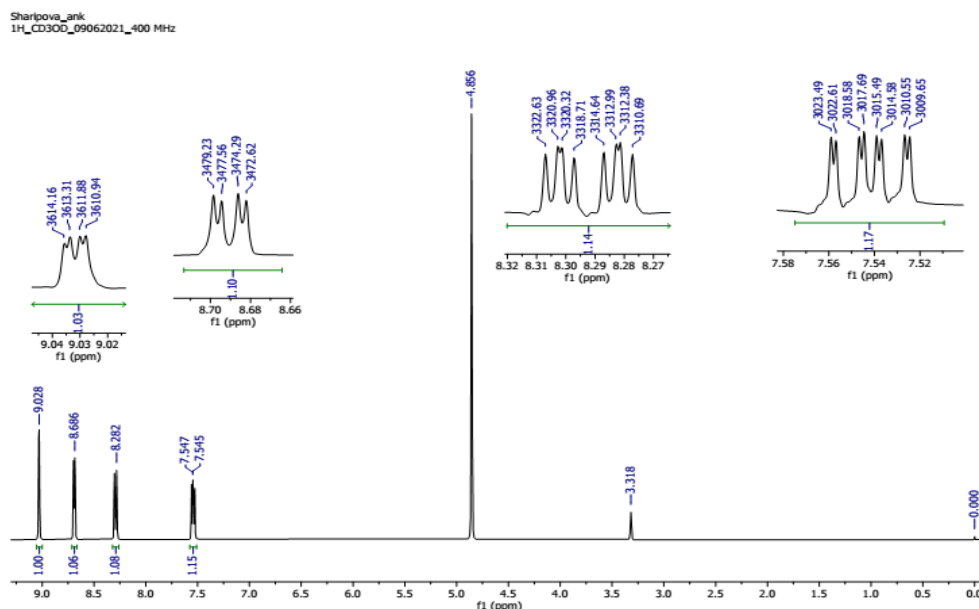


Figure 2. ^1H NMR spectrum of isonicotinamide molecule in CD_3OD

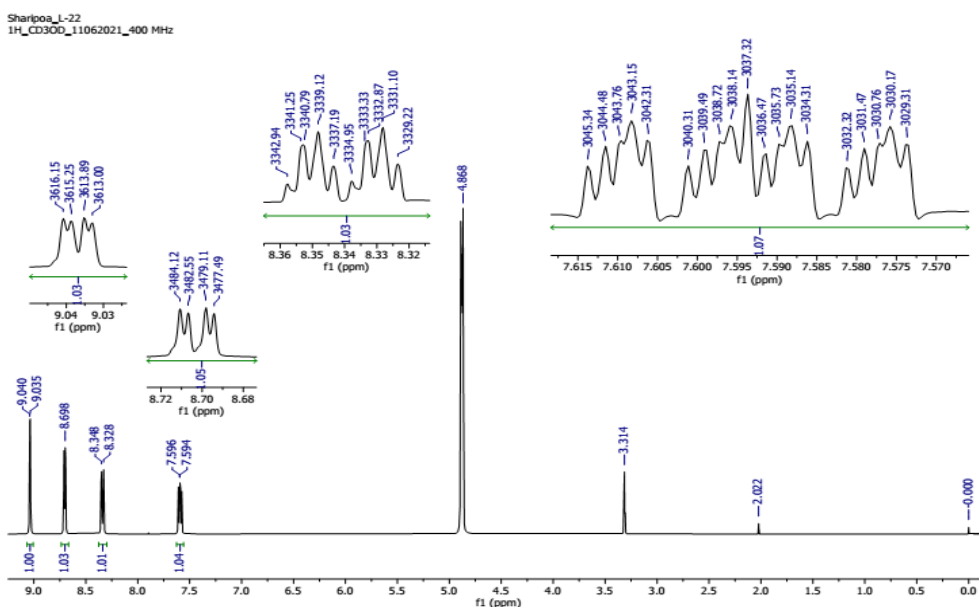


Figure 3. ^1H NMR spectrum of complex compound

Description of Molecular Structure

In the structure of the complex compound, the central zinc atom is triclinically coordinated with the nitrogen atom of the isonicotinamide ring of two ligands and the oxygen atoms of two nitrate residues. In this, isonicotinamide molecules participated as monodentate ligands through nitrogen atom and two nitrate residues through oxygen atoms as bidentate ligands. The central zinc atom has a coordination number of 6 and is hybridized in the sp^3d^2 state (Fig. 4).

The parameters of the unit cell of the crystal are as follows: spatial group C1, $a=21.33(8)$ Å, $b=21.33(13)$ Å, $c=15.08(3)$ Å, $\alpha=90^\circ$, $\beta=90^\circ$, $\gamma=90^\circ$, $V=6868.107\text{Å}^3$, $Z=2$. Complex compound $[\text{Zn}(\text{NO}_3)_2 \cdot 2\text{NC}_5\text{H}_4\text{CONH}_2] \cdot \text{H}_2\text{O}$ is mononuclear, and the complex formed by Zn^{2+} ion with isonicotinamide, nitric acid anion and water molecules has a neutral nature (Table 1).

Table 1. Parameters crystallographic data and structure of complex compound

Formule	C ₁₂ H ₁₂ N ₆ O ₈ Zn, H ₂ O	Size of the crystal, [mm]	0.22×0.18×0.06
Molecular mass	451.68	T, °K	298
Syngonia	Triclinic	θ, ° deg.	2,14; 34,10
Spatial group	C1	Interval h,k,l	999: 99; 999: 99; 999: 99
a, Å	21.33620	Reflex	2146
b, Å	21.33620	Refraction index	1568
c, Å	15.08700	R _{int}	0.71073
α, β, γ, deg	90(14);90(15);90(15)	F ² ≥2σ(F ²)	R ₁ =0.054
V, Å ³	6868.107	Criteria	
Z	2	Parameter	4162
D _x , g/cm ⁻³	0.218	Eligibility Criteria (F ²)	460
		R ₁ , wR ₂ (I>2σ(I))	R ₁ =0.0548, wR ₂ =0.1894
μ(CuKα), mm ⁻¹	0.187		

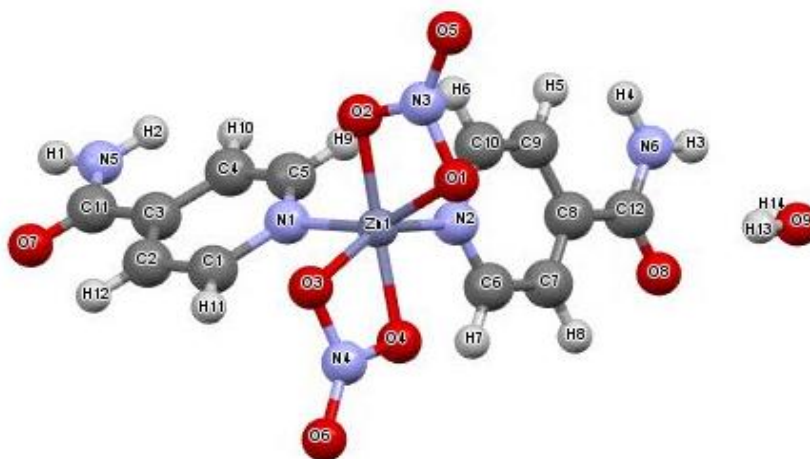


Figure 4. Molecular structure of the synthesized complex compound

Table 2. Valence bonds and bond lengths of complex compound

Bond	d, Å	Bond'	d, Å
Zn(1)-O(1)	1.9737	C(3)-C(4)	1.4645
Zn(1)-O(2)	2.0082	C(3)-C(11)	1.4634
Zn(1)-O(3)	1.9751	C(4)-C(5)	1.3475
Zn(1)-O(4)	2.0088	N(5)-H(2)	1.0121
Zn(1)-N(1)	2.0013	N(5)-H(1)	1.0142
Zn(1)-N(2)	1.9984	N(6)-H(4)	1.0134
O(1)-N(3)	1.4505	C(6)-C(7)	1.4594
O(2)-N(3)	1.3581	N(6)-H(3)	1.0124
O(3)-N(4)	1.4513	C(7)-C(8)	1.3417
O(4)-N(4)	1.3573	C(8)-C(12)	1.4605
O(5)-N(3)	1.4872	C(8)-C(9)	1.4611
O(6)-N(4)	1.4799	C(9)-C(10)	1.3365
O(7)-C(11)	1.2200	C(1)-H(11)	1.0823
O(8)-C(12)	1.2199	C(2)-H(12)	1.0826
N(1)-C(1)	1.5152	C(4)-H(10)	1.0828
N(1)-C(5)	1.3227	C(5)-H(9)	1.0834
N(2)-C(6)	1.3191	C(6)-H(7)	1.0836
N(2)-C(10)	1.5192	C(7)-H(8)	1.0732
N(5)-C(11)	1.3197	C(9)-H(5)	1.0786
N(6)-C(12)	1.3200	O(9)-H(13)	0.9475
C(1)-C(2)	1.4548	O(9)-H(14)	0.9584
C(2)-C(3)	1.3388	C(10)-H(6)	1.0843

The value of the distance between the bonds Zn(1)–O(1), Zn(1)–O(2), Zn(1)–O(3), Zn(1)–O(4) va Zn(1)–N(1), Zn(1)–N(2) in the complex is corresponding to 1.9737Å, 2.0082Å, 1.9751Å, 2.0088Å va 2.0013Å, 1.9984Å accordingly (Fig.5., Tab.2.). It can be seen that the valence angles of the bonds O(1)–Zn(1)–O(2), O(1)–Zn(1)–O(3), O(1)–Zn(1)–O(4), O(2)–Zn(1)–O(3) and O(1)–Zn(1)–N(1), O(1)–Zn(1)–N(2) are equal to 64.61°, 102.42°, 106.12°, 106.88° and 152.37°, 90.56°, respectively (Fig.6., Tab.3.)

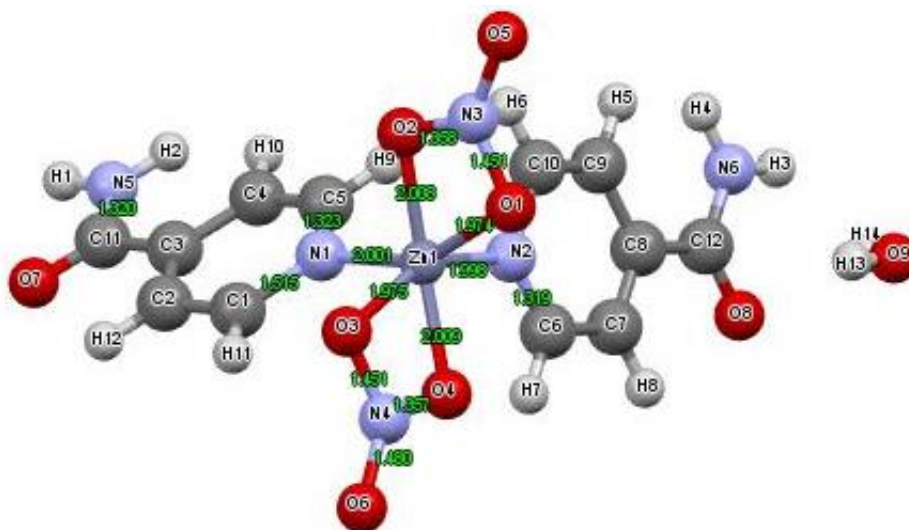


Figure 5. Interatomic bonds and bond length of complex compound

Table 3. Bond angles of a complex compound

Angle	ω , degree	Angle	ω , degree
O(1)–Zn(1)–O(2)	64.61	O(4)–N(4)–O(6)	130.72
O(1)–Zn(1)–O(3)	102.42	N(1)–C(1)–C(2)	118.02
O(1)–Zn(1)–O(4)	106.12	C(1)–C(2)–C(3)	118.46
O(1)–Zn(1)–N(1)	152.37	C(2)–C(3)–C(4)	120.64
O(1)–Zn(1)–N(2)	90.56	C(2)–C(3)–C(11)	119.69
O(2)–Zn(1)–O(3)	106.88	C(4)–C(3)–C(11)	119.68
O(2)–Zn(1)–O(4)	166.73	C(3)–C(4)–C(5)	121.88
O(2)–Zn(1)–N(1)	88.22	N(1)–C(5)–C(4)	121.23
O(2)–Zn(1)–N(2)	102.48	H(1)–N(5)–H(2)	124.21
O(3)–Zn(1)–O(4)	64.63	C(11)–N(5)–H(2)	123.24
O(3)–Zn(1)–N(1)	89.71	C(11)–N(5)–H(1)	126.32
O(3)–Zn(1)–N(2)	150.63	C(12)–N(6)–H(4)	126.34
O(4)–Zn(1)–N(1)	101.52	C(12)–N(6)–H(3)	120.36
O(4)–Zn(1)–N(2)	86.57	N(2)–C(6)–C(7)	119.72
N(1)–Zn(1)–N(2)	90.63	H(3)–N(6)–H(4)	120.23
Zn(1)–O(1)–N(3)	97.62	C(6)–C(7)–C(8)	123.63
Zn(1)–O(2)–N(3)	99.30	C(9)–C(8)–C(12)	119.68
Zn(1)–O(3)–N(4)	97.51	C(7)–C(8)–C(12)	119.67
Zn(1)–O(4)–N(4)	99.28	C(7)–C(8)–C(9)	120.65
Zn(1)–N(1)–C(1)	119.49	C(8)–C(9)–C(10)	119.61
Zn(1)–N(1)–C(5)	120.74	N(2)–C(10)–C(9)	119.27
C(1)–N(1)–C(5)	119.77	O(7)–C(11)–C(3)	120.01
Zn(1)–N(2)–C(6)	119.65	O(7)–C(11)–N(5)	119.18
Zn(1)–N(2)–C(10)	120.45	N(5)–C(11)–C(3)	126.12
C(6)–N(2)–C(10)	119.86	N(6)–C(12)–C(8)	127.16
O(1)–N(3)–O(2)	98.48	O(8)–C(12)–N(6)	119.24
O(1)–N(3)–O(5)	130.76	O(8)–C(12)–C(8)	120.01
O(2)–N(3)–O(5)	130.76	N(1)–C(1)–H(11)	122.32
O(3)–N(4)–O(4)	98.58	C(2)–C(1)–H(11)	122.34
O(3)–N(4)–O(6)	130.71	C(1)–C(2)–H(12)	121.76

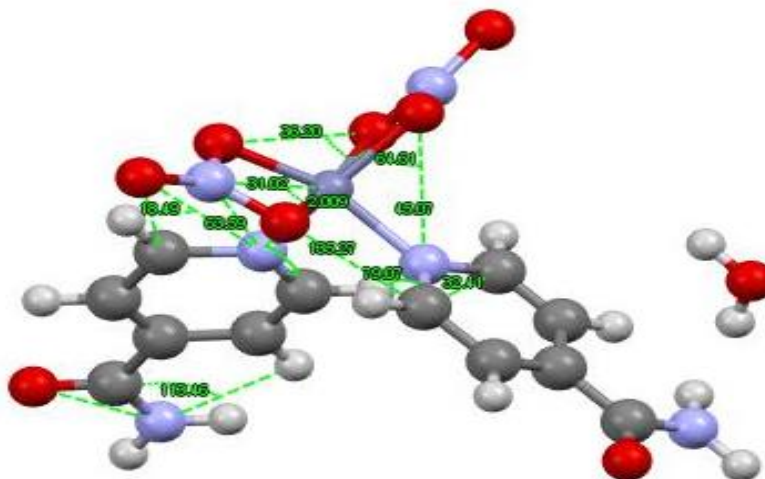


Figure. 6. Sizes of the bond angles of the complex compound

The structure of the complex compound was also previously studied by XAFS (X-ray absorption fine structure) analysis. According to the results of the analysis, Due to the hydrogen bonds C(6)---H(7)... O(4), C(5)---H(9)... N(2), C(1)---H(11)...O(3) with the participation of nitrate residues and nicotinamide molecules in the complex, It is stable due to the formation of a two-dimensional layer parallel to the *bc* plane (Fig.7).

Table 4. Hydrogen bonds in the crystal structure (Å°)

Bonds D—H⋯A	Distance, Å			Angle D—H⋯A, deg.	Coordinates of the atom, A
	D—H	N⋯A	D⋯A		
[C ₁₂ H ₁₄ N ₆ O ₉ Zn]					
C(6)---H(7)... O(4)	1.0800	1.9900	2.6731	118.00	1-x,1-y,1-z
C(5)---H(9)... N(2)	1.0800	2.5500	3.0045	105.00	2-x,2-y,-z
C(1)---H(11)...O(3)	1.0800	2.2500	2.8263	111.00	x,-1+y,z

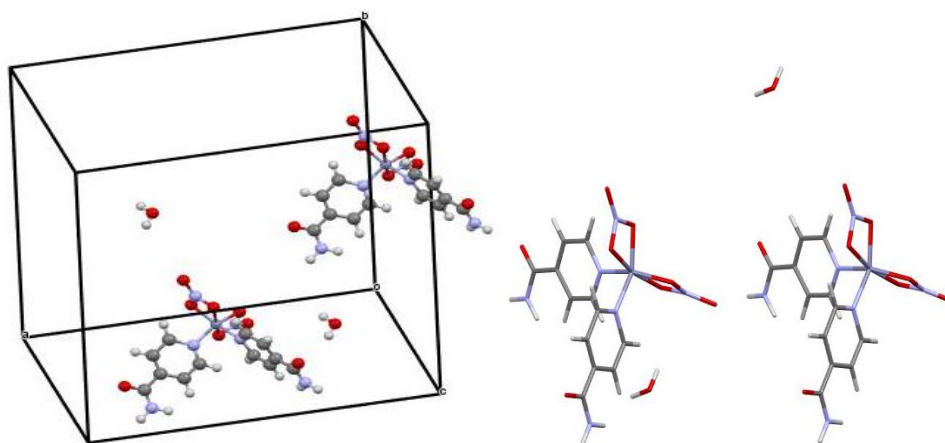


Figure. 7. Location projection of the complex compound in the crystal cell

Conclusion

Based on the changes in values of valence vibrations of functional groups and the values of chemical shifts of magnetic resonance signals by infrared and ^1N NMR spectroscopy methods, it was determined that isonicotinamide is coordinated monodentately through the nitrogen atom of the pyridine ring and bidentately coordinated through zinc nitrate oxygen atoms.

The structure proposed by IR and NMR was confirmed by X-ray. In the synthesized complex, it was found that the water molecule is located in the outer sphere.

Scientific Ethics Declaration

The authors declare that the scientific ethical and legal responsibility of this article published in EPSTEM journal belongs to the authors.

Acknowledgements or Notes

* This article was presented as a poster presentation at the International Conference on Basic Sciences and Technology (www.icbast.net) held in Antalya/Turkey on November 14-17, 2024.

References

- Boldyrev, V.V. (2006) *Mechanochemistry and mechanical activation of solids*. Moskva, M.: Uspekhi khimii.
- Bazhenova, L.N. (2008). *Quantitative elemental analysis of organic compounds*. Yekaterinburg, Ural Stat University.
- Charlot, G. (2007). *Quantitative analysis of inorganic compounds*. Brookfield, WI: Thomas Press. p. 368.
- Ibragimova, M.R., Abdullaeva, F.A. Khasanov, Sh.B., & Azizov, T.A. (2016). Acid amide coordination compounds of magnesium nicotinate. *Journal of Chemical Technology and Metallurgy*, 51(1), 47-52.
- Ibragimov, B.T., Khasanov, Sh.B., Khudoyberganov, O.I., Abdullaeva, Z.Sh., & Eshchanov, E.U. (2022). Synthesis and analysis of coordination compounds of nickel(II) acetate with monoethanolamine and p-nitrobenzoic acid. *Azerbaijan Chemical Journal*, 4, 3–47.
- Jumaniyozova, M.E. (2021). *Mixed amide coordination compounds of formates of a number of 3d-metals*. (Doctor of Philosophy dissertation). National university of Uzbekistan.
- Jumaniyozova, M.E., Azizov, T.A., Ibragimova, M.R., & Khasanov, Sh.B. (2021). Structure of the coordination compound of cobalt(II) formate with nicotinamide. Actual problems of chemistry of coordination compounds. *Republican scientific-practical conference*. Tashkent.
- Jumanazarova, Z.K. (2018). *Synthesis, structure and properties of homogeneous and mixed-ligand coordination compounds of magnesium and calcium nitrates*. (Doctor of Philosophy dissertation). Tashkent. T: National university of Uzbekistan.
- Khudoyberganov, O., Ruzmetov, A., Ibragimov, A., Ashurov, J., Khasanov, Sh., Eshchanov, E., & Ibragimov, B. (2022). Synthesis, crystal structure and Hirshfeld surface analysis of the binuclear Cu(II) complex with 4-nitrobenzoic acid and triethanolamine. *Chemical Data Collections*.
- Khasanov, Sh.B., Ibodullaeva, T.A., Abdullayeva, Z.Sh., & Khudoyberganov, O.I. (2023). Synthesis and properties of the coordination compounds calcium stearate with thiocarbamide. *Azerbaijan Chemical Journal*, 2, 111-115.
- Lomovsky, O. (2001). Applied mechanochemistry: Pharmaceuticals and medical industry. *Processing of dispersed materials and media*. 11, 81-100.
- Nakamoto, K. (1991). IR and Raman spectra of inorganic and coordination compounds. Moscow, M: Mir.
- Sharipova, L.A. (2022). Ecological efficiency of mechanochemical synthesis. *Science and Innovation*. Tashkent, T: 2022.
- Sharipova, L.A., Azizov, T.A., Ibragimova, M.R., & Kholmatov, D.S. (2019). New coordination compounds of zinc nitrate with nitrocarbamide, benzamide and benzoic acid. *NamSU Scientific Bulletin*, 3, 42-48.
- Sharipova, L.A. (2022). *Synthesis, structure and properties of coordination compounds of zinc nitrate with homogeneous and mixed ligand ligands*. (Doctor of Philosophy dissertation). Bukhara, Bukh: Bukhara Stat University.
- Sharipova, L.A., Azizov, T.A., Ibragimova, M.R., & Mamatova, F.K. (2023). Complex compound of zinc nitrate based on formamide and nicotinic acid. *Universum: Chemistry and Biology*. 4(106), 65-68. Retrieved from <http://7uneversum.com/ru/nature/archive/item/15187>
- Sharipova, L.A., Azizov, T.A., & Ibragimova, M.R. (2018). Coordination compounds of zinc nitrate with carbamide, nitrocarbamide and nicotinic acid. *Universum: Chemistry and Biology*. 12(54), 45-49. URL: Retrieved from <http://7uneversum.com/ru/nature/archive/item/6596>
- Sharipova, L.A., Ibragimova, M.R., Azizov, T.A., & Mamatova, F.K. (2023). IR-spectroscopic and thermal analysis of a mixed ligand complex compound of zinc nitrate with formamide and acetamide. *Universum: Chemistry and Biology*. 3(105), 68-71. Retrieved from <http://7uneversum.com/ru/nature/archive/item/15090>
- Volovenko, Yu.M., Kartsev, V.G., Komarov, I.V., Turov, A.V., & Khilya, V.P. (2011). *Nuclear magnetic resonance spectroscopy for chemists*. Moscow, M: Scientific Partnership Foundation.

Yakimov, I.S., & Dubinin, P.S. (2008). *Quantitative X-ray phase analysis*. Krasnoyarsk: Siberian Federal University.

Author Information

Lobar Sharipova

Branch of Kazan federal university in the city of Jizzakh
130000, Republic of Uzbekistan, Jizzakh city, Jizzakhlik
mahalla, Sharof Rashidov street, 295, Uzbekistan
Contact e-mail: sharipovalobar82@gmail.com

Mavluda Ibragimova

Institute of General and Inorganic Chemistry, Academy
Sciences of the Republic of Uzbekistan
77-a MirzoUlugbek, Tashkent 100170, Uzbekistan

Oybek Khudoyberganov

Khorezm Mamun branch of Uzbekistan Academy of
Sciences, 220100, Republic of Uzbekistan, Khorezm
region, Urgench, Babadjanov street, 43A, Uzbekistan

Farhod Khallokov

Bukhara State Medical Institute named after Abu Ali Ibn
Sino, 200118, Bukhara region, Navoi ave., 1, Uzbekistan

Khayrulla Bobakulov

Institute of the Chemistry of Plant Substances
Academy Sciences of the Republic of Uzbekistan
77. MirzoUlugbek, Tashkent 100170, Uzbekistan

Zubayda Abdullaeva

Khorezm Mamun branch of Uzbekistan Academy of
Sciences, 220100, Republic of Uzbekistan, Khorezm
region, Urgench, Babadjanov street, 43A, Uzbekistan

To cite this article:

Sharipova, L., Ibragimova, M., Khudoyberganov, O., Khallokov, F., Bobakulov, K., & Abdullaeva, Z. (2024). Synthesis and study of the complex compound of isonicotinamide with zinc nitrate. *The Eurasia Proceedings of Science, Technology, Engineering & Mathematics (EPSTEM)*, 30, 47-55.

The Eurasia Proceedings of Science, Technology, Engineering & Mathematics (EPSTEM), 2024

Volume 30, Pages 56-63

ICBAST 2024: International Conference on Basic Sciences and Technology

Evaluation of Antioxidant and Anti-Inflammatory Activities of Aqueous Extract of *Malva Sylvestris* Leaves in Association with Serum Albumin

Idir Moualek

Mouloud Mammeri University of Tizi-Ouzou

Karima Benarab

University Hospital Center of Tizi-Ouzou

Karim Houali

Mouloud Mammeri University of Tizi-Ouzou

Abstract: *Malva sylvestris* L., commonly known as common mallow, is an herbaceous plant widely used in traditional Algerian medicine for its anti-inflammatory and antioxidant properties. The richness of its leaves and flowers in phenolic compounds is the source of these therapeutic virtues. In Algeria, various remedies based on this species are commonly used in the treatment of inflammation, joint pain, and digestive disorders. Serum albumin is the most abundant protein in blood plasma and plays a key role in regulating oncotic pressure. Its versatile nature also allows it to transport numerous molecules such as fatty acids, hormones, drugs, and metal ions, thus contributing to the proper functioning of essential physiological processes. This study aims to evaluate certain biological activities resulting from the association between serum albumin and the aqueous extract of *Malva sylvestris* L. leaves. The results obtained highlight a notable antioxidant activity of this association, with respective IC₅₀ values of 3.825 ± 0.422 µg/ml, 296.13 ± 69.33 µg/ml, and 217.9 ± 31.5 µg/ml for the ability to scavenge DPPH, OH, and H₂O₂ radicals. The mixture exhibits a total antioxidant capacity with an IC₅₀ of 310.5 ± 11.33 µg/ml and a ferric ion reducing power with an IC₅₀ of 42.93 ± 46.38 µg/ml. The ferrous ion chelating ability is evaluated with an IC₅₀ of 137.96 ± 30.07 µg/ml. Regarding the anti-inflammatory activity, no stabilizing effect on erythrocyte membranes against osmotic stress, HOCl-induced oxidative stress, and heat was observed with this association. These results clearly demonstrate that the combination of serum albumin and the aqueous extract of *Malva sylvestris* leaves significantly potentiates the antioxidant properties of the plant. This combination represents a promising source of bioactive molecules and constitutes an interesting therapeutic alternative for the treatment of pathologies related to oxidative stress.

Keywords: *Malva sylvestris*, BSA, Antioxidant, Anti-radical, Anti-inflammatory

Introduction

For centuries, medicinal plants have been a valuable source of bioactive molecules, offering numerous therapeutic benefits, particularly in the prevention of oxidative damage. The growing interest in these biomolecules, particularly polyphenols, is justified by their well-documented antioxidant and anti-inflammatory effects (Singh, 2015). At a time when synthetic antioxidants are raising concerns about their safety, natural antioxidants from plants, such as those from *Malva sylvestris*, are seen as a promising alternative (Velioglu et al., 1998).

Malva sylvestris, widely known for its medicinal properties, contains various polyphenols, such as flavonoids and tannins, which are widely studied for their ability to neutralize free radicals (Bhattacharyya et al., 2014). However, beyond the exploration of these antioxidant properties, the association of these compounds with

- This is an Open Access article distributed under the terms of the Creative Commons Attribution-Noncommercial 4.0 Unported License, permitting all non-commercial use, distribution, and reproduction in any medium, provided the original work is properly cited.

- Selection and peer-review under responsibility of the Organizing Committee of the Conference

© 2024 Published by ISRES Publishing: www.isres.org

serum proteins such as HSA (Human Serum Albumin) is attracting increasing attention. HSA, a major plasma protein, plays a crucial role in the transport and stabilization of small bioactive molecules (Zhang et al., 2021). Its interaction with polyphenols, particularly those present in *Malva sylvestris*, could amplify their biological effects by stabilizing these compounds in physiological environments.

In this sense, this study focuses on assessing the antioxidant and anti-inflammatory effects of *Malva sylvestris* in interaction with BSA, with the aim of better understanding the impact of this interaction on the mechanisms of protection against oxidative stress.

Materials and Methods

Plant Collection

Malva Sylvestris leaves were collected in October 2022 from M'sila, Algeria. The plant was identified by Doctor Mahmoud Laribi, botanist at Mouloud Mammeri University of Tizi-Ouzou, department of vegetal biology, where a voucher specimen was deposited (FSBSA/MK/oct2722). The sample was dried and then ground to obtain a powder that was stored at room temperature and in the dark until extraction.

Extract Preparation

20g of powder are dissolved in 200ml of distilled water. After 24 hours of maceration at room temperature, the filtrate was lyophilized.

Determination Of DPPH Radicals Scavenging Activity

The free radical scavenging activity of the extract was measured using the stable free radical DPPH test according to the method described by (Sharma & Bhat, 2009; Santos et al., 2010). 250 µl of 0.8 mM DPPH in ethanol was mixed with 3.65 ml of extract and 100µl of BSA. The reaction was carried out in triplicate and the absorbance was measured at 517nm after 30 minutes in dark. L-Ascorbic acid was used as reference standard.

Hydroxyl Radical Scavenging Assay

Scavenging activity of hydroxyl radical of the extract was measured according to the method of (Rajamanikandan et al., 2011) Three millilitres of the final reaction solution consisted of aliquots (500 µl) of various concentrations of the extract, 100µl of BSA, 1ml FeSO₄ (1.5 mM), 0.7 ml hydrogen peroxide (6 mM) and 0.3 ml sodium salicylate (20 mM). The reaction mixture was incubated for 1 h at 37°C. L-Ascorbic acid was used as the standard. The colour development was measured at 560 nm against a blank.

Hydrogen Peroxide Radical Scavenging Activity

The scavenging ability of water extract of *Malva Sylvestris* on hydrogen peroxide was determined according to the method of (Serteser et al., 2009). A solution of hydrogen peroxide (40 mM) was prepared in phosphate buffer (pH 7.4). BSA (100µl) and extract in distilled water (3.4 ml) was added to a hydrogen peroxide solution (0.6 ml, 40mM). Absorbance of hydrogen peroxide at 230 nm was measured 10 minutes later against a blank solution containing the phosphate buffer without hydrogen peroxide.

Ferrous Ion Chelating Activity

Ferrous ion chelating activity was determined by inhibition of the formation of iron(II)–ferrozine complex, following the method of (Dinis et al., 1994; Nabavi et al., 2012). Briefly, 100 µl of 0.6 mM FeCl₂ was added to 500µl of different concentrations of the extract mixed with 100µl of BSA or EDTA (positive control). The reaction mixture was adjusted to a final volume of 1.5ml with methanol, and then 100µl of 5 mM ferrozine solution were added. The mixture was shaken vigorously and left to stand at room temperature for 5 min. Absorbance was determined at 562nm.

Ferric Reducing Power Assay

Reducing power was determined by the method described by (Oyaizu, 1986; Hazra et al., 2008). Different concentrations of extract and BAS were mixed with 1.25 ml of 0.2 M, pH 6.6 sodium phosphate buffer and 1.25 ml of potassium ferricyanide (1%). The mixture was incubated at 50°C for 20 min. After incubation, the reaction mixture was acidified with 1.25 ml of trichloroacetic acid (10%) and centrifuged at 3000 rpm for 10 min. Finally, 0.5 ml of freshly prepared FeCl₃ (0.1%) was added to this solution, and the absorbance was measured at 700nm. Ascorbic acid at various concentrations was used as standard.

Total Antioxidant Capacity

Total antioxidant capacity was estimated by phosphomolybdenum assay (Prieto et al., 1999; Rao et al., 2010). The tubes containing extract and BSA and reagent solution (0.6 M sulfuric acid, 28 mM sodium phosphate and 4 mM ammonium molybdate) were incubated at 95°C for 90 min. Then the solution was cooled to room temperature and absorbance was read at 695 nm. Ascorbic acid was used as standard.

Antihemolytic Activity

Red Blood Cell Suspension

Blood was obtained by venipuncture from healthy volunteers collected in heparinized tubes and centrifuged at 2 000 r/min for 10 min at 4 °C. After removing the plasma, red blood cells (RBCs) were washed for three successive times using phosphate buffer saline (PBS) (0.9% NaCl). The study protocol was performed according to the Helsinki declaration and approved by Scientific Committee of the Faculty of Biology (CSFB). Informed written consent was obtained from Hospital Department of Hematology (University Hospital Nedir Mohamed of Tizi-Ouzou).

Hypotonic Solution Induced Hemolysis

Membrane stabilizing activity of extract and BSA was assessed using hypotonic solution induced hemolysis, and the method was described by de Freitas et al. (de Freitas et al., 2008). In hypotonic solution, the test sample consisted of washed stock erythrocyte (RBC) suspension (40 mL) with 1 mL of hypotonic solution (0.1%, 0.3% and 0.7% NaCl) in sodium PBS (pH 7.4) containing either of the different concentrations of BSA. The mixture was incubated for 30 min at 37 °C under gentle stirring, centrifuged for 10 min at 2 000 r/min and the absorbance of the supernate was measured at 540 nm.

Heat Induced Hemolysis

Different concentrations of the extract mixed with BSA (mg/mL) or aspirin dissolved in isotonic PBS (pH 7.4) was mixed with 1 mL of 2% RBCs suspension. The reaction mixture was incubated in a water bath at 56 °C for 30 min. After incubation, the tubes were cooled under running tap water, then centrifuged at 2 000 r/min for 10 min and the absorbance of the supernatants was estimated at 560 nm (Sakat et al., 2010).

Oxidant Induced Hemolysis

One milliliter of RBC suspension (5%) in PBS (pH 7.4) was incubated for 15 min at 37°C with 1 ml of the extract mixed with BSA at different concentrations. After preincubation, the mixture was centrifuged at 2 000 r/min for 10 min at 4°C, the supernatant was removed and packed RBCs were resuspended with 0.5 mmol/L HOCl in PBS. After this, the incubation was performed as previously described. The absorbance was determined at 540 nm (Suwalsky et al., 2007; Chandler et al., 2013).

Results and Discussion

The results obtained in this study for both the antioxidant and the anti-inflammatory activity of *Malva sylvestris* aqueous extract alone and in combination with BSA are summarized in the following tables (Tables 1 and 2).

Table 1. IC 50 recorded for antioxidant activity

Test	IC50 standard	IC50 <i>Malva sylvestris</i>	IC50 <i>M sylvestris</i> + BSA
DPPH radicals scavenging activity	2.359 ± 0.091 µg/ml	7.81 ± 0.402 µg/ml	3.825 ± 0.422 µg/ml
Hydroxyl radical scavenging assay	758.83 ± 7.40 µg/ml	971.28 ± 27.12 µg/ml	296.13 ± 69.33 µg/ml
Hydrogen peroxide radical scavenging activity	259.95 ± 9.33 µg/ml	431.06 ± 11.72 µg/ml	296.13 ± 69.33 µg/ml
Ferrous ion chelating activity	57.21 ± 0.44 µg/ml	74.631 ± 1.19 µg/ml	137.96 ± 30.07 µg/ml
Ferric reducing power assay	88.17 ± 1.39 µg/ml	46.7 ± 0.85 µg/ml	42.93 ± 46.38 µg/ml
Total antioxidant capacity	292 ± 7.54 µg/ml	348.357 ± 6.03 µg/ml	310.5 ± 11.33 µg/ml

Table 2. Percentage of protection recorded for erythrocyte membrane stabilization

Test	Protection % <i>Malva sylvestris</i>	Protection % <i>M sylvestris</i> + BSA
Hypotonic solution induced hemolysis	0.3% NaCl: 79.57% 0.7% NaCl: 60.3%	0.3% Na Cl: 80.3% 0.7% Na Cl: 60.7%
Heat induced hemolysis	90%	89.1%
Oxidant induced hemolysis	63.10%.	65.8%

DPPH Scavenging Activity

Table 1 presents the percentage inhibition of DPPH radical scavenging activity by the samples tested. The IC₅₀ value, representing the concentration required to scavenge 50% of DPPH radicals, was used to compare the antioxidant potential of different samples. The IC₅₀ of ascorbic acid was 2.359 ± 0.091 µg/ml, significantly lower than that of the aqueous extract of *Malva sylvestris* (IC₅₀ = 7.81 ± 0.402 µg/ml). However, when combined with BSA, the antioxidant activity of the extract improved notably, with an IC₅₀ value of 3.825 ± 0.422 µg/ml, indicating an enhanced scavenging capacity.

Hydroxyl Radical Scavenging

The ability of *Malva sylvestris* aqueous extract, alone and in combination with BSA, to scavenge hydroxyl radicals was assessed using salicylic acid as a reference compound. As shown in Table 1, scavenging activity increased with increasing concentration. Ascorbic acid (IC₅₀ = 758.83 ± 7.40 µg/ml) showed the most effective scavenging ability, while the extract alone (IC₅₀ = 971.28 ± 27.12 µg/ml) had a lower capacity. Interestingly, the combination of the extract with BSA significantly improved hydroxyl radical scavenging, achieving an IC₅₀ of 296.13 ± 69.33 µg/ml, which is considerably lower than that of the extract alone.

Hydrogen Peroxide Radical Scavenging Activity

The scavenging activity of hydrogen peroxide for the samples was also evaluated, with results showing significant variation. Ascorbic acid (IC₅₀ = 259.95 ± 9.33 µg/ml) exhibited the strongest activity, while *Malva sylvestris* alone had a higher IC₅₀ (431.06 ± 11.72 µg/ml), indicating less scavenging potential. However, the combination with BSA resulted in a marked improvement in activity, with an IC₅₀ of 296.13 ± 69.33 µg/ml, suggesting the potential of BSA to enhance the extract's antioxidant effects.

Ferrous Ion Chelating Activity

The ferrous ion chelating activity of the *Malva sylvestris* extract and its combination with BSA was measured by evaluating the reduction in color intensity of the Fe²⁺-Ferrozine complex. EDTA (IC₅₀ = 57.21 ± 0.44 µg/ml) demonstrated the highest activity. The extract alone showed a lower chelating effect (IC₅₀ = 74.631 ± 1.19 µg/ml).

1.19 µg/ml), while the combination with BSA displayed a significantly higher IC₅₀ of 137.96 ± 30.07 µg/ml, indicating that the combination is less effective at chelating iron than the extract alone.

Ferric Reducing Power Assay

The ferric reducing power of the samples was evaluated, and it was observed that the extract's reducing power was concentration-dependent. The IC₅₀ of *Malva sylvestris* extract alone (46.7 ± 0.85 µg/ml) was higher than that of ascorbic acid (88.17 ± 1.39 µg/ml), indicating strong reducing capacity. When combined with BSA, the IC₅₀ slightly improved to 42.93 ± 46.38 µg/ml, suggesting that the combination maintains the reducing capacity.

Total Antioxidant Capacity

The total antioxidant capacity was determined using the reduction of Mo (VI) to Mo (V). Ascorbic acid (IC₅₀ = 292 ± 7.54 µg/ml) displayed stronger antioxidant capacity compared to the extract alone (IC₅₀ = 348.357 ± 6.03 µg/ml). However, the combination of the extract with BSA showed a moderate improvement, with an IC₅₀ of 310.5 ± 11.33 µg/ml, further confirming the synergistic effect of BSA on the antioxidant potential of the extract.

Heat-Induced Hemolysis

As illustrated in Table 2, both the native *Malva sylvestris* extract and the combination with BSA provided significant protection against heat-induced erythrocyte hemolysis. While aspirin offered maximum protection (62.97 ± 2.1%), both the extract alone and the combination with BSA achieved similar levels of protection, around 90%, with the combination slightly lower at 89.1%.

Hypotonic Solution-Induced Hemolysis

Table 2 demonstrates the protective effects of the samples against hypotonic solution-induced hemolysis. The extract alone provided 79.57% protection at 0.3% NaCl, while the combination with BSA slightly increased this protection to 80%. At 0.7% NaCl, the extract offered 60.3% protection, with a similar result for the combination at 60.7%.

Oxidant-Induced Hemolysis

In the presence of oxidative stress, as shown in Table 2, the *Malva sylvestris* extract alone exhibited 63.10% protection against hemolysis, whereas the combination with BSA increased this protection to 65.8%, further indicating the enhanced bioactivity of the extract when combined with BSA. This study investigates the impact of the combination of *Malva sylvestris* aqueous extract and bovine serum albumin (BSA) on antioxidant and anti-inflammatory activities. The results highlight the potential impact of this combination on the antioxidant and anti-inflammatory activity of the extract studied. The combination of *Malva sylvestris* with BSA demonstrated a remarkable synergy in the inhibition of free radicals, notably DPPH● and OH●. This improvement in free radical scavenging capacity can be attributed to several factors:

The polyphenols present in *Malva sylvestris* probably interact with the thiol residues (Cys-34) of BSA. These residues play a crucial role in the scavenging of reactive oxygen species (ROS), thereby increasing the overall efficiency of radical scavenging (Colombo et al., 2012). BSA can act as a redox buffer, stabilizing polyphenols in biological environments and extending their half-life under physiological conditions (Zhang et al., 2021). This stabilization could explain the observed increase in antioxidant activity. The hydroxyl radical, considered the most reactive of the free radicals, is particularly well neutralized by this combination. This is significant given its ability to interact with intracellular targets such as DNA, causing significant damage (Lushchak, 2014).

In contrast to the synergistic effect observed for free radical scavenging, the combination with BSA showed a negative impact on metal ion chelation capacity and iron reduction. This phenomenon can be explained by: BSA, as a carrier protein, has metal-binding sites that can compete with *Malva sylvestris* polyphenols for the chelation of metal ions, particularly Fe²⁺ (Sugio et al., 1999).

This competition may limit the availability of metal ions to be sequestered by the extract's polyphenols, thus reducing the overall efficiency of iron chelation and reduction. This result highlights the importance of considering the relative concentration of proteins and polyphenols in optimizing the overall antioxidant effect. The combination of *Malva sylvestris* with BSA showed no significant improvement in the protection of erythrocyte membranes against oxidative stress, with a percentage protection of 65.8% versus 63.10% for the extract alone. The integrity of erythrocyte membranes is often used as a model for assessing the stabilization of lysosomal membranes, essential for preventing the release of pro-inflammatory enzymes (Omale & Okafor, 2008). By analogy with BSA, HSA, by stabilizing these membranes, could play a crucial role in inhibiting the release of lysosomal enzymes, thus offering better protection against inflammatory processes (Govindappa et al., 2011).

The stabilizing action of HSA on cell membranes, combined with the intrinsic anti-inflammatory properties of *Malva sylvestris*, suggests a synergistic anti-inflammatory effect that is not very effective *in vitro* but has potential *in vivo*. The complexes formed between BSA and polyphenols of *Malva sylvestris* could modulate the inflammatory response by inhibiting lipid peroxidation and stabilizing lysosomal membranes (Adefegha & Oboh, 2011).

The study did not reveal any significant synergistic or antagonistic effects for H₂O₂ scavenging and for the protection of erythrocyte cells against osmotic and thermal stress. However, these results remain relevant: Although hydrogen peroxide is not highly reactive on its own, it can be toxic to cells by giving rise to the hydroxyl radical (Moualek et al., 2020). The elimination of H₂O₂ therefore remains crucial to cellular antioxidant defense. The fact that the combination with BSA does not diminish these capabilities of *Malva sylvestris* extract is positive, indicating that the combination maintains the extract's efficacy in these specific aspects of cellular protection.

Conclusion

This preliminary study highlights the promising potential of the combination of *Malva sylvestris* aqueous extract and BSA. The results show a significant improvement in certain antioxidant activities, notably free radical scavenging and cell membrane protection, although a moderate impact was observed on metal chelation and iron reduction capacities.

The synergy observed in membrane stabilization and anti-inflammatory activity underlines the protective role of this combination against oxidative damage and inflammatory processes. The interactions between *Malva sylvestris* polyphenols and BSA appear to enhance the bioactivity of the plant extracts, making this combination promising for future therapeutic applications, particularly in the fight against oxidative stress and inflammation. However, the complexity of the interactions observed, with variable effects depending on the tests carried out, highlights the need for further research. It would be pertinent to explore in greater detail the molecular mechanisms underlying these interactions, to optimize the relative concentrations of extract and BSA, and to conduct *in vivo* studies to confirm these beneficial effects under physiological conditions.

In conclusion, this study opens up interesting prospects for the combined use of *Malva sylvestris* and BSA in the development of new antioxidant and anti-inflammatory strategies, while underlining the importance of a nuanced approach to the interpretation of interactions between natural compounds and proteins.

Scientific Ethics Declaration

The authors declare that the scientific ethical and legal responsibility of this article published in EPSTEM Journal belongs to the authors.

Acknowledgements

* This article was presented as an oral presentation at the International Conference on Basic Sciences and Technology (www.icbast.net) held in Antalya/Turkey on November 14-17, 2024.

References

- Adefegha, S. A., & Oboh, G. (2011). Water extractable phytochemicals from some Nigerian spices inhibit Fe²⁺-induced lipid peroxidation in rat's brain – in vitro. *J Food Process Technol*, 2(1), 104.
- Bhattacharyya, A., Chattopadhyay, R., Mitra, S., & Crowe, S. E. (2014). Oxidative stress: an essential factor in the pathogenesis of gastrointestinal mucosal diseases. *Physiological Reviews*, 94(2), 329-354.
- Chandler, J. D., Min, E., Huang, J., Nichols, D. P., & Day, B. J. (2013). Nebulized thiocyanate improves lung infection outcomes in mice. *British Journal of Pharmacology*, 169(5), 1166-1177.
- Colombo, G., Clerici, M., Giustarini, D., Rossi, R., Milzani, A., & Dalle-Donne, I. (2012). Redox albuminomics: oxidized albumin in human diseases. *Antioxidants & Redox Signaling*, 17(11), 1515-1527.
- de Freitas, M. V., Rita de Cássia, M. N., da Costa Huss, J. C., de Souza, T. M. T., Costa, J. O., Firmino, C. B., & Penha-Silva, N. (2008). Influence of aqueous crude extracts of medicinal plants on the osmotic stability of human erythrocytes. *Toxicology in Vitro*, 22(1), 219-224.
- Dinis, T. C., Madeira, V. M., & Almeida, L. M. (1994). Action of phenolic derivatives (acetaminophen, salicylate, and 5-aminosalicylate) as inhibitors of membrane lipid peroxidation and as peroxyl radical scavengers. *Archives of Biochemistry and Biophysics*, 315(1), 161-169.
- Govindappa, M., Naga Sravya, S., Poojashri, M. N., Sadananda, T. S., Chandrappa, C. P., Santoyo, G., ... & Anil Kumar, N. V. (2011). Antimicrobial, antioxidant and in vitro anti-inflammatory activity and phytochemical screening of water extract of Wedelia trilobata (L.) Hitchc. *Journal of Medicinal Plants Research*, 5(24), 5718-5729.
- Hazra, B., Biswas, S., & Mandal, N. (2008). Antioxidant and free radical scavenging activity of *Spondias pinnata*. *BMC Complementary and Alternative Medicine*, 8(1), 63.
- Idir, Moualek., Djedjiga, M., Karima, B., Hillal, S., Karim, B., & Karim, H. (2020). Evaluation of antioxidant potential of algerian malva sylvestris aqueous extract. *Ponte International Journal of Science and Research*, 76(4).
- Lushchak, V. I. (2014). Free radicals, reactive oxygen species, oxidative stress and its classification. *Chemico-Biological Interactions*, 224, 164-175.
- Nabavi, S. F., Nabavi, S. M., Hellio, C., Alinezhad, H., Zare, M., Azimi, R., & Baharfar, R. (2012). Antioxidant and antihemolytic activities of methanol extract of *Hyssopus angustifolius*. *Journal of Applied Botany and Food Quality*, 85(2), 198-201.
- Omale, J., & Okafor, P. N. (2008). Comparative antioxidant capacity, membrane stabilization, polyphenol composition and cytotoxicity of the leaf and stem of *Cissus multistriata*. *African Journal of Biotechnology*, 7(17).
- Oyaizu, M. (1986). Studies on products of browning reaction antioxidative activities of products of browning reaction prepared from glucosamine. *The Japanese Journal of Nutrition and Dietetics*, 44(6), 307-315.
- Prieto, P., Pineda, M., & Aguilar, M. (1999). Spectrophotometric quantitation of antioxidant capacity through the formation of a phosphomolybdenum complex: specific application to the determination of vitamin E. *Analytical Biochemistry*, 269(2), 337-341.
- Rajamanikandan, S., Sindhu, T., Durgapriya, D., Sophia, D., Ragavendran, P., & Gopalakrishnan, V. K. (2011). Radical scavenging and antioxidant activity of ethanolic extract of *Mollugo nudicaulis* by in vitro assays. *Indian Journal of Pharmaceutical Education and Research*, 45(4), 310-316.
- Rao, A. S., Reddy, S. G., Babu, P. P., & Reddy, A. R. (2010). The antioxidant and antiproliferative activities of methanolic extracts from Njavara rice bran. *BMC Complementary and Alternative Medicine*, 10, 1-9.
- Sakat, S., Tupe, P., & Juvekar, A. (2010). Gastroprotective effect of methanol extract of *Oxalis corniculata* Linn (whole plant) experimental animals. *Planta Medica*, 76(12), P090.
- Santos, S. A., Pinto, P. C., Silvestre, A. J., & Neto, C. P. (2010). Chemical composition and antioxidant activity of phenolic extracts of cork from *Quercus suber* L. *Industrial Crops and Products*, 31(3), 521-526.
- Serteser, A., Kargioğlu, M., Gök, V., Bağcı, Y., Özcan, M. M., & Arslan, D. (2009). Antioxidant properties of some plants growing wild in Turkey. *Grasas Y Aceites*, 60(2), 147-154.
- Sharma, O. P., & Bhat, T. K. (2009). DPPH antioxidant assay revisited. *Food Chemistry*, 113(4), 1202-1205.
- Singh, R. (2015). Medicinal plants: A review. *Journal of Plant Sciences*, 8(2), 50-55.
- Sugio, S., Kashima, A., Mochizuki, S., Noda, M., & Kobayashi, K. (1999). Crystal structure of human serum albumin at 2.5 Å resolution. *Protein Engineering*, 12(6), 439-446.
- Suwalsky, M., Orellana, P., Avello, M., & Villena, F. (2007). Protective effect of *Ugni molinae* Turcz against oxidative damage of human erythrocytes. *Food and Chemical Toxicology*, 45(1), 130-135.
- Velioglu, Y., Mazza, G., Gao, L., & Oomah, B. D. (1998). Antioxidant activity and total phenolics in selected fruits, vegetables, and grain products. *Journal of Agricultural and Food Chemistry*, 46(10), 4113-4117.

Zhang, C., Guan, J., Zhang, J., Yang, J., Wang, X., & Peng, X. (2021). Protective effects of three structurally similar polyphenolic compounds against oxidative damage and their binding properties to human serum albumin. *Food Chemistry*, 349, 129118.

Author Information

Idir Moualek

Mouloud Mammeri University of Tizi-Ouzou,
Algeria
Contact e-mail: moualek_idir@yahoo.fr

Karima Benarab

University Hospital Center of Tizi-Ouzou,
Algeria

Karim Houali

Mouloud Mammeri Tizi-Ouzou University,
Algeria

To cite this article:

Moualek, I., Benarab, K., & Houali, K. (2024). Evaluation of antioxidant and anti-inflammatory activities of aqueous extract of *Malva sylvestris* leaves in association with serum albumin. *The Eurasia Proceedings of Science, Technology, Engineering & Mathematics (EPSTEM)*, 30, 56-63.

The Eurasia Proceedings of Science, Technology, Engineering & Mathematics (EPSTEM), 2024

Volume 30, Pages 64-71

ICBAST 2024: International Conference on Basic Sciences and Technology

Phenological and Morphological Characters Analysis of *Vicia Narbonensis* L. and *Vicia Sativa* L. in a Semi-Arid Context

Farid Djellal

Ferhat Abbas Sétif1 University

Selma Mahmah

Ferhat Abbas Sétif1 University

Azeddine Mouhous

M. Mammeri University

Si Ammar Kadi

M. Mammeri University

Amar Mebarkia

Ferhat Abbas Sétif1 University

Abstract: Our study focused on ten *Vicia narbonensis* L. ecotypes in comparison with two *Vicia sativa* L. ecotypes cultivated at the University of Sétif-1 experimental station. The aims work to study these twelve vetches behavior via phenological character (plant height) and some morphological stages (date: start of flowering, 50% of flowering and full flowering) monitoring, under the rainy conditions of the semi-arid region (East Algerian). The Two *Vicia sativa* L. ecotypes are used as controls because this species dominates forage crops in Algeria. The data collected are subjected to variance analysis based on comparison Fisher means (LSD) at the 5% threshold. The relationships between the different measured variables pairs are described and analyzed by calculating phenotypic correlations, based on genotypic means using the XLSTAT software (2014). The variance analysis indicates significant effects of ecotype, year and ecotype \times year interaction ($p < 0.05$), highlighting the great diversity in phenological evolution. Our results indicate that characteristics ecotype tested are strongly affected by interannual variations and the ecotypes are not stable for the parameters measured from one year to the next. According to three year average for *Vicia narbonensis* L., the earliest period at flowering start is recorded by ecotype N-2380 while the latest is recorded by ecotype N-2390. ANOVA indicated significant differences between ecotypes, years and their interaction for plant height. Finally, early ecotypes are preferred in semi-arid regions provided that spring frosts do not coincide with flowering. In other words, as they flower early, they can escape drought at end cycle and therefore give themselves more time to fill their pods.

Keywords: *Vicia narbonensis* L., *Vicia sativa* L., Ecotypes, Semi-arid

Introduction

Livestock farming in Algeria has always retained a traditional character, based mainly on pastoralism and the exploitation of natural resources (Carter, 1974). Among the various challenges faced by livestock farmers, feeding ruminants is particularly problematic due to its heavy reliance on natural vegetation (Merdjane and Yakhlef, 2016). Annual forage legumes, such as those of the *Vicia* genus, are an interesting alternative to replace the fallow year in cereal-fallow rotation (Issolah, 2008). Vetches (genus *Vicia* sp.) are forage legumes frequently grown in rainfed and semi-arid agricultural systems in the Mediterranean region (Turk, 1997). They

- This is an Open Access article distributed under the terms of the Creative Commons Attribution-Noncommercial 4.0 Unported License, permitting all non-commercial use, distribution, and reproduction in any medium, provided the original work is properly cited.

- Selection and peer-review under responsibility of the Organizing Committee of the Conference

© 2024 Published by ISRES Publishing: www.isres.org

are proving particularly suitable and promising as short-term forage crops. One of vetch's major assets is its versatility, enabling it to be grazed as green fodder or harvested and stored as silage or hay. In addition, their grains are sources of protein and energy for ruminant and non-ruminant feed (Sadeghi et al., 2009), while generally being less expensive than concentrates, particularly in developing countries. The contribution of vetch to agricultural and animal production systems worldwide is widely recognized (Berhanu et al., 2003).

Adding value to species of the *Vicia* sp. genus can help to guarantee sufficient, varied and balanced feed for livestock, based on protein-rich forage resources. This could also lead to a reduction in the costs associated with importing concentrated feed, thereby encouraging the development of livestock farming, as well as milk and meat production. The objective of this study is to examine the behavior of ten ecotypes of *Vicia narbonensis* L. in comparison to two ecotypes of *Vicia sativa* L. under the rainy conditions of the semi-arid region of Sétif, focusing on their phenological and morphological characteristics.

Method

Study Area Description

The trials were carried out on plots at the FERHAT Abbas Sétif University Campus (36°12' N; 5°21' E) under rainy conditions in the Sétif region. The climate in this region is continental, with wide annual and daily temperature variations, and two major climatic constraints: frost and sirocco. It is located in the semi-arid bioclimatic zone, at an altitude of 1,025m. Temperatures fall below 0°C in winter and reach peaks of over 40°C in summer. In addition, the difference in temperature between night and day, sometimes reaching 20°C in winter and spring, causes frost, which is very restrictive for plant growth (Bouzerzour & Benmahammed, 1994).

The soils at the test site belong to the steppe soil group (Perrier and Soyer, 1970). The physico-chemical composition of all the plots shows a silty-clay texture, a lumpy structure, a basic water pH (7.81), a total limestone content of 17.7% and an organic matter content ranging from 2.0 to 3.0%. Average annual rainfall is around 450 mm (Seltzer, 1947) and 373.8 mm for the period between 2006 and 2017 (ONM, 2017). However, rainfall is subject to very wide intra- and inter-annual variations. The trial was conducted during three cropping seasons 2017-2018; 2018-2019 and 2019-2020. Climatic conditions for the three seasons are presented in Table 2 (ONM, 2020). The three crop years are characterised by:

- Rainfall was fairly variable over the three cropping seasons, with higher amounts in the first year (469.05 mm), followed by the third year (384.56 mm), compared with only 321.20 mm in the second year;
- The maximum temperatures recorded were consistent across the three seasons, as were the minimum temperatures.

Plant Material Presentation

The experiment involved two species of the *Vicia* genus, represented by ten ecotypes of *Vicia narbonensis* L. of different origins (from ICARDA) and two ecotypes of *Vicia sativa* L. from Algeria. The ecotypes of *Vicia sativa* L. were used as control ecotypes because this species is well known among Algerian farmers (Table 1).

Table 1. Origins of the *Vicia narbonensis* L. and *Vicia sativa* L. ecotypes studied

Species	Ecotype	Code	Origin
<i>Vicia narbonensis</i> L.	1	N-2380	Lebanon
	2	N-2383	Lebanon
	3	N-2390	Lebanon
	4	N-2392	Lebanon
	5	N-2393	Syria
	6	N-2461	Turkey
	7	N-2464	Turkey
	8	N-2466	Turkey
	9	N-2468	Lebanon
	10	N-2561	Syria
<i>Vicia sativa</i> L.	11	S-174	Algeria
	12	S-BBA	Algeria

Essay Presentation

Sowing was carried out from the same seed lot on 04 January 2018 for the first year, 22 December 2019 for the second year and 23 December 2020 for the third year. All ecotypes were sown manually and separately in a completely randomised block design with three replications in a plot with a cereal (durum wheat) as the previous crop. Each elementary plot consisted of 4 rows 4 m long, spaced 30 cm apart. 336 seeds/plot (at a rate of 70 seeds/m²) of vetch were sown in each of these plots.

Various cultivation operations were carried out on this trial. Deep ploughing (25 cm) was carried out using a disc plough just after the first autumn rains (September and October), followed by two cross passes of covercrop to reduce weed infestation and obtain a good seedbed. During the three trial campaigns, the plots were weeded manually throughout the growing season as and when required, and fertilisers were not used. Harvesting was carried out manually; from 30 May to 19 June for the first year; from 11 June to 02 July for the second year and from 17 to 28 June for the third year.

Studied Characteristics

Phenological Stage

The phenological stages observed in this study comprise several key stages. Firstly, the date when flowering begins, which is determined by the number of days from germination to the appearance of the first inflorescence (Berrekia, 1985). Next, the date of 50% flowering is assessed by counting the number of days between germination and the appearance of half the flowers. Finally, the date of full flowering is measured in terms of the number of days from germination to the appearance of the maximum number of flowers. These different phenological stages provide crucial information on the development of the ecotypes studied.

Morphological Characteristics

Plant height (PH), measured in centimetres from the base to the end of the main stem at the time of full flowering.

Statistical Analysis

The collected data were processed using XLSTAT (2014) software, according to an analysis of variance based on the comparison of Fisher means (LSD) at the 5% threshold. The relationships between the different pairs of variables measured were described and analysed by calculating phenotypic correlations based on genotypic means.

Results and Discussion

For each species (*Vicia narbonensis* L. and *Vicia sativa* L.), the analysis of variance showed significant effects of ecotype, year and ecotype × year interaction ($p < 0.05$), highlighting the wide diversity in phenological development and production for the different parameters measured (Table 2).

Phenological Stage

Statistically significant differences ($P < 0.05$) were found between growing seasons (years) in terms of days to reach onset of flowering; 50% flowering and 100% flowering between ecotypes of *Vicia narbonensis* L. and *Vicia sativa* L. (Table 2). This indicates that the characteristics of the ecotypes of the two species tested in the semi-arid region of Sétif are strongly affected by inter-annual variations. The days to reach the three phenological stages in the 2017-2018 growing season were significantly fewer than in the other two seasons. This is probably because the amount of precipitation during the winter months and in March was higher than during the 2019-2020 or 2018-2019 growing seasons (Table 2).

Table 2. Variance of measured parameters of vetches studied (2017-2020)

Variation source	Phenological Stage (Days)				Morphological characteristics PH (cm)
	df	SF	50%F	100%F	
<i>Vicia narbonensis</i> L.					
Total	89	787.2	804.2	830.5	377.2
Ecotype	9	71.39*	21.12*	15.60*	12.55*
Year	2	10463*	11232*	11644.7*	4946.5*
Ecotype* Year	18	46.59*	10.12*	15.03*	16.33*
Overall mean		52.5	61.90	68.13	34.66
Standard deviation		16.17	16.37	16.58	11.43
Variation coefficient (%)		30.80	26.44	24.33	33.00
<i>Vicia sativa</i> L.					
Total	17	1482.7	1491.1	1482.7	1006.8
Ecotype	1	2.00*	3.50*	2.00*	1.10*
Year	2	3678.5*	3708.5*	3678.5*	2474.1*
Ecotype* Year	2	3.50*	3.50*	3.50*	1.67*
Overall mean		57.17	67.67	73.83	39.97
Standard deviation		20.97	20.98	21	17.4
Variation coefficient (%)		36.68	31.00	28.44	45.82

*: Significant at 5%; df: degree of freedom, SF: start flowering; 50%F: 50% flowering; 100%F: Full flowering; PH: plant height

Due to the favourable climatic conditions during the winter months of the 2017-2018 growing season, *Vicia narbonensis* L. and *Vicia sativa* L. ecotypes maintained their growth during the winter months, and they completed their vegetation periods and reached their flowering periods earlier in the growing season. Our results are similar to those reported by Mahdipour-Afa et al. (2021) on the possibility of introducing guar as a grain legume with various trials of pharmaceutical and cosmetic applications in the semi-arid climate of Tehran.

The days to reach the three phenological stages in the 2017-2018 growing season were significantly fewer than in the other two seasons. This is probably because the amount of precipitation during the winter months and in March was higher than during the 2019-2020 or 2018-2019 growing seasons (Table 2). Due to the favourable climatic conditions during the winter months of the 2017-2018 growing season, *Vicia narbonensis* L. and *Vicia sativa* L. ecotypes maintained their growth during the winter months, and they completed their vegetation periods and reached their flowering periods earlier in the growing season. Our results are similar to those reported by Mahdipour-Afa et al. (2021) on the possibility of introducing guar as a grain legume with various trials of pharmaceutical and cosmetic applications in the semi-arid climate of Tehran.

Table 3. Phenological stages observed in the studied ecotypes (2017-2020)

Ecotype	Flowering start (Days)				Flowering 50% (Days)				Flowering 100% (Days)			
	2017- 2018	2018- 2019	2019- 2020	Means	2017- 2018	2018- 2019	2019- 2020	Means	2017- 2018	2018- 2019	2019- 2020	Means
<i>Vicia narbonensis</i> L.												
N-2380	33.00 ^B	57.00 ^I	50.00 ^I	46.67	40.00 ^A	70.00 ^J	68.00 ^H	59.33	46.00 ^A	78.00 ^I	78.00 ^D	67.33
N-2383	33.00 ^B	72.00 ^E	57.00 ^C	54.00	40.00 ^A	76.00 ^G	69.00 ^G	61.67	46.00 ^A	81.00 ^F	79.00 ^C	68.67
N-2390	33.00 ^B	77.00 ^B	58.00 ^B	56.00	40.00 ^A	80.00 ^C	71.00 ^E	63.67	46.00 ^A	85.00 ^C	76.00 ^F	69.00
N-2392	33.00 ^B	69.00 ^G	65.00 ^A	55.67	40.00 ^A	79.00 ^D	75.00 ^C	64.67	46.00 ^A	83.00 ^E	83.00 ^B	70.67
N-2393	32.00 ^C	72.00 ^E	55.00 ^E	53.00	40.00 ^A	78.00 ^E	69.00 ^G	62.33	45.00 ^B	84.00 ^D	74.00 ^G	67.67
N-2461	31.00 ^D	73.00 ^D	58.00 ^B	54.00	39.00 ^B	75.00 ^H	71.00 ^E	61.67	44.00 ^C	80.00 ^G	77.00 ^E	67.00
N-2464	33.00 ^B	64.00 ^H	52.00 ^G	49.67	40.00 ^A	74.00 ^I	67.00 ^I	60.33	46.00 ^A	81.00 ^F	74.00 ^G	67.00
N-2466	32.00 ^C	71.00 ^F	54.00 ^F	52.33	39.00 ^B	75.00 ^H	69.00 ^G	61.00	45.00 ^B	79.00 ^H	76.00 ^F	66.67
N-2468	33.00 ^B	74.00 ^C	51.00 ^H	52.67	40.00 ^A	77.00 ^F	70.00 ^F	62.33	46.00 ^A	86.00 ^B	77.00 ^E	69.67
N-2561	34.00 ^A	69.00 ^G	50.00 ^I	51.00	40.00 ^A	72.00 ^I	72.00 ^D	62.00	45.00 ^B	79.00	79.00 ^C	67.67
Means	32.70	69.80	55.00	52.50	39.80	75.80	70.10	61.90	45.50	81.60 ^H	77.30	68.13
<i>Vicia sativa</i> L.												
S-174	32.00 ^C	82.00 ^A	56.00 ^D	56.67	39.00 ^B	85.00 ^B	78.00 ^A	67.33	45.00 ^B	92.00 ^A	85.00 ^A	74.00
S-BBA	33.00 ^B	82.00 ^A	58.00 ^B	57.67	40.00 ^A	87.00 ^A	77.00 ^B	68.00	46.00 ^A	92.00 ^A	83.00 ^B	73.67
Means	32.50	82.00	57.00	57.17	39.50	86.00	77.50	67.67	45.50	92.00	84.00	73.83

A, B, C, D, E, F, G, H, I, J: Groups of means according to Fisher's test (LSD) at the 5% significant level

According to the average of the three years, for *Vicia narbonensis* L., the earliest period at the start of flowering is recorded by ecotype N-2380 while the latest is recorded by ecotype N-2390. Ecotype N-2380 is also the earliest to reach 50% flowering, while the latest is ecotype N-2392. The latter has the longest period to reach 100% flowering, while ecotype N-2466 has the shortest period. The two ecotypes of *Vicia sativa* L. are late for the same phenological stages compared with the ecotypes of *Vicia narbonensis* L. (Table 3).

Among annual fodder legume species, early flowering ecotypes are of great importance, as they not only give more time to fill their pods before the onset of hot, dry weather, but also allow sufficient time for the crops that follow (Sayar and Han, 2014). Getnet et al (2003) reported that species such as *Vicia narbonensis* and *Vicia sativa* mature relatively earlier than other vetches. Mebarkia et al. (2010) find that an average of 64.0 to 79.0 and 76.0 to 92.0 days is required to reach onset of flowering and full flowering in *Vicia narbonensis* L.; respectively. Yilmaz (2008) reports that 114 to 126 days are required to reach 50% flowering in *Vicia narbonensis* L..

The cause of the differences between previous studies and our results of days to reach onset of flowering, 50% flowering and 100% flowering may be the differences between the ecological environments in which the experiments were conducted as well as the use of different ecotypes. Variation in the phenology of vetch species and their accessions has a significant effect on forage and grain yield productivity (Gezahagn et al., 2013). According to Richards (1991), crop phenology is the most important factor influencing yield and adaptation, especially where growth factors are limited.

The semi-arid region of Sétif is characterised by two major phenomena: spring frost and drought at the end of the cycle. Early ecotypes should be the best, provided that spring frosts do not coincide with flowering. Nevertheless, flowering behaviour in *Arabidopsis* is opportunistic to maximise growth rather than as protection against frost damage (Kinmonth-Schultz et al., 2023). These results have implications for future population success, as climate change may modify the relationship between daylength and temperature.

Morphological Characteristics

The ANOVA indicates significant differences between ecotypes, years and their interaction for plant height (Table 2). The significance of the ecotype*year interaction indicates that the ranking of the vetch ecotypes in terms of plant height is significantly affected by the change of year. In our study, the ranking of means according to the Fisher LSD test at 5% shows that *Vicia sativa* L. has the highest mean values; 37.72 and 38.22 cm compared with *Vicia narbonensis* L.; 33.24 to 36.48 cm (Table 4).

Table 4. Average height of vetch ecotypes studied (2017-2020)

Ecotype	Plant height (cm)			Mean
	2017-2018	2018-2019	2019-2020	
<i>Vicia narbonensis</i> L.				
N-2380	41.72 ^B	18.89 ^H	43.78 ^H	34.80
N-2383	34.89 ^I	21.67 ^A	43.33 ^I	33.30
N-2390	36.56 ^H	20.44 ^D	45.00 ^F	34.00
N-2392	39.28 ^E	19.33 ^G	41.11 ^K	33.24
N-2393	39.11 ^E	19.33 ^G	48.33 ^C	35.59
N-2461	41.39 ^C	19.55 ^F	44.66 ^G	35.20
N-2464	40.56 ^D	21.11 ^B	47.78 ^D	36.48
N-2466	40.67 ^D	20.22 ^E	41.89 ^J	34.26
N-2468	34.17 ^J	20.78 ^C	45.67 ^E	33.54
N-2561	43.11 ^A	20.44 ^D	45.00 ^F	36.18
Mean	39.15	20.18	44.66	34.66
<i>Vicia sativa</i> L.				
S-174	37.72 ^G	16.89 ^J	58.56 ^A	37.72
S-BBA	38.21 ^F	18.44 ^I	58.00 ^B	38.22
Mean	37.97	17.67	58.28	37.97

A, B, C, D, E, F, G, H, I, J: Groups of means according to Fisher's test (LSD) at the 5% significant level

The highest plant height is recorded during the 2019-2020 growing season; 44.66 cm in *Vicia narbonensis* L. and 58.28 cm in *Vicia sativa* L.; and the lowest during the 2018-2019 growing season (20.18 cm and 17.67); respectively (Table 4; Figure 1). In *Vicia narbonensis* L., the highest plant height is obtained for ecotype N-2393 (48.33 cm), and the lowest for ecotype N-2380 (18.89 cm); while for *Vicia sativa* L.; ecotype S-174 has the

highest height during the 2019-2020 growing season (58.56 cm) and the lowest during the 2018-2019 growing season (16.89 cm) (Table 4; Figure 1).

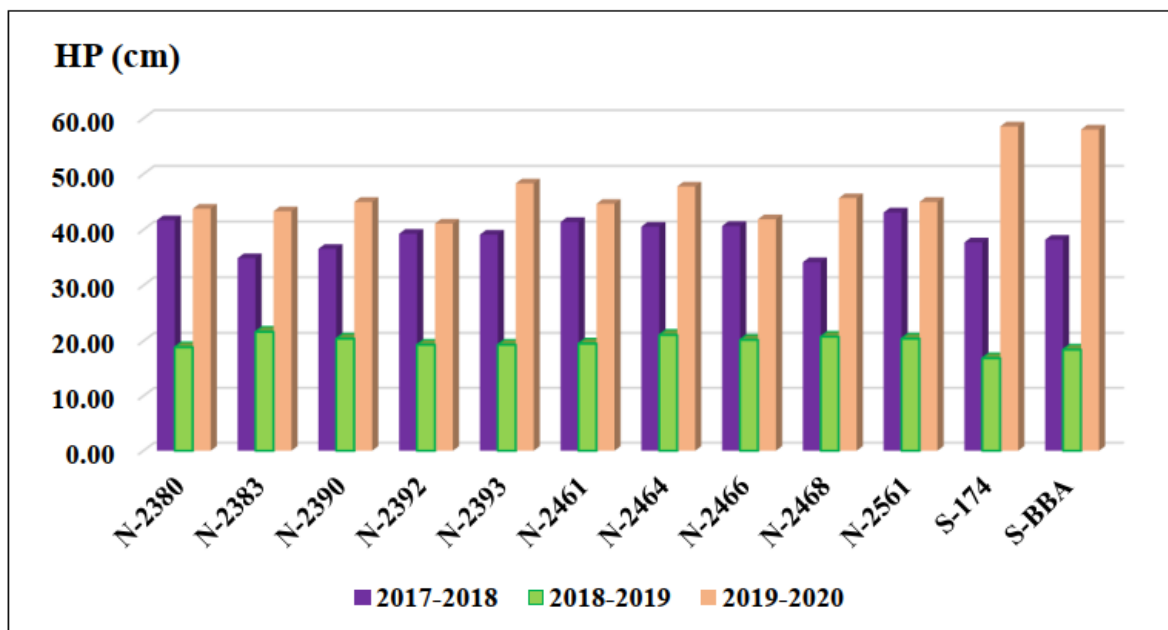


Figure 1. Heights of vetches studied (2017-2020)

Our results are lower in comparison with previous reports on *Vicia sativa* plant height reported by Gezahagn et al. (2013) (57.7-131.1 cm). These same authors find that plant height in *Vicia narbonensis* L. varies from 38.5 to 60.7 cm; which is consistent with the results of our study. Büyükburç and İptas (2001) report that plant height is a genotypic characteristic of Narbonne vetch, this characteristic is strongly affected by spring rainfall; i.e. in a year with a relatively high amount of spring rainfall, plant height is also relatively higher. Siddique et al. (1999) consider that plant height is the least stable characteristic, although it is the variable that best expresses the differences between the ecotypes studied.

Conclusion

Our findings indicate that the characteristics of the tested ecotypes are significantly affected by interannual variations, and that these ecotypes are not consistent in the measured parameters from one year to the next. Over the three-year average for *Vicia narbonensis* L., ecotype N-2380 exhibits the earliest flowering onset, while ecotype N-2390 shows the latest. ANOVA reveals significant differences among ecotypes, years, and their interactions concerning plant height. Ultimately, early-flowering ecotypes are favored in semi-arid regions, as long as spring frosts do not coincide with their flowering period. This early flowering allows them to avoid late-cycle droughts, providing more time for pod filling.

Recommendations

Early ecotypes are preferred in semi-arid regions, provided that spring frosts do not coincide with flowering. In other words, because they flower early, they can escape the drought at the end of the cycle and thus have more time to fill their pods.

Scientific Ethics Declaration

The authors declare that the scientific ethical and legal responsibility of this article published in EPSTEM Journal belongs to the authors.

Acknowledgements or Notes

* This article was presented as a poster presentation at the International Conference on Basic Sciences and Technology (www.icbast.net) held in Antalya/Turkey on November 14-17, 2024.

* We would like to thank all the technical staff at the farm and the laboratory at Ferhat ABBAS University Sétif-1.

References

- Berhanu, G., John, P., et Simeon, E. (2003). Land tenure and land management in the highlands of Northern Ethiopia. Research in Agricultural and applied economics. *Ethiopian Journal of Economics*, 8(2),46-63.
- Berrekia, R. (1985). Contribution à l'étude du genre *Hedysarum* L. en Algérie. *Institut National Agronomique, d'Alger (Algérie)*.
- Bouzerzour, H., & Benmahammed, A. (1994). Environmental factors limiting barley grain yield in the high plateaus of eastern Algeria. *Rachis*, 12, 11-14.
- Büyükburç, U., & İptaş, S. (2001). The yield and yield components of some narbon vetch (*Vicia narbonensis* L.) lines in Tokat ecological conditions. *Turkish Journal of Agriculture & Forestry*, 25(2),79-88.
- Getnet, A., Tekleyohanes, B., Lemma G, Mesfin, D., & Diriba, G. (2003). Major herbaceous forage legumes: Some achievements in species and varietal evaluation in Ethiopia. In: *Kemal, A., Seid, A., Surendra, Gemechu Kenneni, B., Rajendra, M., & Khaled, M. (Ed.). Food and forage legumes of Ethiopia: Progress and prospects*.
- Kebede, G., Assefa, G., Mengistu, A., & Mohammed, H. (2013). Evaluation of vetch species and their accessions for agronomic performance and Nutritive value in the Central Highlands of Ethiopia. *Ethiopian Journal of Agricultural Sciences*, 24(1), 99-121.
- Issolah, R. (2008). Diversité et valorisation des ressources fourragères en Algérie : cas des genres *Trifolium* L. et *Hedysarum* L. (*Fabaceae*). *Congrès national sur les ressources phytogénétiques en Algérie, INRAA*, 87-104.
- Kinmonth-Schultz, H., Sønstebo, J. H., Croneberger, A. J., Johnsen, S. S., Leder, E., Lewandowska-Sabat, A., ... & Fjellheim, S. (2023). Responsiveness to long days for flowering is reduced in Arabidopsis by yearly variation in growing season temperatures. *Plant, Cell & Environment*, 46(11), 3337-3352.
- Mahdipour-Afra, M., AghaAlihani, M., Abbasi, S., & Mokhtassi-Bidgoli, A. (2021). Growth, yield and quality of two guar (*Cyamopsis tetragonoloba* L.) ecotypes affected by sowing date and planting density in a semi-arid area. *Plos one*, 16(9), e0257692.
- Mebarkia, A., Abbas, K., & Abdelguerfi, A. (2010). Phenology and agronomic performances of the species *Vicia narbonensis* L. in the semi-arid region of Setif. *Journal of Agronomy*, 9(3),75-81.
- Merdjane, L., & Yakhlef, H. (2016). Le déficit fourrager en zone semi-aride: une contrainte récurrente au développement durable de l'élevage des ruminants. *Revue Agriculture. Numéro spécial*, 1, 43-51.
- Office National de la Météorologie (ONM). (2017-2020). Bulletin météorologique de la région de Sétif. *Office National de la Météorologie, Algérie*.
- Perrier, A., & Soyer, J. P. (1970). Cereal crop in the highlands: Study of the rotation wheat /fallow in the region of Setif. *Working agricultural Experimental Farm*. Setif, Algeria.
- Richards, R. A. (1991). Crop improvement for temperate Australia: future opportunities. *Field Crops Research*, 26(2), 141-169.
- Sadeghi, G. H., Mohammadi, L., Ibrahim, S. A., & Gruber, K. J. (2009). Use of bitter vetch (*Vicia ervilia*) as a feed ingredient for poultry. *World's Poultry Science Journal*, 65(1), 51-64.
- Sayar, M. S., Anlarsal, A. E., Basbağ, M., & Açıkgöz, E. (2011). Determination of forage yield, its affecting components and relationships among traits of some forage pea (*Pisum arvense* L.) genotypes in Hazro ecological conditions. *Turkey IX. Field Crops Congress, 12-15 September 2011, Bursa, Turkey*, 3, 1716-1721.
- Seltzer, P. (1947). *Le climat de l'Algérie*, (Ed). Institut de Météorologie et de Physique du globe de l'Algérie, Université Alger, Algérie.
- Siddique, K. H. M., Loss, S. P., Regan, K. L., & Jettner, R. L. (1999). Adaptation and seed yield of cool season grain legumes in Mediterranean environments of south-western Australia. *Australian Journal of Agricultural Research*, 50(3), 375-388.
- Turk, M.A. (1997). Comparison between common vetch and barley to phosphorus fertilizer application. *Legume Resources*, 20, 141-147.

Yilmaz, Ş. (2008). Effects of increased phosphorus rates and plant densities on yield and yield-related traits of narbon vetch lines. *Turkish Journal of Agriculture and Forestry*, 32(1), 49-56.

Author Information

Farid Djellal

Département d'agronomie, FSNV, Université Ferhat Abbas-UFAS-1- 19000, Sétif, Alegria.
Campus El Bez. Sétif 19137, Algeria.
Contact e-mail: fariddjellal@yahoo.fr

Selma Mahmah

Département d'agronomie, FSNV, Université Ferhat Abbas-UFAS-1- 19000, Sétif, Alegria.
Campus El Bez. Sétif 19137, Algeria.

Azeddine Mouhous

Faculté des Sciences Biologiques et des Sciences Agronomiques, Université M. MAMMERI, UN1501, Tizi-Ouzou, Alegria
UMMTO. Nouvelle ville BP 17 RP. 15000 Tizi Ouzou. Algeria

Si Ammar Kadi

Faculté des Sciences Biologiques et des Sciences Agronomiques, Université M. MAMMERI, UN1501, Tizi-Ouzou, Alegria
UMMTO. Nouvelle ville BP 17 RP. 15000 Tizi Ouzou. Algeria

Amar Mebarkia

Département d'agronomie, FSNV, Université Ferhat Abbas-UFAS-1- 19000, Sétif, Alegria.
Campus El Bez. Sétif 19137, Algeria

To cite this article:

Djellal, F., Mahmah, S., Mouhous, A., Kadi, S.A. & Mebarkia, A. (2024). Phenological and morphological characters analysis of *Vicia narbonensis* L. and *Vicia sativa* L. in a semi-arid context. *The Eurasia Proceedings of Science, Technology, Engineering & Mathematics (EPSTEM)*, 30, 64-71.

The Eurasia Proceedings of Science, Technology, Engineering & Mathematics (EPSTEM), 2024

Volume 30, Pages 72-77

ICBAST 2024: International Conference on Basic Sciences and Technology

Chemical Properties of Agricultural Soils after Applications of Municipal Sewage Sludge

Rabia Cherfouh

Mouloud Mammeri University

Khaled Ouali

Mouloud Mammeri University

Si Ammar Kadi

Mouloud Mammeri University

Azeddine Mouhous

Mouloud Mammeri University

Ali Bouzouren

Mouloud Mammeri University

Zahia Dorbane

Mouloud Mammeri University

Nacima Zimbri-Zirmi

Mouloud Mammeri University

Houci Guermah

Mohamed Boudiaf University

Farid Djellal

Ferhat Abbas University

Idir Moualek

Mouloud Mammeri University

Dahia Saidj

Saad Dehleb University

Abstract: An alternative technique for disposing and managing municipal sewage sludge is its application to soils associated with crop production. The aim of the present study was to evaluate the suitability of the existing sludge application routes in terms of the fertility of the soil and the accumulation of heavy metals. A chemical analysis was carried out on four agricultural soils located in the north-central region of Algeria, which had been subjected to an irregular application of sewage sludge for more than ten years. Results showed high levels of organic matter, nitrogen, phosphorus and potassium in the sludge samples. The amended soils are characterised by an increased content of organic matter and an improved availability of nutrients, including nitrogen, potassium and phosphorus. In addition, the pH of the soil solution is close to neutral, there is an increase in the cation exchange capacity and there is no change in the electrical conductivity. The total concentrations of cadmium, copper, nickel and zinc were found to be consistently low and below the acceptable limit values for soil. Copper accumulation in P3 soil was slightly above standard (122.4 mg.kg⁻¹). However, amended soils

- This is an Open Access article distributed under the terms of the Creative Commons Attribution-Noncommercial 4.0 Unported License, permitting all non-commercial use, distribution, and reproduction in any medium, provided the original work is properly cited.

- Selection and peer-review under responsibility of the Organizing Committee of the Conference

© 2024 Published by ISRES Publishing: www.isres.org

showed remarkable Cu (+167%) and Ni (+84%) accumulation. Whereas the total concentration of Cd is slightly lower than in the control soil, its speciation indicates a very high bioavailability. The results show that sewage sludge application has a positive effect on the availability of essential elements and the improvement of soil properties. However, inappropriate use and/or inaccurate application rates can lead to soil contamination with potentially toxic heavy metals.

Keywords: Municipal sewage sludge, Nutrients, Heavy metals, soil, Chemical properties.

Introduction

The objectives of land production, the search for the reduction of mineral fertilisers and for a circular economy are driving the agricultural use of sewage sludge (SS). In Algeria, the amount of SS currently produced by urban wastewater treatment plants is about 450,000 tons per year (Cherfouh et al., 2018; Hannachi et al., 2014). The weakness of soil fertility has increasingly promoted agricultural use, as this practice helps to avoid its uncontrolled disposal, recycles nutrients and minimizes soil pollution in terms of direct discharge into the natural environment (Montes et al., 2023; Rehman et al., 2013).

It is established that sewage sludge is a rich source of nutrients, including nitrogen and phosphorus, as well as organic matter and trace elements that are beneficial for plant growth and yield (Cherfouh et al., 2022; Kautale et al., 2005; Wong et al., 1995). Furthermore, sewage sludge is regarded as a viable alternative to commercial fertilisers. Sewage sludge has the potential to enrich soil with macronutrients, including phosphorus, potassium, sulphur, calcium and magnesium, as well as micro-nutrients (Cherfouh et al., 2018).

The dearth of experimental data on the effects of SS on soil properties gives rise to concerns regarding the potential damage caused in terms of soil quality, environmental pollution and human health problems. The necessity to consider the environmental hazards has prompted a multitude of studies and has prompted the authorities of numerous countries to establish regulations for the utilisation of SS in accordance with its heavy metal content and soil characteristics (Merdy et al., 2024; Mishalli et al., 2014).

The objectives of this work are to determine the effect of sewage sludge amendment on agronomic soil properties and to assess the potential contamination with heavy metals. In the absence of regulatory requirements, and as the agricultural use of SS started empirically, our objective is to find indications that the existing use routes for sewage sludge are sustainable in the long term.

Materials and Methods

Soil Sampling

The sampling was conducted in April 2021 to allow for the inclusion of pedological turnover processes. The study area is situated in the Tizi-Ouzou district of northern Algeria. Three representative vineyard soils receiving sewage sludge (S-SS) and a reference soil (RS) that did not receive either SS were sampled. At each site, five soil cores were sampled at the corners and at the centre at a depth of 0 to 10 cm. The five samples were thoroughly mixed together to create a composite soil sample. The samples were then air-dried and sieved at 2 mm. Aliquots of the < 2 mm soil fraction were ground in an agate mortar and stored in polyethylene containers at 4 °C until analysis.

Analysis

The soil texture was determined using the Robinson pipette method. All solutions were prepared using high-purity water and analytical-grade chemicals (Merck). For the sludge and soil samples, the pH and electrical conductivity (EC) were determined using a 1:5 soil-to-water ratio. The organic carbon and total nitrogen content of the solid samples (soils and SS) were determined using a CHNS apparatus (Shimadzu, Flash 2000) following H₃PO₄ pre-treatment (Pastor et al., 2011). For the liquid samples (water extracts), the dissolved organic carbon was determined using a TOC (total organic carbon) analyser (TOC-V CSH, Shimadzu). The cation exchange capacity (CEC) was determined for the sludge and soil samples by the cobaltihexamine procedure (Tarchouna et al., 2010). The metal contents were quantified by ICP-AES (inductively coupled plasma atomic emission spectrophotometry), while the ion concentrations in solution (nutrients and other major species).

Results and Discussion

Main Agronomical Characteristics of the Studied Soils, Sludge, and Wastewater

Tables 1 present the principal agronomical characteristics of the soils and SS. With regard to the soils, the values indicated in Table 1 pertain to the 0-10 cm soil layer. The SS exhibited elevated concentrations of soil organic matter (SOM) and total nitrogen, accompanied by a low C/N ratio (6.3). The water extract of the SS exhibited elevated concentrations of both dissolved organic carbon (WEOC) (1455 mg L^{-1}) and total nutrients. The given values for nutrients confirm the potentially positive agronomical effect of spreading sludge. The SS had high amounts of leachable Ca^{2+} , Mg^{2+} , K^+ , and SO_4^{2-} and lower, but non-negligible, concentrations for the sum of nitrogen species and PO_4^{3-} . Its high SO_4^{2-} value may be related to the possible use of sulphate compounds during the wastewater treatment process, as expected due to their high solubility. These attributes are likely associated with the elevated K^+ , Ca^{++} , NO_3^- and SO_4^{2-} values observed in the studied soils (S1, S2 and S3) when compared to the reference soil (RS), which has not been amended.

Granulometry and Dry Bulk Density.

The three studied soils showed similar mineral particles size distribution. According to the texture triangle, S1 is loam, S2, S3 and RS are silt-loam, this variability being consistent with the natural variability of the parental material. The Values of dry bulk density are in the range expected for the surface soil layer, between 1.1 and 1.3 g.cm^{-3} .

Soil pH

All soils exhibited a neutral to slightly alkaline pH (USDA, 1993). With regard to the reference soil, the application of SS resulted in a slight but significant increase in the average soil pH from 7.05, 7.69, 7.78, and 7.88 respectively (Table 1). The majority of studies have demonstrated that the application of sludge results in a reduction in pH soil. Here the elevated levels of potassium, calcium, and magnesium cations from the SS, when combined with the low organic matter content of the soil, are likely to result in an increase in soil alkalinity and subsequently in soil pH (figure 1).

Cation Exchange Capacity (CEC), Electrical Conductivity (EC) and SOM

The CEC values are within the typical range observed for this soil type, they were higher in amended soils than in the RS. This shows the improvement in the soil's ability to fix nutrients after sludge spreading (figure 2.). The EC values in soil extracts remained below $55.4 \text{ }\mu\text{S.cm}^{-1}$, despite the SS extract exhibiting significant conductivity ($946.5 \text{ }\mu\text{S.cm}^{-1}$). The low EC values in soils indicate sufficient leaching by annual deep drainage of soluble chemical species, indicating a very low risk of injury to all cultivated crops. The soil organic matter (SOM) content of the upper horizon is low (0.94%) in the RS, which is consistent with the characteristics of a Mediterranean soil. The application of sewage sludge resulted in a notable increase in SOM content, with values rising from 1.45, 2.41 and 2.98, respectively.

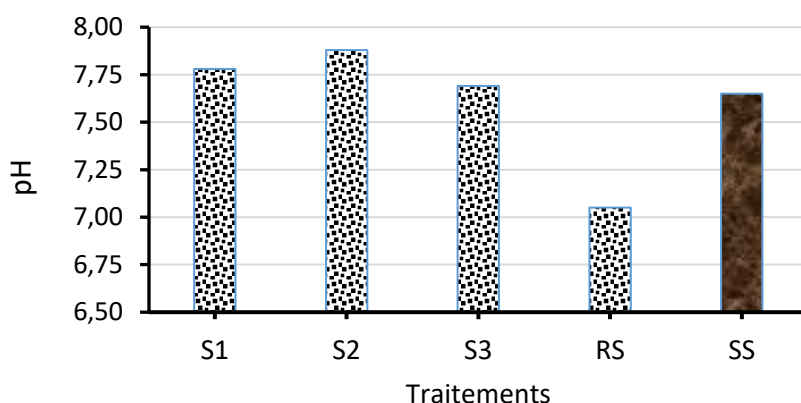


Figure 1. pH of the soil solution in amended soils

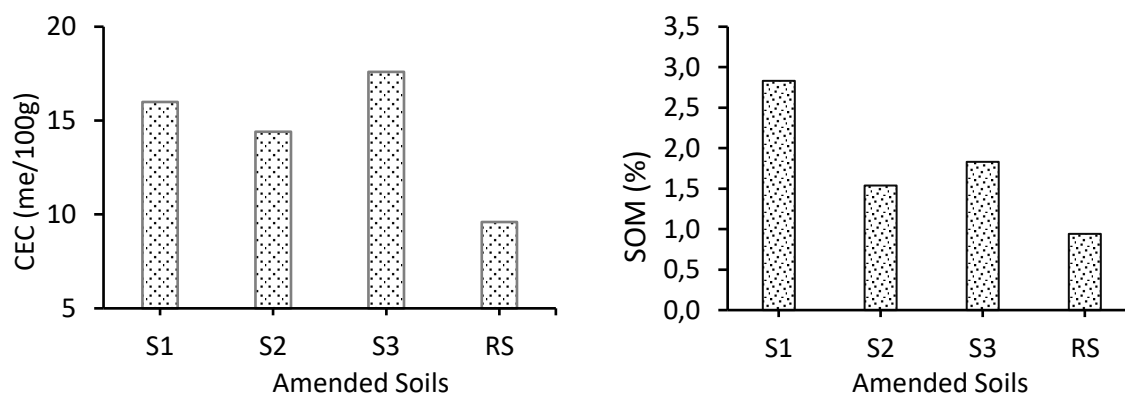


Figure 2. Cation exchange capacity and soil organic matter in amended soils

Water Extractable Nutrients

The sewage sludge exhibited elevated levels of leachable nutrients, including calcium, magnesium, potassium, and sulphate. These attributes are likely associated with the elevated values observed for the S1, S2, and S3 soils when compared to the RS soil. The findings demonstrated that SS amendment enhanced nutrient availability, particularly for potassium and phosphorus, in alignment with previous research.

Total Content of the Heavy Metals in Soils and Sewage Sludge

The sludge SS gave about 0.5, 119.6, 107.1 and 365.6 mg kg⁻¹ for Cd, Cu, Ni and Zn respectively. These heavy metal concentrations remain below the standard value for agricultural purposes. The sludge application leads to higher metal contamination on the soils. The metal accumulation index shows considerable variation among different soil types, with values ranging from 0.8 to 5.2 for copper, from 2.0 to 2.7 for nickel and from 2.2 to 4.1 for zinc. The concentration of Cd was found to be lower than that of the reference soil. This is probably due to the increased mobility of Cd in the studied soils.

Table1. Agronomic parameters for sludge (SS) and studied soils (S1, S2 and S3). Average values for the 0–10 cm soil layer.

Parameter	Unit	S1	S2	S3	RS	SS
CEC	me.100g ⁻¹	16.00	14.4	17.6	9.6	38.5
SOM	%, w/w	2.83	1.54	1.83	0.94	22.78
N total	%, w/w	0.25	0.11	0.14	0.09	3.61
C/N	#	11.52	14.11	13.01	10.38	6.31
WEOC	mg.L ⁻¹	129.8	62.04	65.39	172.42	14550
pH	#	7.78	7.88	7.69	7.05	7.65
CE	μS.cm ⁻¹	55.4	45.2	43	78.2	946.5
Ca ⁺⁺	mg.L-1	28.77	21.98	23.97	14.4	1057.6
Mg ⁺⁺	mg.L-1	2.85	3.16	3	10.03	198.1
K ⁺	mg.L-1	10.66	6.43	4.63	1.57	2487.4
Na ⁺	mg.L-1	2.01	1.76	2.21	1.59	553.6
Cl ⁻	mg.L-1	2.01	1.87	1.76	0.87	784.6
F ⁻	mg.L-1	0.07	0.26	0.27	14.72	nd
NO ₃ ⁻	mg.L-1	2.07	1.54	0.91	0.45	nd
NO ₂ ⁻	mg.L-1	0.77	0.36	0.53	5.55	nd
PO ₄ ⁻⁻⁻	mg.L-1	9.68	0.55	nd	3.59	900.9
SO ₄ ⁻⁻	mg.L-1	4.12	6.92	2.96	3.72	5595.4
Cd	mg.kg-1	0,17	nd	0,05	0,21	0,49
Cu	mg.kg-1	42,27	122,36	20,99	25,07	119,66
Ni	mg.kg-1	31,53	23,11	29,76	11,81	107,15
Zn	mg.kg-1	123,87	68,34	87,02	30,49	365,57

Furthermore, the concentration of Cd was found to be well below the ceiling value (2 mg kg⁻¹). The pH value recorded in the soil solution is indicative of alkalinity, suggesting that the solubility of ETMs is relatively low. The concentration of metals in the soil has a strong influence on the uptake by plants and on the biological life dependent on the soil (wong et al., 1995). The bioavailability regimes of metals vary with total content, leading to differences in the rates of soil processes such as SOM decomposition and soil chemistry. It's essential to determine the chemical speciation of heavy metals in the soil to get the best view of bioavailability. Recently, Merdy et al (2024) found that the Time to Critical Content Index (TCCI) for metals to reach the critical threshold was very different depending on whether the analysis was based on total content or on readily bioavailable fractions of metals.

Conclusion

The application of sludge has been demonstrated to result in elevated nutrient levels and a marked enhancement in soil fertility. These findings demonstrate the potential of urban sewage sludge application as a means of improving soil quality, even in the absence of data on the specific doses and frequencies employed. From an environmental perspective, however, the potential for soil contamination by heavy metals requires assessment.

Scientific Ethics Declaration

The authors declare that the scientific ethical and legal responsibility of this article published in EPSTEM Journal belongs to the authors.

Acknowledgements

* We would like to thank the Algerian Ministry of Higher Education and Scientific Research (MESRS) and the Mouloud Mammeri University of Tizi-Ouzou for the facilities that made it possible to carry out this work and to present it as a poster at the International Conference on Basic Sciences and Technology (ICBAST2024).

* This article was presented as a poster presentation at the International Conference on Basic Sciences and Technology (www.icbast.net) held in Antalya/Turkey on November 14-17, 2024.

References

- Cherfouh, R., Lucas, Y., Derridj, A., & Merdy, P. (2018). Long-term, low technicality sewage sludge amendment and irrigation with treated wastewater under Mediterranean climate: impact on agronomical soil quality. *Environmental Science and Pollution Research*, 25(35), 35571-35581.
- Cherfouh, R., Lucas, Y., Derridj, A., & Merdy, P. (2022). Metal speciation in sludges: A tool to evaluate risks of land application and to track heavy metal contamination in sewage network. *Environmental Science and Pollution Research*, 29(46), 70396-70407.
- Hannachi A, Gharzouli R, Djellouli Tabet Y (2014) Gestion et valorisation des eaux usées en Algérie. *Larhyss J* 19, 51–62.
- Kauthale, V. K., Takawale, P. S., Kulkarni, P. K., & Daniel, L. N. (2005). Influence of flyash and sewage sludge application on growth and yield of annual crops. *International Journal of Tropical Agriculture*, 23(1-4), 49-54.
- Merdy, P., Cherfouh, R., & Lucas, Y. (2024). Long-term agricultural reuse of treated wastewater and sewage sludge: developing a Time to Critical Content Index for metal species. *Environmental Monitoring and Assessment*, 196(9), 1-14.
- Montes, R., Méndez, S., Carro, N., Cobas, J., Alves, N., Neuparth, T., ... & Rodil, R. (2022). Screening of contaminants of emerging concern in surface water and wastewater effluents, assisted by the persistency-mobility-toxicity criteria. *Molecules*, 27(12), 3915.
- Mtshali, J. S., Tiruneh, A. T., & Fadiran, A. O. (2014). Characterization of sewage sludge generated from wastewater treatment plants in Swaziland in relation to agricultural uses. *Resources and Environment*, 4(4), 190-199.
- Ramdani, N., Hamou, A., Lousdad, A., & Al-Douri, Y. (2015). Physicochemical characterization of sewage sludge and green waste for agricultural utilization. *Environmental Technology*, 36(12), 1594-1604.

- Ramdani, N., Hamou, A., Lousdad, A., & Al-Douri, Y. (2015). Physicochemical characterization of sewage sludge and green waste for agricultural utilization. *Environmental Technology*, 36(12), 1594-1604.
- Soil Survey Division Staff. (1993). Soil survey manual. Soil conservation service. *United State Department of Agriculture Handb.* 18.
- Tarchouna, L. G., Merdy, P., Raynaud, M., Pfeifer, H. R., & Lucas, Y. (2010). Effects of long-term irrigation with treated wastewater. Part I: Evolution of soil physico-chemical properties. *Applied Geochemistry*, 25(11), 1703-1710.

Author Information

Rabia Cherfouh

Mouloud Mammeri University
17 RP, Tizi-Ouzou Algeria
Contact e-mail:rabiacherfouh@yahoo.fr

Khaled Ouali

Mouloud Mammeri University
17 RP, Tizi-Ouzou Algeria

Si Ammar Kadi

Mouloud Mammeri University
17 RP, Tizi-Ouzou Algeria

Azeddine Mouhous

Mouloud Mammeri University
17 RP, Tizi-Ouzou Algeria

Ali Bouzouren

Mouloud Mammeri University
17 RP, Tizi-Ouzou Algeria

Zahia Dorbane

Mouloud Mammeri University
17 RP, Tizi-Ouzou Algeria

Nacima Zimbri-Zirmi

Mouloud Mammeri University
17 RP, Tizi-Ouzou Algeria

Houci Guermah

Mohamed Boudiaf University
M'sila, Algeria

Farid Djellal

Ferhat Abbas University
Setif, Algeria

Idir Moualek

Mouloud Mammeri University
17 RP, Tizi-Ouzou Algeria

Dahia Saidj

I. S. V. ,Saad Dehleb University,
Blida, Algeria

To cite this article:

Cherfouh, R., Ouali, K., Kadi, S.A. Mouhous, A., Bouzourene, A., Dorbane, Z., Zirmi-Zembri, N., Guermah H. Djellal, F., Moualek, I. & Saidj, D. (2024). Chemical properties of agricultural soils after applications of municipal sewage sludge. *The Eurasia Proceedings of Science, Technology, Engineering & Mathematics (EPSTEM)*, 30, 72-77.

The Eurasia Proceedings of Science, Technology, Engineering & Mathematics (EPSTEM), 2024

Volume 30, Pages 78-84

ICBAST 2024: International Conference on Basic Sciences and Technology

Energy Audit of an Enterprise from Machine Industry

Slav Valchev

University of Food Technology

Ana Semerdzhieva

University of Food Technology

Stanislava Tasheva

University of Food Technology

Abstract: An energy survey of an enterprise operating in field of machine industry is carried out. During the energy audit, primary information about energy consumed by the enterprise for heating, ventilation, lighting and needs of production process for three year period was collected. Annual energy costs for three consecutive years were compared and highest energy costs were taken as a basis for determining the energy consumption baseline. Proposals for energy-saving measures are defined. The specific energy costs before and after energy-saving measures were calculated and comparisons between them were made. An assessment to optimize number of workers in the enterprise and increase its competitiveness was made. The effect of increasing the productivity of the enterprise was evaluated. Direct and indirect cost savings were estimated, realized during the implementation of energy-saving measures. Annual energy savings in machine industry enterprise as energy saved in kWh/year and in saved carbon emissions/year to the environment were presented.

Keywords: Energy survey, Energy audit, Energy efficiency, Carbon emissions

Introduction

Subject to mandatory energy efficiency audit in accordance with regulation act in Bulgaria are: large enterprises for the production of goods, large service providers, industrial systems whose annual energy consumption is over 3000 MWh (Ordinance №E-RD-04-3, 2016), (Ordinance №E-RD-04-05, 2016). However, in addition to them, many large and small businesses also take advantage of the opportunities of energy auditing to expand their production and implementation of new energy-efficient technological lines (Ivanov et al., 2021; Kamburova et al., 2017; Iliev et al., 2013). The main goals they want to achieve with this are the following:

- achieving low energy costs of the enterprise. The new technological equipment consumes less energy, which leads to a reduction in the specific energy costs per unit. Realized energy savings achieved help reduce the term of repayment for energy-saving measures and realizing greater profits from their implementation (Baev et al., 2015), (Kaloyanov et al., 2020);
- achieving reduction of operating costs in the enterprise. Use of highly efficient technological lines leads to a reduction in costs for repairs, consumables, blanks, etc. Expenses for employee business trips and for paying for services to subcontractors are also reduced;
- increasing the production capacity without increasing the workforce of the enterprise This leads to increased labor productivity, reduced technological waste due to human errors, both in terms of carbon emissions in the environment and technological waste;

- increasing the degree of automation in the production process. Reducing human errors in the production process leads to the production of a high-quality product in a continuous process. The increased level of automation of technological lines makes it easy to monitor energy consumption in real time;
- increasing the level of competence of the staff. The presence of automated technological lines in the enterprise leads to the fact that the enterprise will employ a small number of people, but each of them will have a high level of competence. The presence of highly competent personnel such as engineers, technologists, etc. guarantees the production of high quality products;
- production of products that meet current standards in the European Union. This requires the use of high-quality raw materials and highly efficient technologies in the production process. Under these conditions, the high quality of the product and the sale of the company's products on European markets are guaranteed;
- production of new products. In many cases, the purchased highly efficient technological lines have the ability to produce new products, which allows the company to increase both its productivity and its assortment. By covering a high standard of quality of all manufactured products, the company opens up opportunities to sell its product on new markets;
- low levels of harmful emissions to the environment. During the production of the product, low levels of harmful emissions into the atmosphere must be guaranteed, both from the equipment operating in the enterprise itself and from the sources producing energy that is subsequently supplied to the enterprise.

The presence of highly efficient technological lines and highly qualified personnel in the enterprise creates prerequisites for the company to easily implement and maintain quality standards in its production. In this way, the enterprise can create its own methodologies for waste management, for energy management, which are coordinated and comply with local legislation. Maintaining an enterprise resource planning (ERP) system is additional evidence of the high level of quality of the products produced. All of this is important for the enterprise to be able to participate in interaction with other enterprises for the conditions of circular economy. Assessment of the need and effectiveness of energy-saving measures in an enterprise is carried out with the help of energy audit (Kreith & Goswami, 2007; Rasheva, 2011; Shapiro, 2016; Thuman & Younger, 2008; Turner, 1997).

Method

The object of the present survey for energy efficiency of an industrial system is a machine enterprise in Bulgaria. The enterprise produces components for electric lamps and lighting fixtures. The following technological processes in process are carried out:

- Milling operation on details;
- Drilling operation on details;
- Manual operation - chamfering, plating and assembly on details.

Detailed energy analysis of the enterprises includes:

- collection of primary information on the energy costs of the enterprise for a period of 3 consecutive years and analysis in order to determine the potential for energy savings;
- determination of a reference year, on the basis of which the baseline of energy consumption of the enterprise is determined;
- determination of specific energy consumption depending on the production in the enterprise;
- determining the amount of energy savings as saved energy and as saved carbon emissions to the environment.

The introduction of energy-saving measures in the enterprise, such as the supply of new energy-efficient equipment, should not conflict with the requirements for:

- reducing the amount of waste from the enterprise;
- recycling materials used in production process;
- circular economy.

Results and Discussion

In Table 1 are shown data on installed electrical power of the facilities in the enterprise.

Table 1. Installed electrical power of the facilities in the enterprise

Name	Value	Power, kW	Total power, kW
Lathe with CNC	3	15.36	46.08
Horizontal processing center with CNC	1	27.00	27.00
Lathe universal	1	7.30	7.30
Universal milling cutter	1	7.30	7.30
Milling cutter	1	4.25	4.25
Watchmakers lathe	1	0.22	0.22
Hydraulic hacksaw machine	1	1.25	1.25
Hydraulic hacksaw machine	1	1.65	1.65
Drilling machine	3	1.30	3.90
Compressor for compressed air Working pressure 6 atm	1	1.50	1.50
Compressor for compressed air Working pressure 6 atm	1	1.00	1.00
Total usable power			101.45

In Table 2 are shown data for annual consumption of electrical energy in enterprise for 2021, 2022 and 2023 year.

Table 2. Annual consumption of electrical energy in enterprise for 2021, 2022 and 2023 year

Year	2021	2022	2023
Month	kWh	kWh	kWh
January	4566	4899	5304
February	4850	4340	4578
March	4620	4300	4306
April	5001	5025	5224
May	4200	3930	3873
June	4003	4880	4951
July	4685	4780	4793
August	3895	4222	4545
September	3768	3955	4160
October	3688	3554	4116
November	4935	3333	5066
December	4555	4892	4336
Total	52766	52110	55252

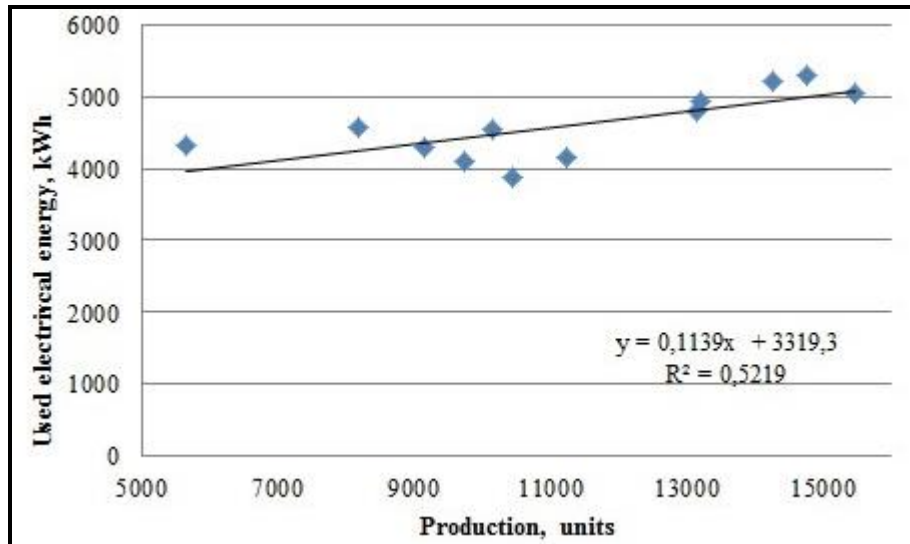


Figure 1. Correlation between used energy in enterprise and number of manufactured unit.

Used electrical energy is reported for production period of three years 2021, 2022 and 2023. Data in table show that annual consumption of electrical energy in enterprise is higher for 2023 year.. This is why this year was chosen as a reference year for energy audit. On Figure 1 are shown correlation between used energy in enterprise and number of manufactured unit. On Figure 2 is shown percentage distribution of electrical energy consumed in enterprise for reference year.

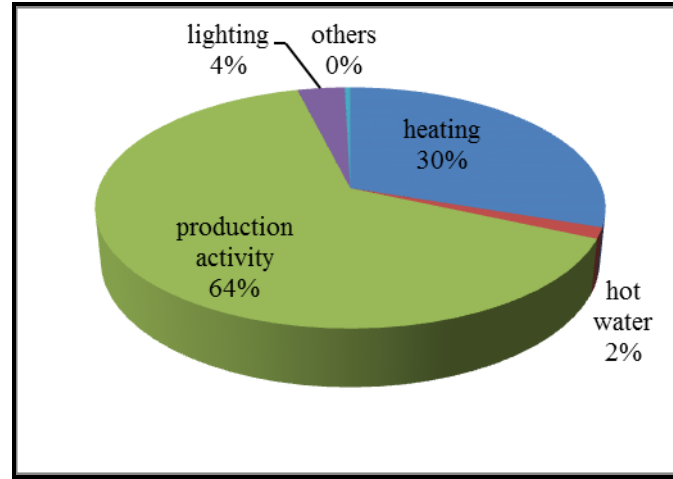


Figure 2. Percentage distribution of energy consumed in enterprise for reference year

The graph shows that there is a great potential for saving energy in machines with which the production activity is carried out. This requires optimization and replacement of facilities consuming electrical energy for production activity. The enterprise intends to make the following investments:

- Vertical processing center with CNC – 1 pieces (existing horizontal processing center will also be used in production process);
- Strip cutting machine - 1 pieces (new equipment - will replace two hydraulic hacksaw machine);
- Anodizing line– 1 pieces (new equipment);
- Spray dyeing line - 1 pieces (new equipment);

In Table 3 are shown data on installed electrical power of facilities in enterprise after energy saving measures. The installation of the new equipment will lead to an increase in the amount of new finished products from the enterprise. Data for the baseline of energy consumption in the enterprise after energy saving measures are shown in a Table 4.

Table 3. Installed electrical power of facilities in enterprise after energy saving measures.

Name	Value	Power, kW	Total power, kW
Lathe with CNC	3	15.36	46.08
Horizontal processing center with CNC	1	27.00	27.00
Vertical processing center with CNC	1	11.00	11.00
Lathe universal	1	7.30	7.30
Universal milling cutter	1	7.30	7.30
Milling cutter	1	4.25	4.25
Watchmakers lathe	1	0.22	0.22
Drilling machine	3	1.30	3.90
Strip cutting machine	1	1.19	1.19
Anodizing line	1	40.00	40.00
Spray dyeing line	1	60.00	60.00
Compressor for compressed air	1	1.50	1.50
Working pressure 6 atm			
Compressor for compressed air	1	1.00	1.00
Working pressure 6 atm			
Total usable power			210.74

Table 4. Baseline of energy consumption in the enterprise after energy saving measures

Name	Value	Unit of measure
Power consumption horizontal processing center with CNC - old	8876	kWh/year
Quantity produced before energy saving measures	10575	Units/ year
Power consumption processing center with CNC – old+new	18366	kWh/year
Quantity produced after energy saving measures old	26025	Units/ year
Power consumption hydraulic hacksaw machines	1075	kWh/year
Quantity produced before energy saving measures	12912	Units/ year
Power consumption strip cutting machine	413	kWh/year
Quantity produced after energy saving measures	19110	Units/ year
Power consumption anodizing line machine – good practice	43610	kWh/year
Quantity produced before energy saving measures	72000	Units/ year
Power consumption anodizing line machine – new	36960	kWh/year
Quantity produced after energy saving measures	72000	Units/ year
Power consumption spray dyeing line machine – good practice	28864	kWh/year
Quantity produced before energy saving measures	29400	Units/ year
Power consumption spray dyeing line machine – new	25099	kWh/year
Quantity produced after energy saving measures	29400	Units/ year
Baseline power consumption	95895	kWh/year

The implementation of a new horizontal processing center with CNC, strip cutting machine, anodizing line machine and dyeing line machine are accordingly marked as energy-saving measures ESM 1, ESM 2, ESM 3 and ESM 4. A comparison of specific costs before and after energy saving measures is shown in Table 5.

Table 5. Comparison of specific costs before and after energy saving measures

	Before ESM				After ESM		
	Energy consumption for related with measures activities	Produced output	Specific energy consumption	Corrected energy consumption for related with measures activities	Energy consumption for related with measures activities	Produced output	Specific energy consumption
	kWh/year	Units/year	kWh/unit	kWh/year	kWh/year	Units/year	kWh/unit
ESM 1	8876	10575	0.839	21835	18366	26025	0.706
ESM 2	1075	12912	0.083	1586	413	19110	0.022
ESM 3	43610	72000	0.606	43610	36960	72000	0.513
ESM 4	28864	29400	0.982	28864	25099	29400	0.854
Total:	82425	-	-	95895	80838	-	-

The share of the enterprise's energy savings compared to the reference year 2019 has been determined in energy value (in kWh) and ecological equivalent (t CO₂/ year). The results are shown in Table 6.

Table 6. Energy savings

Energy saving measures	Energy carrier	Energy savings		Ecological equivalent t CO ₂ / year
		kWh	%	
ESM 1	electricity	3469	15.89	2.8
ESM 2	electricity	1173	73.96	1.0
ESM 3	electricity	6650	15.25	5.4
ESM 4	electricity	3765	13.04	3.1
Total:	-	15057	15.70	12.3

Conclusion

With the introduction of the energy-saving measures, additional benefits will be realized, as follows:

ESM 1 - with implementation of new vertical processing center productivity and quality of the products will increase. Production interruptions in event of technical failures and needs for repair work will be avoided;

ESM 2 - with the implementation of strip cutting machine, savings will be achieved on ongoing operating costs, achieving savings on the loss of cutting material (waste reduction is expected up to 3 times, which will reduce the cost of purchasing materials for production);

ESM 3 - with the implementation of anodizing line machine savings will be generated from costs to a subcontractor company for performing service, fuel costs, travel expenses and remuneration of a seconded employee, carrying out the transport of the details to a subcontractor company;

ESM 4 - with the implementation of dyeing line machine savings will be generated from costs to a subcontractor company for performing service, fuel costs, travel expenses and remuneration of a seconded employee, carrying out the transport of the details to a subcontractor company;

No new personnel are expected to be hired to service new anodizing and dyeing line machines, as after implementation of new processing center, the company's existing employees will be able to perform maintenance activities on this machines. Upon implementation of the energy-saving measure, object of investment intention, the enterprise will realize an energy saving of 15.70% compared to the baseline of energy consumption, which is equal to an energy saving of 15057 kWh/ year with an ecological equivalent of 12.3 tons of CO₂ emissions saved.

Scientific Ethics Declaration

The authors declare that the scientific ethical and legal responsibility of this article published in EPSTEM Journal belongs to the authors.

Acknowledgements or Notes

* This article was presented as an oral presentation at the International Conference on Basic Sciences and Technology (www.icbast.net) held in Antalya/Turkey on November 14-17, 2024.

References

- Baev, D., Georgiev, Z., Manchev, P., Simeonov, K., Ivanova, D., Hristov, H., Canev, D., Haladzhova, R., & Stankov, A. (2024, 16 October). *Manual on energy efficiency management in enterprises (In Bulgarian)*. Retrieved from <https://seea.government.bg/documents/narachnik.pdf>
- Iliev, I., Kaloyanov, N., Gramatkov, P., Terziev, A., Pavlov, I., Stefanov, S., Sirakov, K., & Kamburova, V. (2024, 16 October). *Energy efficiency and energy management handbook*, Retrieved from https://www.exergia-max.com/sites/default/files/documents/EEEM_Handbook_ENG.pdf
- Ivanov, K., Georgieva, N., Tasheva, S., Gandova, V. (2021). Analysis of energy efficiency of an industrial system. *IOP Conference Series: Materials Science and Engineering*, 1031(1), 012080.

- Kaloyanov, N., Kasabov, I., Bojkov, C., Matanov, N., Penkova, N., Vasilev, M., Cekov, R., Tomova, M., Djabarska, S., Markova, S., & Todorov, C. (2024, 16 October). *Methodological instructions for do a survey for energy efficiency and evaluation of industrial energy savings systems and enterprises (In Bulgarian)*, Retrieved from https://seea.government.bg/documents/metodicheski_ukazania.pdf
- Kamburova, V., Iliev, I., Velikanov, M., Terziev, A., Ahmedov, A., & Iliev, K. (2017). Energy efficiency of large industrial enterprises. *Journal Energetika*, 3, 40-50.
- Kreith, F., & Goswami, D. (2007). *Energy Efficiency and Renewable Energy*. CRC Press.
- Ordinance № E-RD-04-3 of 4.05.(2016). *On admissible measures for implementation of energy savings in final consumption, ways of proving the achieved energy savings, requirements to methodologies for their evaluation and ways for their confirmation (In Bulgarian)*. Retrieved from https://seea.government.bg/documents/NAREDBA_ERD043_ot_4052016_g_za_dopustimite_merki_za_osyestvqvane_na_energijni_spestqvaniq_v_krajnot.pdf
- Ordinance № E-RD-04-05 of 8 (2016). *On determining energy consumption indicators, energy performance of enterprises, industrial systems and outdoor artificial lighting systems, as well as on determining conditions and procedure for conducting inspections for energy efficiency and preparation of energy savings assessment (in Bulgarian)*. Retrieved from <https://seea.government.bg/documents/Naredba%20ERD0405.pdf>
- Rasheva, V. (2011). *Energy technology analysis of industrial enterprise*. Academic publishing house of UHT - Plovdiv.
- Shapiro, I. M. (2016). *Energy audits and improvements for commercial buildings*. John Wiley & Sons.
- Thuman A., & Younger, W. (2008). *Handbook of energy audit*. The Fairmont Press Inc.
- Turner, W.(1997). *Energy Management Handbook*. Third Edition, The Fairmont Press, Inc.

Author Information

Slav Valchev

University of Food Technology
Plovdiv, Bulgaria, 26 Maritza Boulevard, Bulgaria
Contact e-mail: slav_vul4ev@abv.bg

Ana Semerdzhieva

University of Food Technology
Plovdiv, Bulgaria, 26 Maritza Boulevard, Bulgaria

Stanislava Tasheva

University of Food Technology
Plovdiv, Bulgaria, 26 Maritza Boulevard, Bulgaria

To cite this article:

Valchev, S., Semerdzhieva, A. & Tasheva, S. (2024). Energy audit of an enterprise from machine industry. *The Eurasia Proceedings of Science, Technology, Engineering & Mathematics (EPSTEM)*, 30, 78-84.

Early Predictors of Cognitive Decline and Stroke

Galya Atanasova
Medical University Pleven

Abstract: *Background* Insulin resistance can affect multiple tissues and organs, from the classic “triumvirate” (myocyte, adipocyte, and hepatocyte) to possible effects on organs such as the central nervous system. This review explores shared pathophysiological mechanisms between MCI and MS and establishes a hypothesis of a possible MCI role in the development of IR and the appearance of MS. *Objective* The objective of the study was to investigate new biomarkers for early diagnosis of MS, cognitive decline as a follow-up and stroke. A cardiological, neuropsychological and neurological study was conducted among 75 Bulgarian participants. All data and samples derived from the University Hospital of Pleven. Beta amyloid in the blood, procalcitonin (PCT), NT-proBNP as predictors of cognitive impairment in patients with MS were identified. *Methods* Clinical, anthropometric, biochemical, neuropsychological, cognitive and statistical data processing. Plasma amyloid beta ($A\beta$) levels, procalcitonin, NT-proBNP in MS were investigated in participants with MS and in healthy controls. **RESULTS** In the present study, an inverse relation between NT-proBNP and diastolic blood pressure, waist circumference, triglycerides, HDL- and LDL cholesterol was found. Plasma levels of $A\beta_{42}$ and $A\beta_{40}$ were found to be reduced in MetS participants. Regression analysis showed a positive relationship between NT-proBNP and systolic blood pressure ($p < 0.001$) and fasting blood glucose ($p < 0.05$). *Conclusions* There was a positive association between PCT levels, decreased levels of $A\beta_{42}$ and $A\beta_{40}$, as well as elevated NT-proBNP and cognitive impairment in people with MS and stroke. A concentration of NT-proBNP of 60 pg / ml or greater could be an indicator of metabolic abnormalities and early cognitive decline. Large-scale studies and longer follow-up periods will be necessary to establish a direct and accurate causal relationship between MS and MCI pathologies.

Keywords: Metabolic syndrome, Cognitive decline, Healthcare engineering

Introduction

Metabolic syndrome (MetS), a risk factor for many vascular conditions, may be a prodromal manifestation of vascular cognitive impairment. Diagnosing early stages of cerebrovascular pathology can lead to prevention and delay of the progression of pathological conditions such as vascular cognitive impairment. It can be said that MetS, which is considered as risk factor for the development of diabetes, hypertension, dyslipidemia, and coronary artery disease can also act as an important risk factor for the development of dementia.

Dementia is among the leading causes of disability in developed societies, affecting approximately 6% of the population aged 65 and older, and its prevalence increases exponentially with age: 40–70% at the age of 95 years and over suffer from dementia. The vascular and vascular-related factors that have been associated with dementia and cognitive decline included high blood pressure (BP) and hypertension, total cholesterol and other lipid parameters, diabetes and insulin resistance, body mass index (BMI) and obesity, and the metabolic syndrome (MetS).

Metabolic-Cognitive Syndrome: Is This Understanding Useful?

- This is an Open Access article distributed under the terms of the Creative Commons Attribution-Noncommercial 4.0 Unported License, permitting all non-commercial use, distribution, and reproduction in any medium, provided the original work is properly cited.

- Selection and peer-review under responsibility of the Organizing Committee of the Conference

© 2024 Published by ISRES Publishing: www.isres.org

It is suggested that possibly the metabolic-hormonal changes which occur over the course of MetS may be detrimental for neuronal cells and are resultantly responsible for development of dementia. The current level of understanding suggests that the concept of Metabolic Cognitive Syndrome (MCS) provides an important window for primary prevention of dementia (Panza et al., 2006). Changing the modifiable risk factors can reduce the incidence of dementia and also possibly delay the onset of dementia. There are strong links between obesity, insulin resistance, and components of the metabolic syndrome. Chronic low-grade inflammation has been implicated in the pathophysiology of these three intertwined entities. Procalcitonin polypeptide, is the precursor of calcitonin hormone produced by neuroendocrine C-cells of the thyroid and K-cells of the lung, encoded from the calcitonin chromosome 11.

Procalcitonin is best known as a biomarker of infection and severe systemic inflammation. Recent studies show that adipose tissue is capable of expressing and secreting procalcitonin. This makes Procalcitonin a potential biomarker for obesity-related low-grade inflammation. There are no data addressing the significance of variation in plasma procalcitonin levels in the general population. So far, procalcitonin level in the normal population has been studied only in a small sample, and only an association of procalcitonin with sex was acknowledged. We hypothesize that plasma procalcitonin may be associated with measures of obesity, insulin resistance, and metabolic risk factors.

Method

Data were statistically processed using variation and regression analyses. To analyze data, parametric and non-parametric methods were applied, and the value of chi-square was used for analyses of qualitative variables. Evaluation of statistical reliability for the groups studied was made according to the p-value for the meaning of chi-square, and differences were considered significant at $p < 0.05$. Statistical studying of dependences between variables to a great extent depends on the way the variables are measured. When studying the statistical dependence between two qualitative variables, it is convenient to present data in a table reflecting mutual connection of the characteristics. In this table, the categories of the first variable (subdivisions, varieties) are entered along the rows, and the categories of the other variable are entered down the columns. In the points where the rows and columns cross, the frequencies (numbers) of the respective combinations of categories of the variables.

The sums of those are figures that are called borderline (marginal) frequencies. Relative frequencies, expressed in per cent, are calculated by dividing the frequencies of cells by dividing the borderline frequencies in the respective row in the excerpt, and the figures obtained are multiplied by 100 (percent along the rows). Looking for statistical dependence between the variable implies whether the relationship between the variables is a natural characteristics of the population, a sample of which is selected, or this relationship is the result from the influence of accidental factors, i.e. the latter relationship is found in the actual sample but it is not characteristic of the population. It makes sense to take this into consideration only if the population sample investigated has been collected at random, and the population has been strictly defined. That would mean that each person on a population, that is well-differentiated from the environment should have an equal chance to be in the sample selected. To find the statistical dependence between two variables measured in qualitative scales, the chi-square criterion is used. This allows to ascertain the hypothesis that the variables forming the rows and the columns are independent, without defining the extent and tendency in the dependence.

From data about the sample, as presented in a table, the respective value of the chi-square statistics and its empirical level of significance (p-value) is calculated. If this empirical level is lower than 0.05 (this being the most common level of dependence a researcher chooses) then the hypothesis of lack of dependence between the characteristics in the population, from which the samples is selected, is rejected. In this case, a hypothesis is proposed for the presence of statistically significant dependence (alternative hypothesis).

The chi-square criterion (Fischer's exact test) make it possible to only answer the question regarding the presence or absence of dependence. When the two variables are qualitative, it is impossible to conclude whether the dependence is positive or negative. The chi-square value shows whether the difference between the percentages expected and those found is big enough to allow the assumption that it exists (presents regularly) in the whole population, or it is too small, which implies that there is no significant relationship between the variables in this population. When $p < 0.05$, this means that the differences established in the percentages are regular, and not due to the influence of accidental factors.

Logistic Regression Analysis

Regression analysis is applied to describe the dependence between one dependent variable and one or more independent variables. In the “case-control epidemiological studies, odds ratio is used as a measure for the degree of dependence between one risk factor and a certain disease. The risk factor can be a quantitative or a qualitative variable, but the simplest situation is that in which the factor also has two characteristics: presence of the factor, coded as “1”, and absence of the factor, coded as “0”. Under such circumstances, the linear regression analysis is not applicable. When the dependent variable is discrete, i.e. when it can have most commonly, two values, then the standard method for analysis is the logistic regression analysis. It makes it possible to study the individual impact of each factor. In addition, logistic regression analysis may help to find the most appropriate and cost-effective, as well as the most acceptable biomedical model, which can describe the relationship between the outcome of a disease and a multitude of independent variables (factors). In this study, most of the potential risk factors were qualitative and their characteristics were coded in a relevant manner. The odds ratio is used as an approximate measure for risk regarding the outcome of the disease, depending on a certain risk factor or a certain group of risk factors.

Results and Discussion

Heart rate was 77.53/min for oncology patients and 81.24/min for other people in the study. Systolic (SBP) blood pressure, diastolic (DBP) blood pressure and BMI were measured. The 67 serum samples of patients with different tumors were evaluated for CBC. We also collected 31 serum samples from 31 patients without cancer as controls in April 2018. The number of women was 17 and the number of men was 14. The following CBC parameters were analyzed: red blood cell count (RBC), hemoglobin (Hb), hematocrit (Hct), mean corpuscular volume (MCV), mean corpuscular hemoglobin (MCH), mean corpuscular hemoglobin concentration (MCHC), red blood cell distribution width (RDW), platelet count (PLT), mean white blood cell count (WBC), and leukocyte differential count.

One way ANOVA test was performed on ECGs by splitting the participants into four groups:

- 1) men with cancer
- 2) men without cancer
- 3) women with cancer
- 4) women without cancer.

Multiple comparison test of means was used to obtain the differences between every two groups. Multiple logistic regression analysis was implemented to estimate OR of cancer. The box plots for one way ANOVA test of pulse pressure (Figure 1) showed that the difference between persons with and without MS is more significant for women. The ANOVA F-statistic was 3.683 with p-value 0.0145 and the hypothesis that the all groups' means were equal had to be rejected.

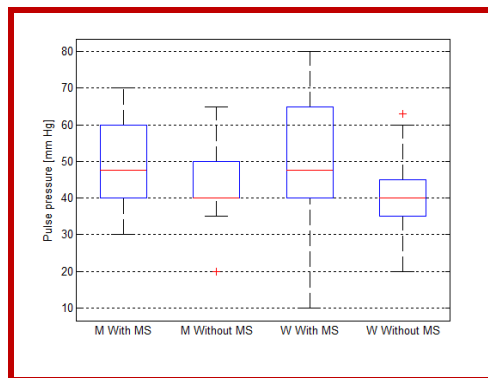


Figure 1: Box plots for one way ANOVA test of pulse pressure for groups: Men with MS, Men without MS, Women with MS and Women without MS

The multiple comparison tests indicated statistically significant difference in the PP mean values between groups of women with and without MS (Table 1). A considerable difference in means between groups of men without MS and women without MS was obtained (Table 1). Some difference in means was observed between groups of men with and without MS (Table 1). The difference in means between groups of men with MS and women with MS was very small (Table 1).

Table 1. Table of multiple comparison test for men and women with and without MS.

First group	Second group	Lower boundary of the CI	Difference between means	Upper boundary of the CI
Men with MS	Men without MS	-6.303	4.001	14.323
Men with MS	Women with MS	-10.866	-0.033	10.801
Men without MS	Women without MS	-2.565	5.085	12.736
Women with MS	Women without MS	0.788	9.128	17.464

MODEL 1

The results indicated that the increasing of OR with increasing of PP for men was similar to that for women when the men's APO B/APO A1 ratio was with about 0.1 greater. The obtained model showed that for increase of PP with 5 mm Hg it was expected about 1.2314 times increase in the odds ratio of MS and for increase of APO B/APO A1 ratio with 0.1 it was expected about 1.6363 times increase in the odds ratio.

MODEL 2: WC, HDL-CHOL, GLU, TG

In the second model-- in addition to PP-- four dichotomous variables were included and the model was adjusted for gender. The dichotomous variables were composed using the following components of MS: waist (WC), HDL cholesterol, blood glucose (Glu) and serum triglycerides (Tg). Each dichotomous variable received value 1 if the criterion for corresponding component in NCEP-ATP III definition was met. The p-value for overall model fit statistic was less than 1×10^{-6} . The p-values of regression coefficients were 0.0001 for $WC > 102/88$ cm (men/women), 0.0302 for $HDL < 1.03/1.3$ mmol/l (men/women), 0.0097 for $Glu > 6$ mmol/l and 0.0002 for $Tg > 1.7$ mmol/l.

The p-value of regression coefficient for PP was 0.0061. These p-values showed that all model variables contribute significantly to the odds ratio of MS. This model was used to study the relation between the odds ratio of MS and the value of pulse pressure when only one of the other MS components met criterion (Figure 4). The results demonstrated when only HDL-cholesterol or blood glucose met criterion the odds ratio was less than 1 even for PP up to 80 mm Hg (Figure 4).

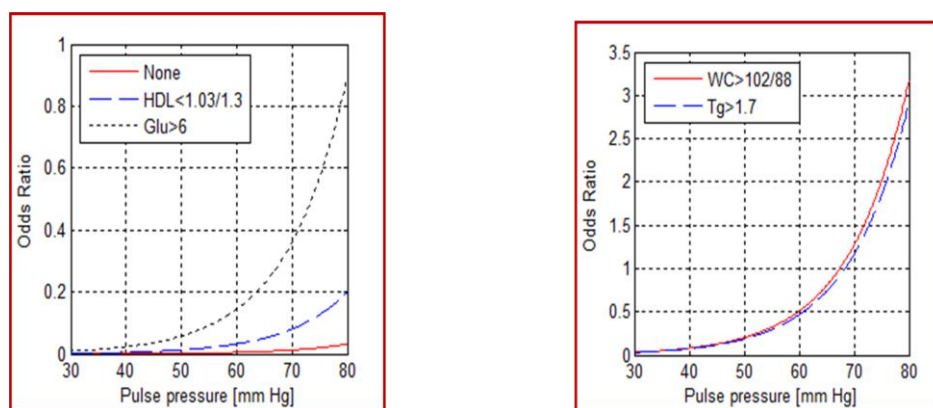


Figure 2. Odds ratio as function of PP when only one of the MS components was met criterion.

When waist or triglycerides met criterion the odds ratio was more than 1 for wide PP. The models for waist and triglycerides were very similar. The obtained model showed that for increase of PP with 5 mm Hg it was expected about 1.5787 times increase in the odds ratio of MS. In the second model in addition to PP four dichotomous variables were included and the model was adjusted for gender. The dichotomous variables were composed using the following components of MS – waist (WC), HDL cholesterol, blood glucose (Glu) and serum triglycerides (Tg).

The MCS model could also help us to explain the complex relationship between metabolic disorders and cognitive disturbances and the boundaries between normal and pathological conditions, with a better understanding of clinical and neuropathological features of these metabolic-based cognitive disorders. At

present, there is gross lack of data in terms of association of MetS and cognitive decline. There is an urgent need to study this association in community samples. Understanding the progress from MetS to overt NCDs and development of dementia can also help in identifying other associated risk and protective factors for development of dementia.

Conclusion

There was a positive association between PCT levels, decreased levels of A β 42 and A β 40, as well as elevated NT-proBNP and cognitive impairment in people with MS and stroke. A concentration of NT-proBNP of 60 pg / ml or greater could be an indicator of metabolic abnormalities and early cognitive decline. Large-scale studies and longer follow-up periods will be necessary to establish a direct and accurate causal relationship between MS and MCI pathologies.

Scientific Ethics Declaration

The author declares that the scientific ethical and legal responsibility of this article published in EPSTEM Journal belongs to the author.

Acknowledgements or Notes

* This article was presented as an oral presentation at the International Conference on Basic Sciences and Technology (www.icbast.net) held in Antalya/Turkey on November 14-17, 2024.

References

- Alberti, K. G. M. M., & Zimmet, P. Z. (1998). Definition, diagnosis and classification of diabetes mellitus and its complications. Part 1: diagnosis and classification of diabetes mellitus. Provisional report of a WHO consultation. *Diabetic Medicine*, 15(7), 539-553.
- Grodstein, F. (2007). Cardiovascular risk factors and cognitive function. *Alzheimer's & Dementia*, 3(2), S16-S22.
- Grundy, S. M., Brewer Jr, H. B., Cleeman, J. I., Smith Jr, S. C., & Lenfant, C. (2004). Definition of metabolic syndrome: report of the National Heart, Lung, and Blood Institute/American Heart Association conference on scientific issues related to definition. *Circulation*, 109(3), 433-438.
- Luis, C. A., Loewenstein, D. A., Acevedo, A., Barker, W. W., & Duara, R. (2003). Mild cognitive impairment: directions for future research. *Neurology*, 61(4), 438-444.
- Frisardi, V., Panza, F., Seripa, D., Imbimbo, B. P., Vendemiale, G., Pilotto, A., & Solfrizzi, V. (2010). Nutraceutical properties of Mediterranean diet and cognitive decline: possible underlying mechanisms. *Journal of Alzheimer's Disease*, 22(3), 715-740.
- Panza, F., Capurso, C., D'Introno, A., Colacicco, A. M., Capurso, A., & Solfrizzi, V. (2006). Prevalence rates of mild cognitive impairment subtypes and progression to dementia. *Journal of the American Geriatrics Society*, 54(9), 1474-1475.

Author Information

Galya Atanasova

Medical University Pleven, Bulgaria

Contact e-mail: maa_05@abv.bg

To cite this article:

Atanasova, G. (2024). Early predictors of cognitive decline and stroke. *The Eurasia Proceedings of Science, Technology, Engineering & Mathematics (EPSTEM)*, 30, 85-89.

The Eurasia Proceedings of Science, Technology, Engineering & Mathematics (EPSTEM), 2024

Volume 30, Pages 90-96

ICBAST 2024: International Conference on Basic Sciences and Technology

Basic Principles of Infection Control and Implementation Strategies

Mehmet Erdem
Gaziantep University

Makhzuna Khamdamova
Tashkent State Pedagogical University after named Nizami

Mehmet Ozaslan
Gaziantep University

Abstract: Hand hygiene plays a vital role in controlling infections and ensuring patient safety in healthcare settings. The World Health Organization (WHO) and CDC emphasize the critical role of hand hygiene in patient safety. Research conducted worldwide clearly demonstrates the positive effects of hand hygiene adherence by healthcare workers on patient health. Effective implementation of hand hygiene in healthcare settings is essential for reducing infection rates and ensuring sustainable quality within healthcare systems. However, low adherence to hand hygiene among healthcare workers can lead to the spread of hospital-associated infections. This paper emphasizes the critical role of hand hygiene in preventing infections in healthcare settings and details the strategies proposed to enhance healthcare workers' compliance with hand hygiene. The role of training, observation, feedback, and leadership support is discussed. The aim of this study is to review the current literature on the applicability of hand hygiene in healthcare settings. Literature searches were conducted using academic databases such as PubMed, Google Scholar, Scopus, and Cochrane Library. The search focused on articles published between 2000-2024. This study reviews research assessing the effectiveness of training programs, observation and feedback methods, leadership support, and accessibility to hygiene products in hospital settings. The development and implementation of hand hygiene strategies has significant potential in improving healthcare quality and reducing healthcare-associated infections.

Keyword: Hygiene, Healthcare-associated infections, Infection control, Healthcare engineering.

Introduction

Healthcare-associated infections (HAIs) represent one of the most significant risks to patient safety in healthcare settings. HAIs are widespread in hospitals, clinics, and other healthcare facilities. The World Health Organization (WHO) defines hand hygiene as a fundamental component of infection control in healthcare settings. Proper hand hygiene helps prevent the spread of infections and enhances the safety of healthcare workers, patients, and visitors (Pittet et al., 2009; Boyce, 2021). However, adherence to hand hygiene often faces various challenges, which can contribute to the spread of healthcare-associated infections (Larson et al., 2007). For effective implementation of hand hygiene in healthcare services, strategic planning is required. This planning should not only include training and awareness activities but also incorporate tools such as observation, feedback, and leadership support to encourage healthcare workers' behavior (Pittet et al., 2009; Boyce, 2021). Furthermore, it is crucial to create environments that address barriers such as healthcare workers' workload and time constraints and facilitate easy access to hygiene products. Recent studies have shown that educational programs aimed at increasing hand hygiene awareness, along with observation, feedback strategies, leadership support, and accessibility to hygiene products, effectively improve healthcare workers' compliance with hand hygiene. WHO's 2023 research agenda on hand hygiene highlights its role in preventing infections in healthcare settings.

- This is an Open Access article distributed under the terms of the Creative Commons Attribution-Noncommercial 4.0 Unported License, permitting all non-commercial use, distribution, and reproduction in any medium, provided the original work is properly cited.

- Selection and peer-review under responsibility of the Organizing Committee of the Conference

© 2024 Published by ISRES Publishing: www.isres.org

Method

This study aims to review the existing literature on the applicability of hand hygiene in healthcare services. Literature searches were conducted using academic databases such as PubMed, Google Scholar, Scopus, and Cochrane Library. The search focused on articles published between 2000 and 2024. Keywords such as "hand hygiene", "healthcare-associated infections", "compliance", "education programs", "feedback", "infection control", "hospital hygiene", and "leadership support" were used. The study reviews research assessing the effectiveness of training programs, observation and feedback methods, leadership support, and the accessibility of hygiene products in healthcare settings (Pittet et al., 2009; Boyce, 2021; WHO, 2023).

Importance of Hand Hygiene

Prevents Infections: In hospital environments, bacteria, viruses, and other pathogens can spread easily. Healthcare workers, if they neglect hand hygiene, may transfer these pathogens to patients or themselves.

Increases Patient Safety: Hand hygiene is particularly critical for immunocompromised patients. It is essential in sensitive areas such as postoperative care, intensive care units, and dialysis, where vulnerable patients are at greater risk.

Reduces Cross-Contamination: It prevents the spread of disease-causing agents between different patients. This helps protect both patients and healthcare workers (WHO, 2009).

5 Moments for Hand Hygiene: The "5 Moments for Hand Hygiene" approach identifies critical times when healthcare workers should perform hand hygiene. The World Health Organization (WHO) recommends the following 5 key moments for healthcare professionals to clean their hands:

Before Contact with a Patient: Healthcare workers should wash their hands before direct contact with a patient. This prevents germs from spreading to the patient (Duckro et al., 2005; Hayden et al., 2008; Creamer et al., 2010).

During Contact with a Patient: Hands should be cleaned during direct contact with the patient, for example, when performing an examination or providing care (Hirschmann et al., 2001; CDC, 2002; Loveday et al., 2014).

After Contact with Patient Body Fluids: Hands should be washed after contact with body fluids (e.g., blood, urine, saliva) to prevent infection spread.

After Contact with Environmental Surfaces: Hands should be cleaned after touching surfaces near the patient, such as bed rails, devices, or other equipment.

After Contact with the Patient: Hand hygiene after patient contact helps prevent the spread of microbes to other patients or individuals.

These five key moments are critical for the effective implementation of hand hygiene in healthcare settings (CDC, 2002; WHO, 2009; WHO, 2012; AORN, 2022).

Your 5 Moments for Hand Hygiene

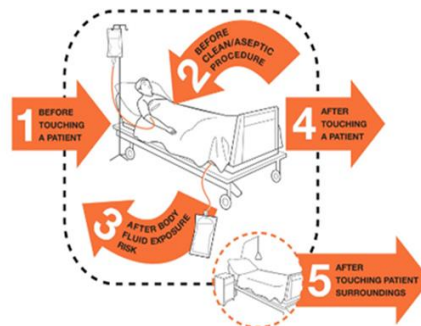


Figure 1. The five indications for hand hygiene

The Importance of Hand Hygiene in Healthcare

Hand hygiene is emphasized by the World Health Organization (WHO) as a fundamental strategy to prevent the spread of infections in healthcare settings (Pittet et al., 2009). Compliance with hand hygiene is identified as an

effective method for preventing hospital-acquired infections (Boyce, 1999; Kampf, Löffler, & Gastmeier, 2009). However, healthcare workers often exhibit low compliance rates, which can contribute to the spread of healthcare-associated infections (Larson et al., 2007). Improving hand hygiene not only ensures patient safety but also helps healthcare workers protect themselves and their patients from infections. Both WHO and the Centers for Disease Control and Prevention (CDC) highlight the importance of increasing compliance with hand hygiene and have made its implementation mandatory across all areas of healthcare (CDC, 2002; WHO, 2009).

Challenges in Ensuring Compliance with Hand Hygiene

Although hand hygiene is critical for infection prevention and health protection, individuals often face challenges in adopting and adhering to proper hand hygiene practices. These challenges arise across various contexts, from healthcare settings to schools and daily life at home. Several factors impede compliance with hand hygiene in healthcare environments. Among the key factors are heavy workloads, skin irritation caused by antiseptic use, and a lack of awareness regarding the importance of hand hygiene (Larson, 1994; Almansour, 2021). Overcoming these challenges is essential to promote hand hygiene compliance among healthcare workers. WHO has developed various educational materials, protocols, and compliance assessment tools to increase healthcare workers' awareness about hand hygiene (WHO, 2009; Kilpatrick et al., 2011). The primary factors inhibiting compliance with hand hygiene are outlined below:

Lack of Education and Awareness

A lack of knowledge and awareness about the importance of hand hygiene is one of the leading causes of non-compliance. Many individuals are unaware of the situations in which handwashing is necessary or the correct washing methods. Specifically, incomplete knowledge about the role of hand hygiene in preventing infections can negatively affect individuals' handwashing habits (Larson & Sabin, 2006).

Time Constraints and Workload

In groups with high workloads, such as healthcare workers, time constraints can hinder hand hygiene compliance. In hospitals, for instance, staff are often faced with emergencies, making it difficult for them to find time for handwashing. Additionally, neglect of hygiene in some workplaces can be related to time management issues and external stressors (Pittet et al., 2000).

Infrastructure and Access Challenges

Access to hygiene materials and infrastructure deficiencies pose significant barriers to hand hygiene compliance. A shortage of basic hygiene tools such as soap, water, and disinfectants can make it difficult to maintain proper hand hygiene. This issue may be more pronounced in rural areas or developing countries, where access to hygiene products can be more challenging (WHO, 2009).

Cultural and Social Barriers

Cultural and social norms can influence individuals' compliance with hand hygiene. In some cultures, frequent handwashing may not be considered necessary, or hygiene habits may be shaped by traditional beliefs. Additionally, some individuals may believe that hygiene is only required before becoming sick, rather than as a regular practice (Aunger & Curtis, 2016).

Lack of Motivation and Forgetfulness

Individuals' motivation to comply with hand hygiene practices can be influenced by external factors. For example, people with lower personal health risks may not feel adequately motivated to wash their hands. Moreover, busy work schedules or daily life stress can lead to forgetting or neglecting hand hygiene (Novák et al., 2019).

Incorrect Use or Insufficiency of Hygiene Products

Incorrect use of hygiene products can reduce their effectiveness. For instance, some individuals may believe they have achieved adequate hygiene by simply washing their hands with water, but water alone may not be sufficient to kill microbes. Additionally, improper use of disinfectants can lead to compliance issues (Boyce & Pittet, 2002; Rumano et al., 2022).

Psychological Barriers and Insufficient Awareness

Psychological barriers to hand hygiene compliance also exist. Particularly in high-risk groups, such as healthcare workers, fatigue and psychological stress can negatively affect adherence to hand hygiene. Furthermore, some individuals may fail to fully grasp the importance of hand hygiene or may neglect hygiene rules (Larson et al., 2007). Ensuring hand hygiene compliance is a multifaceted process. Factors such as educational deficiencies, time constraints, infrastructure challenges, cultural influences, lack of motivation, and psychological barriers all present obstacles to this process. Addressing these challenges requires more comprehensive and effective health policies, infrastructure, and educational strategies.

Strategies to Increase Hand Hygiene Compliance

Various strategies have been developed to improve compliance with hand hygiene practices. Education programs are one of the most essential tools for healthcare workers to understand the importance of hand hygiene and incorporate it into their daily practices. Education should not only provide theoretical knowledge but also include practical exercises that aim to change behavior. Furthermore, leadership support is crucial for increasing hand hygiene compliance rates, as strong leadership ensures that hand hygiene remains a continuous priority within healthcare institutions (Gould et al., 2017a). Additionally, observation and feedback methods play a significant role in improving compliance. These methods involve monitoring healthcare workers' hand hygiene behaviors and providing necessary feedback to encourage behavior change. Observations inform employees about correct practices and motivate them to adjust their behaviors (Gould et al., 2017b). Increasing the availability of hygiene products in hospitals and reinforcing hygiene culture in healthcare settings are also key components of this strategy (Pittet et al., 2009). Below are various strategies that can be employed to enhance hand hygiene compliance:

Education and Awareness Campaigns

Education is one of the most important strategies to improve hand hygiene compliance. Regular training for healthcare workers, coupled with materials that encourage compliance, is crucial. Providing this education during orientation and at regular intervals can significantly improve compliance with hand hygiene (Boyce & Pittet, 2002; Fuadi et al., 2024). Public awareness campaigns emphasizing the importance of proper handwashing should also be integrated into schools, hospitals, and community centers (WHO, 2009).

Targeted Behavior Change Interventions

Behavior change theories can be used to improve hand hygiene compliance. These theories offer strategies to help individuals adopt healthier behaviors. Approaches such as Cognitive Behavioral Therapy (CBT), social learning theory, and motivational interviewing can be effective in encouraging proper hand hygiene practices (Larson & Sabin, 2006).

Enhancing Accessibility and Convenience

Making hygiene products (soap, water, disinfectants) easily accessible and user-friendly is essential for improving compliance. In hospitals, schools, and public areas, increasing the number of handwashing stations and making hygiene products more visible can encourage better compliance (Pittet et al., 2000).

Digital Observation and Tracking Systems

Modern hospitals can use sensor-based and camera monitoring systems to track hand hygiene compliance. These systems enable healthcare workers to receive real-time feedback on their hand hygiene practices and evaluate their performance (Sax et al., 2007).

Feedback Mechanisms

Hand hygiene compliance can be increased through regular monitoring and feedback. Setting up systems to track compliance rates and providing staff with regular feedback plays an important role in improving adherence. Such feedback can encourage individuals to be more vigilant and improve their hygiene habits (Dubbert et al., 1990; Boyce & Pittet, 2002; Binyamin, 2022).

Considering Cultural and Social Factors

Hand hygiene strategies should be tailored to cultural and social contexts. Compliance with hand hygiene can be influenced by social norms, traditions, and cultural values. Customizing hygiene programs to fit the cultural characteristics of a community can improve compliance (Aunger & Curtis, 2016; Lee et al., 2019).

Motivational Approaches and Rewards

Using rewards and incentives can motivate individuals to adhere to hand hygiene practices. For example, fun rewards or class competitions can encourage children to be more attentive to hygiene. Reward programs aimed at healthcare workers can also boost compliance in the workplace.

Reminder Materials

In healthcare settings, reminder materials such as posters, flyers, and brochures can help increase awareness and prompt staff to adhere to hand hygiene guidelines (Kampf, Löffler, & Gastmeier, 2009). These strategies can collectively promote better hand hygiene practices and ensure they are sustained over time. Through a combination of education, access to materials, digital monitoring, and cultural sensitivity, hand hygiene compliance can be significantly improved in various environments.

Findings of Research on Hand Hygiene

Recent studies have shown that educational interventions, observation and feedback strategies, leadership support, and the accessibility of hygiene products significantly enhance healthcare workers' compliance with hand hygiene practices. The WHO's 2023 research agenda on hand hygiene emphasizes its crucial role in preventing infections within healthcare settings. Research indicates that hand hygiene training is effective in changing healthcare workers' behaviors and improving hygiene standards in hospitals. Studies conducted by the WHO and CDC found that increased compliance with hand hygiene led to a significant reduction in hospital infection rates (Pittet et al., 2006). Hand hygiene practices are particularly critical in reducing mortality rates among high-risk patient groups.

Raising Public Awareness

Hand hygiene is important not only for healthcare workers but also for patients and visitors. Raising public awareness plays a significant role in controlling hospital-acquired infections. Informational materials can be placed at hospital entrances to educate patients and visitors about the importance of hand hygiene (Sax et al., 2007).

Conclusion

Hand hygiene is an indispensable practice for ensuring patient safety in healthcare services. Enhancing healthcare workers' compliance with hand hygiene is crucial for preventing hospital infections and safeguarding patient safety. Hand hygiene is a simple but effective method in infection control. To improve healthcare workers' compliance, systematic education programs, infrastructure improvements, and digital monitoring systems should be adopted. Regular audits by healthcare institutions and the establishment of a hygiene culture are essential. These measures will contribute to reducing infection rates and improving the overall quality of healthcare services. Adopting proper hand hygiene habits by healthcare workers will help decrease hospital-acquired infections and enhance patient safety. Research on hand hygiene indicates that strategies like training, leadership support, monitoring, and feedback are effective tools for increasing compliance. Improving hand hygiene in healthcare institutions is an important step towards enhancing patient safety. The development and implementation of hand hygiene strategies have the potential to improve healthcare quality and reduce healthcare-associated infections.

Scientific Ethics Declaration

The authors declare that the scientific ethical and legal responsibility of this article published in EPSTEM Journal belongs to the authors.

Acknowledgements or Notes

* This article was presented as an oral presentation at the International Conference on Basic Sciences and Technology (www.icbast.net) held in Antalya/Turkey on November 14-17, 2024.

References

- Allegranzi, B., & Pittet, D. (2009). Role of hand hygiene in healthcare-associated infection prevention. *Journal of Hospital Infection*, 73(4), 305-315.
- Al-Mansour, B. (2021). Review on the medicinal properties of some aromatic hydrosols. *Zeugma Biological Science*, 2(1), 1-19.
- Aunger, R., & Curtis, V. (2016). Behaviour centred design: towards an applied science of behaviour change. *Health psychology review*, 10(4), 425-446.
- Binyamin, S. S. (2022). Understanding factors affecting the use of mobile health innovation, Attitude and synthesis. *The Eurasia Proceedings of Health, Environment and Life Sciences*, 7, 1-7.
- Boyce, J. M. (1999). It is time for action: improving hand hygiene in hospitals. *Annals of Internal Medicine*, 130(2), 153-155.
- Boyce, J. M., & Pittet, D. (2002). Guideline for hand hygiene in health-care settings: recommendations of the healthcare infection control practices advisory committee and the HICPAC/SHEA/APIC/IDSA hand hygiene task force. *Infection Control & Hospital Epidemiology*, 23(S12), S3-S40.
- Boyce, J. M. (2021). Hand hygiene, an update. *Infectious Disease Clinics*, 35(3), 553-573.
- Centers for Disease Control and Prevention (CDC). (2002). *Guideline for hand hygiene in health-care settings. MMWR*, 51(RR-16). Retrieved from <https://www.cdc.gov/mmwr/pdf/rr/rr5116.pdf>
- Creamer, E., Dorrian, S., Dolan, A., Sherlock, O., Fitzgerald-Hughes, D., Thomas, T., ... & Humphreys, H. (2010). When are the hands of healthcare workers positive for meticillin-resistant *Staphylococcus aureus*?. *Journal of Hospital Infection*, 75(2), 107-111.
- Dubbert, P. M., Dolce, J., Richter, W., Miller, M., & Chapman, S. W. (1990). Increasing ICU staff handwashing: effects of education and group feedback. *Infection Control & Hospital Epidemiology*, 11(4), 191-193.
- Duckro, A. N., Blom, D. W., Lyle, E. A., Weinstein, R. A., & Hayden, M. K. (2005). Transfer of vancomycin-resistant enterococci via health care worker hands. *Archives of Internal Medicine*, 165(3), 302-307.
- Duckro, A. N., Blom, D. W., Lyle, E. A., Weinstein, R. A., & Hayden, M. K. (2005). Transfer of vancomycin-resistant enterococci via health care worker hands. *Archives of Internal Medicine*, 165(3), 302-307.
- Fuadi, D. S., Hufad, A., Ismawati, D., Jaya, A., Pratama, A., Haryanto, H., & Hidayat, T. (2024). Building public awareness: Education and campaigns to prevent stunting in the next generation. *The Eurasia Proceedings of Health, Environment and Life Sciences*, 13, 88-97.
- Gould, D. J., Creedon, S., Jeanes, A., Drey, N. S., Chudleigh, J., & Moralejo, D. (2017b). Impact of observing hand hygiene in practice and research: a methodological reconsideration. *Journal of hospital infection*, 95(2), 169-174.

- Gould, D. J., Moralejo, D., Drey, N., Chudleigh, J. H., & Taljaard, M. (2017a). Interventions to improve hand hygiene compliance in patient care. *Cochrane Database of Systematic Reviews*, (9).
- Hayden, M. K., Blom, D. W., Lyle, E. A., Moore, C. G., & Weinstein, R. A. (2008). Risk of hand or glove contamination after contact with patients colonized with vancomycin-resistant enterococcus or the colonized patients' environment. *Infection Control & Hospital Epidemiology*, 29(2), 149-154.
- Hirschmann, H., Fux, L., Podusel, J., Schindler, K., Kundi, M., Rotter, M., & with assistance of EURIDIKI, G. W. (2001). The influence of hand hygiene prior to insertion of peripheral venous catheters on the frequency of complications. *Journal of Hospital Infection*, 49(3), 199-203.
- Kampf, G., Löffler, H., & Gastmeier, P. (2009). Hand hygiene for the prevention of nosocomial infections. *Deutsches Ärzteblatt International*, 106(40), 649.
- Kilpatrick, C., Allegranzi, B., & Pittet, D. (2011). WHO first global patient safety challenge: Clean care is safer care, contributing to the training of health-care workers around the globe. *International Journal of Infection Control*, 7(2).
- Larson, E. L. (1994). Draft APIC guideline for handwashing and hand antisepsis in health care settings. *American Journal of Infection Control*, 22(5), A25-A47.
- Larson, E. L., Quiros, D., & Lin, S. X. (2007). Dissemination of the CDC's Hand Hygiene Guideline and impact on infection rates. *American Journal of Infection Control*, 35(10), 666-675.
- Larson, E. L., & Sabin, S. L. (2006). The effectiveness of health care worker hand hygiene compliance interventions: A systematic review. *American Journal of Infection Control*, 34(10), 535-545.
- Lee, Y. F., McLaws, M. L., Ong, L. M., Amir Husin, S., Chua, H. H., Wong, S. Y., & Zingg, W. (2019). Hand hygiene—social network analysis of peer-identified and management-selected change agents. *Antimicrobial Resistance & Infection Control*, 8, 1-7.
- Loveday, H. P., Wilson, J. A., Pratt, R. J., Golsorkhi, M., Tingle, A., Bak, A., & Wilcox, M. (2014). Epic3: national evidence-based guidelines for preventing healthcare-associated infections in NHS hospitals in England. *Journal of Hospital Infection*, 86, S1-S70.
- Novák, M., Breznický, J., Kompaniková, J., Malinová, N., & Hudečková, H. (2019). Impact of hand hygiene knowledge on the hand hygiene compliance. *Medicinski Glasnik*, 17(1), 194-199.
- Pittet, D., Hugonnet, S., Harbarth, S., Mourouga, P., Sauvan, V., Touveneau, S., & Perneger, T. V. (2000). Effectiveness of a hospital-wide programme to improve compliance with hand hygiene. *The Lancet*, 356(9238), 1307-1312.
- Pittet, D., Allegranzi, B., Storr, J., Donaldson, L., & WHO Global Patient Safety Challenge, Clean Care is Safer Care. (2006). The WHO guidelines on hand hygiene in health care and their consensus recommendations. *Journal of Hospital Infection*, 63(3), 268-279.
- Rumano, M., Rumano, E., Joti, J., & Hasanbelli, B. (2022). Food supplements usage during Covid-19 pandemic. *Zeugma Biological Science*, 4(1), 6-17.
- Sax, H., Allegranzi, B., Uckay, I., Larson, E., Boyce, J., & Pittet, D. (2007). 'My five moments for hand hygiene': a user-centred design approach to understand, train, monitor and report hand hygiene. *Journal of Hospital Infection*, 67(1), 9-21.
- WHO (2009). *WHO guidelines on hand hygiene in health care: first global patient safety challenge clean care is safer care*. <https://www.ncbi.nlm.nih.gov/books/NBK144013/>

Author Information

Mehmet Erdem

Department of Health Services Vocational School, Gaziantep University, 27310, Gaziantep-Türkiye,
Contact e-mail: merdem@gantep.edu.tr

Makhzuna Khamdamova

Tashkent State Pedagogical University after named Nizami,
Tashkent, Uzbekistan

Mehmet Ozaslan

Department of Biology, Gaziantep University, 27310,
Gaziantep-Türkiye,
Contact e-mail: ozaslanmd@gantep.edu.tr

To cite this article:

Erdem, M., Khamdamova, M. & Ozaslan, M. (2024). Basic principles of infection control and implementation strategies. *The Eurasia Proceedings of Science, Technology, Engineering & Mathematics (EPSTEM)*, 30, 90-96.

The Eurasia Proceedings of Science, Technology, Engineering & Mathematics (EPSTEM), 2024

Volume 30, Pages 97-106

ICBAST 2024: International Conference on Basic Sciences and Technology

The Properties of Waste Cooking Oil Soap with Avocado Waste Extract as Filler

Nisrina Zahira Putri Irawan
Universitas Pendidikan Indonesia

Heli Siti Halimatul Munawaroh
Universitas Pendidikan Indonesia

Sjaeful Anwar
Universitas Pendidikan Indonesia

Abstract: The research investigated the production of bar soap formulation using waste cooking oil (WCO) and avocado waste extract as a filler to enhance its functional properties and provide additional benefits for human skin. The research involved refining WCO, extracting avocado seed and peel bioactive compounds, preparing the solid soap formulation, and conducting various tests to evaluate its pH, cleansing ability, organoleptic properties, and irritation potential. The results indicated that all of the soap formulations met Indonesia National Standard (SNI) for pH and exhibited comparable cleansing power to commercial soaps. Organoleptic tests revealed moderate levels of hardness, foam, odor, texture, and tight impression. Irritation tests identified WCO bar soap that four of six formulations did not cause skin irritation. Overall, the WCO bar soap containing 10% (w/w) avocado peel extract, demonstrated promising properties and met all the established criteria. Future research should focus on characterizing specific chemical compounds in the soap, exploring additional natural extracts with antioxidant and anti-allergic activities, and further analysis quantitatively is required to ensure the product's quality and clinical efficacy.

Keywords: Avocado waste extract, Cleansing ability, Organoleptic test, Soap formulation, Waste cooking oil.

Introduction

Waste cooking oil (WCO) notably resulted from a product of used oil derived from domestic and industrial culinary (Azhar et al., 2024; Azme et al., 2023). WCO is produced from the frying process at high temperatures after several cycles of utilization. WCO contains hazardous chemicals that, when handled inappropriately, potentially pollute the water and soil environment and cause human health problems. WCO is widely produced by countries with high populations (Azhar et al., 2024; Foo et al., 2022). WCO has been utilized to recycle environmentally friendly and economical products with special techniques to overcome the impact of this waste. Some of the reported utilisations of WCO include being used as a green solvent, raw material for making biodiesel, bio-asphalt, and surfactant (Foo et al., 2022). The use of waste cooking oil to make soap is a sustainable option because it creates no waste and requires minimal energy (Azme et al., 2023). Soap is biodegradable, which can generate income for villagers and homemakers. Soap production has economic and environmental benefits and can educate the community about environmental awareness and waste recycling (Azme et al., 2023).

One of the products produced by WCO is an environmentally friendly soap for personal hygiene purposes (Azhar et al., 2024). Several prior studies show waste cooking oil-based soaps have advantages regarding stain-cleaning ability. Therefore, waste cooking oil soap is applied to soap for washing clothes or cutlery (Abera et al., 2023; Hartini et al., 2021). Waste cooking oil soap will have another beneficial value when added with

- This is an Open Access article distributed under the terms of the Creative Commons Attribution-Noncommercial 4.0 Unported License, permitting all non-commercial use, distribution, and reproduction in any medium, provided the original work is properly cited.

- Selection and peer-review under responsibility of the Organizing Committee of the Conference

© 2024 Published by ISRES Publishing: www.isres.org

bioactive substances from natural products, so waste cooking oil soap is not only applied as a cleaner for clothes or cutlery, but also safe and has more benefits for human skin such as antioxidants, anti-aging, and emollient (Ahmed et al., 2020).

Avocado peels and seeds are disposed of during industrial processing and daily consumption (Zaki et al., 2020). However, peels and seeds appeared typically disposed of as useless when consumed or processed, causing environmental waste problems (Zaki et al., 2020). Recovering valuable plant compounds from food industry waste, such as avocado peels and seeds, is an economical and eco-friendly approach (Zaki et al., 2020). These by-products are abundant in antioxidants such as phenolics, carotenoids, and flavonoids, making them valuable resources for producing functional foods, nutritional supplements, or cosmetics (Zaki et al., 2020). Avocado seed and peel waste have some fatty acid content. Avocado seeds are composed of 17-19% palmitic acid, 22-24% oleic acid, and 35-38% linoleic acid, whereas avocado peels contain 15-16% palmitic acid, 4.8-5.7% palmitoleic acid, 0.2-0.4% stearic acid, 68-69% oleic and vaccenic acids, 8-10% linoleic acid, and 0.16-1.1% linolenic acid (Ramadan & Farag, 2022). The oleic acid in avocado seeds can improve skin permeability, aiding in the delivery of additional nutrients or moisturizers in soaps (Charles et al., 2022).

It is widely recognized that avocado waste is a material that contains bioactive compounds with biological properties such as polyphenolic compounds and antioxidant activity (Jimenez et al., 2020; Ong et al., 2022).

Phenolic compounds are more abundant in the avocado seed and peel (Jimenez et al., 2020). Avocado seed contains procyanidin B1, hydroxycinnamic acid, while avocado peel contains procyanidin B2, chlorogenic acid (Jimenez et al., 2020; Ramadan & Farag, 2022). Phenolic compounds in seeds are grouped into many classes, such as phenolic acids (hydroxybenzoic and hydroxycinnamic acids), phenolic alcohol derivatives, flavonoids, catechins, and tannins (Jimenez et al., 2020; Ramadan & Farag, 2022). Other non-polar compounds contained in the seeds are polyhydroxylated fatty alcohols. It has been shown that polyhydroxylated fatty alcohols in avocado seeds can play an essential role as photoprotective agents in skin damage caused by UV rays (Martín-del-Campo et al., 2023). It is noted that the concentration of phenolic compounds in avocado skin is higher than in avocado seed in raw extract. The polyphenolic compounds contained in avocado peels are hydroxybenzoic acid, hydroxycinnamic acid, flavan-3-ols, catechins and epicatechins, procusinin dimer, and quercetin (Martín-del-Campo et al., 2023; Ramadan & Farag, 2022).

This study aims to determine the optimum formulation of solid soap made from waste cooking oil with avocado waste extract added as a filler. Avocado waste is extracted simply by utilizing the waste cooking oil solvent. Furthermore, the soap was made based on several formulations, and several tests were carried out, such as pH, cleansing ability test, organoleptic test, and irritation test. This solid soap formulation is expected to contribute to developing a high-value product from waste cooking oil soap.

Method

Refining of Waste Cooking Oil

Waste cooking oil refining aims to remove impurities and carcinogenic substances contained in waste cooking oil. This waste cooking oil is then used to extract the oil content in avocado seeds and peels. The refining of waste cooking oil follows this procedure. Waste cooking oil is obtained from waste oil used by households and fried food vendors. Waste cooking oil is filtered to separate the oil from food residue, then heated until 80°C. The heating of the waste cooking oil was continued with the addition of activated carbon and cooked for 30 minutes. After that, the heating was stopped, and the activated carbon was left submerged in the oil for 24 hours to adsorb the dirt. Then, the oil and activated carbon were filtered using filter paper (Hartini et al., 2021). Waste cooking oil refining continued using Na_2CO_3 to absorb some of the oil color and residual impurities with the help of heating until the foam from the Na_2CO_3 disappeared. After that, the oil and Na_2CO_3 sediment is filtered again using filter paper (Gharby, 2022).

Extraction of Avocado Seeds and Peels Using Waste Cooking Oil Solvent

Extraction is one of the chemical separation techniques used to separate one or more compounds in a sample based on phase differences or solubility using a suitable solvent as a separating agent. Avocado peels and seeds waste is obtained from fruit juice sellers, which is then extracted conventionally with waste cooking oil (WCO) as the solvent. The production of avocado peels and seeds extract utilizes WCO as an organic solvent to extract the fatty acid and bioactive compounds in avocado seeds and peels. The conventional method used in extracting

avocado seeds and peels waste is through a heating process with the following steps. First, the avocado peels and seeds are washed with water and cut into small pieces. Next, avocado peels and seeds are dried in an oven for 6 hours at 70-75°C or roasted first and then dried in the sun for about three days. The dried avocado peels and seeds are blended into powder and put into WCO until soaked. The mixture is cooked for 30 minutes until the WCO changes color. After that, the oil was filtered using filter paper, and avocado waste extract was obtained.

Production of Bar Soap from Waste cooking oil with Avocado Seeds and Peels Extract

The preparation of bar soap from waste cooking oil with avocado seeds and peel extract involves a saponification reaction between oils with sodium hydroxide lye solution; then, the product is bar soap. The production of this soap uses the cold process method (without heating process), so it requires a curing process for 2-4 weeks until the soap solidifies and is not overly alkaline. In this study, several formulations of the bar soaps are shown in Table 1. Bar soap production uses a cold process. Various types of oils are then mixed and stirred until evenly blended according to the specified formulation. Then, a certain amount of sodium hydroxide solution was added as a reaction and stirred quickly until thick and well-blended. Finally, fragrance oil was added and stirred until well mixed (Sukeksi et al., 2021).

Table 1. WCO soap with avocado waste extract formulations

No.	Formulation 1	Formulation 2	Formulation 3	Formulation 4	Formulation 5	Formulation 6
1.	10% (w/w) WCO+ Avocado seeds extract	10% (w/w) WCO+ Avocado peels extract	10% (w/w) WCO+ Avocado seeds and peels extract	20% (w/w) WCO+ Avocado seeds extract	20% (w/w) WCO+ Avocado peels extract	20% (w/w) WCO+ Avocado seeds and peels extract
2.	70% (w/w) WCO	70% (w/w) WCO	70% (w/w) WCO	50% (w/w) WCO	50% (w/w) WCO	50% (w/w) WCO
3.	20% (w/w) Coconut oil	20% (w/w) Coconut oil	20% (w/w) Coconut oil	30% (w/w) Coconut oil	30% (w/w) Coconut oil	30% (w/w) Coconut oil
4.	25% (w/w) NaOH (aq)	25% (w/w) NaOH (aq)	25% (w/w) NaOH (aq)	25% (w/w) NaOH (aq)	25% (w/w) NaOH (aq)	25% (w/w) NaOH (aq)
5.	Fragrance Oil	Fragrance Oil	Fragrance Oil	Fragrance Oil	Fragrance Oil	Fragrance Oil

pH Test

The pH measurement of bar soap was carried out using the following steps. One gram of bar soap sample was measured and dissolved in 10 mL of water. The soap solution was then tested for pH using a digital pH meter (LAQUA Horiba PH-2000 Series). The pH value is recorded and adjusted to the applicable standard according to the Indonesian National Standard (SNI). According to SNI, the pH standard of bar soap is 9-11 (Diningsih et al., 2022; Sukeksi et al., 2021).

Soap Cleansing Ability Test

To assess the cleaning effectiveness of the prepared soaps, three drops of lubricant oil were applied to strips of filter paper. Each piece of filter paper was then immersed in a beaker glass containing each soap solution formulation. The filter paper was stirred vigorously for one minute, after which the filter papers were removed, rinsed with distilled water, and visually inspected for cleanliness. This process was repeated using commercial soap samples and regular WCO soap for comparison (Usman & Mukhtar, 2021).

Soap Organoleptic and Irritation Test

To evaluate the sensory properties and potential skin irritation of the solid soap made from waste cooking oil and avocado waste extract, a small-scale organoleptic and irritation test was conducted involving ten non-standard panelists. The panelists assessed the soap's odor, texture, tight impression, hardness, and foam production. The irritation test was conducted by panelists to provide information related to the effects felt after using solid soap from waste cooking oil and avocado waste extract. An irritating effect occurs if the panelist

feels symptoms such as skin dryness, redness, itching, or burning 30 minutes after using the solid soap (Ircham et al., 2022; Sany et al., 2019).

Results and Discussion

Characteristic of Refined Waste Cooking Oil (WCO)

WCO refining involves two essential processes: neutralization using Na_2CO_3 and bleaching using activated carbon (Sukmawati & Sunarto, 2020). The results of oil blanching by activated carbon are observed based on checking the peroxide value using the titration method according to the AOCS-AOAC 965.33 standard (Abera et al., 2023; Mariana et al., 2020). The results of neutralization of waste cooking oil using Na_2CO_3 are observed based on checking the pH of the oil using a universal indicator. Data of the pH and peroxide values before and after refining waste cooking oil using activated carbon can be seen in Table 2.

Table 2. The WCO pH and peroxide value		
Aspects	Before refining	After refining
pH	5	8
Peroxide value	22 meq O_2/kg	10 meq O_2/kg

The pH data indicates that the neutralization process effectively reduces the acidity of waste cooking oil. This occurs because the alkaline solution reacts with the free fatty acids present in the oil. Neutralization aims to separate the free fatty acids contained in waste cooking oil with the help of Na_2CO_3 . By adding sodium carbonate (Na_2CO_3), the free fatty acids are separated and removed as a sediment, resulting in a less acidic oil. (Sukmawati & Sunarto, 2020). The bleaching process, specifically using activated carbon, effectively reduces the peroxide value of waste cooking oil. This indicates a decrease in free radical compounds like peroxide compounds. Activated carbon functions through adsorption, capturing and removing various substances, including peroxide compounds, metal particles, and other toxic compounds, from the waste cooking oil (Sukmawati & Sunarto, 2020). The appearance of waste cooking oil before and after refining can be seen in Figure 1.



Figure 1. Discolouration of waste cooking oil in refining process.

The effectiveness of adsorption is directly linked to the surface area of the adsorbent. A larger surface area allows for greater adsorption capacity, leading to increased adsorption. By reducing the particle size of the carbonized adsorbent, its surface area can be significantly increased. This, combined with suitable surface functional groups, enhances the overall adsorption capacity (Haryanto et al., 2024). The adsorption process by activated carbon in the refining process of waste cooking oil involves physical adsorption. In chemistry, this interaction arises due to van der Waals forces. These van der Waals forces are weak. When interacting with components in oil, adsorbents can adsorb organic contaminants with three types of interactions. First, activated carbon can experience electrostatic interactions with organic contaminants. Second, activated carbon can interact with parts of organic compounds that are polar (hydrophilic). Third, activated carbon can interact with parts of organic compounds that are nonpolar (hydrophobic) (Adegoke et al., 2023).

Characteristic of Avocado Seeds and Peels Extract

The appearance of several variations of avocado waste extract using WCO as the solvent can be seen in Figure 2. The description of each part in Figure 2 is: a) avocado seed extract; b) avocado seed and peel extract; c) avocado peel extract.

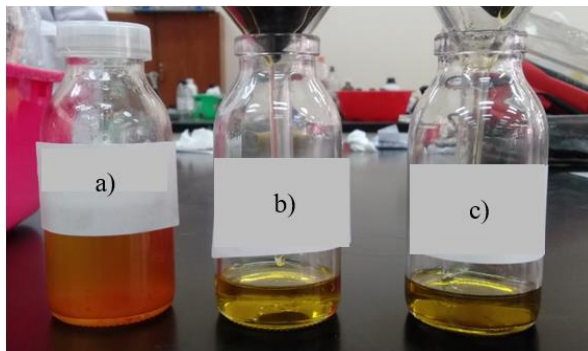


Figure 2. WCO with the addition of avocado waste extract.

The avocado waste extraction is a simple extraction marked by a change in the color of waste cooking oil (yellow) to an orange color in the extraction of the avocado seeds sample and a greenish color in the extraction of avocado peels and avocado seeds+peels sample. The difference in the apparent color between avocado seeds and avocado peels extract sample is due to the difference in the dominance of pigment compounds contained in avocado seeds and peels. Avocado seeds contain more carotenoid compounds that contribute to the orange color, while avocado skin contains more chlorophyll compounds that contribute to the greenish color (Oliveira et al., 2022; Tesfaye et al., 2022). Extracting bioactive compounds and other ingredients from plant materials is a crucial step in the process. Avocado waste extraction is included in solid-fluid extraction, which is the extraction or separation of metabolite compounds from solid material in the form of certain parts or all parts of plant material using certain solvents (Ong et al., 2022).

Analysis of Bar Soap from Waste Cooking Oil and Avocado Waste Extracts Tests

This soap made from avocado waste oil involves a saponification reaction between the triglycerides in the oil and NaOH lye solution, and the product is bar soap (Arasaretnam & Venujah, 2019). The bar hand soap samples from three variations of avocado waste extract are shown in Figure 3.

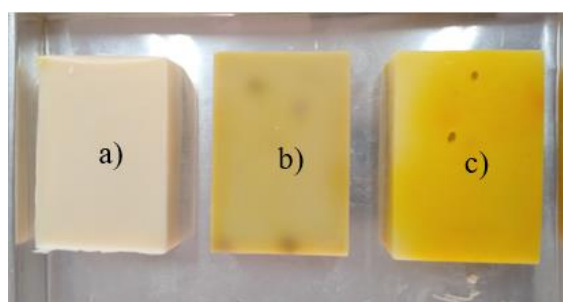


Figure 3. Sample of wco soap with avocado waste extract.

The description of each part in Figure 3. is: a) WCO soap with avocado seed extract; b) WCO soap with avocado peel extract; c) WCO soap with avocado seed and peel extract. Based on Figure 3, the addition of avocado waste extract in cooking oil soap does not actually cause a difference in the color of each soap sample. The original color of each soap is as in the soap labeled a). This was observed when the soap batter was formed. Therefore, the samples were given additional synthetic dyes to differentiate each sample based on its formulation so that the yellow and green colors in soaps b) and c) came from synthetic dyes.

Soap pH Testing

The soap pH test is conducted to ensure that the solid soap made is within the acidity level that is safe for the skin. According to the Indonesian National Standard (SNI), the pH of bar soap that is safe for the skin is 9-11

(Sukeksi et al., 2021). The pH value data obtained from each bar soap formulation from waste cooking oil and avocado waste extract are shown in Table 3.






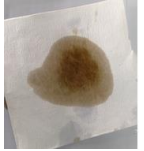
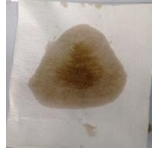
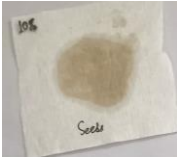





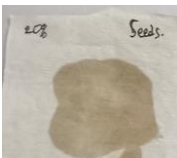


Table 3. pH of wco soap with waste avocado extract

Soap Compositions	pH	
	10% (w/w)	20 % (w/w)
WCO + Avocado Seeds Extract	9.88	9.80
WCO + Avocado Peels Extract	10.03	9.83
WCO + Avocado Seeds and Peels Extract	10.09	9.96

Based on the data in Table 2, all six bar soap samples have pH values that comply with SNI standards. Knowing the pH of soap is essential because soap with a high pH will cause dry skin and irritation. Under normal conditions, the skin's pH will return to normal 30 minutes after rinsing the skin from soap foam with water (Sany et al., 2019).

Qualitative Test of Soap Cleansing Ability

Table 4. Qualitative results of soap cleansing ability

Percents of WCO and waste avocado extract (w/w)	Cleansing Ability				
	WCO + Avocado Seeds Extract	WCO + Avocado Peels Extract	WCO + Avocado Seeds and Peels Extract	Commercial Soap	WCO Soap
0%	-	-	-	Before 	Before 
	-	-	-	After 	After 
10%	Before 	Before 	Before 	-	-
	After 	After 	After 	-	-
20%	Before 	Before 	Before 	-	-
	After 	After 	After 	-	-

The test of the cleansing ability of bar soap from waste cooking oil and avocado waste extract was carried out qualitatively by comparing the results of cleaning stains in the form of lubricant oil droplets using samples of WCO with avocado waste extract soap solution with the results of cleaning stains using commercial soap and regular WCO soap (without the addition of avocado waste extract) (Usman & Mukhtar, 2021). Each sample was tested for cleanliness on filter paper within 1 minute. The qualitative soap cleansing ability test results can be seen in Table 4.

Based on Table 3, the cleansing ability for all variations of solid soap from waste cooking oil and avocado waste extract shows results that are similar to waste cooking oil soap (without the addition of avocado waste extract). As for commercial soap, it looks cleaner (lifts more stains) than other soap samples, except for the sample with the formulation of 1) Waste cooking oil and 20% avocado peel and seed extract, and 2) Waste cooking oil and 10% avocado peel extract. Both waste cooking oil soap and 20% avocado peel and seed extract, as well as waste cooking oil and 10% avocado peel extract, have a cleansing ability that is close to the cleansing ability of commercial soap when viewed from the remaining stains that remain on filter paper.

Soap Organoleptic Test

Organoleptic tests were conducted on ten panelists aged 19-27 using a questionnaire with a 3-point Likert scale. Table 5 shows the results of the organoleptic test of soap from waste cooking oil and avocado waste extract.

Table 5. Organoleptic test of each soap formulation

Aspects	Soap Formulation						Description
	F1	F2	F3	F4	F5	F6	
Hardness	2,1	2,4	2,4	1,9	1,9	1,9	Low Level: $\bar{x} < 1,5$
Amount of foam produced	2,2	2,2	2,3	2,4	2,2	2,1	
Odor	2,0	1,9	2,0	1,8	1,6	1,9	Medium Level: $1,5 \leq \bar{x} \leq 2,5$
Texture	1,9	2,0	2,3	1,6	1,9	2,0	High Level: $\bar{x} > 2,5$
Tight Impression	2,0	2,3	2,4	2,0	1,9	2,0	

The good and preferred waste cooking oil soap with avocado waste extract filler is a soap that has a medium level of hardness, amount of soap produced, odor, texture, and tight impression. In this organoleptic test, all soap formulations fell into the medium category for all aspects assessed. The hardness of the soap is affected by the amount of water in the soap. The more water in the soap, the softer the soap. Hard soap is more durable than soft soap. The amount of foam produced on the soap affects the process of transferring the scent from the soap to the human skin. Too much foam does not always indicate that the soap has a high cleansing power; it can cause the skin to become dry.

Conversely, too little foam is an indication of low cleansing power. Fragrance influences panelists' preference for the soap used. Overall, panelists reported that all soap formulations had a mild scent. In addition, the texture of the soap also affects the panelists' preference for the soap. Cold-process soap has a texture that is neither soft nor rough. A tight impression is assessed to ensure that there is no slippery or greasy feeling and that the skin of the hands feels tight after using the soap. Tight impression is one of the most critical parameters in soap as it affects the consumer's interest in choosing a soap.

Soap Irritation Test

Based on the soap irritation test results, 2 out of 10 panelists experienced symptoms of irritation with the soap used. One panelist reported that the Formulation 6 soap sample experienced slight itching symptoms 30 minutes after using the soap. The other panelist reported experiencing symptoms of slight redness on the skin 30 minutes after using the Formulation 5 soap sample. A person can experience allergic symptoms to soap products or surfactants based on the last product used (Ilomuanya et al., 2020). Based on these reports, it can be concluded that soap samples in certain formulations cause irritating effects on some people with a history of allergies. Several factors cause soap products to potentially cause irritating effects on the skin, including the overly strong alkaline nature of soap and fragrance oils incorporated into soap formulations (Ilomuanya et al., 2020).

The addition of quercetin compound concentration in soap formulations from waste cooking oil and avocado waste extract can be suggested to provide anti-allergic effects for the skin. Quercetin is one of the substances

from the flavonoid polyphenol group, which is not only an antioxidant but also acts as an anti-inflammatory and anti-histamine (Jafarinia et al., 2020).

Conclusion

The production of solid soap from waste cooking oil and avocado waste extract filler has undergone a series of quantitative and qualitative test processes. Based on the soap pH test results, all soap samples started from formulations 1-6 meet SNI standards. Based on the results of the soap cleanability test, Formulation 2 (WCO soap with the addition of 10% (w/w) avocado peel extract) and Formulation 6 (WCO soap with the addition of 20% (w/w) avocado peel and seed extract) have almost the same cleanability as commercial soap. The results of the soap organoleptic test show that all soaps fall into the moderate category in terms of hardness level, foam produced, odor, texture, and tight impression. The results of the irritation test show that soap formulations that do not irritate are soaps with formulations 1-4. Overall, it can be concluded that solid soap with Formulation 2 is a soap that fulfills all the criteria of the pH test, cleansing ability test, organoleptic test, and irritation test.

Recommendations

The research is limited to the production of bar soap from WCO and avocado waste extract and qualitative tests, including small-scale cleansing ability tests and organoleptic and irritation tests. Future research is expected to be related to the characterization of specific chemical compounds, such as quercetin from waste cooking oil soap and additional natural product extracts with antioxidant and anti-allergic activities. In addition, quantitative testing of bar soap also needs to be further investigated so that the quality of bar soap can be more clinically tested and according to standards.

Scientific Ethics Declaration

The authors declare that the scientific ethical and legal responsibility of this article published in EPSTEM Journal belongs to the authors.

Acknowledgements

* This article was presented as an oral presentation at the International Conference on Basic Sciences and Technology (www.icbast.net) held in Antalya/Turkey on November 14-17, 2024.

* The authors would like to thank to Indonesia Endowment Fund for Education/Lembaga Pengelola Dana Pendidikan (LPDP), Ministry of Finance, Republic of Indonesia for the scholarship, research, international conference, and publication funding.

* The authors would like to thank to Chemistry Education Department, Universitas Pendidikan Indonesia for the facility, guidance, and support for this research.

References

- Abera, B.H., Diro, A., & Beyene, T.T. (2023). The synergistic effect of waste cooking oil and endod (*Phytolacca dodecandra*) on the production of high-grade laundry soap. *Heliyon*, 9(6).
- Adegoke, K.A., Akinnawo, S.O., Adebusi, T.A., Ajala, O.A., Adegoke, R.O., Maxakato, N.W., & Bello, O.S. (2023). Modified biomass adsorbents for removal of organic pollutants: a review of batch and optimization studies. *International Journal of Environmental Science and Technology*, 20, 11615–11644
- Ahmed, I. A., Mikail, M. A., Zamakshshari, N., & Abdullah, A. S. H. (2020). Natural anti-aging skincare: role and potential. *Biogerontology*, 21, 293-310.
- Arasaretnam, S. & Venajah, K. (2019). Preparation of soaps by using different oil and analyze their properties. *Natural Products Chemistry & Research*, 7(1), 1-4.

- Azhar, A.N.S., Safarin, N.S.M., & Razak, S.N.A. (2024). Green eco-soap hand wash. *Multidisciplinary Applied Research and Innovation*, 5(2), 87-92.
- Azme, S. N. K., Yusoff, N. S. I. M., Chin, L. Y., Mohd, Y., Hamid, R. D., Jalil, M. N., & Zain, Z. M. (2023). Recycling waste cooking oil into soap: Knowledge transfer through community service learning. *Cleaner Waste Systems*, 4, 100084.
- Charles, A.C., Dadmohammadi, Y., & Abbaspourrad, A. (2022). Food and cosmetic applications of the avocado seed: a review. *Food & Function*, 13, 6894-6901.
- Diningsih, A., Yaturramadhan, H., & Batubara, S. (2022, December). Physical properties testing soap from citronella oil with red spinach (*amaranthus gangeticus*) extract. In *Tapanuli International Health Conference 2022 (TIHC 2022)* (pp. 19-26). Atlantis Press.
- Esfarjani, F., Khoshtinat, K., Zargaraan, A., Mohammadi-Nasrabadi, F., Salmani, Y., Saghafi, Z., ... & Bahmaei, M. (2019). Evaluating the rancidity and quality of discarded oils in fast food restaurants. *Food science & Nutrition*, 7(7), 2302-2311.
- Foo, W. H., Koay, S. S. N., Chia, S. R., Chia, W. Y., Tang, D. Y. Y., Nomanbhay, S., & Chew, K. W. (2022). Recent advances in the conversion of waste cooking oil into value-added products: A review. *Fuel*, 324, 124539.
- Gharby, S. (2022). Refining vegetable oils: Chemical and physical refining. *The Scientific World Journal*, 2022(1), 6627013.
- Hartini, S., Fiantika, Y., Widharto, Y., & Hisjam, M. (2021). Optimal treatment combination for dishwashing liquid soap based on waste cooking oil according to the requirement of Indonesian quality standards. *EVERGREEN Joint Journal of Novel Carbon Resource Sciences & Green Asia Strategy*, 08 (02), 492-498.
- Haryanto, B., Hutagaol, L.N., Sianturi, N.C., Fazira, M., Sitorus, J., & Alexander, V. (2024). Purification of waste cooking oil using natural corn cob and carbon corn cob as adsorbent with batch operation. *IOP Conference Series: Earth and Environmental Science*, 1302(1), 012067.
- Ilomuanya, M., Ayanlowo, O., Ubani-ukoma, U., Ologunagba, M., Odafe, R., & Nwankanna, U. (2020). Safety evaluation of different variants of a topically applied toilet bar soap range using skin irritancy testing methods in the Nigerian population. *Journal of Pharmaceutical Technology*, 1(2), 40-45.
- Ircham, M.M., Mubarak, A.S., & Saputra, E. (2022). Physical characteristic and antioxidant activities of liquid bath soap with substitution of β -carotene crude extract from *Gracilaria* sp. *IOP Conference Series: Earth and Environmental Science*, 1036, 012047.
- Jafarinia, M., Sadat Hosseini, M., Kasiri, N., Fazel, N., Fathi, F., Ganjalikhani Hakemi, M., & Eskandari, N. (2020). Quercetin with the potential effect on allergic diseases. *Allergy, Asthma & Clinical Immunology*, 16, 1-11.
- Jimenez, P., Garcia, P., Quitral, V., Vasquez, K., Parra-Ruiz, C., Reyes-Farias, M., & Soto-Covasich, J. (2021). Pulp, leaf, peel and seed of avocado fruit: A review of bioactive compounds and healthy benefits. *Food Reviews International*, 37(6), 619-655.
- Mariana, R. R., Susanti, E., Hidayati, L., & Wahab, R. A. (2020). Analysis of peroxide value, free fatty acid, and water content changes in used cooking oil from street vendors in Malang. In *AIP Conference Proceedings*, 2231(1). AIP Publishing.
- Martin-del-campo, S.T., Cardador-Martinez, A., & Ramirez-Anaya, J.D.P. (2023). *Food byproducts: valorization through nutraceutical production*. New York: Nova Science Publishers, Inc.
- Oliveira, C. S. D., Andrade, J. K. S., Rajan, M., & Narain, N. (2022). Influence of the phytochemical profile on the peel, seed and pulp of margarida, breda and geadia varieties of avocado (*Persea Americana* Mill) associated with their antioxidant potential. *Food Science and Technology*, 42, e25822.
- Ong, E. S., Low, J., Tan, J. C. W., Foo, S. Y., & Leo, C. H. (2022). Valorization of avocado seeds with antioxidant capacity using pressurized hot water extraction. *Scientific Reports*, 12(1), 1-13.
- Ramadan, M. F., & Farag, M. A. (Eds.). (2022). *Mediterranean fruits bio-wastes: chemistry, functionality and technological applications*. Cham, Switzerland: Springer International Publishing.
- Sany, I.P., Romadhon, Fahmi, A.S. (2019). Physicochemical characteristics and antioxidant activity of solid soap enriched with crude *Eucheuma cottoni* Extract. *IOP Conference Series: Earth and Environmental Science*, 246, 012066.
- Sukeksi, L., Iriany, Grace, M., & Diana, V. (2021). Characterization of the chemical and physical properties of bar soap made with different concentrations of bentonite as a filler. *International Journal of Technology*, 12(2), 263-274.
- Sukmawati, S.H. & Sunarto. (2020). Utilization of coffee waste as active charcoal for purification of waste cooking oil. *Indonesian Journal of Chemistry and Environment*, 3(2), 29-38.
- Tesfaye, T., Ayele, M., Gibril, M., Ferede, E., Limeneh, D. Y., & Kong, F. (2022). Beneficiation of avocado processing industry by-product: A review on future prospect. *Current Research in Green and Sustainable Chemistry*, 5, 100253.

- Usman, A.H. & Mukhtar, B. (2021). Investigation of qualitative parameters in soap produced from blend of neem and castor oil. *Journal of the Nigerian Society of Chemical Engineers*, 36(2), 20-27.
- Zaki, S.A.E., Ismail, F.A.E., Abdelatif, S.H., El-Mohsen, N.R.A., & Helmy, S.A. (2020). Bioactive compounds and antioxidant activities of avocado peels and seeds. *Pakistan Journal of Biological Sciences*, 23(3), 345-350.

Author Information

Nisrina Zahira Putri Irawan

Universitas Pendidikan Indonesia

Jl. Dr. Setiabudi No. 229, Bandung, West Java, Indonesia

Heli Siti Halimatul Munawaroh

Universitas Pendidikan Indonesia

Jl. Dr. Setiabudi No. 229, Bandung, West Java, Indonesia

Contact e-mail: heli@upi.edu

Sjaeful Anwar

Universitas Pendidikan Indonesia

Jl. Dr. Setiabudi No. 229, Bandung, West Java, Indonesia

To cite this article:

Irawan, N.Z.P, Munawaroh, H.S.H., & Anwar, S. (2024). The properties of waste cooking oil soap with avocado waste extract as a filler. *The Eurasia Proceedings of Science, Technology, Engineering & Mathematics (EPSTEM)*, 30, 97-106.

The Eurasia Proceedings of Science, Technology, Engineering & Mathematics (EPSTEM), 2024

Volume 30, Pages 107-113

ICBAST 2024: International Conference on Basic Sciences and Technology

Cluster Analysis of Sleep Health and Lifestyle Data Using Ward Algorithm and Euclidean Distance

Mawar Idah Shonia
Universitas Gadjah Mada

Noorma Yulia Megawati
Universitas Gadjah Mada

Gunardi Gunardi
Universitas Gadjah Mada

Asrul Khasanah
Universitas Gadjah Mada

Abstract: The intention of this study is to identify and assess groups based on their sleep quality and duration, physical activity levels, and stress levels. Next, we will investigate the relationship between sleep habits and stress levels. There were 374 respondents, with a total of 13 variables. The researchers utilized Ward's algorithm to identify groups and Euclidean distance to compare them. This study technique employs statistical computer tools, specifically R. This study's processes begin with data processing, which is followed by data standardization and clustering. There are four categories, namely (1) a group with an average sleep duration of 6 hours and a sleep quality scale worth 6 out of 10, but conducting physical activity less than 30 minutes per day, the stress level is high. (2) in a group with an average sleep duration of 6 hours and a sleep quality scale worth 6 out of 10, but doing physical activity for two hours each day, the stress level is very high. (3) in the group with an average sleep duration of 7 hours, a sleep quality scale of 8 out of 10, and 65 minutes of physical activity each day, the stress level is medium, (4) the group with an average sleep duration of 8 hours and a sleep quality rating of 9 out of 10 maintains a low stress level despite one hour of physical exercise. A dendrogram plot is used in data visualization to show how closely connected the data sets are. This study suggests that a person's sleep habits and daily physical activity have a major impact on their stress level, providing readers and the community with knowledge into how to improve overall health.

Keywords: Cluster, Sleep health, Lifestyle, Ward algoritmn, Euclidean distance, Healthcare engineering

Introduction

Sleep is a crucial health practice that affects all areas of well-being (Grandner, 2014). Sleep can also help the body recover from weariness and become more rejuvenated. Sleep difficulties can cause behavioral changes such as decreased endurance, loss of attention, easy exhaustion, sadness or stress, and interference with other daily tasks. Sleep length and quality are two aspects that influence whether a person's sleep requirements are met (Lemma et al., 2012). The factors that cause a person's stress level are classified into three categories: (1) biological factors, which include genetics, sleep patterns, diet, fatigue, and so on; (2) psychological factors, which include emotional factors, behavior, situations, and feelings; and (3) environmental factors, which include physical, social, and biotic activities. Stress levels can range from one to ten. Level one indicates that a person is not stressed and is free of pressure and worry. Level two denotes a little stress that does not interfere with regular activities. Level three stress refers to mild or low stress in which pressure is present but may be

- This is an Open Access article distributed under the terms of the Creative Commons Attribution-Noncommercial 4.0 Unported License, permitting all non-commercial use, distribution, and reproduction in any medium, provided the original work is properly cited.

- Selection and peer-review under responsibility of the Organizing Committee of the Conference

© 2024 Published by ISRES Publishing: www.isres.org

regulated. Level four refers to mild stress that can still be managed. Level five is defined as medium-level stress, which causes pressure and interferes with daily tasks. Level six is moderately stressful and has an effect on mental health. Level seven indicates a high level of tension that significantly interferes with tasks. Level eight indicates extremely high stress, making it difficult to focus on regular activities. Levels nine and ten represent high and extraordinary levels of stress when you are unable to manage them and require intensive medical treatment. The 10 levels can be classified into two types of stress levels. Eustress is a stress condition in which the individual remains cheerful and enthusiastic about participating in activities, typically at levels one through five. And distress is defined as stress that has a negative effect, typically at levels six to ten.

A person's stress level can be reduced by a variety of means, one of which is participating in sports or other physical activities. Physical activity is an effective way to manage stress and become more organized (Scott, 2021). Physical activity can take several forms, including exercise, which involves moving the body in such a way that sweat is produced. The World Health Organization (WHO) defines physical activity as a body movement that requires energy expenditure (World Health Organization, 2020). As a result, there is a strong link between stress-causing sleep disturbances and stress-reducing physical activity. Researchers obtained secondary data from the Kaggle.com website in the form of a data set containing 13 variables. We will cluster the data and evaluate each group separately. Cluster analysis seeks to create multiple natural groupings, or clusters, of individuals. This is accomplished by categorizing "similar" individuals based on some relevant criteria. Once the groups have been identified, it is useful to display the data to describe each group using dendrograms in order to have a better understanding of the distinctions that exist between the formulated groupings. Cluster analysis is used in many sectors, including natural science, medical science, economics, marketing, and others. Cluster analysis is divided into two fundamental steps: (1) selecting the proximity measure of each object to determine the similarity of its values, so that the "closer" they are, the more homogeneous they are; and (2) selecting a group formation algorithm based on the proximity measure, the objects are assigned into groups so that the differences between groups become large and the observations within the groups become as close as possible. The study's criteria include four variables: sleep length, sleep quality, physical activity level, and stress level. Then, the link between sleep habits and stress levels will be investigated. Ward's technique is used to group and identify the data set, while the Euclidean distance is utilized to compare groups.

Ward Algorithm

To group the dataset Ward's approach is another algorithm for identifying partitions with a minimal number of squares. It begins with a large number of squares and reduces them before beginning with a small number of squares (using many clusters) and increasing them.

1. Begin with each point in a cluster by itself (sum of squares = 0).
2. Combine two clusters with the minimum total of squares to minimize merging costs.
3. Repeat merging until k clusters are reached. To identify it, Ward's method is utilized, and the Euclidean distance is used to compare groups.

If two items or groups, say P and Q, are combined, the distance between the resulting group P + Q and group R can be determined using the following distance function (Härdle & Simar, 2007):

$$d(R, P + Q) = \delta_1 d(R, P) + \delta_2 d(R, Q) + \delta_3 d(P, Q) + \delta_4 |d(R, P) - d(R, Q)|$$

δ_j is the weighting element that determines the different agglomeration algorithms.

$$\delta_1 = \frac{n_R + n_P}{n_R + n_P + n_Q}, \delta_2 = \frac{n_R + n_Q}{n_R + n_P + n_Q}, \delta_3 = -\frac{n_R}{n_R + n_P + n_Q}, \delta_4 = 0$$

Here, $n_P = \sum_{i=0}^n I(x_i \in P)$ is the number of objects in group P. The values n_Q and n_R are defined analogously.

Euclidean Distance

The Euclidean distance is the smallest distance between two objects in N-dimensional space, also known as Euclidean space. It is a broad metric for determining the similarity of two data objects and is utilized in a variety of domains, including geometry, data mining, deep learning, and others. It also goes by the titles Euclidean

norm, Euclidean metric, L2 norm, L2 metric, and Pythagorean metric. The Euclidean distance is a special instance of the L_r norm for $r \geq 1$, (Härdle & Simar, 2003) :

$$d_{ij} = \|x_i - x_j\|_r = \left\{ \sum_{k=1}^p |x_{ik} - x_{jk}|^r \right\}^{\frac{1}{r}}$$

Where x_{ik} represents the value of the k-th variable as measured on the i-th person.

Method

The data used in this study is secondary data from Kaggle.com. The data comes in the form of "sleep health and lifestyle" data, with 374 respondents and 13 columns containing various variables linked to sleep and daily activities. This data covers parameters such as gender, age, occupation, sleep duration, sleep quality, physical activity level, stress level, BMI category, blood pressure, heart rate, number of steps per day, and presence or absence of sleep disorders, as well as the definition of each variable:

- X_1 : Person ID
- X_2 : Gender (Male or Female)
- X_3 : Age (years)
- X_4 : Occupation
- X_5 : Sleep duration (hours per day)
- X_6 : Quality of Sleep (scale 1-10)
- X_7 : Physical activity level (minutes per day)
- X_8 : Stress level (scale 1-10)
- X_9 : BMI Category
- X_{10} : Blood Pressure (systolic or diastolic)
- X_{11} : Heart Rate (bpm)
- X_{12} : Daily Steps
- X_{13} : Sleep Disorder

Person ID is essentially an identifier for each individual. Each individual's BMI falls into one of three categories: underweight, normal, or overweight. Daily steps refers to the number of steps a person takes each day. Insomnia, sleep apnea, or the absence of any abnormalities. Individuals with problems sleeping suffer from insomnia (inappropriate sleep). Sleep apnea happens when a person's sleep pattern disturbance causes them to cease breathing while sleeping. The variables studied in this study are X_5, X_6, X_7 , and X_8 , which represent sleep length, sleep quality, physical activity, and a person's stress level. The respondents ranged in age from 27 to 59 years old. These variables share the same association, so they will be analyzed as a group. The set of data management techniques makes use of software applications, specifically R. In addition to cluster analysis, principal component analysis will be performed, with results provided in the form of plots. The following diagram depicts the flow from data loading to cluster analysis:

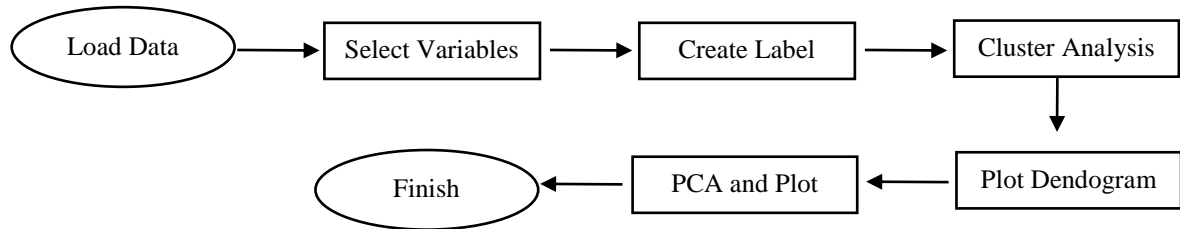


Figure 1. Cluster analysis diagram

The collected data was then put into the R software application using the `load()` command. Then, using the `par()` command, configure the chart layout to display two plots side by side in a single row. Next, use the `hclust(dist(file[:]), "ward.D")` command to execute the "Ward" cluster analysis, and the `dist(file[:])` function to compute the Euclidean distance matrix between rows and columns. With the `cutree(hc, 4)` command, visualize data using a dendrogram plot of cluster analysis results divided into four clusters; the item names of the four clusters are also presented. The following phase is PCA (Principal Component Analysis), which tries to reduce

these variables into principal components capable of explaining the majority of the data variance, also known as data reduction, to make it easier to grasp the relationship structure between variables in the dataset.

Results and Discussion

This is an overview of the "Sleep Health and Lifestyle" data that was processed:

Table 1. Person's typical sleep time

Person ID	Age (years)	Sleep Duration (hours/day)	Quality of Sleep (1-10)	Physical Activity Level (minutes/day)	Stress Level (1-10)
1	27	6.1	6	42	6
2	28	6.2	6	60	8
3	28	6.2	6	60	8
⋮	⋮	⋮	⋮	⋮	⋮
372	59	8.1	9	75	3
373	59	8.1	9	75	3
374	59	8.1	9	75	3

Table 1. Shows that a person's typical sleep time ranges between 6.1 and 8.1 hours per day. Physical activity levels vary from 42 to 75 minutes each day. Sleep quality indicators on a scale of 1 to 10 with interpretations, namely scale 1 is very bad, scale 2 is bad, scale 3 is not good, scale 4 is below average, scale 5 is moderate, scale 6 is quite good, scale 7 is good, scale 8 is very good, scale 9 is exceptional, and scale 10 is extraordinary without interruption and very sound. The ward approach is used to process this data, resulting in four clusters as follows:

Table 2. Cluster analysis results

Cluster	Sleep Duration (hours/day)	Quality of Sleep (1-10)	Physical Activity Level (minutes/day)	Stress Level (1-10)
1	6.249412	5.800000	38.41176	7.40000
2	7.294624	7.586022	64.73118	4.913978
3	8.243662	9.000000	55.56338	3.028169
4	6.065625	6.000000	90.00000	8.000000

Table 2. Shows the findings of the cluster analysis, which revealed four clusters with varying signals for each. The reasoning for each cluster is as follows:

- (1) The group with an average sleep duration of 6.3 hours per day and a sleep quality scale score of 5.8 is close to 6, indicating that sleep is relatively sound with a reasonably effective sleep period despite slight interruptions. Physical activity averages 38 minutes per day, and the stress level on a scale of 7.4 is high enough to interfere with daily tasks.
- (2) The group with an average sleep duration of 7.3 hours per day and a sleep quality scale worth 7.6 close to 8 indicates that the quality of sleep is very good, and with 65 minutes of physical activity per day, the stress level on a scale of 4.9 close to 5 remains moderate.
- (3) The group with an average sleep length of 8.2 hours per day and a sleep quality rating of 9 indicates no sleep disturbance and is at an exceptional level. The average daily physical activity is two hours and 56 minutes, indicating a low stress level.
- (4) The group with an average sleep duration of 6 hours per day and a sleep quality scale of 6 indicates that the quality of sleep is fairly good, and with 90 minutes of physical activity per day, the stress level is quite high.

To further comprehend, the dendrogram visualization is as follows:

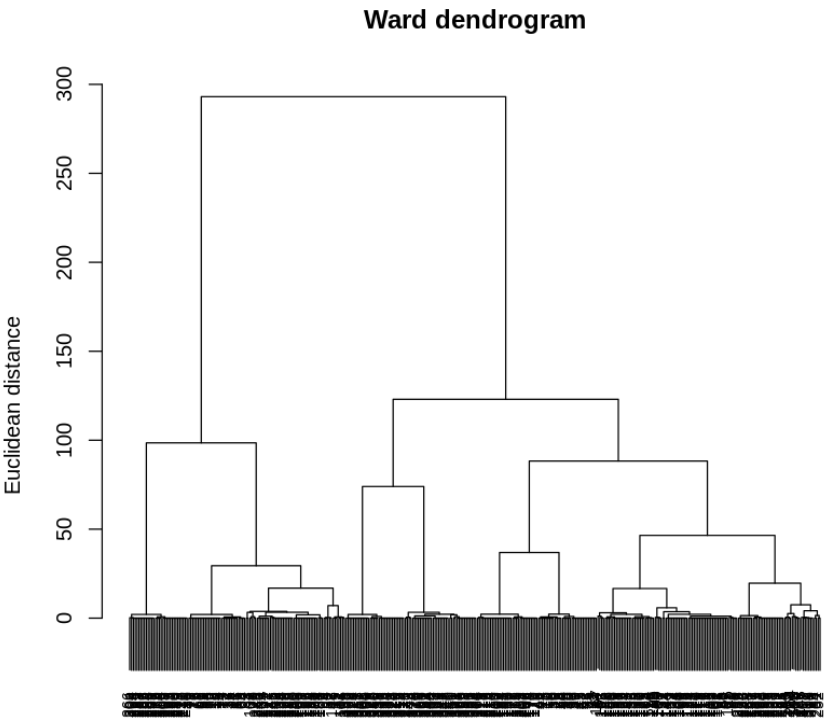


Figure 2. Shows that the six factor branches of the data can be more clearly interpreted and understood by applying PCA. Here's a PCA plot:

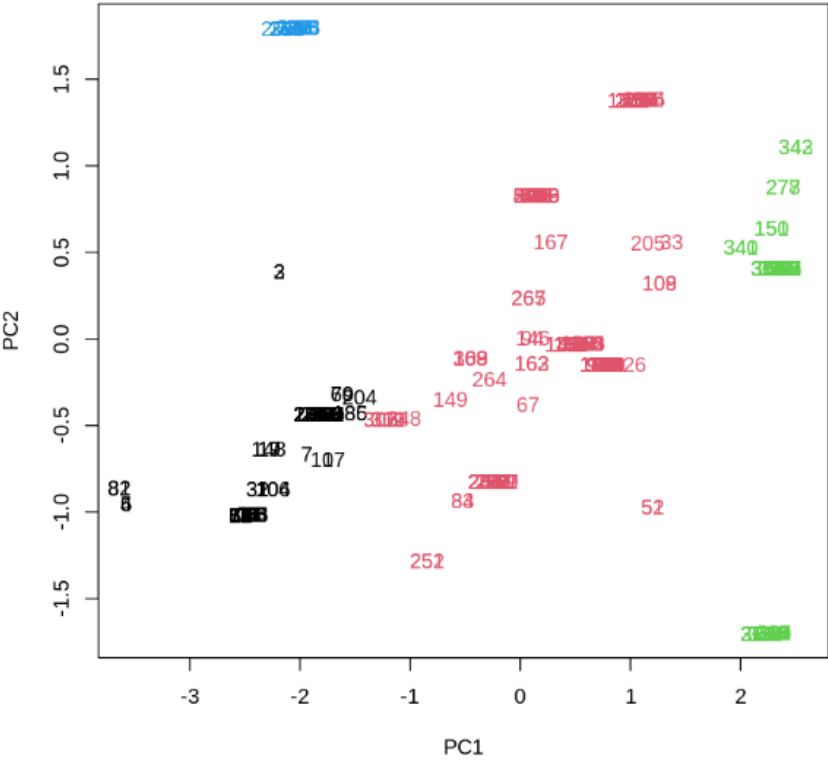


Figure 3. Color gruping

Figure 3. Shows four color groupings: blue, black, pink, and green. The number on the plot represents the individual's identity number. The blue color is in the positive area of the Y-axis, suggesting that the group is distinct from other groups and belongs to cluster 1. The dark hue appears in the negative region on PC1 and PC2, but slightly in the positive area on PC2. The pink color is more evenly distributed in the middle, ranging from -1 to 1 in both PC1 and PC2, indicating that it is in cluster 3. The green color appears in the positive

section of both PC1 and PC2, indicating cluster 4. The few points that are not part of the group suggest data variation.

Conclusion

Based on the results of cluster analysis on "Sleep Health and Lifestyle" data using the ward algorithm and the Euclidean distance approach, it is possible to conclude that there are four groups from the cluster analysis process visualized using a dendrogram and then using PCA, which produces four different colors as follows:

- (1) Blue (cluster 1) is a group with an average sleep length of 6.3 hours per day and a sleep quality scale score of 5.8, which is near to 6, indicating that sleep is pretty sound with a fairly effective sleep period despite slight interruptions. The average physical activity was 38 minutes per day, so the stress level on a scale of 7.4 was high enough to interfere with everyday tasks.
- (2) Black (cluster 2) is a group with an average sleep duration of 7.3 hours per day and a sleep quality scale of 7.6 close to 8, indicating that the quality of sleep is very good. They also do 65 minutes of physical activity per day, and their stress level on a scale of 4.9 close to 5 remains medium.
- (3) Pink (cluster 3) is a group with an average sleep length of 8.2 hours per day and a sleep quality rating of 9 out of 10, indicating no sleep disturbance. The average daily physical activity is two hours and 56 minutes, indicating a low stress level.
- (4) Green (cluster 4) is a group with an average sleep duration of 6 hours per day and a sleep quality scale of 6, indicating that the quality of sleep is fairly good, and with 90 minutes of physical activity per day, the stress level is quite high.

There are certain spots that appear to be close together, indicating that the primary components are more comparable.

Scientific Ethics Declaration

The authors declare that the scientific ethical and legal responsibility of this article published in EPSTEM Journal belongs to the authors.

Acknowledgements or Notes

* The authors would like to express their sincere gratitude to Indonesia Endowment Fund for Education Agency (LPDP) under the Ministry of Finance of the Republic of Indonesia for supporting and funding the authors to attend this conference. Their assistance was crucial in facilitating the author's participation in the conference and encouraging collaboration on this project.

* This article was presented as an oral presentation at the International Conference on Basic Sciences and Technology (www.icbast.net) held in Antalya/Turkey on November 14-17, 2024.

References

- Bull, F. C., Al-Ansari, S. S., Biddle, S., Borodulin, K., Buman, M. P., Cardon, G., ... & Willumsen, J. F. (2020). World Health Organization 2020 guidelines on physical activity and sedentary behaviour. *British Journal of Sports Medicine*, 54(24), 1451-1462
- Grandner, M. A. (2014). Addressing sleep disturbances: an opportunity to prevent cardiometabolic disease?. *International Review of Psychiatry*, 26(2), 155-176.
- Härdle, W., & Simar, L. (2007). Conjoint measurement analysis. *Applied Multivariate Statistical Analysis*, 347-358.
- Lemma, S., Gelaye, B., Berhane, Y., Worku, A., & Williams, M. A. (2012). Sleep quality and its psychological correlates among university students in Ethiopia: a cross-sectional study. *BMC Psychiatry*, 12, 1-7.
- Maronna, R. (2005). [Review of the book Wolfgang Härdle and Léopold Simar: Applied multivariate statistical analysis, Springer, Berlin, New York, 2003]. *Statistical Papers*, 46(1), 147.
- Scott, E. (2021). *Top 10 stress management techniques for students.* Verywell Mind.

<https://static1.squarespace.com/static/5dafb59e6bdcaa043c952968/t/5ef67f29c852723c9ddb3ca/1593212713649/Lead+Health+--+Stress+Article.pdf>

Author Information	
Mawar Idah Shonia Universitas Gadjah Mada Yogyakarta, Indonesia Contact e-mail: mawaridahshonia@mail.ugm.ac.id	Dr. Noorma Yulia Megawati, S.Si., M.Sc. Universitas Gadjah Mada Yogyakarta, Indonesia
Asrul Khasanah Universitas Gadjah Mada Yogyakarta, Indonesia	Dr.Drs. Gunardi, M.Si. Universitas Gadjah Mada Yogyakarta, Indonesia

To cite this article:

Shonia, M. I., Megawat, N. Y., Gunardi, G., & Khasanah, A. (2024). Cluster analysis of sleep health and lifestyle data using Ward algorithm and Euclidean distance. *The Eurasia Proceedings of Science, Technology, Engineering & Mathematics (EPSTEM)*, 30, 107-113.

The Eurasia Proceedings of Science, Technology, Engineering & Mathematics (EPSTEM), 2024

Volume 30, Pages 114-120

ICBAST 2024: International Conference on Basic Sciences and Technology

The Impact of Climate Change on the Morphology of Marine Topography Using GNSS

Sotiris Lycourghiotis
Hellenic Open University

Elizabeth Paraskevi Crawford
Edinburgh Napier University

Abstract: In recent decades, very important scientific studies have focused on the effect of climate change on the average Sea Level Rise (SLR). Recent data has shown that 44% of the increase is due to the melting of glaciers and 42% to the thermal expansion of water due to the increase in average temperature. Research has focused mainly on the rate of Sea Level Rise from radar altimetry data (showing an average rise of 2.3 – 3.1 mm/year since 1970), or from coastal tide gauge data. In particular, although the coastal observations in closed seas agree with the data showing there is a trend towards an increase in sea levels, which is a result of climate change, they show significantly different rates of change. The question therefore arises: does climate change also affect the morphology of the Mean Sea Level (MSL) topography? In this paper, the research focuses for the first time not only on the change in MSL but also on the change in the morphology of the MSL topography. Research expeditions were carried out in the Gulf of Patras in 2011 and 2023. The method used is the new GNSS-on-boat method that, for the first time, makes it possible to examine the morphology of the MSL with an accuracy of up to 1 cm. The results show that in the area which was studied there was a significant change in mean sea level of the order of 2.78 cm in 12 years, which corresponds with the estimates of other researchers. However, what we observe for the first time is an obvious change in the shape of the sea surface. The significant changes in both the maxima and the slopes of the geoid exceed 8%.

Keywords: GNSS, Climate Change, Sea level rise, GNSS-on-boat, Environmental engineering

Introduction

The rate of Sea Level Rise (SLR) has never been constant. Geological research has shown that at the end of the last ice age (about 20,000 years ago) a rapid rise in ocean levels began, but it gradually slowed down and essentially stopped about 7,500 years ago (Leo et al., 2019). From this point until the industrial revolution the ocean level rose at a rate of less than 1mm/year (Griggs & Reguero, 2021). As is widely accepted, from the mid-19th century to the present, the widespread use of fossil fuels has doubled the amount of carbon dioxide in the atmosphere (from ~200 to ~400 ppm) and this has contributed to an increase in the average temperature of the planet by ~ 1.2 °C (Lindsey & Dahlman, 2020; Lycourghiotis et al., 2017; Lycourghiotis, 2022). This increase has been reflected in rising ocean levels both due to the expansion of water and the melting of continental glaciers. According to the most recent report of the IPCC (Fox-Kemper, 2022) the global increase in the average sea level has reached a quarter of a meter (25 cm) from 1880 to the present day (figure 1). Bearing in mind that the phenomenon of SLR lags behind its cause, i.e. global warming, by many tens of times, it becomes clear that SLR will not stop for a long time, even if the rise in temperature were halted (Skea et al., 2022).

In recent years, research on the effects of SLR has focused mainly on the data provided by the Topex & Poseidon altimetry satellite missions since 1999, followed by the Jason-1, -2 and -3 satellites (Nerem & Hamlington, 2024). These missions give us an insight into SLR on a global level. The data show an average

- This is an Open Access article distributed under the terms of the Creative Commons Attribution-Noncommercial 4.0 Unported License, permitting all non-commercial use, distribution, and reproduction in any medium, provided the original work is properly cited.

- Selection and peer-review under responsibility of the Organizing Committee of the Conference

© 2024 Published by ISRES Publishing: www.isres.org

increase of nearly 11cm from 1999 to the present, with the rate of SLR increasing dramatically in recent years up to 4.8mm/year (Veng & Andersen, 2021). However, the influence of SLR is not the same in all parts of the planet. As tide gauge data show, the rate of increase in mean sea level varies significantly (Adebisi et al., 2021). Several local factors, such as tidal magnitude, ocean currents, and geological sedimentation can greatly influence the effects. Recent studies have shown that island regions near the equator, such as the Caribbean, the Philippines, Indonesia, etc. will experience multiple impacts from SLR within the next few years (Martyr-Koller et al., 2021)

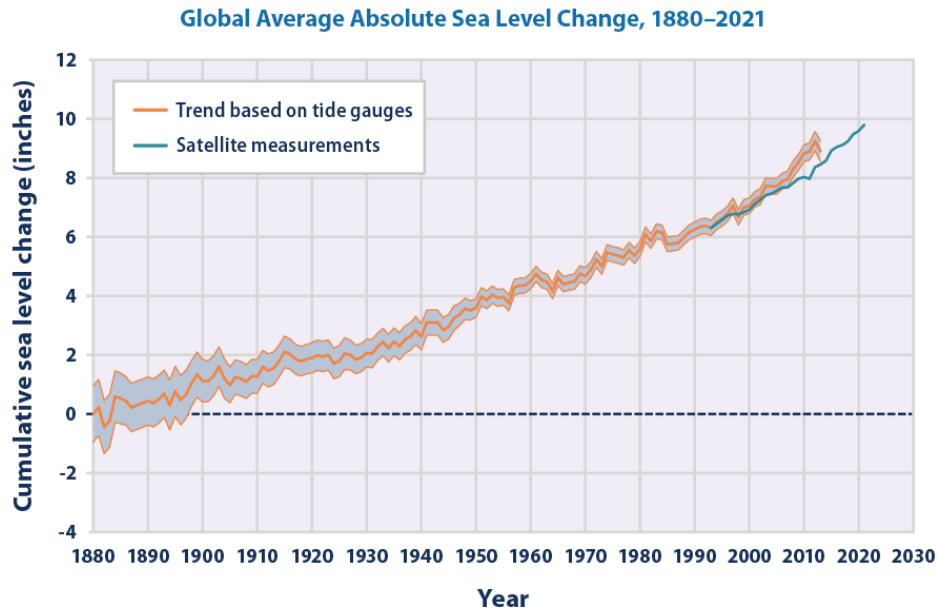


Figure 1. The global average sea level has rise since 1880 [Data source: Climate change indicators: sea level / absolute sea level change. EPA.gov. U.S. Environmental Protection Agency (EPA) (July 2022)]

Altimetry satellite measurements cover certain zones of the oceans (over the track of the satellites' orbit) while tide gauges measure only at specific and fixed coastal points and are not spread evenly over the planet. The limits and limitations of both methods make it imperative to add floating GNSS measurements to the study of SLR (Adebisi et al., 2021). In recent years a relatively new methodology has opened up a new field of research in the study of marine topography. This is the *GNSS-on-boat* technique (Lycourghiotis & Kariotou, 2022). This technique makes it possible to study the marine topography in coastal areas and closed seas where satellite and airborne methods usually fail, achieving an accuracy that reaches even 1cm (Lycourghiotis & Stiros, 2010; Lycourghiotis 2017a; 2017b; 2021). Although the GNSS-on-boat method succeeds in determining both mean sea level (MSL) and sea surface topography (SST) with very high accuracy, to date it has not been used to study climate change and in particular SLR. This is because the expeditions that have published data to date have focused their measurements on short periods of time, from a few days to a few weeks, and thus it is not possible to study the effect of SLR.

In this Paper, the GNSS-on-boat method is used for the first time in the study of climate change. Measurements made in the same area in two periods 12 years apart, in 2011 and 2023, are utilized. The area chosen was the Gulf of Patras (Greece), which is of great interest in terms of tectonic movements as it is an area which contains many active seismic faults (Ferentinos et al., 1985).

Significance of the Study Area in Light of SLR

The Gulf of Patras (Greece) is located between the Peloponnese and Western Greece (figure 2). To the west it is a natural extension of the Ionian Sea, from the island of Oxia to the cape of Araxos, while to the east it is bounded by the Rio-Antirion bridge. The bay has an area of 370 km² with a length of 40 to 50 km and a width of 10 to 20 km. Its deepest point (132m) is found approximately in the area of its geometric center. The gulf exhibits intense seismic activity while many active faults are present (Chronis et al., 1991). The city of Patras, the third largest city in Greece with a population of 200 thousand, lies on the south-eastern coast of the Gulf. The city is also a very important commercial port (Lycourghiotis, 2020; Lycourghiotis et al., 2021). The area is

characterized by significant vertical geological movements. Several intense climatic events, such as the floods of January 1, 2010 (Lycourghiotis & Kontoni, 2012), April 18, 2012 (Lycourghiotis & Kontoni, 2014) and the most recent one (November 2017), which almost destroyed the city's marina (figure 2), have demonstrated the vulnerability of the region to climate change and specially to rising sea levels. Although the average astronomical tide in the area does not exceed 12cm (Lycourghiotis & Stiros, 2013; Lycourghiotis & Kontoni, 2012b), geological movements combined with extreme weather events make the need for a systematic study of the phenomenon imperative.

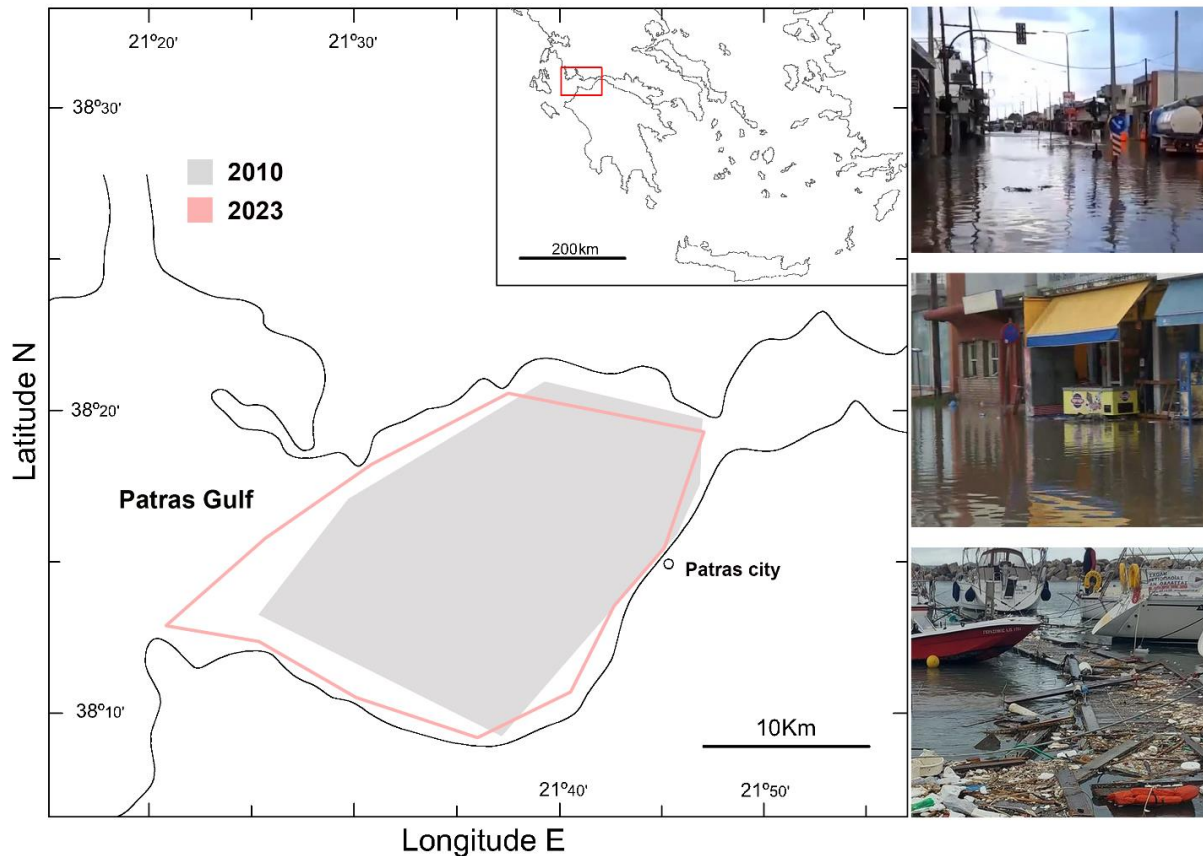


Figure 2. Location map of the study area and images of flood damages. The study area of the first mission (2010) is shown in grey, the of the second mission (2013) in red outline.

The Two Research Expeditions in the Study Area

Two research missions were carried out in the area of the Gulf of Patras, using the same GNSS-on-boat method. The first, in November 2010, employed a sailing vessel and a floating platform. The platform was of the catamaran type and carried 4 GNSS HiperPro receivers, which recorded at a rate of 1 Hz (Lycourghiotis, 2017a). The second expedition was carried out in the same area using a special research platform that carried 2 GNSS receivers and an accelerometer (Lycourghiotis & Kariotou, 2024). The sampling rate was 10 Hz. In both expeditions the central area of the Gulf of Patras was swept almost in its entirety. In the first mission, 3 days of data were collected, while in the second, data was recorded over a period of 7 days. In addition, tide prediction models, namely TASK, as well as tide gauge data in the port of Patras were used. The processing of data noise was affected using special software developed by us (Galani et al., 2021)

Methodology

The raw data of the first expedition was resolved using two methods, DGNSS and Precise Point Positioning (PPP) (Li et al., 2011). Figure 3 summarizes the overall methodology as presented in earlier work [16].

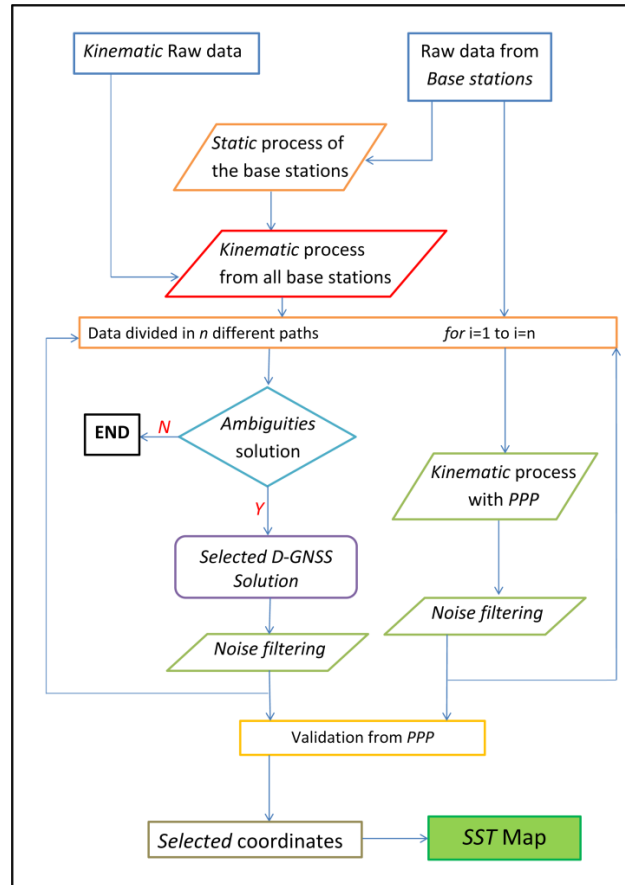


Figure 3. Illustration of the basic methodology of the first expedition [16, figure 16]

The raw data of the second expedition was resolved using the PPP method, while data noise was corrected using a special code. Ripple oscillations were corrected using data from the accelerometer, while the random noise was dealt with by testing successive moving average fitters, using the Savitzky-Golay method (Schafer, 2011). The tide was corrected using the tide gauge measurements and confirmed by the TASK software estimates. The final accuracy of the Sea Surface Topography estimates was calculated using the law of transmission of errors and was estimated at 1.3 cm. In contrast, the accuracy of the results of the first expedition was estimated at 5.43 cm. The main reason for this difference was that in the first expedition there was no reliable tide data and so it was estimated using data from remote stations (Lycourghiotis, 2017b).

Results and Discussion

Table 1 shows the results for the average value of the marine topography (MSL) in both expeditions. As can be observed, in the 12 years between the two expeditions there was an increase in the MSL of the common experimental area by 2.78 cm. This increase is generally in line with the estimates of other researchers (Meli, 2023). This fact confirms that the GNSS-on-boat method is suitable for SLR estimation. If we also consider that the method makes it possible to study, with extreme precision, marine areas that are not covered by the range of satellites, or coastal areas and closed seas where satellite methods fail, then we can say that a new field of research is opening.

Table 1. Mean sea levels in experimental areas. Differences in the common study area.

Mission	2010	2023	Differences
MSL (m) in their original study area	24.8534	24.6792	
MSL (m) in common area	24.6653	24.6931	+2.78 cm

Figure 4 shows the estimates of MSL Topography as obtained from the two research expeditions. On the top left we see the results of the first mission (2010). At the top right we see the results of the second mission (2023). While at the bottom right we see the results of both missions in their common study area. As can be seen, a

small but statistically significant change in the shape of the sea surface is detected. The differences in the shape of the sea surface are particularly evident at points A and B (bottom right), where the slope of the topography and curves change significantly. Trying to estimate these differences statistically, we took a canvas of 42,546 points throughout the common study area and calculated the differences between the two estimates. From the analysis it emerged that the differences in the shape of the sea surface are statistically significant and reach the level of 8%.

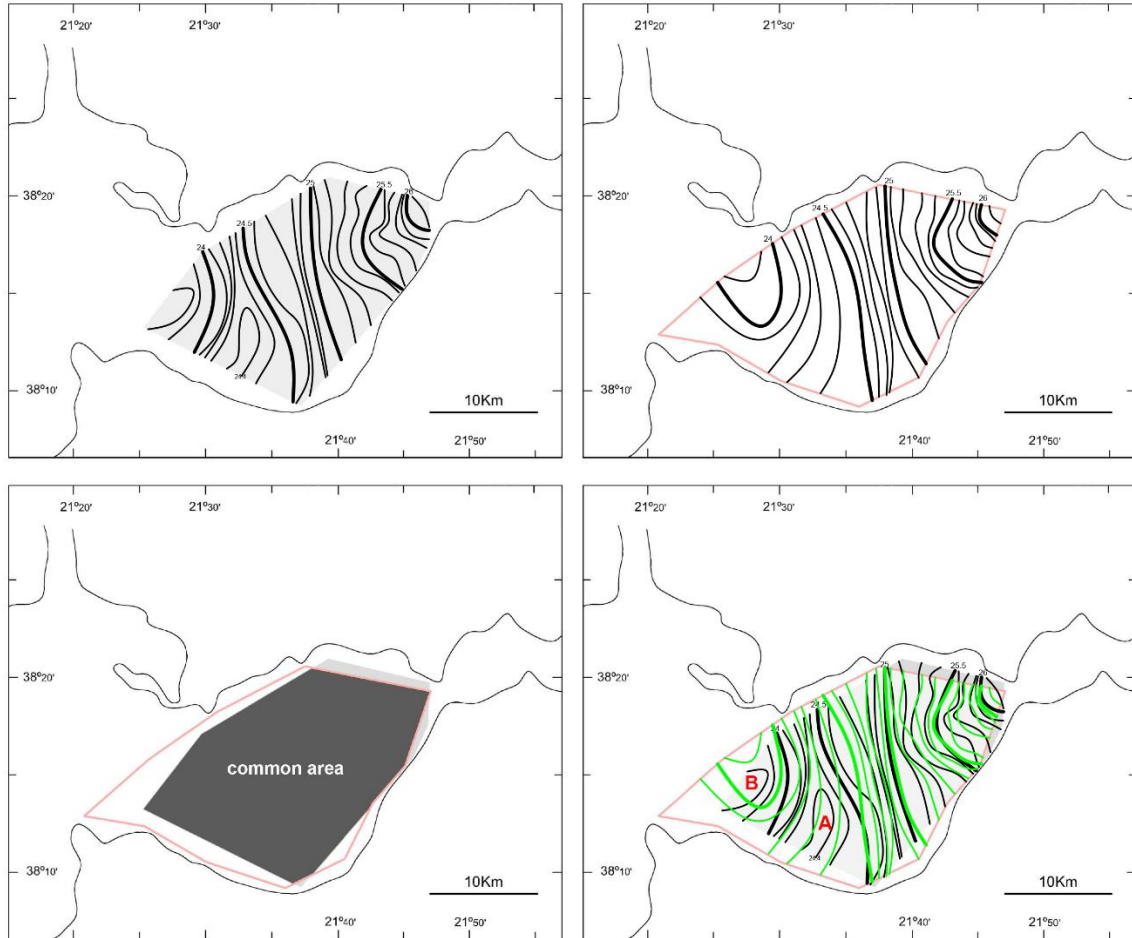


Figure 4. Results of the assessment of MTS from the two research expeditions in Patras Bay. (Above) Left and right show the first and second expeditions. (Bottom). Their common research area and comparison of their results. The contour interval of the contour lines is equal to 10cm. Heights were calculated above the WGS84 ellipsoid.

Despite the statistical significance of these differences, it would be risky to claim that the observed change in sea surface shape is due to climate change and SLR. The significant tectonic variability of the region could lead to such changes. We should also be wary of the small but significant differences observed in the results of the GNSS-on-boat analyses used in the two expeditions. In any case, the observations made here open up an important research question that future research is called upon to answer.

Scientific Ethics Declaration

The authors declare that the scientific ethical and legal responsibility of this article published in EPSTEM Journal belongs to the authors.

Acknowledgements or Notes

* This article was presented as an oral presentation at the International Conference on Basic Sciences and Technology (www.icbast.net) held in Antalya/Turkey on November 14-17, 2024.

References

- Adebisi, N., Balogun, A. L., Min, T. H., & Tella, A. (2021). Advances in estimating Sea Level Rise: A review of tide gauge, satellite altimetry and spatial data science approaches. *Ocean & Coastal Management*, 208, 105632.
- Chronis, G., Piper, D. J., & Anagnostou, C. (1991). Late Quaternary evolution of the Gulf of Patras, Greece: Tectonism, deltaic sedimentation and sea-level change. *Marine Geology*, 97(1-2), 191-209.
- Ferentinos, G., Brooks, M., & Doutsos, T. (1985). Quaternary tectonics in the Gulf of Patras, western Greece. *Journal of Structural Geology*, 7(6), 713-717.
- Fox-Kemper, B. (2021, December). Ocean, cryosphere and sea level change. In AGU fall meeting abstracts (Vol. 2021, pp. U13B-09).
- Galani, P., Lycourghiotis, S., & Kariotou, F. (2021, November). On the determination of a locally optimized Ellipsoidal model of the Geoid surface in sea areas. In IOP Conference Series: *Earth and Environmental Science*, 906(1), 012036. IOP Publishing.
- Griggs, G., & Reguero, B. G. (2021). Coastal adaptation to climate change and sea-level rise. *Water*, 13(16), 2151.
- Leo, K. L., Gillies, C. L., Fitzsimons, J. A., Hale, L. Z., & Beck, M. W. (2019). Coastal habitat squeeze: A review of adaptation solutions for saltmarsh, mangrove and beach habitats. *Ocean & Coastal Management*, 175, 180-190.
- Li, X., Huang, J., Li, X., Shen, Z., Han, J., Li, L., & Wang, B. (2022). Review of PPP-RTK: Achievements, challenges, and opportunities. *Satellite Navigation*, 3(1), 28.
- Lindsey, R., & Dahlman, L. (2020). *Climate change: Global temperature*. Climate. gov, 16.
- Lycourghiotis, A., Kordulis, C., & Lycourghiotis, S. (2017). *Beyond fossil fuels: the return journey to renewable energy*. Πανεπιστημιακές Εκδόσεις Κρήτης ISBN: 978-960-524-492-7
- Lycourghiotis, S. (2022). Trends in renewable energy: an overview. *Global Nest Journal*, 24(3), 505-525.
- Lycourghiotis, S., & Kariotou, F. (2022). The “GPS/GNSS on boat” technique for the determination of the sea surface topography and geoid: A Critical Review. *Coasts*, 2(4), 323-340.
- Lycourghiotis S., Stiros S., (2010). Sea surface topography in the gulf of Patras and the southern Ionian Sea using GPS. *Bull. Geo. Soc. Greece*, XLIII (2), pp. 1029-1034,
- Lycourghiotis, S. (2017, July). Improvements of GNSS-on-boat methodology using a catamaran platform: Application at the gulf of Patras. In *Proceedings of the 7th International Conference on Experiments/Process/System Modeling/Simulation/Optimization*, Athens, Greece (pp. 5-8).
- Lycourghiotis, S. (2017, July). Sea surface topography determination. Comparing two alternative methods at the gulf of Corinth. In *Proceedings of the 7th International Conference on Experiments/Process/System Modeling/Simulation/Optimization*, Athens, Greece (pp. 5-8).
- Lycourghiotis, S. (2021). Sea topography of the Ionian and Adriatic seas using repeated GNSS measurements. *Water*, 13(6), 812.
- Lycourghiotis, S. (2020). The fluid geography of rubbish: An analysis of the Patras refugee camp (1999–2009). *Worldwide Waste*, 3(1), 8-8.
- Lycourghiotis, S., Mpelogianni, V., & Groumpos, P. P. (2021, July). Smart cities and intelligent transportation in traditional cities. Ten design principles and one case study. In *2021 12th International Conference on Information, Intelligence, Systems & Applications (IISA)* (pp. 1-7). IEEE.
- Lycourghiotis, S. A., & Kontoni, D. P. N. (2012). Flood phenomena in the Aegean and Ionian Sea on the 25th December 2009 and 1st January 2010: a numerical analysis of the surge amplitude. *5th International Conference from Scientific Computing to Computational Engineering*, Athens, Greece, 4-7, Volume II, pp. 263-268.
- Lycourghiotis S., Kontoni D.-P.N. (2014). Topographic leveling, numerical simulation and digital video analysis of marina damage: Evidence from the 18th of April 2012 fierce storm. *6th International Conference from Scientific Computing to Computational Engineering*, Athens, Greece, 9-12 Vol. II, pp. 505-510.
- Lycourghiotis, S. A., & Stiros, S. C. (2013). Coastal flooding hazard in low-tide and high-tide coasts: Evidence from the north Aegean coast. *Coastal Hazards*, 231-243.
- Lycourghiotis, S., & Kontoni, D. P. N. (2012, July). Analysing the flood risk in Mediterranean coastal areas with a new methodology. In *Proceedings of the 5th International Conference from Scientific Computing to Computational Engineering*, Athens, Greece (pp. 4-7).
- Lycourghiotis, S., Crawford, E. P., & Kariotou, F. (2024). A study of the geoid and marine topography in Lagoons. *Inżynieria Mineralna*, 1(1), 181-185. <https://doi.org/10.29227/IM-2024-01-19>
- Martyr-Koller, R., Thomas, A., Schleussner, C. F., Nauels, A., & Lissner, T. (2021). Loss and damage implications of sea-level rise on small island developing states. *Current Opinion in Environmental Sustainability*, 50, 245-259.

- Meli, M., Camargo, C. M., Olivieri, M., Slangen, A. B., & Romagnoli, C. (2023). Sea-level trend variability in the Mediterranean during the 1993–2019 period. *Frontiers in Marine Science*, 10, 1150488.
- Nerem, R. S., & Hamlington, B. D. (2024, March). Satellite measurements of sea level change: Past, present, and future. In *2024 IEEE Aerospace Conference* (pp. 1-4). IEEE.
- Schafer, R. W. (2011). What is a savitzky-golay filter? [lecture notes]. *IEEE Signal Processing Magazine*, 28(4), 111-117.
- Skea, J., Shukla, P. R., Reisinger, A., Slade, R., Pathak, M., Al Khourdajie, A., ... & Winkler, H. (2022). Summary for policymakers. In *Climate change 2022: Mitigation of climate change: Contribution of working group iii to the sixth assessment report of the intergovernmental panel on climate change*. Cambridge University Press.
- Veng, T., & Andersen, O. B. (2021). Consolidating sea level acceleration estimates from satellite altimetry. *Advances in Space Research*, 68(2), 496-503.

Author Information

Sotiris Lycourghiotis

Hellenic Open University,
Greece

Contact e-mail: slykour@email.com

Elizabeth Paraskevi Crawford

Edinburgh Napier University,
United Kingdom

To cite this article:

Lycourghiotis, S. & Crawford, E.P. (2024). The impact of climate change on the morphology of marine topography using GNSS. *The Eurasia Proceedings of Science, Technology, Engineering & Mathematics (EPSTEM)*, 30, 114-120.

The Eurasia Proceedings of Science, Technology, Engineering & Mathematics (EPSTEM), 2024

Volume 30, Pages 121-128

ICBAST 2024: International Conference on Basic Sciences and Technology

Research into Alternative Resources to Improve Animal Feed: The Case of *Azolla*

Azeddine Mouhous

Mouloud Mammeri University of Tizi-Ouzou

Amina Ait-Allaoua

Mouloud Mammeri University of Tizi-Ouzou

Lisa Chettouh

Mouloud Mammeri University of Tizi-Ouzou

Nadir Semsoum

Mouloud Mammeri University of Tizi-Ouzou

Nassima Zirmi-Zembri

Mouloud Mammeri University of Tizi-Ouzou

Zahia Dorbane

Mouloud Mammeri University of Tizi-Ouzou

Dyhia Saidj

SAAD Dahleb University

Hocine Guermah

Mohammed Boudiaf University of M'sila

Farid Djellal

Ferhat Abbas University of Setif

Rabia Cherfouh

Mouloud Mammeri University of Tizi-Ouzou

Ali Bouzourene

Mouloud Mammeri University of Tizi-Ouzou

Si Ammar Kadi

Mouloud Mammeri University of Tizi-Ouzou

Abstract: In countries where the animal feed are mainly imported, the search for alternative resources is a key way of reducing these costs. We have chosen to use the *Azolla filiculoides* plant. It is an aquatic fodder plant that is rich in protein. Its cultivation is simple. For the assessment of its development and yield, *Azolla* has been grown in two different environments. The first experiment was carried out in two open-air ponds with a surface area of 02 m². The water depth was 3 cm and 5 cm, respectively. The second was carried out in the laboratory, using a system of small caissons arranged on shelves. Water was added to these caissons at different depths. In both experiments, nutrient solution consisting of cow dung and some NPK was added. After 20 days of

- This is an Open Access article distributed under the terms of the Creative Commons Attribution-Noncommercial 4.0 Unported License, permitting all non-commercial use, distribution, and reproduction in any medium, provided the original work is properly cited.

- Selection and peer-review under responsibility of the Organizing Committee of the Conference

© 2024 Published by ISRES Publishing: www.isres.org

growing, the outdoor experiment showed that *Azolla filiculoides* could tolerate depths of 3 and 5 cm and could multiply easily. Daily production reached a yield of 305 g/m². This corresponds to about 10 kg per month. On the other hand, the laboratory trial was a failure. The *Azolla* gradually deteriorated over the course of the trial until it died. The reason for this was the inefficiency of the lighting system due to the use of ordinary fluorescent lamps that are unsuitable for *Azolla* cultivation. We recommend the use of fluorescent lamps specially designed for this purpose. It is possible to grow *Azolla* in a closed environment as long as the environmental parameters are well controlled. These promising results suggest that *Azolla* has interesting potential as an alternative source of protein to feed livestock. However, further research will be necessary in order to improve yields and optimize growth conditions.

Keywords: *Azolla filiculoides*, Animal feed, Alternative resource, Protein source, *Azolla* cultivation, Agricultural engineering

Introduction

Worldwide demand for animal protein is constantly increasing due to population growth. Animals need to consume more energy and plant proteins than they produce for human consumption (Laisse et al., 2019). In the new forms of livestock farming, which are often more intensive, field crops (cereals, oilseeds, protein crops) and their co-products (oilcake, bran and milling waste) are widely used throughout the world. There is competition for arable crop resources between humans and animals, as well as competition for available farmland (Dronne, 2018).

Current production methods certainly provide higher yields, but at the high cost of some raw materials, particularly soya meal (Adouko et al., 2021). The use of local, non-conventional feedstuffs appears to be an endogenous solution to the high cost of imported raw materials (Adouko et al., 2021). These resources are an alternative to supplementation with concentrates and intensification of fodder production (Geoffroy et al., 1991).

Alternative or non-conventional food resources are foods of plant, animal or mineral origin that do not compete with human food. They include seeds (*Mucuna spp.*, *Lablab purpureus*, *Canavalia ensiformis*, *sesame*), leaves (*Moringa oleifera*, *Leucaena leucocephala*, *Azolla pinnata*), tubers and various animal products (Dahouda et al., 2009). Introducing these resources into animal feed has become the only way of reducing the cost of the ration supplemented with concentrate without affecting herd productivity (Lassoued et al., 2011).

In the case of this study, the interest is focused on the fern *Azolla filiculoides*, an inexpensive alternative that offers an excellent protein supply. *Azolla* can be a valuable protein supplement for many animal species, including ruminants, poultry, pigs and fish (Ouedraogo et al., 2021).

Method

To test the *Azolla filiculoides* plant, two systems were set up in order to grow this plant. The first set-up consisted of two basins, each measuring 02 m² and dug into the soil with a water depth of 03 and 05 cm respectively, set up in the open air. The second system consists of 06 small caissons of different volumes and depths installed on a shelf and set up in a laboratory, where the environmental parameters (water pH, H[°], air and water T[°]) are controlled. The volumes and depths were as follows: 02 caissons A1 (volume 0.025 m³, depth 5 cm); 02 caissons A2 (volume 0.035 m³, depth 7 cm); 02 caissons A3 (volume 0.045 m³, depth 9 cm). For each depth, there were two repetitions. 18W neon lamps were superposed on each tank and operated for 20 hours per day using a timer.

The test lasted 20 days, after a 10-day adaptation period. It began on 18 May 2023. All the caissons were filled with water. The laboratory basins were covered by a thin layer of soil from the open-air basin. A nutrient solution was prepared and left to stand for 10 days. It consists of 10 kg of cow dung + 40 litres of water + 80 g of NPK. For the open-air tank, 02 litres of nutrient solution are added each week. For each laboratory tank, a volume of 500 ml / week is added (figure 1).

Azolla was planted on the same day for all the basins (in the lab and outdoors). The quantity of *Azolla* planted in the laboratory caissons was 250 g/0.5 m² of water surface. In the open-air basins, which each had a water surface area of 02 m², an area of 0.5 m² was marked off with a board, where the quantity of *Azolla* planted was 250 g.



Figure 1. Experimental device used

Results and Discussion

The Development of *Azolla filiculoides* in Open-Air Basins

Air temperature monitoring recorded an average of 19.3°C, with values ranging from 12.8 to 26°C. For *Azolla*, ambient temperature is the main factor that has a direct influence on the plant. According to Van Hove (1989), the temperature that favours plant growth is between 20 and 30°C (figure 2). The water temperature varied between 13 and 21°C, with an average of 16.2°C. The drop in temperature was due to the *Azolla* mat on the surface of the water, which prevented the sun's rays from penetrating the two pools.

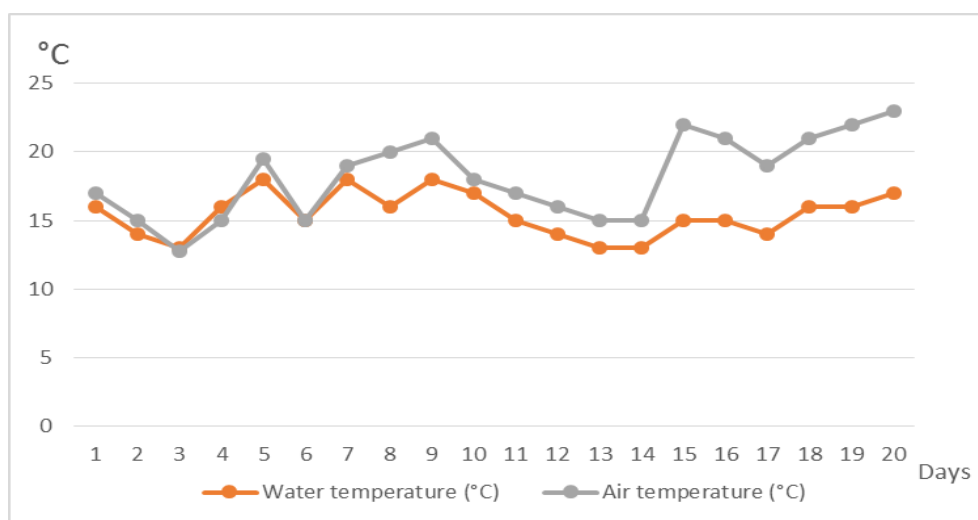


Figure 2. Evolution of water and air temperatures in the two open-air basins.

The pH of the water varies between 6.5 and 6.8 (Figure 3). It is basic and is suitable for the proper development of the plant, and encourages its growth and multiplication. The adequate pH for growing *Azolla* varies between 4.5 and 7 (Peters et al., 1980; Lumpkin and Plucknett, 1980). The average humidity level recorded during the trial was 67.3%. It varied between 48% and 92%. The optimum humidity for the growth of this plant varies between 85 and 90% (Rajesh, 2020). Although the humidity level recorded over the days varied, this did not have a negative influence on the plant's development (figure 3). Even when the humidity level was below 60%, the growth and multiplication of the *Azolla* were not affected, and we observed a positive evolution of the plant in both cultivation basins.

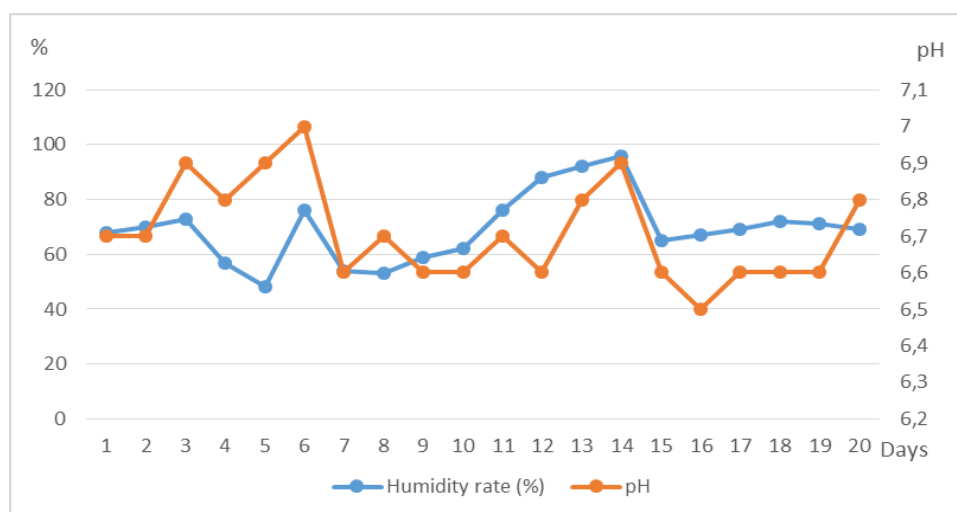


Figure 3. Evolution of humidity levels and water pH in the two open-air basins

Azolla Harvest and Yield in the Open-Air Basins

Once the plant had matured and adapted, it was found that the *Azolla* could resist and grow without difficulty in open-air basins at depths of 03 and 05 cm. The first harvest was made 20 days after planting the fern (figure 4).



Figure 4. Evolution of *Azolla* development in open-air basins

The second harvest took place on day 28. For basin 1 (5 cm deep), a quantity of 3350 g was harvested for the first time, taking into account the need to leave an initial quantity for later multiplication (the entire basin was still covered with *Azolla* after harvesting).

The second harvest was carried out 08 days after the first. The quantity harvested was 3110 g of *Azolla*. In basin 2 (3 cm deep), the first harvest was 3240 g, and the second was 3040 g (Table 1). *Azolla* dries by spreading it out on a ventilated surface. It can take up to 48 hours. The following table shows the weight differences between the fresh and dried states of the plant.

Table 1. Weight of fresh, dry *Azolla* in both basins.

	Fresh <i>Azolla</i>	Dry <i>Azolla</i>
		Basin 1 (05 cm depth)
Harvest 1	3350 g	301,5 g
Harvest 2	3110 g	280,9 g
		Basin 2 (03 cm depth)
Harvest 1	3240 g	298,08 g
Harvest 2	3040 g	273,6 g

After drying, *Azolla* loses almost 91% of its initial weight. Dry matter only represents nearly 9%. This result is close to that of Parashuramulu et al. (2013), who indicated a rate of 8.7% dry matter. Despite this considerable loss of weight, the process has little effect on the nutritional value of the plant (Van Hove, 1989). It should also be noted that there are no moulds, which gives the plant a good health quality. To estimate the yield of *Azolla* per m², the quantity reproduced was estimated using the following formula:

Quantity multiplied = total quantity harvested - initial quantity

If we take into account the second harvest, which took place on day 28, giving us 08 days of cultivation, we get the following figure:

For basin 1 (05 cm deep) :

3110 g - 250 g = 2860 g / 2 m². i.e. production of 357.5 g/day/2 m².

i.e. a production of 178.75 g / day / m². The 2 m² basin can produce 10.7 kg of *Azolla* / month.

For basin 2 (03 cm deep) :

3040 g - 250 g = 2790 g / 2 m². i.e. production of 348.75 g/day/2 m².

i.e. a production of 174.37 g / day / m². The 2 m² basin can produce up to 10.4 kg of *Azolla* / month.

On average, a 2 m² basin will produce 10.55 kg of *Azolla*. The plant multiplies very quickly. This is one of its advantages. This is also reported by Kumar and Chander (2017).

***Azolla* Developement in the Laboratory Set-up**

Given the three basins (with repetition) were subjected to the same environmental conditions, we measured, for the three parameters, the average of all the basins. In the laboratory, near the device, the air temperature varied between 19 and 26°C during the test period. This temperature range is in line with standards. According to Van Hove (1989), the temperature that favours plant growth is between 20 and 30°C. The temperature inside the caissons varied between 16 and 23°C (figure 5).

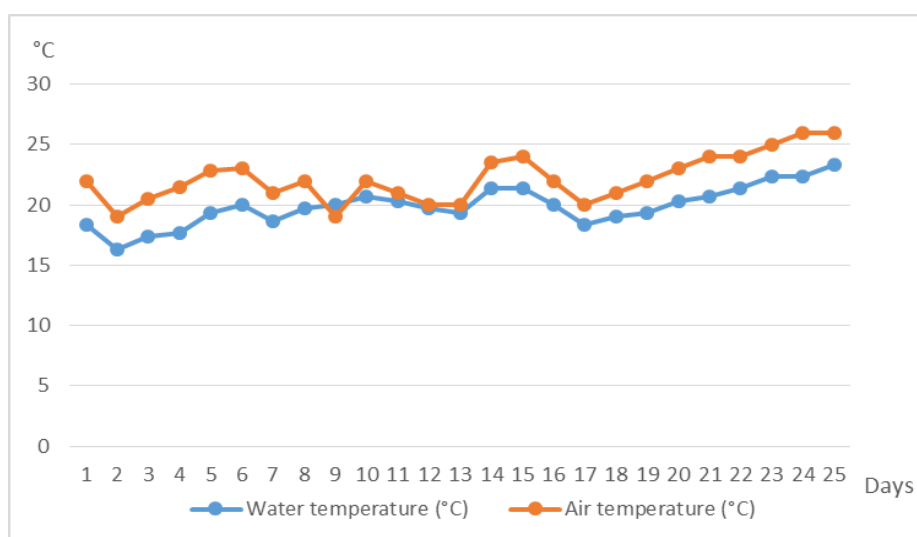


Figure 5. Evolution of water and air temperatures in the laboratory set-up basins

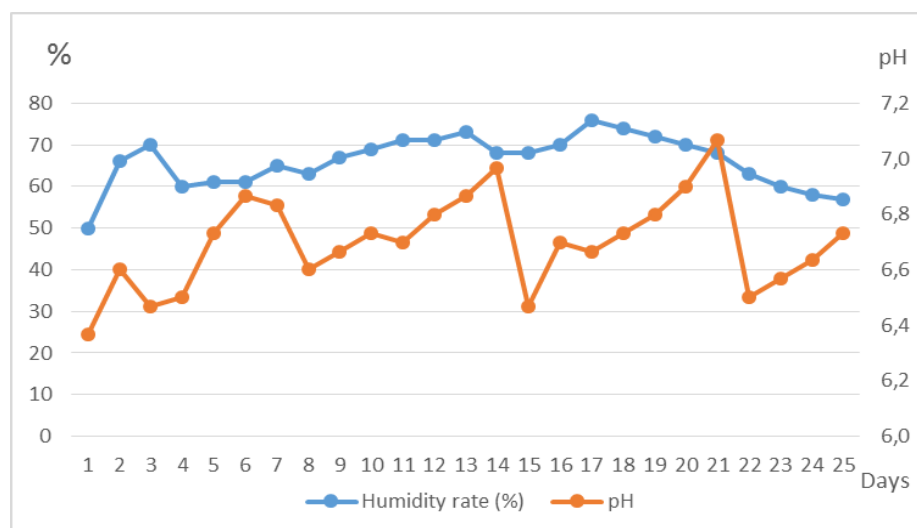


Figure 6. Evolution of the humidity level and pH of the water in the basins of the laboratory set-up

Humidity levels varied between 50 and 76% (figure 6). This is thought to be due to the variations in temperature between mid-May and mid-June during the trial period. While the pH varied between 6.4 and 7.1, *Azolla* is particularly tolerant of environmental pH, surviving in a range from 3.5 to 10 (Peters et al., 1980; Lumpkin and Plucknett, 1980).

Monitoring the Development of *Azolla*

The *Azolla filiculoides* developed normally until the 5th day, and its density was increasing. From day 8 onwards, the roots take a long time to develop. They become fragile, and when they reach a certain stage of growth, they detach from the frond and new regrowth appears. On the other hand, the fern continued to grow and an increase in its density was observed.

On the 10th day, the end of the adaptation phase, the density had increased. However, the roots had not developed and had not reached maturity (figure 7). On day 15, a deterioration in the condition of the plant was observed, with a significant decrease in density and the absence of roots. On day 20, there was no improvement and the plant continued to deteriorate despite the addition of artificial light and NPK fertiliser (20%).



Figure 7. Evolution of *Azolla* development in the laboratory caissons

The laboratory device did not give positive results. There was a lack of light. The neon lights placed in the boxes did not provide enough light for the *Azolla* to develop. According to Lumpkin and Plucknett (1980), *Azolla* growth declines rapidly if light levels are below 1500 lux.

Conclusion

The aim of growing *Azolla filiculoides* in two different environments (in the open air and in a closed environment) was to assess the plant's profitability in the field of animal nutrition. In the open-air trial, the fern showed very promising performance; a 2 m² basin can produce up to 10.4 kg of *Azolla* per month. *Azolla* can grow in water depths of between 3 and 5 cm. *Azolla* loses up to 90% of its weight when it dries out. In the laboratory test, there was a lack of light. The *Azolla* deteriorated over the last few days, until it disappeared. To

improve this system, it would be necessary to carefully control the level of light (in Lux) required for the *Azolla* to develop.

Recommendations

Azolla filiculoides is an alternative source that we strongly recommend for animal feed because of its high protein content, its increasing multiplication and its less expensive production, which requires less water and cultivation area. The laboratory set-up we have proposed could increase *Azolla* productivity and reduce production costs by improving the amount of light needed for *Azolla* development.

Scientific Ethics Declaration

The authors declare that the scientific ethical and legal responsibility of this article published in EPSTEM Journal belongs to the authors.

Acknowledgements or Notes

* This article was presented as a poster presentation at the International Conference on Basic Sciences and Technology (www.icbast.net) held in Antalya/Turkey on November 14-17, 2024.

References

- Adouko, S. J., Guedegbe, O. A. U. G., Ohouko, O. H. F., Soha, S. A. S., Youssao, A. K. I., & Dougnon, T. J. (2021). Effets de *Moringa oleifera* substitué au tourteau de soja chez des poules pondeuses. *Livestock Research for Rural Development*, 33(2), 1-15.
- Dahouda, M., Toleba, S. S., Senou, M., Youssao, A. K. I., Hambuckers, A., & Hornick, J. L. (2009). Les ressources alimentaires non-conventionnelles utilisables pour la production aviaire en Afrique: valeurs nutritionnelles et contraintes. In *Annales de Médecine Vétérinaire* (Vol. 153). ULg-Université de Liège, Liège, Belgium.
- Dronne, Y. (2018). Agricultural raw materials for food and feed: the EU and France. *INRA Productions Animales*, 31(3), 181-200.
- Geoffroy, F., Naves, M., Saminadin, G., Borel, H., & Alexandre, G. (1991). Utilisation des ressources alimentaires non conventionnelles par les petits ruminants. *Revue D'élevage et de Médecine Vétérinaire Des Pays Tropicaux*, 44(special), 105-112.
- Kumar, G., & Chander, H. (2017). Study on the potential of *Azolla pinnata* as livestock feed supplement for climate change adaptation and mitigation. *Asian J. Adv. Basic Sci*, 5(2), 65-68.
- Laisse, S., Baumont, R., Dusart, L., Gaudré, D., Rouillé, B., BeNOIT, M., ... & PeYRAUD, J. L. (2019). L'efficience nette de conversion des aliments par les animaux d'élevage: une nouvelle approche pour évaluer la contribution de l'élevage à l'alimentation humaine. *INRA Productions Animales*, 31(3), 269-288.
- Lassoued, N., Rekik, M., Ben Salem, H., & Mahouachi, M. (2011). Utilisation des ressources alimentaires alternatives et performances de reproduction des ovins en Tunisie. *Mutations des systèmes d'élevage des ovins et perspectives de leur durabilité, Zaragoza: CIHEAM/IRESA/OEP*, 67-72.
- Lumpkin, T. A., & Plucknett, D. L. (1980). *Azolla*: botany, physiology, and use as a green manure. *Economic Botany*, 34, 111-153.
- Ouedraogo, B., Nikiema, Z. S., Zoundi, J. S., & Sawadogo, L. (2021). Effets de l'incorporation de la biomasse d'*azolla* (*Azolla pinnata*) séchée dans les rations du poulet en aviculture traditionnelle améliorée. *International Journal of Biological and Chemical Sciences*, 15(1), 212-223.
- Parashuramulu, S., Swain, P. S., & Nagalakshmi, D. (2013). Protein fractionation and in vitro digestibility of *Azolla* in ruminants. *Online Journal of Animal and Feed Research*, 3(3), 129-132.
- Peters, G. A., Toia, J. R., Robert, E., Evans, W. R., Crist, D. K., Mayne, B.C., & Pool, R.E. (1980). Characterization and comparisons of five N₂-fixing *Azolla*-*Anabaena* associations, I. Optimization of growth conditions for biomass increase and N content in a controlled environment. *Plant, Cell & Environment*, 3(4), 261-269.

- Rajesh, S. (2020). Production of azolla as livestock feed supplement in India. Pashudhan praharee. *Indian Dairy & Poultry Industry*, 43 p.
- Van Hove, C. (1989). Azolla: and its multiple uses with emphasis on Africa. Food and Agriculture Organization of the United Nations. AGRIS-International System for Agricultural Science and Technology. <https://agris.fao.org/search/en/providers/123819/records/64735fc92c1d629bc97df1a8>

Author Information

Azeddine Mouhous

Department of Agronomic Sciences, Faculty of Biological Sciences and Agronomic Sciences, Mouloud Mammeri University of Tizi-Ouzou, Hasnaoua, BP17 Tizi-Ouzou, Algeria
Contact e-mail: mouhousazeddine@yahoo.fr

Amina Ait Allaoua

Department of Agronomic Sciences, Faculty of Biological Sciences and Agronomic Sciences, Mouloud Mammeri University of Tizi-Ouzou, Hasnaoua, BP17 Tizi-Ouzou, Algeria

Lisa Chettouh

Department of Agronomic Sciences, Faculty of Biological Sciences and Agronomic Sciences, Mouloud Mammeri University of Tizi-Ouzou, Hasnaoua, BP17 Tizi-Ouzou, Algeria

Nadir Semsoum

Department of Agronomic Sciences, Faculty of Biological Sciences and Agronomic Sciences, Mouloud Mammeri University of Tizi-Ouzou, Hasnaoua, BP17 Tizi-Ouzou, Algeria

Nacima Zirmi-Zembri

Department of Agronomic Sciences, Faculty of Biological Sciences and Agronomic Sciences, Mouloud Mammeri University of Tizi-Ouzou, Hasnaoua, BP17 Tizi-Ouzou, Algeria

Zahia Dorbane

Department of Agronomic Sciences, Faculty of Biological Sciences and Agronomic Sciences, Mouloud Mammeri University of Tizi-Ouzou, Hasnaoua, BP17 Tizi-Ouzou, Algeria

Dyhia Saidj

Veterinary Sciences Institute, SAAD Dahleb University, Blida1, Algeria

Hocine Guermah

Faculty of Agronomic Sciences, Mohammed Boudiaf University of M'sila, Algeria

Farid Djellal

Faculty of Agronomic Sciences, Ferhat Abbas University of Setif, Algeria

Rabia Cherfouh

Department of Agronomic Sciences, Faculty of Biological Sciences and Agronomic Sciences, Mouloud Mammeri University of Tizi-Ouzou, Hasnaoua, BP17 Tizi-Ouzou, Algeria

Ali Bouzourene

Department of Agronomic Sciences, Faculty of Biological Sciences and Agronomic Sciences, Mouloud Mammeri University of Tizi-Ouzou, Hasnaoua, BP17 Tizi-Ouzou, Algeria

Si Ammar Kadi

Department of Agronomic Sciences, Faculty of Biological Sciences and Agronomic Sciences, Mouloud Mammeri University of Tizi-Ouzou, Hasnaoua, BP17 Tizi-Ouzou, Algeria

To cite this article:

Mouhous, A., Ait-Alloua, A., Chettouh, L., Semsoum, N., Zirmi-Zembri, N., Dorbane, Z., Saidj, D., Guermah, H., Djellal, F., Cherfouh, R., Bouzourene, A., & Kadi, S. A. (2024). Research into alternative resources to improve animal feed: The case of *Azolla*. *The Eurasia Proceedings of Science, Technology, Engineering & Mathematics (EPSTEM)*, 30, 121-128.